

STATUS OF THESIS

Title of thesis

PERFORMANCE AND CHARACTERIZATION OF
SUPPORTED IRON NANOCATALYST IN FISCHER-
TROPSCH REACTION

I, SARA FAIZ HANNA TASFY

hereby allow my thesis to be placed at the Information Resource Center (IRC) of Universiti Teknologi PETRONAS (UTP) with the following conditions:

1. The thesis becomes the property of UTP.
2. The IRC of UTP may make copies of the thesis for academic purposes only.
3. This thesis is classified as

Confidential

Non-confidential

If this thesis is confidential, please state the reason:

The contents of the thesis will remain confidential for _____ years.

Remarks on disclosure:

Endorsed by

Signature of Author

Signature of Supervisor

Permanent Address:

Name of Supervisor

University of Gizera

Assoc. Prof. Dr. Noor Asmawati

Faculty of Chemical Engineering

Mohd Zabidi

P.O. Box. 11111

Date: _____

Date: _____

UNIVERSITI TEKNOLOGI PETRONAS
PERFORMANCE AND CHARACTERIZATION OF SUPPORTED IRON
NANOCATALYST IN FISCHER-TROPSCH REACTION

By

SARA FAIZ HANNA TASFY

The undersigned certify that they have read, and recommend to the Postgraduate Studies Programme for acceptance this thesis for the fulfillment of the requirements for the degree stated.

Signature: _____

Main Supervisor: Assoc. Prof. Dr. Noor Asmawati Mohd Zabidi

Date: _____

Signature: _____

Co-Supervisor: Prof. Dr. Duvvuri Subbarao

Date: _____

Signature: _____

Head of Department: Assoc. Prof. Dr. Shuhaimi Mahadzir

Date: _____

UNIVERSITI TEKNOLOGI PETRONAS

PERFORMANCE AND CHARACTERIZATION OF SUPPORTED IRON
NANOCATALYST IN FISCHER-TROPSCH REACTION

By

SARA FAIZ HANNA TASFY

A Thesis

Submitted to the Postgraduate Studies Programme
as a Requirement for the Degree of

MASTER OF SCIENCE

CHEMICAL ENGINEERING DEPARTMENT

UNIVERSITI TEKNOLOGI PETRONAS

BANDAR SRI ISKANDAR

PERAK

February 2011

DECLARATION OF THESIS

Title of thesis

PERFORMANCE AND CHARACTERIZATION OF
SUPPORTED IRON NANOCATALYST IN FISCHER-
TROPSCH REACTION

I, SARA FAIZ HANNA TASFY

hereby declare that the thesis is based on my original work except for quotations and citations which have been duly acknowledged. I also declare that it has not been previously or concurrently submitted for any other degree at UTP or other institutions.

Witnessed by

Signature of Author

Signature of supervisor

Permanent Address:

Name of Supervisor

University of Gizera

Assoc. Prof. Dr. Noor Asmawati

Faculty of Chemical Engineering

Mohd Zabidi

P.O. Box. 11111

Date: _____

Date: _____

To my parents

To my sweet aunt

To all my relative

To my grandfather and uncle's souls

To my friends

To everyone I meant something to

ACKNOWLEDGEMENT

My Strength is Made Perfect in Weakness (2Cor 12:9)

First I would like to thank God for the inspired and strength that keeps me standing to finish what I have started and for the motivation and hope that keeps me believing that this affiliation would be possible and more interesting.

I would like to express my acknowledgment and appreciation to my great supervisor, Associate Professor Dr. Noor Asmawati Mohd Zabidi as well as my Co-supervisor, Prof. Duvvuri Subbarao for their encouragement. Where without their support, guidance, patience, and encouragement I would not able to complete this work.

Special acknowledgment and thank goes to my parents, I would not have gone through this years without their and unlimited spiritual support, love, inspired, and believe and confident in me. I am deeply indebted to them. In addition I would like to record my deepest gratitude to my family members especially my aunt Atiat and my uncle Joseph and Sami for their encouragement and help.

My thanks and gratitude are also extended to my friends, who have stood beside me, providing a social atmosphere and supporting me wherever I face any difficulties or problem while conducting this research. My sincere thanks also goes to my research group members for their assistance and friendship throughout this research period.

Last but not least, I would like to pass my appreciation to Universiti Teknologi PETRONAS for providing me the opportunity to study at UTP. Special thanks for the staff in Chemical Department, and PG office. Not to be missed, my appreciation goes to all UTP laboratory technicians for their assistance and co-operation during experimental period. Special acknowledgment to MOSTI for the E-science research grant (project NO: 03-02-02-SF0036).

ABSTRACT

Fischer-Tropsch synthesis (FTS) has received considerable attention as it offers alternative route to produce liquid fuels and chemicals from abundant energy sources other than crude oil such as natural gas, coal, and biomass. The objective of this work is to synthesize, characterize and study the performance of supported iron (Fe) nanocatalyst with Fe particle less than 30nm in Fischer-Tropsch synthesis. Supported Fe nanoparticles have been formulated using impregnation and precipitation methods. Fe nanoparticles loading (3, 6, 10, 15 wt %) were deposited on silica (SiO₂) and alumina-silica (Al₂O₃-SiO₂) supports. The effect of alkali promoters such as potassium (K) and copper (Cu) on the physicochemical properties of the catalyst has been investigated. The physicochemical properties of the catalysts were studied using N₂ physical adsorption, field emission scanning electron microscopy (FESEM), transmission electron microscopy (TEM), X-ray diffraction (XRD), and H₂ temperature-programmed reduction (TPR). The FTS performance of the synthesized catalysts was examined in a fixed-bed microreactor at atmospheric pressure and various reactant ratio (H₂/CO), temperature, and space velocity. The size of Fe nanoparticle was affected by the Fe loading, synthesis technique, and the type of catalyst support. More uniformly distributed and smaller particle size was obtained at lower Fe loading. The 6% Fe/SiO₂ synthesized via the impregnation method had Fe average particles size of 8.6±1.1 nm, as measured by TEM. It resulted in CO conversion of 54% and C₅₊ selectivity of 20% at 523K, 1.5H₂/CO v/v ratio, and 3L/g-cat.h. Under the same reaction conditions, 6%Fe/SiO₂ prepared by precipitation method with Fe average particles size of 12.8±4.2 nm resulted in CO conversion of 45% and C₅₊ selectivity of 8%. The CO conversion trend correlated to the size of Fe nanoparticles where the results show that catalysts with average particles size less than 9 nm yielded in CO conversion >50% as well as higher selectivity of C₅₊ and olefins, and lower selectivity for light hydrocarbons (C₁-C₄) compared of those of larger particles.

ABSTRAK

Sintesis Fischer-Tropsch telah menerima banyak tumpuan kerana ia menjanjikan satu langkah alternatif untuk menghasilkan bahan-bahan api dalam bentuk cecair dan juga bahan-bahan kimia daripada sumber-sumber tenaga yang banyak selain minyak mentah seperti seperti gas asli, arang batu dan biomas. Objektif penyelidikan ini ialah untuk menghasilkan dan mencirikan mangkinnano ferum tersokong serta mengkaji aktiviti mangkin yang membunyai saiz zarah Fe kurang dari 30 nm dalam sintesis Fischer-Tropsch. Zarahnano ferum yang disokong telah diformulasikan melalui kaedah-kaedah penyatuan dan mendakan. Zarahnano ferum mengandungi (3, 6, 10, 15 berat %) telah dihasilkan di atas penyokong-penyokong silika (SiO_2) and alumina-silika ($\text{Al}_2\text{O}_3\text{-SiO}_2$). Kesan pembantu-pembantu alkali seperti kalium (K) dan kuprum (Cu) terhadap sifat-sifat fizikalkimia mangkin turut diuji. Sifat-sifat fizikalkimia bagi mangkin-mangkin telah dikaji dengan menggunakan penjerapan fizikal nitrogen, mikroskopi pengesanan elektron medan pemancaran (FESEM), mikroskopi transmisi elektron (TEM), tenaga pembelauan sinar-X (XRD) dan program penurunan suhu (TPR). Aktiviti FTS bagi mangkin-mangkin yang dihasilkan telah diuji dalam satu mikroreaktor lapisan tetap pada tekanan atmosfera serta nisbah bahan suapan (H_2/CO), suhu dan kelajuan ruang yang berbeza. Kandungan ferum, kaedah sintesis dan jenis penyokong mangkin mempengaruhi saiz zarahnano ferum. Pengagihan yang lebih seragam dan saiz zarah yang lebih kecil telah didapati pada kandungan ferum yang rendah. Mangkin 6%Fe/ SiO_2 yang dihasilkan menggunakan kaedah penyatuan mempunyai purata saiz Fe 8.6 ± 1.1 nm berdasarkan kajian TEM. Ia telah menghasilkan penukaran CO sebanyak 54% dan pemilihan C_{5+} sebanyak 20% pada 523K, nisbah $1.5\text{H}_2/\text{CO}$ v/v, dan 3L/g.cat.h . Dalam keadaan-keadaan yang sama, mangkin 6%Fe/ SiO_2 yang dihasilkan melalui kaedah pemendakan mempunyai purate saiz Fe 12.8 ± 4.2 nm menunjukkan penukaran CO sebanyak 45% dan pemilihan C_{5+} sebanyak 8%. Corak penukaran CO didapati berhubung kait dengan saiz zarah-zarah nano ferum dimana keputusan-keputusan menunjukkan mangkin dengan purata saiz zarah kurang dari 9 nm menghasilkan penukaran CO $>50\%$ dan juga tahap pemilihan

C_{5+} dan olefin yang lebih tinggi serta tahap pemilihan yang rendah untuk hidrokarbon yang ringan (C_1-C_4) berbanding dengan hasil dari mangkin-mangkin yang mempunyai zarah-zarah yang lebih besar.

In compliance with the terms of the Copyright Act 1987 and the IP Policy of the university, the copyright of this thesis has been reassigned by the author to the legal entity of the university,

Institute of Technology PETRONAS Sdn Bhd.

Due acknowledgement shall always be made of the use of any material contained in, or derived from, this thesis.

© Sara Faiz Hanna Tasfy, 2010

Institute of Technology PETRONAS Sdn Bhd

All rights reserved.

TABLE OF CONTENTS

| | |
|--|------|
| STATUS OF THESIS | I |
| APPROVAL PAGE | II |
| TITLE PAGE | III |
| DECLARATION OF THESIS | IV |
| ACKNOWLEDGEMENT | VI |
| ABSTRACT | VII |
| ABSTRAK | VIII |
| COPYRIGHT PAGE | X |
| TABLE OF CONTENTS | XI |
| LIST OF TABLES | XIV |
| LIST OF FIGURES | XVI |
| LIST OF ABBREVIATION..... | XXII |
| CHAPTER 1..... | 1 |
| INTRODUCTION..... | 1 |
| 1.1 INTRODUCTION | 1 |
| 1.2 BACKGROUND | 3 |
| 1.3 FISCHER-TROPSCH SYNTHESIS | 5 |
| 1.4 PROBLEM STATEMENT..... | 8 |
| 1.5 RESEARCH OBJECTIVES..... | 8 |
| 1.6 HYPOTHESIS | 9 |
| 1.7 SCOPE OF THIS STUDY | 9 |
| 1.8 ORGANIZATION OF DISSERTATION | 10 |
| CHAPTER 2..... | 11 |
| LITERATURE REVIEW..... | 11 |
| 2.1 INTRODUCTION | 11 |
| 2.2 FISCHER-TROPSCH PROCESS | 12 |
| 2.2.1 Reactor system..... | 14 |

| | |
|---|----|
| 2.2.2 Reaction mechanism..... | 16 |
| 2.2.3 Fischer-Tropsch Catalysts..... | 18 |
| 2.2.4 Active metal | 19 |
| 2.2.5 Support..... | 24 |
| 2.2.6 Promoters | 29 |
| 2.2.7 Synthesis technique | 32 |
| 2.2.8 Catalysts activation..... | 37 |
| 2.2.9 Catalyst activity and selectivity..... | 38 |
| 2.3 CATALYST CHARACTERIZATION | 41 |
| 2.3.1 Surface area and pore size measurement | 41 |
| 2.3.2 Catalytic morphology | 44 |
| 2.3.3 X-ray powder diffraction (XRD)..... | 48 |
| 2.3.4 Temperature-programmed reduction (TPR) | 49 |
| 2.4 SUMMARY | 50 |
| CHAPTER 3 | 51 |
| RESEARCH METHODOLOGY | 51 |
| 3.1 INTRODUCTION | 51 |
| 3.2 MATERIALS | 53 |
| 3.3 SYNTHESIS TECHNIQUE OF THE FT CATALYSTS | 54 |
| 3.3.1 Preparation of the catalyst support | 54 |
| 3.3.2 Preparation of the FT catalysts | 55 |
| 3.4 CHARACTERIZATION TECHNIQUES..... | 57 |
| 3.4.1 N ₂ -physical adsorption..... | 57 |
| 3.4.2 Field-emission scanning electron microscopy (FESEM) | 59 |
| 3.4.3 Transmission electron microscopy (TEM) | 59 |
| 3.4.4 X-ray diffraction (XRD) | 60 |
| 3.4.5 Temperature-programmed reduction (TPR) | 60 |
| 3.5 GENERAL DESCRIPTION OF REACTOR RIG | 61 |
| 3.5.1 Gas supplying system | 63 |
| 3.5.2 Fixed-bed microreactor..... | 63 |
| 3.5.3 On-line gas chromatograph (GC) system | 64 |
| 3.6 CATALYST PRETREATMENT | 67 |

| | |
|--|-----|
| 3.7 CATALYSTS TESTING | 67 |
| 3.8 REACTION CONDITION | 68 |
| CHAPTER 4..... | 69 |
| RESULTS AND DISCUSSIONS | 69 |
| 4.1 INTRODUCTION | 69 |
| 4.2 CHARACTERIZATION OF CATALYSTS | 69 |
| 4.2.1 Physical properties | 69 |
| 4.2.2 Catalyst reducibility | 90 |
| 4.3 SUMMARY OF THE CATALYSTS PROPERTIES | 96 |
| 4.4 FISCHER-TROPSCH PERFORMANCE..... | 97 |
| 4.4.1 Pretreatment..... | 98 |
| 4.4.2 Stability | 98 |
| 4.4.3 Activity and Selectivity..... | 101 |
| 4.4.4 Kinetics of the FT reaction over Fe-based catalysts | 116 |
| 4.5 EFFECT OF THE REACTION CONDITIONS ON THE CATALYST PROPERTIES | 121 |
| 4.6 SUMMARY OF THE REACTION STUDIES..... | 125 |
| CHAPTER 5..... | 127 |
| CONCLUSION AND RECOMMENDATIONS | 127 |
| 5.1 CONCLUSION | 127 |
| 5.2 RECOMMENDATION..... | 129 |
| REFERENCES..... | 130 |
| APPENDIX A | 139 |
| APPENDIX B | 146 |
| APPENDIX C | 151 |
| APPENDIX D | 155 |
| APPENDIX E..... | 158 |
| APPENDIX F..... | 165 |

LIST OF TABLES

| | |
|---|-----|
| Table 2-1: Summary of the studies on the FT performance..... | 40 |
| Table 3-1: List of chemicals and gases used in this study..... | 53 |
| Table 3-2: Specification of GC columns..... | 65 |
| Table 3-3: valve setting of the front detector | 66 |
| Table 3-4: valve setting of the back detector..... | 66 |
| Table 4-1: Textural properties of the supports | 70 |
| Table 4-2: Textural properties of Fe/SiO ₂ catalysts synthesized via impregnation and precipitation methods | 73 |
| Table 4-3: Textural properties of Fe-based catalyst on SiO ₂ and Al ₂ O ₃ -SiO ₂ supported synthesized via impregnation method..... | 74 |
| Table 4-4: BET surface area, pore volume and average pore size of the promoted catalysts prepared via impregnation method | 75 |
| Table 4-5: EDX elemental analyses over Fe-based catalysts supported by SiO ₂ and Al ₂ O ₃ | 82 |
| Table 4-6: EDX elemental analyses over SiO ₂ supported Fe-based catalysts prepared by impregnation and precipitation | 82 |
| Table 4-7: EDX elemental analyses over SiO ₂ supported Fe-based catalysts and promoted catalyst with Cu, K, and Cu/K | 82 |
| Table 4-8: Average particle size of the synthesis supported Fe-based catalysts | 89 |
| Table 4-9: Summary of the TPR results for all the synthesized catalysts..... | 96 |
| Table 4-10: Effect of promoter on catalytic performance in fixed-bed microreactor (523K, 1.5H ₂ /CO, 3L/g-cat.h) | 110 |
| Table 4-11: Activation energy | 120 |

| | |
|--|-----|
| Table 4-12: Textural properties of the supported Fe-based catalysts before and after the FT reaction | 121 |
| Table 4-13: EDX elemental analyses of the fresh and spent catalysts | 123 |
| Table 4-14: Comparison of the Fe-based catalyst performance in FTS | 126 |

LIST OF FIGURES

| | |
|--|----|
| Figure 1-1: Overall process for synthetic hydrocarbon [4] | 2 |
| Figure 2-1: Types of Fischer-Tropsch reactors [22] | 14 |
| Figure 2-2: Chain initiation [6] | 17 |
| Figure 2-3: Chain propagation and termination [6] | 17 |
| Figure 2-4: Hydrogen reduction profile of Fe-based catalyst [10] | 38 |
| Figure 2-5: Standard adsorption isotherms [68] | 42 |
| Figure 2-6: Concept of multimolecular layers adsorption [70] | 42 |
| Figure 2-7: TEM and SEM system [71] | 44 |
| Figure 2-8: Type of electrons that is used for different analysis [72] | 46 |
| Figure 2-9: Field emission column [74] | 46 |
| Figure 2-10: Electron source at the TEM [75] | 47 |
| Figure 2-11: Schematic diagram of a transmission electron microscope column | 48 |
| Figure 2-12: Flow diagram of the X-ray diffractometer and reflection of the X-ray [78] and [79] | 49 |
| Figure 3-1: Methodology layout | 52 |
| Figure 3-2: Micromeritics (ASAP 2000) equipment used to measure the surface area | 58 |
| Figure 3-3: Overall reactor diagram | 61 |
| Figure 3-4: Schematic diagram of a microreactor system separator | 62 |
| Figure 3-5: Schematic diagram of a fixed bed micro tubular reactor | 64 |
| Figure 3-6: Gas sampling valve diagram in the GC | 65 |
| Figure 4-1: Desorption pore volume plot by BJH method of SiO ₂ support | 71 |

| | |
|---|----|
| Figure 4-2: Desorption pore volume plot by BJH method of Al ₂ O ₃ -SiO ₂ (25:50) support | 71 |
| Figure 4-3: Isotherm linear plot of SiO ₂ support..... | 71 |
| Figure 4-4: Isotherm linear plot of Al ₂ O ₃ -SiO ₂ support | 72 |
| Figure 4-5: FESEM micrographs of Fe/SiO ₂ catalysts prepared via impregnation method at Fe loading (A) 3, (B) 6, (C) 10, and (D) 15 wt % | 77 |
| Figure 4-6: FESEM images of Fe/SiO ₂ catalysts prepared by precipitation method at Fe loading (A) 3, (B) 6, (C) 10, and (D) 15wt% | 78 |
| Figure 4-7: FESEM images Fe nanoparticles on Al ₂ O ₃ -SiO ₂ prepared by impregnation method at Fe loading (A) 3, (B) 6, (C) 10, and (D) 15wt%..... | 79 |
| Figure 4-8: FESEM images of promoted and unpromoted Fe nanoparticles catalyst prepared by impregnation method..... | 80 |
| Figure 4-9: EDX spectrum of (a) Fe/SiO ₂ catalyst prepared by impregnation method, (b) Fe/Al ₂ O ₃ -SiO ₂ catalyst prepared by impregnation method, and (c) Fe/SiO ₂ catalyst prepared by precipitation method | 81 |
| Figure 4-10: TEM image for silica supported Fe catalyst prepared by impregnation method at Fe loading (A) 3, (B) 6, (C) 10, and (D) 15wt%..... | 84 |
| Figure 4-11: Particle size distribution for 3, 6, 10, and 15 wt %Fe/ SiO ₂ catalysts prepared by impregnation method..... | 84 |
| Figure 4-12: TEM image of silica supported Fe-based catalysts prepared by precipitation method at Fe loading (A)3, (B)6, (C) 10 and (D) 15wt% | 85 |
| Figure 4-13: Particle size distribution for 3, 6, 10, and 15 wt %Fe on SiO ₂ support prepared by precipitation method..... | 85 |
| Figure 4-14: TEM image of Al ₂ O ₃ -SiO ₂ supported Fe-based catalyst at different Fe content (A) 3, (B) 6, (C) 10, and (D) 15 wt% | 86 |
| Figure 4-15: Particle size distribution for 3, 6, 10, and 15 wt %Fe on Al ₂ O ₃ -SiO ₂ support | 87 |
| Figure 4-16: TEM image of promoted catalyst (A) 6%Fe/Cu/SiO ₂ , (B) 6%Fe/K/SiO ₂ and (C) 6%Fe/Cu/K/SiO ₂ | 88 |

| | |
|---|-----|
| Figure 4-17: X-ray diffraction patterns of the Fe/SiO ₂ catalyst prepared by impregnation method at Fe loading of 6, 10 and 15 wt% | 90 |
| Figure 4-18: TPR profiles of impregnated Fe/SiO ₂ catalysts with different Fe loading after calcination at 873K for 4h..... | 91 |
| Figure 4-19: TPR profile of Fe/SiO ₂ catalysts with different Fe loading prepared by precipitation method after calcination at 873K for 4h | 92 |
| Figure 4-20: TPR profiles of Fe/Al ₂ O ₃ -SiO ₂ catalysts with different Fe loading after calcination at 873K for 4h..... | 93 |
| Figure 4-21: TPR profiles of Fe/Cu/SiO ₂ catalysts with different Fe loading after calcination at 873K for 4h..... | 94 |
| Figure 4-22 TPR profiles of Fe/K/SiO ₂ catalysts with different Fe loading after calcination at 873K for 4h..... | 95 |
| Figure 4-23: TPR profiles of Fe/Cu/K/SiO ₂ catalysts with different Fe loading after calcination at 873K for 4h..... | 95 |
| Figure 4-24: Stability of impregnated SiO ₂ supported Fe-based catalyst at different Fe loadings 3, 6, 10, and 15 wt %Fe under reaction conditions of 523K, 1.5H ₂ /CO, and 3L/g-cat.h..... | 99 |
| Figure 4-25: Stability of precipitated SiO ₂ supported Fe-based catalyst at different Fe loadings of 3, 6, 10, and 15%Fe under reaction conditions of 523K, 1.5H ₂ /CO, and 3L/g-cat.h..... | 100 |
| Figure 4-26: Stability of Al ₂ O ₃ -SiO ₂ supported Fe-based catalyst at different Fe loadings of 3, 6, 10, and 15% Fe prepared by impregnation method under reaction conditions of 523K, 1.5H ₂ /CO, and 3L/g-cat.h..... | 100 |
| Figure 4-27: Stability of SiO ₂ supported Fe-based catalyst incorporated with the promoter under reaction conditions of 523K, 1.5H ₂ /CO, and 3L/g-cat.h..... | 101 |
| Figure 4-28: The activity of supported Fe-based catalysts prepared by impregnation and precipitation methods under reaction conditions 523K, H ₂ /CO=1.5, and SV=3 L/g-cat.h | 103 |

| | |
|---|-----|
| Figure 4-29: Comparison of the preparation methods on the selectivity of the hydrocarbons for SiO ₂ supported Fe-based catalyst at different Fe loading at 523K, 1.5H ₂ /CO ratio, and 3L/g-cat.h..... | 103 |
| Figure 4-30: The activity of Fe-based catalysts supported on SiO ₂ and Al ₂ O ₃ -SiO ₂ under reaction conditions 523K, H ₂ /CO=1.5, and SV=3 L/g-cat.h | 104 |
| Figure 4-31: Selectivity of the hydrocarbons for Fe-based catalyst with different Fe loading prepared by impregnation method on SiO ₂ and Al ₂ O ₃ -SiO ₂ support under reaction conditions of 523K, H ₂ /CO=1.5, and SV=3 L/g-cat.h | 105 |
| Figure 4-32: Effect of the Fe loading on the CO conversion for SiO ₂ supported Fe-based catalyst at 523K, 1.5H ₂ /CO, and 3L/g-cat.h..... | 106 |
| Figure 4-33: Effect of the Fe loading on the selectivity of hydrocarbons over SiO ₂ supported Fe-based catalyst prepared by impregnation method at 523K, 1.5H ₂ /CO ratio, 3L/g-cat.h..... | 107 |
| Figure 4-34: Variation of activity and hydrocarbon selectivity with Fe average particles size for the impregnated Fe-based catalysts supported by SiO ₂ | 108 |
| Figure 4-35: Variation of activity and hydrocarbon selectivity with Fe average particles size for the precipitated Fe-based catalysts supported by SiO ₂ | 108 |
| Figure 4-36: Variation of activity and hydrocarbon selectivity with Fe average particles size for the Fe-based catalysts supported by Al ₂ O ₃ -SiO ₂ | 109 |
| Figure 4-37: Effect of H ₂ /CO ratio on the CO conversion over Fe/SiO ₂ catalysts prepared by impregnation method at 3, 6, 10, and 15% Fe loading..... | 111 |
| Figure 4-38: Effect of H ₂ /CO ratio at variety of the Fe loading on the selectivity of the light hydrocarbon (C ₁ -C ₄) for SiO ₂ supported Fe-based catalyst..... | 112 |
| Figure 4-39: Effect of H ₂ /CO ratio at variety of the Fe loading on the selectivity of the heavy hydrocarbon for SiO ₂ supported Fe-based catalyst..... | 112 |
| Figure 4-40: Effect of H ₂ /CO ratio at variety of the Fe loading on the selectivity of the olefins (C ₂ ⁼ -C ₄ ⁼) for SiO ₂ supported Fe-based catalyst..... | 113 |
| Figure 4-41: Effect of space velocity on CO conversion over 6% Fe/SiO ₂ catalysts at 0.5 and 1.5 H ₂ /CO ratio | 114 |

| | |
|--|-----|
| Figure 4-42: Effect of the space velocity on the selectivity of hydrocarbons for SiO ₂ -supported 6%Fe-based catalyst..... | 114 |
| Figure 4-43: Effect of reaction temperature on the CO conversion for 6% Fe/ SiO ₂ catalysts prepared by impregnation method at 0.5 and 1.5H ₂ /CO ratio..... | 115 |
| Figure 4-44: Effect of temperature on the selectivity of hydrocarbons for supported 6%Fe/ SiO ₂ catalyst at 1.5H ₂ /CO ratio and 3L/g-cat.h..... | 116 |
| Figure 4-45: Variation of the CO conversion with residence time at different reaction temperature of impregnated 6%Fe/SiO ₂ at 1.5H ₂ /CO ratio | 117 |
| Figure 4-46: Variation of the CO conversion with residence time at different reaction temperatures over precipitated 6%Fe/SiO ₂ at 1.5H ₂ /CO ratio | 118 |
| Figure 4-47: Comparison between rate constant of impregnated (I) and precipitated (P) Fe/SiO ₂ at 523K and 1.5 H ₂ /CO ratio | 119 |
| Figure 4-48: Comparison between rate constant of impregnated (I) and precipitated (P) Fe/SiO ₂ at 543K and 1.5 H ₂ /CO ratio | 119 |
| Figure 4-49: Comparison between rate constant of impregnated (I) and precipitated (P) Fe/SiO ₂ at 563K and 1.5 H ₂ /CO ratio | 119 |
| Figure 4-50: Arrhenius plot of 6%Fe/SiO ₂ prepared by impregnation (I) and precipitation (P) methods at 1.5 H ₂ /CO | 120 |
| Figure 4-51: FESEM images of Fe/SiO ₂ catalyst prepared by impregnation method before (A) and after (B) FTS reaction..... | 122 |
| Figure 4-52: FESEM images of Fe/SiO ₂ catalyst prepared by precipitation method before (A) and after (B) FTS reaction..... | 122 |
| Figure 4-53: FESEM images of Fe/Al ₂ O ₃ -SiO ₂ catalyst prepared by impregnation method before (A) and after (B) FTS reaction | 122 |
| Figure 4-54: Comparison between the Fe particle distribution for impregnated 6%Fe/SiO ₂ catalyst (a) before reaction and (b) after reaction..... | 124 |
| Figure 4-55: Comparison between the Fe particle distribution for precipitated 6%Fe/SiO ₂ catalyst (a) before reaction and (b) after reaction..... | 124 |

Figure 4-56: Comparison between the Fe particle distribution for impregnated 6%Fe/Al₂O₃-SiO₂ catalyst (a) before reaction and (b) after reaction..... 124

LIST OF ABBREVIATION

| | |
|-------|---|
| FTS | Fischer-Tropsch synthesis |
| BTL | Biomass to liquid |
| CTL | Coal to liquid |
| GTL | Gas to liquid |
| HTFT | High temperature Fischer-Tropsch |
| LTFT | Low temperature Fischer-Tropsch |
| WGS | Water gas shift reaction |
| ppm | Parts per million |
| BET | Brunauer, Emmett and Teller method |
| BJH | Barrett-Joyner-Halenda |
| SEM | Scanning electron microscopy |
| TEM | Transmission electron microscopy |
| EDX | Energy-dispersive X-ray spectroscopy |
| FESEM | Field emission scanning electron microscopy |
| XRD | X-ray diffraction |
| TPR | Temperature-programmed reduction |
| GC | Gas chromatography |
| TCD | Thermal conductivity detector |
| FID | Flame ionization detector |

| | |
|-----|---|
| PID | Proportional-integral-derivative controller |
| RGA | Refinery gas analysis |
| HC | Hydrocarbon |
| TOS | Time on stream |

CHAPTER 1

Introduction

1.1 Introduction

The rapid depletion of the world liquid fuel reserves and the dwindling of petroleum reserves stimulated the interest to find new routes to hydrocarbon feedstock. Finding a suitable way to exploit world's abundant resource other than crude oil has attracted considerable attention in recent years. Several synthetic routes have been existed and one method of accomplishing the goal is via the Fischer-Tropsch synthesis (FTS). This process was first used in Germany in 1923 for the production of liquid and gaseous hydrocarbon fuels, such as gasoline or gas oil, and it was named after the German chemists, Franz Fischer and Hans Tropsch. FTS has been considered as a promising route for the production of clean transportation fuels and chemical feedstock from synthesis gas, a mixture of predominantly CO and H₂. Thus, FTS also contributed in preserving our environment and in the diversification of our resources. Additionally, FTS has two unavoidable characteristics: the production of a wide range of hydrocarbon products (olefins, paraffin, and oxygenated) and the liberation of a large amount of heat from the highly exothermic synthesis reactions [1].

FTS can be based on several synthesis gas feedstocks and it has expanded to include biomass, coal, and natural gas. Synthesis gas can be synthesized from a carbonaceous feedstock, where the only essential requirement for the feed is that it has to contain carbon as well as hydrogen to increase the efficiency to produce the desired products [2]. Coal and natural gas can be converted into synthesis gas by either partial oxidation or steam reforming processes. The conversion of coal to synthesis gas is called gasification while for the case of natural gas it is known as methane reforming process. The H₂/CO ratio of the synthesis gas obtained from these two sources is different. The syngas produced from coal has a much lower H₂/CO

ratio than the one produced from the natural gas. The difference in H_2/CO ratio between these two resources leads to production of different yields of desired hydrocarbon products [3]. Due to the ability of applying different feedstocks in the Fischer-Tropsch process, FTS has been considered as a part of the biomass to liquid (BTL), coal to liquid (CTL), or gas to liquid (GTL) technologies.

Generally, there are four main steps in these technologies: syngas generation, syngas purification, liquefaction or FTS and, product upgrading. Figure 1-1 shows the process flow schematics for production of the synthetic hydrocarbons [4]. The Fischer-Tropsch product spectrum consists of a complex multicomponent mixture of linear and branched hydrocarbons and oxygenated products. The fuels produced from the FT process have high quality due to very low aromaticity and absence of sulfur compared to fuels derived from crude oil.

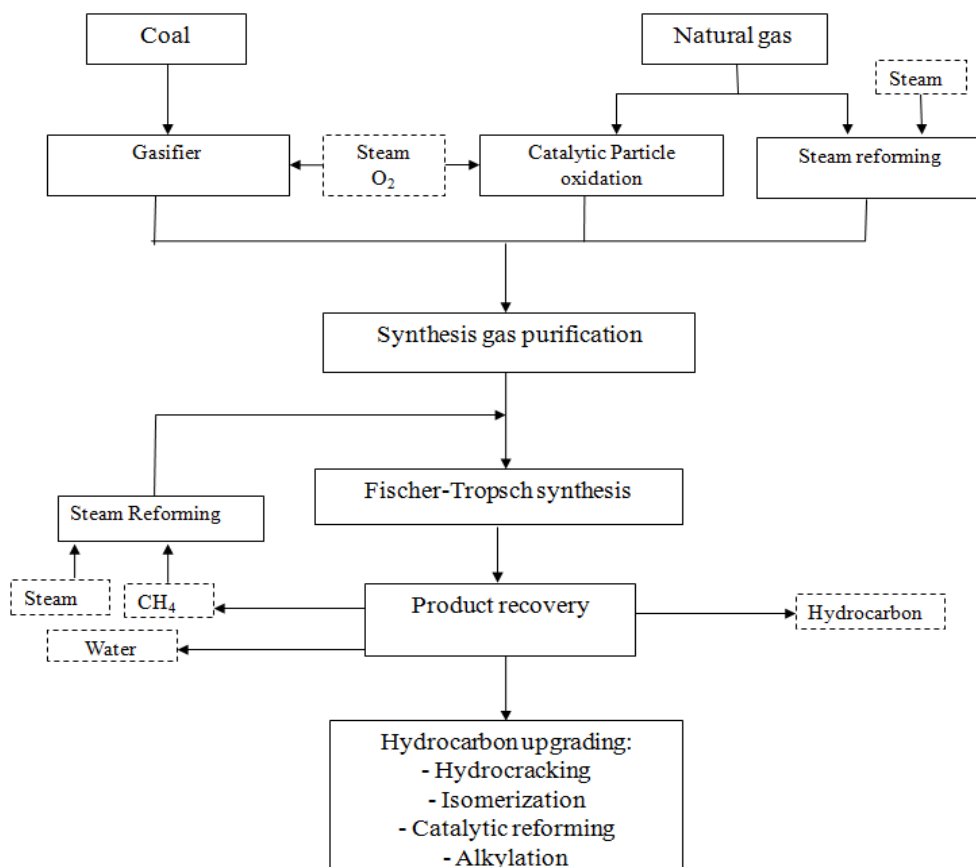


Figure 1-1: Overall process for synthetic hydrocarbon [4]

1.2 Background

The beginning of the 20th century was an exciting period in the development of catalysis. During this time Germany faced a severe energy problem due to the lack of petroleum reserves, in addition to the growing population. Therefore, looking for cheap energy and chemical feedstock to supply the industries received high consideration. As a result, great deal of research was focused to investigate alternative methods of obtaining fuels and chemical feedstock from several abundant resources other than crude oil [5]. The first genesis of this technology started in the early 1902 when Sabatier and Senderens discovered the ability to hydrogenate the CO over cobalt and nickel catalysts and converted it to methane. In 1913, BASF observed the potential to produce liquids hydrocarbons over Cobalt (Co)-based catalyst under unrealistically severe condition, at the same time the Kaiser Wilhelm Institute was constructed. Several research projects were conducted towards developing new process to convert coal reserves to fuel and chemicals feedstocks because of the availability of the abundant coal reserve in Germany and the dwindling of the crude oil resource. Franz Fischer and Hans Tropsch discovered the synthesis of linear hydrocarbons and paraffin using coal-derived gas over Fe-based catalyst in 1923. This observation led to the development of the modern FT catalysts. Moreover, the synthesis of oxygenated hydrocarbons over alkalized Fe was noted in 1925. In 1925, the industrial applications of FTS have been carried out. By 1938, there were fifteen plants came on stream, nine plants in Germany having a combined capacity of about 660×130 ton per year [6], four in Japan, and one each in France and Manchuria [1]. During the Second World War, Fischer and Pichler developed the Co medium-pressure catalyst for producing middle distillates and wax [2]. As a consequence of the war effort, supply of Co became scarce which resulted in the development of Fe catalysts [1].

In spite of the huge oil fields discovery in the Middle East between 1955 and 1970, the world energy was governed by expensive oil supply which led to the commercial proposition of FTS. This elucidates that the economic viability of the FTS depends on the price of the crude oil which has varied over the last 30 years. In the last decades during the oil crises, an unpredictable forecasts about the fading of world oil reserves in the mid of 1970s, the interest as well as the environmental demands,

technological developments and change in fossil energy reserves, all of these factors enhanced the consideration of the FTS to produce clean transportation fuels and chemicals.

At present, FTS is being practiced at SASOL in South Africa for producing fuel and hydrocarbons from coal-derived syngas. Increasing the price of the crude to US\$30 per barrel prompted SASOL to construct two FTS pilot plants which came online in 1980 and 1982. In addition to coal reserves, FTS has been also practiced at Moss gas plant in South Africa and Shell in Bintulu, Malaysia which came on stream in 1992 and 1993, respectively using the natural gas as a resource for producing the syngas. Owing to the difficulty of transporting natural gas by pipeline or liquefying it to consumer market, FT process became an interesting option to convert natural gas to more readily transportable liquid. Furthermore, Shell built the first FT plant in 1993 for production of the middle distillates based on natural gas. Approximately 8-10 plants are in either construction or planning and by 2008-2010 could be producing two million barrels per day of premium sulfur-free diesel [7].

Syngas can be produced from the partial oxidation or steam reforming of natural gas. In addition, gasification process was also used to convert coal to syngas. These processes are highly endothermic and expensive. The use of natural gas results in lower carbon dioxide (CO₂) emission (20%) than the use of coal (50%) but higher than the use of crude oil. The low cost of coal and natural gas made the FTS competitive with producing the fuel from the crude oil [8]. Currently gasification of coal is used at the SASOL plant as primary source of the syngas. During gasification of coal several saleable products were produced such as ammonia (NH₃OH), aromatic tars, oil, naphtha and phenol, which have to be separated from the main product. Syngas produced by coal was found to be suitable as a feedgas to the wax production at low temperature Fischer-Tropsch (LTFT) reactions. While at high-temperature Fischer-Tropsch (HTFT) reaction, gasoline and light hydrocarbon will be achieved. On the other hand, Shell used methane as a primary source of the syngas. Syngas is produced during the partial oxidation of CH₄ at high pressure and temperature resulted in H₂/CO ratio of 1.7 to 2.5. This H₂/CO ratio is raised by adding the H₂-rich gas produced by catalytic steam reforming to the tail gas of FT reactors [6].

1.3 Fischer-Tropsch synthesis

Recently, FTS has been enjoying renewed attention as an option to fabricate a clean transportation fuel and chemical feedstock from the carbonaceous abundant resource. FTS provides surprising phenomena in heterogeneous catalysts whereas a variety of transition metals such as ruthenium (Ru), nickel (Ni), Fe, and Co was used. Moreover, FTS was known as an exothermic surface polymerization reaction or carbon chain building process. The original process was carried out with Fe filling promoted with potassium. The current generation of catalysts includes cobalt and ruthenium as well as Fe promoted with copper, potassium, and other oxides [9]. Both Fe and Co are commercially used at temperature of 200 to 300 °C and pressure of 10 to 60 bar. Synthesis gas can be reacted in the presence of the catalyst to produce hydrocarbons and other aliphatic compounds such as methane, synthetic gasoline, waxes, olefin and alcohols. Water and carbon dioxide are considered as byproducts. The FT products are endowed with a tremendous environmental value because it is free from sulfur and nitrogen as well as lack of aromatic structures [10]. FT reaction is highly exothermic which makes the heat transfer a major issue in the design of FTS reactors. Temperature control is required to avoid catalyst deterioration and carbon formation. Depending on the reaction temperature the process will be classified as low temperature processes (LTFT) at 200-240°C and high temperature Fischer-Tropsch (HTFT) process at 300-350°C. This classification influences the selectivity of the hydrocarbon chain. At HTFT process, the selectivity of light hydrocarbon and olefin is obtained, while at LTFT process, the selectivity of heavy hydrocarbon and wax was improved. The product distribution for FTS was obtained from the stepwise addition of carbon atoms to growing chain. According to these phenomena, several mechanisms have been proposed to determine the chain growth probability.

A simplified reaction model proposed for FTS comprises the adsorption of CO, the formation of a surface-intermediate monomer by reaction with hydrogen, and a chain growth of surface intermediates with this monomeric species. Moreover, the chain close or termination can proceed either by hydrogenation of the surface species yielding an n-alkane or by a reductive abstraction to a 1-alkene [11].

FT process is a complex system in which a number of different reactions are combined. The FT reaction is shown as follows



Where $-\text{[CH}_2\text{]}-$ is the basic building unit of the hydrocarbon molecules in the FT reactions. According to the FT reaction equation, this reaction requires H_2/CO ratio of 2. Using lower H_2/CO ratio requires catalyst to have the ability to facilitate the water-gas-shift (WGS) reaction to make up the deficit in H_2 . Coal is one of the main resources for producing syngas with H_2/CO ratio of 0.67-1.7. Therefore, Fe-based catalysts are proposed as main catalysts used for the syngas derived from coal with low H_2/CO ratio because Fe has the ability to facilitate the WGS reaction as well as the FT reaction. Therefore, it is possible to assume that FT synthesis can be simplified as a combination of the FT reactions and two side-reactions namely the WGS reaction and the Boudouard reaction. The occurrence of these two reactions depends strongly on the nature of the catalyst.

There are many parameters playing a role in the FTS, nevertheless temperature and pressure are the important factors in hydrogenation capability and polymerization process. Temperature influences the number of molecules hitting the surface of the catalyst as well as increasing the diffusivity and the velocity of those molecules. Although beyond a certain point, temperature shows a reversal effects where the velocity of the molecules will increase and hitting the surface very fast and these lead to decrease in the contact time between the surface of the active sites and the reactant thus decrease the reaction rate. Pressure affects the chain growth probability. Therefore, pressure and temperature are both depending on each other in addition to the type of the catalysts and reactors that were used [12].

FT reactions are strongly exothermic reaction, for these reason reactors with highly capability of heat removal are important to achieve an optimum performance for the overall process, the catalysts and the reactor should be comprehensively optimized. Generally many reactors have been proposed and developed for FTS with proper heat control. Currently there are various types of reactors which are commercially used for FTS such as [2]:

- Circulating fluidized bed reactor
- Fluidized bed reactor
- Tubular fixed bed reactor
- Slurry phase reactor

For designing FT reactors many variables should be considered such as the type of the catalysts, feed composition, the range of the desired hydrocarbons, and the operational objective. Therefore, it has been observed that the reactor and catalyst should be fabricated at the combined fashion where it shows strong interaction between the design of the FT reactor and the choice of technology to provide the feed (syngas composition or the H₂/CO ratio) to the FT process. In addition, separation techniques are also important in order to isolate various product components as well as the tail gas to generate the recycle streams.

At present, more than 90% of industrial processes are based on catalytic mechanism where the catalytic action accelerates useful reactions at the expense of other thermodynamically possible transformation. It is well known that the research and development of the catalyst plays an important role in all catalytic reactions [13]. Catalytic system is a very complex system. The vast majority of industrial catalysts are solids. Solid catalysts often contain two or several solid components, different in composition, porosity, and specific surface area. Careful control of the catalytic properties leads to optimal activity, selectivity and stability during the catalytic reaction. One of the major challenges in catalysts preparation is to synthesize highly dispersed solids with a uniform composition at the atomic scale [14]. One of the most important applications of the catalytic systems in industries is in the FTS technology where the conversion of syngas to hydrocarbon products takes place over the catalyst. Consequently, the choice of a suitable catalyst is very important where it is largely dictated by the synthesis gas feed composition and the process conditions [15]. A series of transition metals was chosen due to preferable active sites for the FT process such as ruthenium, nickel, cobalt, and iron [16]. Fe and Co are preferred catalytic metals and remaining until today the only ones for industrial applications while ruthenium and nickel are not common due to their high cost, limited world source, and limitation of product selectivity. Although cobalt is expensive and highly sensitive to the process conditions and is less flexible compared to Fe, Co is still

widely used for FTS, in addition to Fe [8]. Nevertheless, Fe produced unwanted products through the WGS where this reaction helps to make up the deficit of H₂ in the syngas derive from coal gasification. Fe also has many advantages such as availability, low cost, wide range of operating conditions and high WGS activity. In addition, Fe catalysts are more useful at low H₂/CO ratio for the production of alkenes, oxygenates, and branched hydrocarbons which depend on the promoters and process conditions employed. In order to obtain a catalyst with high activity, stability and optimal selectivity, structural promoters are often added. Several structural promoters in the form of metal oxides such as silica, alumina, zeolite, titanium oxide, and carbon nano-tube are investigated for applications in the FTS to stabilize the small catalyst crystallites from sintering and improve the catalytic mechanical properties [17].

1.4 Problem statement

Due to the potential for producing liquid fuels and chemical feedstock from abundant resources other than crude oil, FTS process is considered as a valuable commercial approach to generate a wide product spectrum consisting of complex multi-component mixture of the hydrocarbons. Moreover, there is a continuing requirement for developing the FT catalysts with improved properties to cover the demand of the alternative fuels supplies. Although, the use of Fe-based catalysts to catalyze the FT reaction dates as far back for more than eight decades, there are no studies performed on the effects of the Fe particle size on the performance of the FTS. Therefore correlation between the average Fe particle size and the catalytic activity and selectivity has been investigated in this study.

1.5 Research Objectives

Although FTS has been commercialized for a long time and many studies have been reported on the design of the FT reactors and catalysts, there are still attempts to improve factors that affect the catalyst performance. Therefore, development of FT catalysts is one of the key technology challenges. The impact of metal dispersion and

support on the catalytic performance are two particularly important areas. Therefore, the preparation of supported Fe catalyst with high metal dispersion still poses a big challenge.

The objectives of this research are:

- To develop well-dispersed Fe nanocatalyst on oxide supports at the nanoscale range for FTS.
- To evaluate the catalytic performance of supported Fe nanocatalyst for FTS in a microreactor under different reaction conditions.
- To correlate the catalytic performance in FTS to the catalyst properties.

1.6 Hypothesis

The physicochemical properties of the catalyst influence its catalytic activity. The catalytic performance of the supported Fe-based catalyst depends on the Fe particle size. The correlation between Fe particle size and catalytic activity and product selectivity can be established.

1.7 Scope of this study

Synthesizing well-distributed catalysts with high uniformity and small catalyst particles size presented a challenge in FT synthesis. This study aimed to synthesize Fe-based Fischer-Tropsch catalysts with Fe particle size less than 25nm on oxide supports. Fe loading on the oxide supports were varied at 3, 6, 10, 15 wt%.

Owing to the influence of catalyst preparation methods on the physicochemical properties and the catalytic performance, impregnation and precipitation methods were applied to synthesize Fe nanocatalysts. The impregnated and precipitated catalysts were subjected to the same pretreatment and reaction conditions in order to determine the effect of the synthesis technique on the catalytic properties (structural, morphology, and reducibility) and FT performance (activity and selectivity).

In this study, Fe-based catalysts were prepared on two types of support, namely silica (SiO_2) and alumina-silica ($\text{Al}_2\text{O}_3\text{-SiO}_2$) supports. Silica support was chosen due

to several advantages that made it one of the most common supports, especially for Fe-based catalyst. Alumina was added to silica to improve the acidity of the support which can result in higher metal-support interaction and better dispersion of Fe nanoparticles. The effects of the support and metal-support interaction on the catalysts properties, activity, and selectivity in FTS have been studied.

The catalytic properties of the supported Fe nanocatalyst were modified by introduction of Cu and K promoters. Three sets of Fe-based catalysts have been prepared and each contained a promoter such as copper, potassium, and mix of copper and potassium.

The synthesized catalyst samples were characterized by various techniques such as N₂-physical adsorption, field emission scanning electron microscopy (FESEM), transmission electron microscopy (TEM), X-ray diffraction (XRD), and H₂-temperature programmed reduction (TPR). The FT performance of oxide-supported Fe nanocatalyst prepared under different conditions was evaluated in a fixed-bed microreactor system at atmospheric pressure. The effect of operational conditions such as H₂/CO volumetric feed ratio, reaction temperature, and the space velocity on the FTS activity and product selectivity were investigated. Furthermore, the correlation between catalyst properties and their catalytic performance in FTS has been carried out.

1.8 Organization of Dissertation

This dissertation is divided into five chapters. Chapter one serves as introductory chapter. The second chapter reviews pertinent literature of catalyst, FT process, and the characterization techniques used to determine the physicochemical properties of catalyst. The third chapter describes the experimental methods, material and equipment used. The fourth chapter overviews the results for the physicochemical properties of the catalysts and the FT reactions study using the microreactor system at different reaction conditions. Chapter five provides principal conclusions of this work and recommendation for further work.

CHAPTER 2

Literature Review

2.1 Introduction

Shortage of petroleum fuel derived from crude oil coupled with the unpredictable price of crude oil led to significant increase in demand for alternative resources. Therefore, FTS has received considerable attention because it offers the possibility to produce clean hydrocarbon and liquid fuels which are environmentally friendly, free from sulfur, using syngas derived from natural gas, coal or biomass. FTS is a catalytic reaction where the syngas (a mixture of CO and H₂) is converted to hydrocarbons with carbon number ranging from 1 to over 100 [18]. Syngas with different H₂/CO ratios (0.5-2.5) is usually derived from natural gas, coal, and biomass. In recent years, FTS has come into the picture again especially as a means to convert natural gas to liquid fuels. FTS is a catalytic polymerizing process where several metals such as ruthenium, iron, cobalt, and nickel have been proposed as active sites for this reaction. Although, the FT chemistry is complex, it can be simplified as a combination of FT reaction and WGS reaction. The principle purpose of the FT process is to produce a synthetic petroleum substitute [4]. Syngas is reacted in the presence of catalyst to produce hydrocarbon products such as methane (CH₄), gasoline (C₄-C₁₂), diesel (C₈-C₂₁), wax (C₂₅₊), and alcohol (CH₂OH). FT products are a mixture of different species such as linear paraffin, branched hydrocarbons, and oxygenates [4].

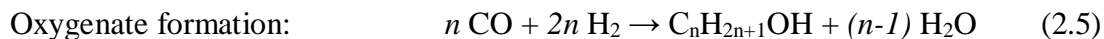
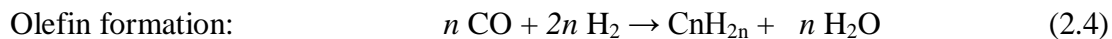
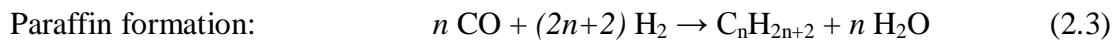
2.2 Fischer-Tropsch process

Fischer-Tropsch synthesis as an option for synthesis of hydrocarbons has been existed for more than 80 years. Recently, FTS received more attention than ever due to the limitation of petroleum reserves and environmental constraints as well as availability of other abundant resources such as coal, biomass, and natural gas. FTS is directed towards the manufacturing of liquid hydrocarbons involving three process steps: generation of the syngas, conversion of the syngas to hydrocarbons product, and product upgrading to produce clean transportation fuel [19]. The chemistry of FTS has been described as a surprising phenomenon where the gases feed (a mix of CO and H₂) is passed over a catalyst placed inside the reactor and liquid hydrocarbon exits [2].

FTS is essentially a polymerization process which can be generically represented as following stoichiometric reaction [9]



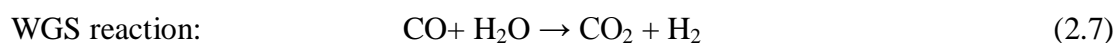
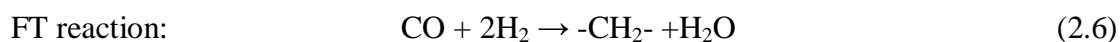
Where, n and m represent the number of C and H, respectively. C_nH_m represents the formation of hydrocarbons (alkanes and alkenes) in addition to the formation of the oxygenated hydrocarbons. The following reactions illustrate the possibility of producing different types of hydrocarbons during the FT reaction (equation 2.2-2.5) [20].



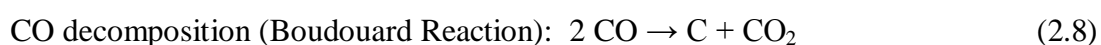
Referring to equation 2.2-2.5, we can conclude that the hydrocarbon formation is strongly depended on the chain growth probability where, the length of the chain is determined by the nature of the catalyst and the operating conditions. Therefore, an appropriate choice of the catalysts and reaction conditions leads to shifting the value

of the chain growth probability and results in the production of compounds with different compositions. The product distribution was obtained from the stepwise addition of carbon atoms to a growing chain. Thus FT process resembles polymerization where producing the hydrocarbons start from producing a monomer then hydrogenate this monomer to produce the products. This step goes through two branches. The first one known as a propagation step leads to the production of hydrocarbons chains of various lengths. The second one, the termination step, leads to stopping of the polymerization reaction and results in the production of low molecular weight hydrocarbons [2]. Therefore, in order to obtain higher selectivity to the intermediate, it is necessary to control the rate of carbon deposition and the rate of its hydrogenation, in other words the average molecular weight of the product is increased when the rate of the propagation step is relatively higher than the rate of termination step. In contrast, the same carbon atoms that are the precursor of the monomer could also be the precursor of inactive carbon species which cause the catalytic deactivation by decreasing the number of the active metal sites. Several mechanisms have been proposed to explain this type of product distribution [4].

FTS is a complex system for producing hydrocarbons with various chain lengths through different reactions. FT reactions can be simplified as a compensation of two main reactions: FT reaction (equation 2.6) and the WGS reaction (equation 2.7). WGS reaction occurs simultaneously with the production of the hydrocarbons during FTS over Fe-based catalysts. The extent of the WGS reaction rate can be shown by determining the selectivity of CO₂, which corresponds to the consumption of CO in WGS reaction [21].



WGS reaction is also known as one of the two FTS side reactions in addition to the Boudouard reaction which is represented in equation 2.8.



The occurrence of these two side-reactions is mainly dependent on the nature of the catalyst and the prevailing gas composition. The existence of the WGS reaction is

controlled by the availability of water during the reactions. Most of the water formed in FT reaction will be consumed in the WGS reaction, resulting in the appearance of CO₂ in the product stream. In addition, determining the rate of WGS reaction is extremely important, especially in the case of using syngas with low H₂/CO ratio where it provided a makeup of the hydrogen for FTS.

The performance of the FTS depends mainly on the feed composition (H₂/CO ratio), formulation of the catalyst, and operation conditions [2].

2.2.1 Reactor system

Different reactors have been used in FTS. Catalysts formulation, operation conditions, and the operational objectives influence the choice of the reactor. Accordingly, FT reactors are classified as LTFT such as tubular fixed-bed reactors and slurry phase reactors and HTFT such as fluidized-bed reactor (Figure 2-1) [22].

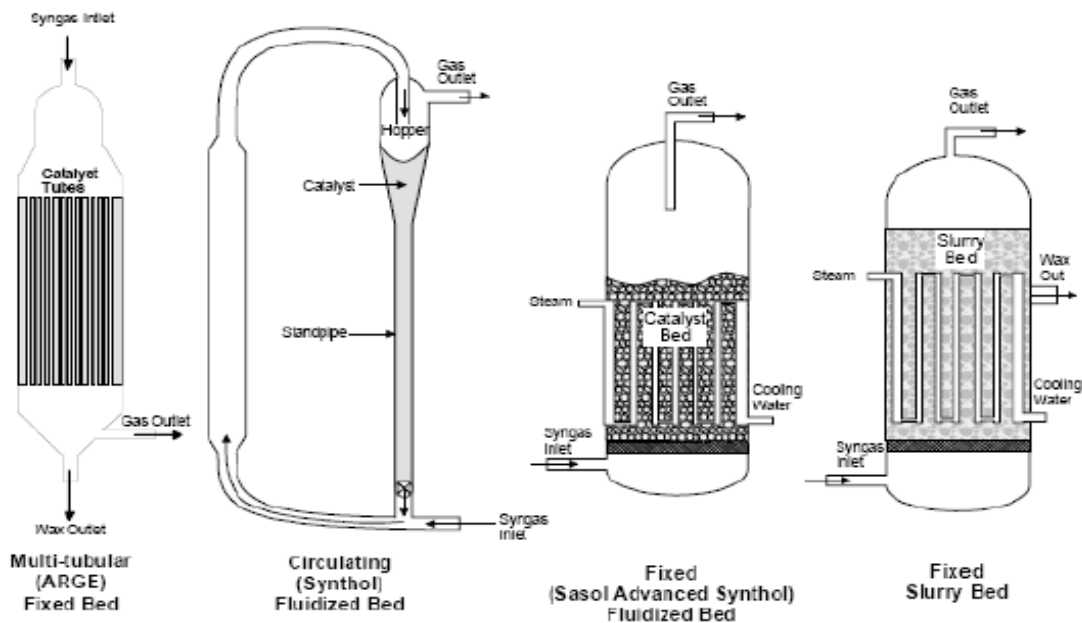


Figure 2-1: Types of Fischer-Tropsch reactors [22]

The HTFT reactor operates in the temperature range between 573 to 623K; where it is higher by 100K than the LTFT which operates in the temperature range from 473-523K. When the main objective is the production of long chain hydrocarbons, the

LTFT reactor is chosen while for producing light hydrocarbons and alkenes the HTFT system is more preferable than the LTFT reactors. HTFT system operates at high temperature which accelerates the production of undesirable methane and caused catalyst damage. Therefore, controlling the rate of the heat transfer from the catalyst particles to the heat exchanger is very important [2].

Fixed-bed reactor is easy to operate compared to the other reactor systems, and it provides an easy way to separate the required product from the catalysts. On the other hand, strong mass transfer resistance inherent in a catalyst suspended in a slurry reactor, resulted in troublesome separation of catalysts from the liquid product [23]. Therefore, addition of other equipment is required to achieve the complete separation of the catalyst from the product. Furthermore, fixed bed reactor undergoes low catalytic deactivation compared with the slurry reactor. Only the upper section of the catalysts will deactivate at the tubular fixed-bed reactor while a complete catalytic deactivation can be obtained in the slurry reactor. However, the slurry bed reactor has the following advantages: lower fabrication cost, minimizing temperature rise across the reactor, and preferable hydrocarbon distribution [2].

In addition to the abovementioned difference between the two types of the LTFT reactors, following paragraph illustrate the advantage and disadvantage of using the fluidized bed reactor as an example for the HTFT reactor. Formation of the liquid phase in the fluidized bed reactor will cause a serious problem due to particles agglomeration, de-fluidization of the catalyst bed, and cease the function of the process. Therefore, the operation on this reactor required the use of catalysts with low alpha values to ensure that the products are in the gas form at the reaction temperature. Due to the obvious limitation of using fluidize-bed reactor, this reactor cannot be used for producing long chain hydrocarbons product other than gasoline (C_5-C_{11}).

Recently, the use of microchannel reactor for the FTS has also been investigated. Modeling of a monolithic reactor for the FTS has shown promising result in terms of the catalytic performance compared with other reactors. Microchannel reactors have become a keen area of interest for parallel catalyst screening involving heat and mass transfer. The heat and mass transfer limitations that often plague catalytic processes

can be largely avoided through the use of microchannel reactor due to the small transportation distance [24].

2.2.2 Reaction mechanism

FTS is a catalytic polymerization reaction in which the monomers are being produced due to the dissociation of gases reactants (carbon monoxide and hydrogen) over the catalyst surface. Therefore, understanding of the fundamental processes taken place at the metal surface during the FTS reaction led to mechanistic description for the rate of product formation in addition to improved the catalyst design. FT reaction pass through three different reactions section (1) generation of the chain initiator, (2) propagation or chain growth, (3) desorption or chain termination. Parallel operation pathways have been proposed to observe the product distribution in the FTS. A large number of the surface species can be generated from the reactants (H_2 and CO) and exist on the catalyst surface in the FTS. Hydrogen is the one of those surface species where the chemisorption of the hydrogen yield monoatomic hydrogen which has a high surface mobility and this make the adsorption of the hydrogen and its consumption does not take place at the same metallic site. Carbon monoxide is one of the surface species chemisorbed to form surface carbon and oxygen. The diffusion of the surface carbon into the bulk of the metal produces carbide carbon or agglomerate yielding graphitic carbon which causes the metal deactivation. The hydrogenation of the surface carbon yields other surface species such as methylidyne, surface methylene, and surface methyl [25].

Generally a numerous reaction mechanisms have been proposed for the FT reaction and one of the most popular mechanisms is methylene insertion mechanism, where at the beginning the reactant adsorbed and dissociated at the surface of the catalyst. H_2 will be adsorbed at the surface of the active site of the catalyst to form chemisorbed hydrogen and then chemisorbed carbon monoxide dissociated to yield surface carbon and oxygen. Additionally, the surface carbon may diffuse into the bulk of the metal yielding carbidic carbon or agglomerated yielding graphitic carbon [2]. The sequential hydrogenation of surface carbon yields surface methylene (CH_2) which acts as a

monomer or initiator for producing the hydrocarbon chain and water. Figure 2-2 shows the production of the initiator on the catalyst surface [6].

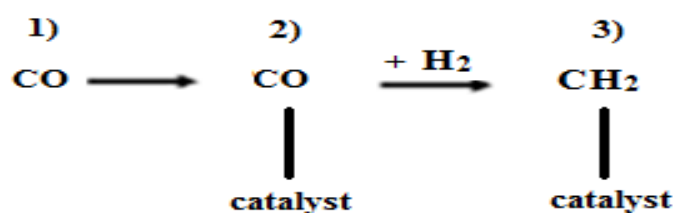


Figure 2-2: Chain initiation [6]

The CH_2 group can be hydrogenated to CH_3 species, which ultimately from CH_4 or they can insert into growing chain (propagation steps). Olefin and paraffin are presumed due to a propagation step. This steps were followed by a termination step, which is known as chain close (Figure2-3) [6]. In order to obtain high activity and desired product selectivity, maintaining the balance between the rate of carbon deposition and its hydrogenation is required. Increasing the rate of carbon deposition and unreactivity of this species lead to decrease of active site and caused catalytic deactivation [16]. On the other hand, when the rate of hydrogenation is excessive the production of low molecular weight will increase.

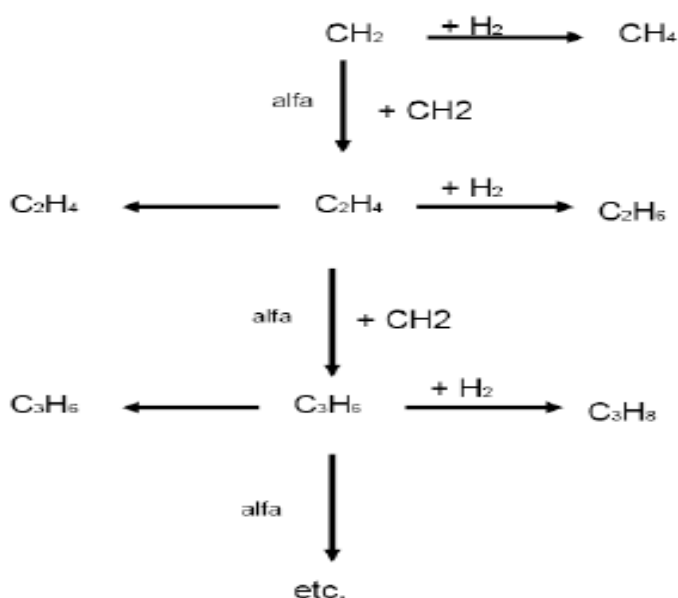


Figure 2-3: Chain propagation and termination [6]

Gaube and co-workers [26] developed a new mechanism of the FTS involving two incompatible mechanisms which are methylene insertion and carbon monoxide insertion.

2.2.3 Fischer-Tropsch Catalysts

Catalysis is a key to chemical transformation and it is an important technology in environmental protection. Catalysis was introduced by Berzelius in 1836 in order to explain various decomposition and transformation reactions. In 1895, catalyst was defined by Ostwald as an accelerator species for chemical reactions without affecting the position of the equilibrium [27]. Catalysts are classified as homogenous and heterogeneous. Heterogeneous catalysts are distinguished from homogeneous catalysts by the presence of different phases during reaction. Generally heterogeneous catalysts are preferable due to the relative ease of catalyst separation from the products stream and their tolerance to extreme operation conditions. A heterogeneous reaction involves several steps. It starts with adsorption or diffusion of the reactants onto a solid surface, surface reaction of adsorbed species, followed by desorbing the product and termination.

Catalyst design involves many steps: catalysts synthesis, catalysts activation, characterization of catalysts, and evaluation of catalytic performance. One of the most relevant requirements for solid catalysts to be particularly useful is an appropriate dispersion of the active species. FTS is one of the most important processes involving catalysts. It is used to produce different hydrocarbon chains from syngas derived from different resources. Many catalysts have been utilized for studies of the FTS for example ruthenium, cobalt, iron, and nickel. FT catalysts are generally presented in the metal oxide form [9]. Fe and Co-based catalysts are widely used compared to the other metals and those two catalysts are the ones receiving serious consideration today. FT catalysts must break the carbon-oxygen bonds and catalyze the formation of carbon-carbon and carbon-hydrogen bonds [28]. Development of effective FT catalysts requires an improvement of the attrition resistance, by introducing a suitable support without sacrificing either the catalyst activity or selectivity [29]. Preparation of FT catalysts involves several important steps: choice of appropriate catalyst carrier

or support, choice of suitable method for depositing the active phase, catalyst promotion, and reductive treatments. In order to produce good catalysts with excellence performance, many attempts were made, such as addition of promoters like K, Cu as well as supports including metals oxides such as SiO₂, Al₂O₃, ZnO, and TiO₂.

2.2.4 Active metal

A variety of metals have been used as an active phase for FTS. Transition metals appear to be the most active sites for FTS. However, selection of the active phase is largely dictated by the composition of the feed. Ru followed by Fe, Co, and Ni are the most active metals for hydrogenation of carbon monoxide, however, using those active metals affect the production of different average molecular weight of the hydrocarbons. Vannice *et al.* [30] showed that the production of various molecular weights of hydrocarbons in presence of the active metals decreased in the following sequence Ru>Fe>Co>Rh>Ni>Ir>Pt>Pd. Thus, these metals are considered as the most common active components for FTS. These catalysts must be subjected to an activation treatment before the catalysts became active for FTS [9].

Fe and Co are the metals proposed by Fischer and Tropsch as the first catalysts for syngas conversion and are also economically feasible on an industrial scale [25]. Due to the limitation of using Ru in terms of their high price, Ru was found to be insufficient for large-scale industry. Ni is responsible for producing too much methane under practical conditions in addition to poor performance at high pressure and lead to production of volatile carbonyls. Accordingly, Co and Fe catalysts were selected as stable catalysts for the industrial scale. Although cobalt-based catalysts are widely investigated to date, the use of Fe-based catalyst in FTS is also attractive for commercial applications [31]. Both Fe and Co can be used in LTFT (473-523K) processes for synthesis of linear long hydrocarbons, waxes, and paraffins while Fe can be operated at HTFT (573-623K) and pressure.

Consequently Ru, Fe, Co, and Ni catalysts must be subjected to an activation treatment before the catalysts become active for FTS [9]. Ru, Co, and Ni are reduced

in flowing hydrogen to form the active phase, which is the metallic state. Different activation parameters could be applied in the case of Fe catalysts due to appearance of various states (metallic, oxide, and carbide) that constitute the active site for FTS.

2.2.4.1 Cobalt-based catalysts

Co-based catalyst has a high activity for hydrogenation of CO and tends to produce long chain of paraffins generated from syngas with high H₂/CO ratio. Although Co and Fe are the preferred catalysts for FTS, the major difference between them is the formation of oxygen-containing product where Co rejected the oxygen in the form of water while Fe produces CO₂. Since Co has lower WGS activity compared to Fe, the feed gas must have higher H₂/CO ratio (2.0-2.3) and this tend to lower the overall operating cost [19]. Co has considerable appeal due to its ability to produce clean diesel fuels with extremely low content of sulfur and aromatics from natural gas [32]. Co is more expensive compared to Fe but is more resistant to deactivation [33]. Co catalysts operate at a very narrow range of temperatures and pressure because the CH₄ selectivity increase with increasing reaction temperature. Due to their stability, higher per pass conversion, longer life, lower WGS activity, and higher hydrocarbon productivity, cobalt catalysts represent the optimal choice for synthesis of long-chain hydrocarbon at LTFT process [25].

2.2.4.2 Iron-based catalyst

Fe-based catalysts are preferred for FTS utilizing synthesis gas with low H₂/CO ratio (0.5-2.5) derived from coal and biomass due to their excellent activity for the water-gas-shift reaction [21]. Due to the instability of Fe-based catalyst during the reduction or reaction, different phases of Fe have been proposed [28]. In addition, Fe is a preferable catalyst due to its ability to offer different types of active sites e.g. Fe-carbides sites are responsible for producing hydrocarbon (FT reaction) while magnetite (Fe₃O₄) sites are the most active phase for CO₂ formation (WGS reaction) [29]. Fe-based catalysts are considered as attractive catalyst for FTS due to their low cost and excellent WGS activity. WGS reaction helps to make up the deficit of H₂ in the syngas. Fe catalysts are also less resistant to deactivation, and flexible to any

change of the operation conditions such as temperature and pressure. Fe catalyst is more versatile than Co catalyst. Fe results in production of less CH₄ and geared for the production of alkenes oxygenates, and branched hydrocarbons, depending on the promoters and process conditions employed. In spite of the sensitivity of Fe-based catalyst; sulfur (S) could contaminate and poison Fe catalyst. Therefore, the reactant feed should not contain more than 0.2 ppm sulfur when using Fe in FTS. Additionally, the main disadvantage of the Fe catalysts is that it can be deactivated due to the production of water during the reaction [10].

Although Fe-based catalyst has many advantages compared to Co-based, Fe catalyst is not stable during FTS. Four kinds of Fe species have been identified: iron carbide (Fe₂C₅), magnetite (Fe₃O₄), hematite (Fe₂O₃), and metallic (Fe) [34]. Accordingly, Fe catalyst is considered to be more complicated catalysts for FTS due to extensive Fe phase changes during reaction. This is why the chemistry of Fe FT catalysts is so complicated. Since Fe is present in multiphase, this makes it difficult to correlate the phase composition with the FT activity and there are no clear suggestions on the nature of active sites for Fe catalyst during the FT reaction [35]. Moreover the nature and composition of Fe-based catalysts undergo changes during the reaction and these changes depend not only on the temperature and the time of exposure to the reactant feed but also on the nature and composition of the reactant feed and activation conditions (time and temperature). Since the solid state phase transformation of Fe catalysts play a major role in determining catalyst activity, longevity, and attrition, many works have been done on this area to investigate the active site of Fe-based catalyst during the FTS.

Many factors affect the phase composition and one of those factors is the pretreatment condition such as temperature, type of the pretreated gases, and duration of the pretreatment. Generally Fe-based catalyst has been reported to be successfully activated with hydrogen, carbon monoxide, or syngas. Hydrogen activation is performed to reduce the catalyst to metallic iron while carbon monoxide and syngas treatments led to the production of a mixture of Fe₃O₄ and Fe₂C₅.

Two models for the role of the Fe₂C₅ phase have been suggested in a series of review articles: the carbide models and the composition model. In the first model

(carbide) the active surface sites are located on the bulk carbide phase and it was proposed to be responsible for the catalytic activity. The second model proposed that the catalytic activity is due to surface Fe atoms and there is competition for the CO molecules between the bulk carbidization and hydrocarbon formation. Furthermore, it appears that the nature of the carbon may also play an important role in the catalytic activity and selectivity. Amorphous carbon may not deactivate the catalysts but it influences the catalytic activity while graphitic carbon reinforces the catalyst deactivation.

Bukur *et al.* [36] studied the effect of activation condition (temperature, time, activated media) on the transformation of Fe-based catalysts for FTS as well as the FT performance. They found that H₂ activation resulted in a mixture of metallic and oxide phase at higher temperature (>673^oC) while at the low temperature only metallic phase was obtained. On the other hand, Fe₂C₅ phase appeared due to CO and syngas activation. However, the picture is still unclear about the composition of the catalytically active phase of Fe. Many scientists proposed Fe₂C₅, which can easily be produced from the CO and syngas pretreatment, as an active phase for FTS [37]. Nevertheless, hydrogen pretreatment is more favorable in industrial scale because it is less expensive and easier to purify [38]. In contrast with the favorability of H₂ pretreatment, Yamada *et al.* [37] proposed that the reduction with CO provide high catalytic activity, on the contrary, low catalytic stability was obtained with H₂. This result was elucidated due to the significant sintering of the Fe species during the H₂ reduction where lower catalytic surface area was observed. Conversely, during CO reduction the sintering did not occur and the catalyst surface area was five times bigger than that of H₂ reduced catalysts. In addition, mixture of metallic iron and Fe₂C₅ was obtained from the XRD pattern. While only metallic iron phase was found from the H₂ reduction process. They also concluded that iron carbide played an important role in enhancing the catalytic activities of the sample. Both metallic and Fe₂C₅ have high ability for CO dissociation.

The importance of formation of iron carbide phase was suggested by Shroff *et al.* [9], where they studied the effect of the activation and reaction treatment on the catalyst phase transformation and catalytic performance of Fe/Cu/K catalyst. Their

results also presented that CO-activated catalyst show higher FT activity (30%) as well as higher methane formation compared with those reduced in H₂ and syngas (H₂/CO=0.7). This could be due to increasing of the carbide content in the catalysts. CO-activation was able to reduce the FeO rapidly into Fe₂C₅ which was found to be the most activate site for FTS. They found a correlation between the iron carbide phase and activity and concluded that carbide formation is important before Fe-FT catalyst can exhibit any activity. Neither magnetite nor hematite was found to have any FT activity.

Several research groups have reported the influence of pretreatment parameters on the catalysts activity and selectivity. During the initial German work on FTS, the Kaiser Wilhelm Institute favored pretreating catalysts with carbon monoxide at sub-atmospheric pressure and they suggested that Fe carbide not metallic Fe play a critical role in the activity of Fe-based catalysts for FTS.

O'Brien *et al.* [38] suggested the effect of the nature of the pretreatment agent in addition to the pretreatment conditions (temperature and pressure) on the precipitated Fe/SiO₂/K catalysts on the performance of FTS. From their report, syngas treatment (H₂/CO=0.7) at 543K and 1.3MPa resulted in poor FTS activity. By decreasing the pressure to 1.0MPa, a dramatic increase in the FTS activity was observed. CO pretreatment is pressure-independent and it also showed higher FTS activity due to formation of Fe₂C₅ phase, less methane selectivity, and more liquid products compared with the syngas pretreatment. Their studies support the hypothesis of proposing Fe₂C₅ as the active sites for FTS reaction.

Ding *et al.* [39] studied the phase transformation of precipitated Fe-based catalyst for FTS under different reduction duration and syngas (H₂/CO=1.2) as a reducing agent. Different analysis technique such as N₂ physisorption, X-ray diffraction, X-ray photoelectron spectroscopy, Raman spectroscopy and Mössbauer effect spectroscopy were applied to characterize the textural properties and the surface phase composition of the catalyst. Their results confirmed that the catalytic surface area decreased with increasing reduction time until it reached a stable state and the active phase was transformed from hematite to magnetite. With increasing duration of reduction, iron carbide phase was progressively formed. They also reported that any change in phase

composition influenced the catalytic activity and selectivity. They also found that formation of iron carbide, due to increasing reduction time enhanced the catalytic activity as well as the selectivity to the gaseous hydrocarbons while it suppressed the selectivity to the heavy hydrocarbons.

2.2.5 Support

The use of massive Fe-based catalysts led to a serious problem: production of catalyst fines due to volume change during reaction and the physical degradation. These catalyst fines caused plugging of the fixed-bed reactor which led to large pressure drop and difficulty in catalyst separation for the slurry reactor. To overcome these problems, adding structural materials or supports was suggested [10]. Support is a thermally-stable material used to fix and disperse small metal particles and inhibit sintering. The addition of structural material or supports may improve the catalytic mechanical properties by increasing the surface area, stabilizing the small catalyst crystallites against sintering, keeping the catalyst away from structure breakage during the reactions, and stabilizing the active phase. A support may be used as a refractory surface on which an active catalysts substance is dispersed since the volume of the support used is considerably greater than that of the active catalytic species [25]. The support may also be used in the form of finely divided refractory crystals than that of the catalytic species. Based on the desired characteristic of the support, selection of the support depends on the following factors:

- Low cost
- Inertness
- Surface area and porosity
- Desirable mechanical properties such as attrition resistance, hardness, and compressive strength
- Stability under reaction and regeneration condition.

A wide range of materials can be used as support, however, only SiO₂, Al₂O₃, and activated carbon possess a good combination of the defined properties. For FTS, structural supports have been used to provide stabilization of metal surface area, improving the catalytic mechanical properties, decreasing the deactivation rate, and improving the catalysts selectivity [40]. Nevertheless, supported catalysts usually suffer from lowered FTS activity and these have been attributed to the strong interaction between the active metal and support having high surface electron density which resulted in lowered reducibility, retarded the FT reaction rates and enhanced the selectivity to methane [41].

Recent studies by Yang *et al.* [42] have shown that the structural promoters display far-reaching effects on the FTS performance of Fe-based catalyst due to the strong metal-support interaction. Iglesia *et al.* [43] concluded that the activity of the FTS and hydrocarbon synthesis was proportional to the metal dispersion and independent of the metal oxide support. However, this hypothesis was challenged by other studies.

The effect of supports such as SiO₂, Al₂O₃, titanium oxide (TiO₂), alumina-silica (Al₂O₃-SiO₂), and carbon nano-tubes (CNT) on the FTS performance have been reported in several studies [17]. SiO₂ has been widely studied and proved to be the most preferable structural promoter for FTS in terms of activity and productivity. Al₂O₃ was also one of the preferable supports especially for cobalt-based catalyst and it is frequently used for Fe-based catalyst [42] and [44]. SiO₂ supported FT catalysts showed high activity, high selectivity to the liquid hydrocarbons as well as high attrition resistance in a stirred tank reactor [21].

Wan *et al.* [45] conducted a study on the influence of silica on the performance of precipitated Fe-based catalyst for FTS as well as the contact between Fe/Cu and Fe/K. They found that SiO₂ influenced the catalyst surface area and resulted in higher surface area than that without SiO₂. Adding SiO₂ suppressed the catalyst reduction due to improved dispersion of Fe₂O₃ and CuO and enhanced contact between them. Due to the stronger Fe-SiO₂ interaction, weakened contact between Fe/K was observed and led to weak surface basicity and a shift of the product distribution to the

light hydrocarbon. Their results also show that SiO₂ suppressed the carburization, catalyst activity, and improve the catalyst stability due to the weak CO adsorption.

SiO₂ is preferred as a support for FT catalyst because it plays an important role in the catalyst reducibility, carburization, surface basicity, and FTS performance. In recent years, SiO₂ was also chosen as the principal structural promoter for the preparation of Fe-based catalysts with high attrition resistance using co-precipitated method and spray-drying technology. Study of FTS catalyst incorporated with silica is extensive. Although SiO₂ was chosen as an excellent structural promoter for Fe-based catalysts with high catalyst stability and attrition resistance, but it usually suffers from lower catalysts activity [45]. Therefore, enormous studies were carried out to investigate the effect of SiO₂ on FTS performance. Hayakawa *et al.* [21] studied the catalytic performance of co-precipitation for SiO₂ supported Fe-based catalyst. They concluded that the addition of silica to Fe-based catalyst enhanced the surface area and greatly changed the structural properties of the catalysts and catalytic performance. In addition, catalyst containing SiO₂ showed slightly lower activity of FTS along with lower selectivity to methane, higher productivity to C₅₊ and higher stability. They also discovered that increasing the reaction temperature improved selectivity to the gases hydrocarbons compared to C₅₊, while increasing the pressure enhanced the selectivity of higher hydrocarbons (C₅₊). The optimized ratio for H₂/CO was found to be between 0.4-1.

Hou *et al.* [46] reported that the addition of binder SiO₂ to a precipitated Fe-based catalyst for FTS influence the catalyst stability, activity, selectivity and attrition resistance. They concluded that increasing the SiO₂ content has little effect on the textural properties compared to the catalyst reduction and carburization. SiO₂ improved distribution of FeO phase and led to decrease in crystallite size. Generally, the small crystallites were reduced at high temperature; therefore, the addition of SiO₂ resulted in higher reduction temperature. The activity, stability, and product selectivity were studied in continuously stirred tank reactor (CSTR) at 250°C, 1.5MPa, 2NL/g-cat/h, and H₂/CO ratio of 2. Their results showed that increasing the silica content led to the low FT activity as well as higher WGS reaction and high stability due to less carbon deposition. Also, increasing the silica content improved

the selectivity to light hydrocarbons and suppressed the selectivity to heavy hydrocarbons.

A large number of studies were carried out to investigate the relation between the strong interaction between metal and structural promoter and catalyst performance. The interaction of the support with the active species is not only physical in nature but there is always a more or less pronounced influence of a chemical nature. However, Fe can easily react with the support to form compounds and often suffered from the difficult in reduction due to the highly dispersed metal on refractory oxides. Consequently, the catalysts containing structural promoter usually suffer from lower FT activity due to the strong metal-support interaction.

The interaction between Fe-Al₂O₃ in precipitated Fe catalyst for FTS was studied by Wan *et al.* [31] and they reported that a large surface area was observed for the Fe/Al₂O₃ catalyst due to the small catalyst crystallite size. Strong interaction existed between Fe-Al₂O₃ and this interaction suppressed the catalyst reducibility. Reduction occurred in two stages; one for transforming the Fe₂O₃ to Fe₃O₄ phase or Fe₂O₃ to Fe₃O₄ and the second for transforming the magnetite phase to metallic phase or Fe₃O₄ to Fe. Addition of Al₂O₃ as a structural promoter or support changed the phase transformation from Fe₂O₃→ Fe₃O₄→ Fe to Fe₂O₃→ Fe₃O₄→ FeO. Al₂O₃ also retard the transformation of FeO, which is a metastable phase of FeO to Fe. Furthermore, the strong Fe-Al₂O₃ interaction weakens surface basicity which suppresses CO adsorption and further suppresses the catalyst carburization, and the FTS and WGS activities. During the FTS, the incorporation of Al₂O₃ improved the catalyst stability and probably suppresses the reoxidation of iron carbide. The strong interaction of Fe-Al₂O₃ enhanced the selectivity of light hydrocarbon and suppressed the selectivity to heavy hydrocarbon due to the weak surface basicity. Therefore, further study on incorporation of structural promoters into Fe-based FT catalysts is highly desired. Dlamini *et al.* [47] suggested that the different degrees of metal-support interaction influenced catalyst activity. They also found that the strong interaction between Fe and SiO₂ hinder the catalytic reducibility and carburization due to intimate mixing of those two components.

The effect of the SiO₂ and Al₂O₃ supports individually on the catalytic performance of the Fe-based FT catalyst was conducted by Hai-jun et al. [13]. They reported that the addition of SiO₂ to Fe-based catalysts enhanced the adsorption of the CO compared to that of the Al₂O₃, which enhanced the adsorption of H₂ and suppressed the CO adsorption. They also concluded that Al₂O₃ has strong acidity compared to the SiO₂ which suppressed the CO adsorption. Therefore, their results are in good agreement with most of the literature findings which suggest that strong surface basicity facilitated the adsorption of the CO and suppress the H₂ adsorption. On the other hand, the addition of SiO₂ enhanced the FT activity as well as the WGS reactivity, while it slowly facilitated the catalytic deactivation compared to that of the Al₂O₃ support, which suppressed the catalytic activity while improved the stability of the catalyst due to suppressed carburization and carbon deposition. Additionally, the catalyst incorporated with Al₂O₃ has higher selectivity to methane and light hydrocarbons and lower selectivity to the heavy hydrocarbons (C₅₊), where SiO₂ support provides an opposite trend on the hydrocarbon selectivity compared to that of Al₂O₃.

Bukur and co-workers [48] and Gaube *et al.* [49] studied the effect of SiO₂ and Al₂O₃ binders on the performance of the precipitated Fe-based (Fe/Cu/K) FT catalysts. They found that the change of the catalytic performance became pronounced at the high content of the binders where the FT and WGS activity decreased with increasing SiO₂ content, whereas Al₂O₃ showed an opposite trend. They also found that the addition of SiO₂ enhanced the catalysts stability and selectivity to the long chain hydrocarbon while it suppressed the selectivity of the light hydrocarbon and the catalytic deactivation due to decreasing carbon deposition in contrast to that of Al₂O₃ support.

Li *et al.* [17] evaluated the influence of Al₂O₃/SiO₂ ratio and they found that increasing Al₂O₃/SiO₂ ratio enlarged the crystallite size and decreased the catalytic surface area. The lower Al₂O₃/SiO₂ ratio weakens the interaction between Fe-SiO₂ and resulting in lower reduction temperature and they also reported that the ratio between Al₂O₃/SiO₂ influenced the activity and selectivity for FTS. They found that the FTS activity increased with increasing ratio between Al₂O₃ and SiO₂ until a

certain value and after that the activity shows reverse relation. Although the individual effects of Al_2O_3 or SiO_2 supported Fe-based FT catalysts have been extensively investigated, there are still some contraries about the effects of SiO_2 and Al_2O_3 on the FTS activity and selectivity.

All these studies revealed that using different supports varied the FT performance. Due to the degree of metal-support interaction, strong interaction ascribed to the higher supports acidity and resulted in decreasing of the catalysts activity as well as enhancing light hydrocarbon selectivity.

2.2.6 Promoters

Properties of the catalysts, number of the metal sites as well as their characteristics and localization on the support could be controlled by promotion with noble metals. Promoters have been used to facilitate the reduction of the catalyst in addition to the adsorption and dissociation of CO which consequently affects the activity and selectivity of the product.

Structural promoters were often added into Fe-based catalysts to improve the catalytic attrition resistance without sacrificing their activity and selectivity. Alkali promoters improved the catalytic stability and enhanced the stabilization of Fe against the oxidation by water during the FT reaction [49]. Therefore, one of the most common promoters used for Fe-based FT catalyst is the alkaline metal group such as K, Cu, Na, Mg, and Ca. In particular, K and Cu promoters have been suggested to enhance the Fe-based catalytic reduction as well as playing an important role in the performance of the FTS. Furthermore, K is well known as a chemical promoter, where it was found that adding K to the catalysts enhanced the CO chemisorption, increased the rate of WGS reaction, and suppressed the adsorption of H_2 . These factors play important roles at decreasing the selectivity of the light hydrocarbons and enhancing the selectivity of longer-chain hydrocarbons and olefin as well as the catalytic activity for both reactions (FT and WGS reactions) [50]. Cu, which is also known as a reduction promoter, facilitating the reduction of Fe_2O_3 to Fe_3O_4 or metallic Fe [51] as a result of segregation of Cu from Fe caused the Fe_2O_3 to Fe_3O_4

transformation to shift to higher temperature. Since both Fe_2O_3 and Fe_3O_4 are prone to sintering at elevated temperature, copper became beneficial because it facilitates the reduction of Fe_2O_3 to lower temperature. In addition, Cu is also used to enhance the mechanical stability of the catalyst and improve the CO conversion.

Hayakawa *et al.* [52] have patented the finding on the effect of Cu on the precipitated fused catalysts Fe/Cu/SiO₂. They found that Cu promoted the catalysts reduction as well as the activity. The effect of Cu and K promoters was mostly due to formation of Fe_2C_5 with higher dispersion which increased the catalytic activity [53]. K and Cu were widely used as promoters for FTS on Fe catalyst to facilitate the reduction of FeO, stabilize the high metal surface area, and improve the hydrocarbon selectivity. However, the effect of Cu is usually smaller compared to that of K. While several studies have been published on the individual effect of K or incorporated with Cu or other structural promoters, only a few investigations have been made on the individual effect of Cu.

In addition to the above-mentioned advantages of adding promoters to Fe-based catalysts, a promoter also influenced the catalytic properties due to increase in the surface basicity and this was reported by Pour *et al.* [54]. They tested the effect of earth alkali metals such as Mg, La, and Ca promoters on the structure, basicity, and the catalytic behavior of precipitated Fe/Cu/SiO₂ FT catalyst. They found that the alkali promoters have a negligible effect on the catalytic structural properties but influenced the catalytic basicity which enhanced the carburization and decreased the catalysts reducibility by H₂. Moreover, the catalytic activity and selectivity to the higher hydrocarbon was enhanced and the methane formation was suppressed by addition of one of these promoters, in the order Ca>Mg>La> unpromoted. The addition of these alkaline promoters increased the catalytic deactivation due to enhanced deposition of carbon during the reaction.

Numerous studies have shown the effect of alkali metals and many reports illustrate that the addition of alkali metals can result in an enhancement of the activity and selectivity of Fe-based FTS catalysts. For instance, Raje and his co-workers [55] discovered the effect of adding different K loadings for the precipitated Fe catalysts on the FT activity, selectivity, and the reaction kinetics. They found that increasing

the K content enhanced the FT activity due to the increase in the rate of WGS reaction. In contrast, increasing K loading lowered the rate constant. They also reported that the selectivity to methane and alkenes depended on the K content as well as CO conversion, where above 50% conversion the methane selectivity increased with decreasing K loading.

K can provide high surface basicity on the catalyst which can apparently suppress the selectivity to methane. Several studies illustrate the interaction between the K promoter and the structural promoters. Zhao *et al.* [56] discovered the influence of the interaction between the K and different structural promoters such as SiO₂, Al₂O₃, and zeolite on the performance FTS for Fe-based catalysts. They concluded that the interaction of K and the structural promoters influenced the catalytic carburization in the sequence of K-Al₂O₃>K-SiO₂>K-ZSM-5>K-free. This sequence mainly depends on the acidity of the structural promoters and their ability to facilitate the migration of K promoter from the support's surface to the iron surface. Al₂O₃ was found to yield high catalytic activity as it contains only Lewis acid sites and lower mobility compared to zeolite which is a complex mixture of silica and alumina. Zeolite contains both Lewis and Brønsted acid sites as well as inhibiting the migration of K. SiO₂ has higher interaction with potassium although silica does not contain any high acidic site. Therefore, SiO₂ was found to provide lower catalytic activity and methane selectivity [56].

A few studies were also carried out to illustrate the influence of the individual promotion of K and Cu and the double promotion of K and Cu without adding any of the structural promoters on the FTS performance. These structural promoters may significantly influenced the catalytic activity and stability and suppress the effect of the promoters. Wan and co-workers [57] discovered the effect of K, Cu, and mixed promotion of K/Cu promoters on precipitated Fe-based FTS catalysts. They reported that addition of Cu promoter resulted in larger catalyst (Fe/Cu) surface area and smaller pore size compared to that of the fresh catalyst (Fe), while addition of K promoter decreased the catalysts surface area on Fe/K and Fe/Cu/K catalysts due to enhanced aggregation of the catalysts crystallites which led to plugging of pores of the catalysts. They also found that Cu promoter promoted the catalyst reducibility by

shifting the reduction peak to lower temperature, and suppressed the adsorption of CO as well as the carburization. K promoter suppressed the reduction of the catalysts and enhanced the catalytic carburization. They have also found that the addition of Cu promoter suppressed the catalytic activity and stability and enhanced the deactivation and the selectivity for the light hydrocarbon. However, K promoter improved the FTS activity, stability, and the chain growth while it suppressed the catalytic deactivation. Compared to the individual promotion of K and Cu, the double promotion was found to provide better activity and stability.

Referring to these aforementioned studies about the effect of the promoters on the Fe-based FT catalysts, it can be summarized that addition of the alkali promoters increased the catalytic activity due to enhance of catalytic carburization and also increasing the selectivity to the higher hydrocarbons. K promoter was found to be an essential promoter in Fe catalysts for the FTS, since it enhanced the formation of the longer chain and olefins hydrocarbons.

2.2.7 Synthesis technique

Catalysts are highly sophisticated products derived from several types of chemicals through different techniques. Therefore, the catalytic performance of FT catalyst strongly depends on the preparation method. The preparation condition controlled the distribution of an active phase over the support. Different synthesis methods were applied in FTS catalysts such as impregnation, precipitation, microemulsion, and colloidal. Three main categories can be used to classify the catalysts with respect to the synthesis method which are bulk catalysts, impregnated catalysts, and mixed agglomerated catalysts [25]. Bulk catalysts mainly consist of the active substance, whereas the impregnated catalysts are usually formed by impregnating the support with the active substance. A mixed agglomerated catalyst comprises those catalysts obtained by mixing the active sites with support precursors and then agglomerated the mixture [58].

2.2.7.1 *Synthesis of nanoparticles*

Fabrication of nanomaterials with control over size, shape, and crystalline structure has inspired the application of nanoparticles to numerous fields including catalysis, medicine, and electronics [59]. The use of nanomaterials requires the development of methods for nanoparticles assembly. Formation of nanoparticles starts with short burst of nucleation followed by slow diffusive growth and then formation of monodisperse crystalline nanoparticles [60]. Generally, synthesis methods of nanoparticles are typically grouped into two categories: the first one involves division of a massive solid into smaller portions, whereas the second one deals with condensation of atoms or molecular entities in solution or gas phase. The interest in synthesizing nanomaterials as catalyst grows rapidly for a variety of homogeneous and heterogeneous catalysis applications. In homogeneous catalysis, the colloidal transition metal nanoparticles are dispersed in an organic or aqueous solution. Heterogeneous nanocatalyst prepared by adsorption of nanoparticles onto supports. The most well-known approaches to synthesize nanoparticles are impregnation, precipitation, sol-gel, colloidal, and microemulsion methods.

2.2.7.2 *Impregnation method*

Incipient wetness impregnation method is the most common method for preparing the supported catalyst. Impregnation method involved three steps: deposition, drying, and calcinations [25].

I. Deposition of active metal on support

Deposition of the active metal on the support can be observed by using a solution of metal precursors. It is possible to start with dry or wet support. As we classify the type of impregnation methods by the starting state of the support [25]. In the case of wet support, the support is pre-wetted by the solvent and the metal will distribute according to diffusion and adsorption; this method is known as wet impregnation or diffusional impregnation. While in the case of dry support, the solution of metal precursors is added directly to the dry support. After being contacted, the solution is aspirated by the capillary force inside the pores of the support and this is referred as dry

impregnation or capillary impregnation methods. Immediately after the impregnation, the interaction between the active phase and support is relatively weak [25].

II. Drying

It is necessary to dry the impregnated sample to eliminate the solvent from the pores of the solid. Removal of this solvent resulted in a certain collapse of the structure. Therefore, care must be taken to control the drying rate. In addition, drying step led to redistribution an active phase over the support which led to initiate strong interaction between them.

III. Calcination

Calcine the dried catalyst facilitate the interaction between the active phase and the support [25]. Calcination is a further treatment beyond the drying process, which resulted in the following: modification of the textural (turn the small particles to bigger size), modification of the structure (surface area and porosity), generation of the active sites, and stabilization of the mechanical properties.

Reproducing synthesis of the catalysts through impregnation method requires a careful control of all impregnation parameters: temperature and time of drying the support, rate of addition of the salt solution, temperature and time of the drying.

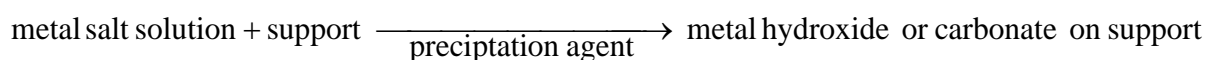
Referring to the amount of the metal salt solution used, two methods of contacting the metal and the support are distinguished as follows [58]:

- Excess solution, also as known incipient wetness impregnation method. During this method, support will be placed in an excess quantity of solution for a certain time required for total impregnation
- Appropriate amount of the solution and this method known as dry impregnation. The support is contacted with appropriate amount of the solution which is equal to the total pore volume or slightly less.

Assaf et al. [61] reported the effect of impregnation parameters on the diffusion profiles experimentally and also compared the experiment results with the mathematical models. The concentration of impregnation solution affects the penetrated distance and degree of coverage of nickel inside the catalytic pores. They showed that the degree of coverage increased by increasing the concentration of the solution. By fixing the concentration, the penetrated distance increased due to increasing impregnation time.

2.2.7.3 *Precipitation method*

Precipitation aimed to precipitate a solid from the liquid solution. Generally precipitation occurs in three main steps: super-saturation, nucleation, and growth. Perego and villa [58] illustrated that the super-saturation step was mainly affected by three parameters: concentration, temperature, and pH. Super-saturation can be approached by increasing the concentration via solvent evaporation or increasing the temperature or pH. The particles which were created during the super-saturation region developed in two stages namely nucleation and growth. These stages are mainly affected by the concentration, temperature, and the pH of the solution. Rapid nucleation and growth in a bulk solution must be avoided as it can cause the deposition of the active species only at the outside the support pores. Precipitation can be explained by the following reaction [25]:



Choosing of the salt depends on several factors, such as the solubility of the salt, thermal decomposition to oxide, safety and environmental impact. Of a wide possibility of salt precursor only nitrate, hydroxide and carbonate precursors possess a good combination of the characteristics mentioned.

Precipitation method is usually a preferred deposition route for loading metal higher than 10-20%, below this range impregnation is usually practiced [25].

2.2.7.4 Deposition-precipitation method

This method is a combination of precipitation and deposition method. It combined all the advantages of precipitation method for controlling the size and it diminishes the risk of formation of the bulk mixed compounds of support and active phase. The process occurs in two main steps (1) precipitation of the bulk solution on the support and (2) nitration of the precipitate on the support's surface. The deposition of metal onto the support surface is enhanced by introducing a precipitating agent, which initiate a fine and homogenous phase by involving surface OH groups of the support. The support's surface acts as a nucleation media to accelerate the adsorption of the metal over it because it coincides with growth and nucleation of a surface compound [25]. Therefore, a proper controlling of the preparation variables plays an important role in controlling the catalytic behavior of the precipitated catalysts.

Diffenbach *et al.* [62] investigated the influence of pH by using two types of precipitating agents which are NH_4OH and Na_2CO_3 for the preparation of precipitated Fe catalyst. They suggested that Na_2CO_3 -precipitated catalysts at low pH (3.7 and 4.7) showed higher activity and higher olefin selectivity compared with the Na_2CO_3 -precipitated catalyst at high pH (5.8, 7.6, and 9.8) while NH_4OH -precipitated catalyst obtained lower olefin selectivity and higher catalytic stability.

Previous studies have indicated the importance of pH on the structure and the performance of the catalysts where most of the studies suggested the dependence of pH on the type of the precipitating agent. Motjope and his co-workers [63] reported the effect of using different precipitating agents (NH_3 , K_2CO_3 , and Na_2CO_3) on the catalysts performance in the FT reaction by using Mössbauer spectroscopy. They found that the nature of the precipitant affect not only the physical properties of the catalyst but also the phase composition. They also concluded that increasing the precipitation pH (9-10) and irrespective of the precipitating agent resulted in formation of larger hematite crystallite compared to the ones at lower pH (7-8). The Mössbauer spectroscopy was used to show the influence of the precipitation agent on the catalytic composition during the reduction and FT reaction. They also found that NH_3 and K_2CO_3 precipitating catalysts exhibited higher CO conversion, due to increasing iron carbide phase compared to those catalysts precipitated by Na_2CO_3 . The formation of the hydrocarbons has an opposite trend compared to the FT activity,

where the catalyst prepared by addition of Na_2CO_3 resulted in higher selectivity to the hydrocarbons compared to that of K_2CO_3 . This suggested that most of the carbon atoms dissociated from the CO over the Na_2CO_3 -precipitated catalyst were consumed in the production of hydrocarbons.

2.2.8 Catalysts activation

Pretreatment of the catalysts before the FTS reaction, especially for the Fe-based catalysts plays an important role on the FT performance (activity and selectivity). There are three gases that can be employed for activating Fe catalyst: carbon monoxide, hydrogen, or syngas. It is well known that the iron oxide ($\alpha\text{-Fe}_2\text{O}_3$) is firstly transformed to Fe_3O_4 irrespective of the activation gas then the magnetite is converted to different Fe phases depending on the activation parameters. Variations in pretreatment conditions (temperature, pressure, and duration) as well as the reactor system would influence the chemical microscopic structure of Fe-based catalysts. Numerous studies have been performed to investigate the relation between the activation condition and the FT performance. Some reports proposed Fe_3O_4 as a main active site for FT reaction while other studies claimed iron carbides as the active phase for FTS. Davis [19] found that the laboratory-scale activation with CO at 270°C for 24h provided the maximum CO conversion compared to the other activation procedures. Pure H_2 is highly recommended for the commercial scale due to their availability and the low cost compared to pure CO, where it is only applied at the laboratory scale. Reduction of iron oxide (Fe_2O_3) by H_2 proceeds in two or three steps. Herranz and his coworkers [10] reported that the reduction of the Fe_2O_3 proceeds in three steps as shown in Figure 2-4. The first step displayed transformation of Fe_2O_3 to Fe_3O_4 , second step for reducing Fe_3O_4 to FeO , and the last step showed the transformation of FeO to Fe . Activation with the syngas is highly desirable since a common gas supply can be used for activation and synthesis [64].

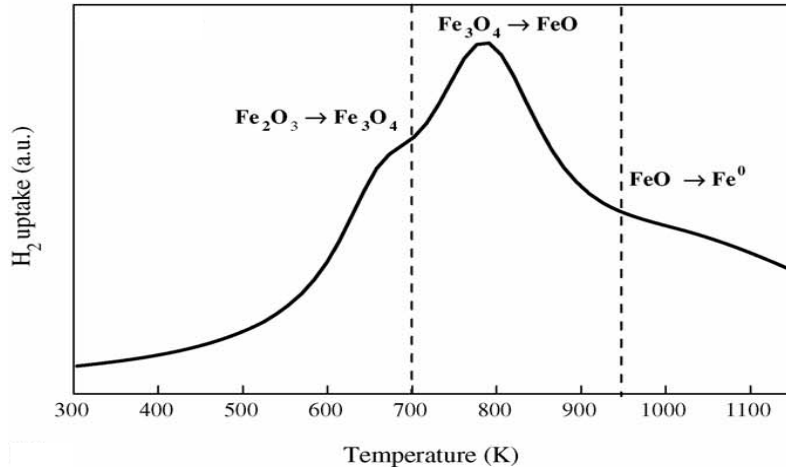


Figure 2-4: Hydrogen reduction profile of Fe-based catalyst [10]

2.2.9 Catalyst activity and selectivity

Several factors influenced the activity and selectivity of FT catalysts, which is strongly affected by the catalysts chemistry and structural compositions. The activation procedure, especially for Fe-based catalysts has a great influence on their activity and selectivity. The term selectivity is used to explain the way in which the products are distributed. Generally the product selectivity should be controlled to minimize the production of undesired products and maximize the production of the primary product. According to most of the literature, it was found that the catalyst activity and selectivity were influenced by one or more of the following factors: catalyst composition, nature of the support, metal dispersion, metal loading, preparation method, type of the reactor, pretreatment conditions, and operation conditions. Since Fe-based catalyst has different active sites for FTS therefore, the pretreatment has an important influence on the FTS activity and selectivity compared to cobalt-based catalyst, which is usually activated with H₂ to produce metallic phase which is considered as an active site for the FTS [50].

The nature of the active sites of Fe-based catalysts for FTS is still being debated. Activation treatment such as H₂, CO, or syngas activation plays an important role at initiating different sites of Fe catalysts. Therefore, a lot of works have been published regarding to the main active site of Fe catalysts for FTS. Hayakawa and co-workers [52] suggested iron carbide as the main active site for FTS because the catalytic activity was increased due to the presence of the carbide sites. Conversions with Fe-

catalysts have been carried out over a wide range of the operation condition such as the H₂/CO ratio, temperature, and pressure. Bukur *et al.* [48] provided detailed information about the influence of promoters (K, Cu, and Cu/K), reaction temperature, and space velocity for the precipitated Fe-based catalysts on the FTS and WGS activity in addition to the product selectivity. They found that the activity for the catalyst that was promoted by using different promoters increased with increasing of the reaction temperature as well as the time on stream. Furthermore, small shift toward the selectivity of the higher molecular weight products was obtained at the higher gas space velocity whereas the opposite trend was observed with increasing reaction temperature. The olefin selectivity may increase or decrease with the reaction temperature and this was interpreted in terms of accelerating the primary or secondary reactions. They found that the selectivity of the olefin increased with increasing reaction temperature for the catalysts promoted with potassium in contrast to the catalyst K with Cu.

Catalytic activity is influenced by changes in the chemical composition of the catalyst and the reaction conditions during some period of time (time-on-stream or induction period). The time-on-stream is longer at the lower reaction temperature and for the catalysts with higher alkali content. Moreover, a slight dependence of the catalytic activity and selectivity on the H₂/CO ratio was observed. Reaction temperature and pressure also influence the performance of the FTS. Therefore, to produce liquid product lower temperature was utilized due to the lower WGS activity. Temperature also played an important role in determining the WGS activity. This is the major difference between high or low reaction temperatures. Moreover, the temperature also affected the formation of different catalyst phase [19].

The basicity of the Fe-based catalysts is the one of the key factors that controls the product selectivity which is maintained by the amount and type of the alkali promoters. The amount and the type of alkali group as well as the amount and type of the structural promoters and impurities affect the basicity of the catalyst [65]. Table 2-1 is a summary of the studies that have been performed on the effects of the catalyst and reaction conditions on the performance of FTS. As shown in Table 2-1, the effects of the Fe particles size on the catalytic performance and the correlation between the catalyst properties and the FT performance have not been reported.

Table 2-1: Summary of the studies on the FT performance

| Catalyst | Synthesis technique | Fe particle size | Reaction condition | CO conversion (%) | Product selectivity (%) |
|--|----------------------------------|------------------|---|-------------------|--|
| 100Fe/20SiO ₂ ^A [44] | Precipitation | - | T=523K P=1.5MPa H ₂ /CO=0.67 | 47.2 | C ₁ -C ₄ = 48.1 C ₅ + = 51.8 |
| 100Fe/6Cu/5K/3Al ₂ O ₃ /22SiO ₂ ^A [17] | Co-precipitation and spray dried | - | T=523K P=20MPa H ₂ /CO=2 | 74.4 | C ₁ -C ₄ = 39 C ₅ + = 61.4 |
| 50Fe/50Mn/10SiO ₂ ^A [66] | Co-precipitation | - | T= 673K P= 1atm H ₂ /CO=0.5 | 73 | C ₁ -C ₄ = 74.9 C ₅ + = 2.1 |
| 57Fe/1.9Cu/1.6K/40%SiO ₂ ^A [67] | Impregnation | - | T=523K P=1.31MPa H ₂ /CO=0.7 | 32 | 0.2 [*] |
| 5%Fe/SiO ₂ ^B [10] | Microemulsion | - | T=573K P=1.01MPa H ₂ /CO=2 | 13.5 | C ₁ -C ₄ = 88.7 C ₅ + = 10.1 |
| 100Fe/6Cu/5K ^A [57] | Co-precipitated and spray-dried | - | T=533K P=1.5MPa H ₂ /CO=0.67 | 82.2 | C ₁ -C ₄ = 18.9 C ₅ + = 81.1 |
| 100Fe/5Cu/4.2K/ 15SiO ₂ ^A [46] | Co-precipitated and spray-dried | - | T=523K P=1.5MPa H ₂ /CO=0.67 | 48.4 | C ₁ -C ₄ = 20.3 C ₅ + = 80.6 |
| 100Fe [21] | Precipitation | - | T=513K P=0.1MPa H ₂ /CO=1 | 85.9 | C ₁ -C ₄ = 32.4 C ₅ + = 67.6 |

*productivity of lower molecular weight 0.2g.h⁻¹.g⁻¹Fe

^A The amount of the element in mass ratio

^B Fe loading (%)

2.3 Catalyst characterization

The performance of the catalysts is strongly influenced by the catalyst properties. Therefore, characterization of the catalysts is important at any stage of designing the catalysts. For FTS catalysts, properties that must be classified are the surface chemical and physical properties, catalyst reducibility, catalytic activity and selectivity. Since the active catalyst for FTS is likely to possess a complex microstructures that include several co-existing phase, therefore, many different types of analysis have been used to explain the catalyst properties.

2.3.1 Surface area and pore size measurement

Since the catalytic phenomena occur at the surface of the solid catalysts thus, porous solids with a high internal surface are often required in order to achieve the responsible value of the activity. Therefore, several techniques were applied to determine the surface area for the solid materials. There are relatively large portion of the atoms of the solid material which are near the surface. The surface atoms were found to be more reactive than the same atoms in bulk form where it suppressed the sintering of catalyst at higher temperature and it exhibits great catalytic activity. Therefore, the influence of the surface area and structure is pronounced as physical composition. The surface area is usually described by the gas adsorption or desorption isotherms. Firstly, the sample is evacuated from the moisture by passing non-adsorbing gas such as helium over the sample. Then the temperature of the evacuated sample (adsorbent) is reduced to that of coolant appropriate such as liquid nitrogen or argon and the adsorbate allowed gas to be adsorbed via attractive force between the exposed surface of the solid material and the gas molecules (adsorbate). The relations between the accumulated gas quantities adsorbed versus gas pressure are graphed to generate the adsorption isotherm and the data are treated in accordance of gas adsorption theories to arrive at a specific surface area for the sample. Generally the adsorption isotherms follow one of six IUPAC standard forms as shown in Figure 2-5 [68]. Type I shows the characteristic of adsorbents with extremely small pores, which is known as micropores ($d_{\text{pore}} < 2\text{nm}$) solid material. Type II illustrates the characteristic of the adsorbents having relatively large pores, indicative of nonporous

adsorbents. Type III and V arise under the condition of vapor adsorption or they can be observed when the interactions between the adsorbate and adsorbent are weak. Type IV appears at the solid that possess mesopores (2-50nm) which is analogous to type II. Finally, the rare type VI, is indicative of a nonporous adsorbent with an almost completely uniform surface [69].

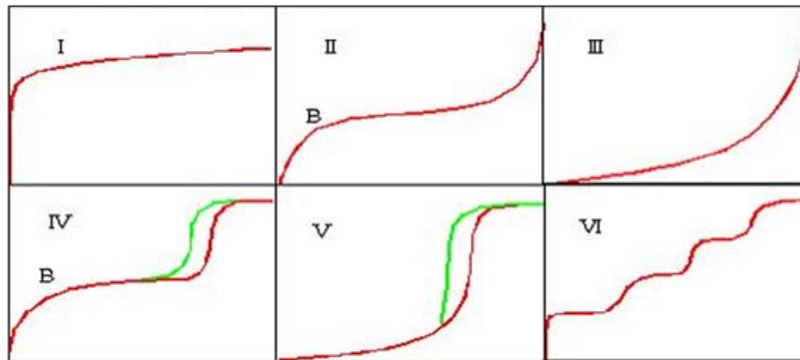


Figure 2-5: Standard adsorption isotherms [68]

The phenomena of gas adsorption have been illustrated through many theories to provide a clear understanding of the surface characteristics. One of the most applicable theories is the BET theory, which is named after the surnames of its originators; Brunauer, Emmett and Teller. This theory takes the main advantage from the Langmuir theory which only considered the adsorption of monolayer molecule and the concept of multimolecular layer adsorption [69], as shown at Figure 2-6 [70].

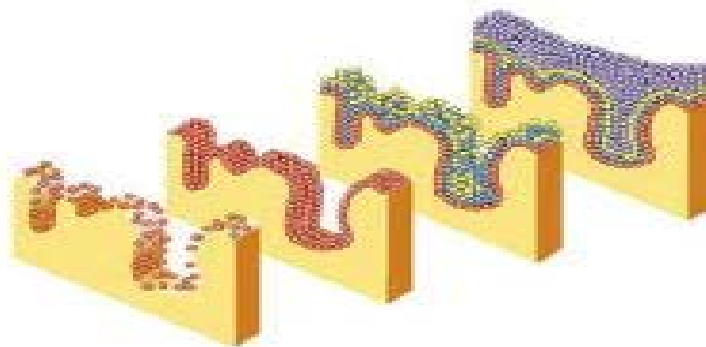


Figure 2-6: Concept of multimolecular layers adsorption [70]

The fundamental assumption of the BET theory is that the gas molecules are physically adsorbed on a solid in an infinite layer. The layers initiated from the force active in the condensation of the adsorbate gas responsible for the binding energy in

multimolecular adsorption. Also assumed that there are no interactions between the adsorption layers. The BET theory can be expressed through this following equation (2.9) [68].

$$\frac{P}{V_{\alpha}(P_0 - P)} = \frac{1}{V_m C} + \frac{C-1}{V_m C} \left(\frac{P}{P_0} \right) \quad (2.9)$$

Where P and P_0 are the equilibrium and the saturation pressure of the adsorbate respectively, at the temperature of adsorption, V and V_m are the total and monolayer adsorbent gas quantity, respectively. The constant C is expressed by equation (2.10) [68].

$$C = \exp \frac{q_1 - q_L}{RT} \quad (2.10)$$

Where q_1 is the heat of adsorption of the first layer onto solid surface, q_L is the latent heat of condensation of the adsorbate, R the gas constant, and T the absolute temperature.

The plot of $P/V_{\alpha}(P_0 - P)$ versus P/P_0 from equation (2.9) should yield straight line where the value of V_m and C can be obtained from the plot with intercept of $1/V_m C$ and slope of $(C-1)/V_m C$. The surface area can be easily calculated after the determination of the volume of the monolayer by the following equation (2.11) [68].

$$\sigma = (4)(0.866) \left[\frac{M}{4(2N_A \rho)^{1/2}} \right]^{2/3} \quad (2.11)$$

Where σ is the area per molecules, M the molecular weight, N_A Avogadro's number, and ρ the density of the liquid adsorbate. BET has achieved wide usage for measuring the surface area and has become the basis for a number of later theories developments.

The pore size distribution was determined through Barrett-Joyner-Halenda (BJH) method. This technique follow the adsorption branch of the isotherm downward from high to low pressure or the desorption branch. The condition must be set arbitrarily where all the considered pores are filled [64]. The calculation of BJH method scheme

on mesopore distribution from nitrogen adsorption data is summarized using equation (2.12) [64].

$$V_{\text{ads}}(x_k) = \sum_{i=1}^k \Delta V_i [r_i \leq r_c(x_k)] + \sum_{i=k+1}^n \Delta S_i t_i [r_i > r_c(x_k)] \quad (2.12)$$

Where,

$V_{\text{ads}}(x_k)$ = volume of (liquid) adsorbate [cm^3/g] at relative pressure x_k (calculated from the value of adsorption expressed in [cm^3/g STP] by $V_{\text{ads}}(x) = 0.0015468 a(x)$)

V = pore volume [cm^3/g]

S = surface area [m^2/g]

t = thickness of adsorbed layer (in appropriate units)

r = pore radius (in appropriate units)

2.3.2 Catalytic morphology

Electron microscopy is used to visualize the morphology of the catalysts via the bombardment of electrons instead of using photons as a source of image formation.

The most common types of the electron microscopy are scanning electron microscopy (SEM) and transmission electron microscopy (TEM) as shown in Figure 2-7. TEM offer the internal study of the material while SEM observes the surface properties [71].

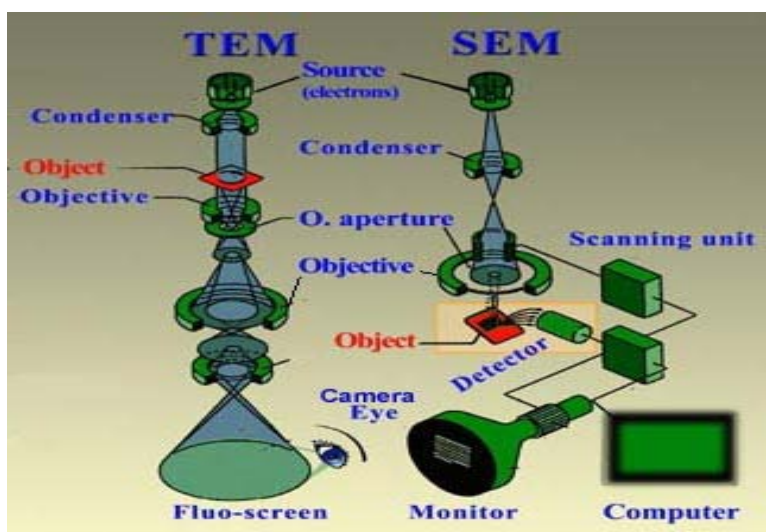


Figure 2-7: TEM and SEM system [71]

2.3.2.1 Scanning electron microscopy (SEM)

SEM is one of the most common techniques used to determine the catalytic surface properties. SEM is used to determine the morphological change by scanning the sample with a high-energy beam of electrons. The surface topography can be studied due to the interaction between the electrons emitted from the electron source and the atoms that exist at surface of the sample. The electron is generated from an electron source and accelerated under influence of a strong electrical voltage gradient (field) with electromagnetic coils. This electron is known as the primary electron and this electron is focused and deflected by electronic lenses to produce a narrow scan beam that bombards the object (Figure 2-8). The secondary electrons are produced by interaction of the electron beam with the atoms at the surface of the sample. The signal formed from this interaction provides information that is employed to reconstruct a very detailed image of the topography of the surface of the sample [72]. The type of the signals produced from the interaction of the electron beam with the sample include not only the secondary electrons but also backscattered electrons, characteristic X-rays, and other photons at various energy. These signals can be used to examine many characteristics of the sample such as surface topography, crystallography, and composition. The characteristic X-rays which are also produced by the interaction of electrons with the sample, may also be detected in SEM equipped for energy-dispersive X-ray spectroscopy (EDS or EDX).

The EDS system offers rapid phase identification of the sample [73]. The electrons that are not captured by the detector would hang like a cloud masking around the sample, thus masking the image. In scanning electron microscopy samples are coated in advance by a very thin layer of conductive material to clear away superfluous electrons [72].

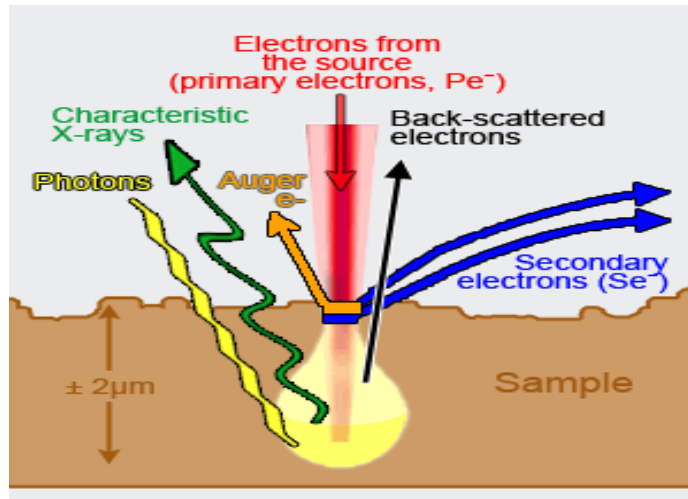


Figure 2-8: Type of electrons that is used for different analysis [72]

The basic components of the FESEM microscopy are lens system, the electron gun, the electron collector, the photo-recording cathode ray tube, and the associated electronics (Figure 2-9).

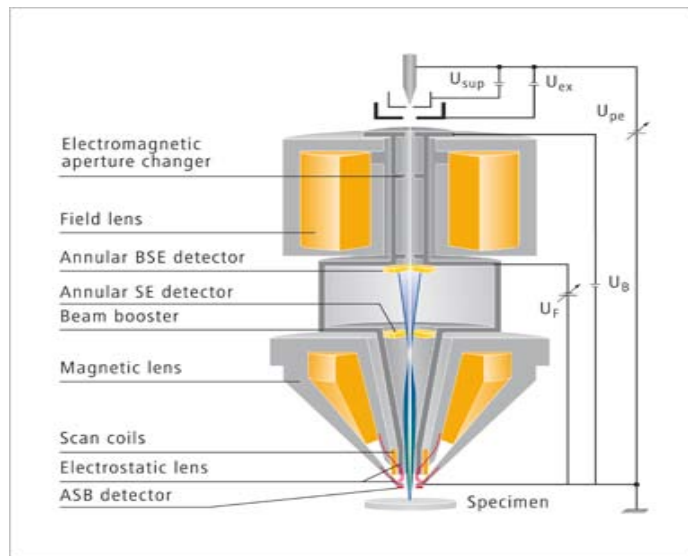


Figure 2-9: Field emission column [74]

2.3.2.2 Transmission electron microscopy (TEM)

TEM is found to be a very powerful system to characterize the nanocrystal materials, particularly when the determination of the particle shape and size is important. TEM is likely used for revealing the atom distributions on nanocrystal surfaces. TEM is

composed of vacuum system, illumination system, a specimen stage, an objective lens system, the magnification system, the data recording system, and the chemical analysis system (Figure 2-10) [75]. Vacuum system is used to increase the mean free path of electron gas interaction. The illumination system includes the electron gun which typically uses a field emission source or thermionic emission source to produce high spatial resolution microanalysis. The illumination system consists of the condenser lenses that are vitally important for forming a fine electron probe. The specimen stage is a key to carrying out structure analysis and giving the possibility of characterizing the physical properties of individual nanostructures. The objective lens is the heart of a TEM which determines the limit of image resolution. The magnification system consists of intermediate lenses and projection lenses, and it gives a magnification up to 1.5 million. The data recording system tends to be digital.

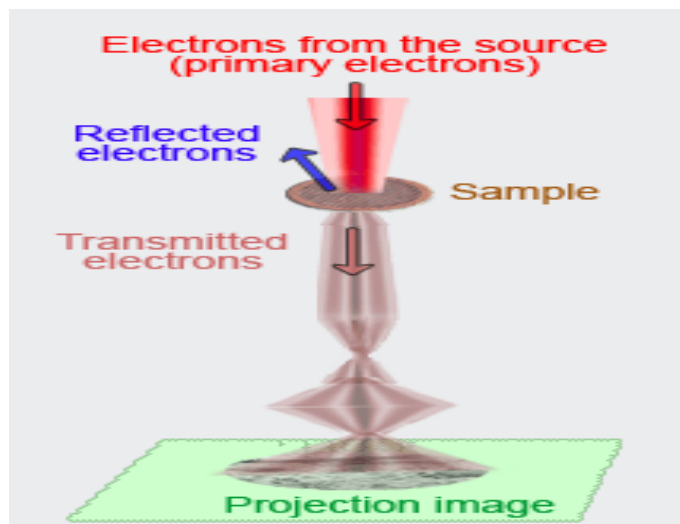


Figure 2-10: Electron source at the TEM [75]

The image formation of the specimen is caused by the interference of the reflected electron beams. Areas that scatter few electrons (electron-lucent areas) appear as bright areas in the image, while areas that scatter more electrons or absorb electrons (electron-dense areas) appear as dark areas (mauricewilkinscentre.org) [76]. Figure 2-11 shows the schematic diagram of the TEM column.

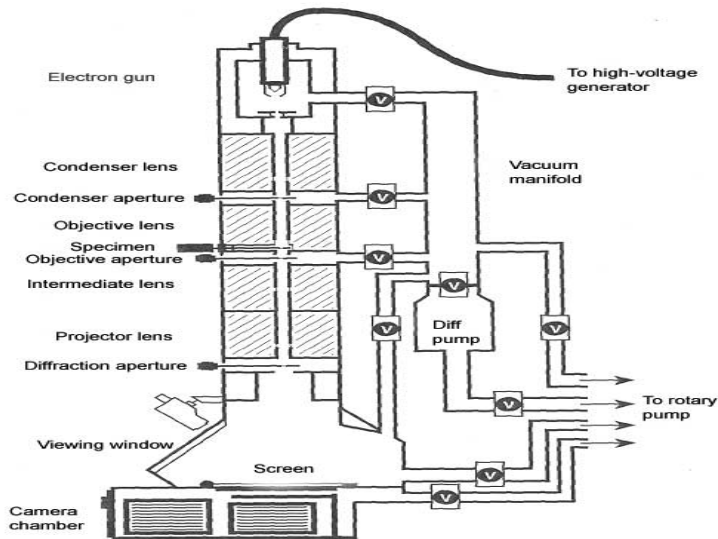


Figure 2-11: Schematic diagram of a transmission electron microscope column

[76]

2.3.3 X-ray powder diffraction (XRD)

XRD is a versatile technique that reveals detailed information about the chemical composition and crystallographic structure of the material. This method is ideally suited for characterization and identification of crystalline phases [77]. The XRD pattern of a pure substance is like a fingerprint of the substance. The main use of powder diffraction is to identify components that existed in the sample by a search and match procedure where a thousand components such as organic, inorganic, and crystalline phase have been collected and stored on magnetic or optical media as standards. The solid material can be described as amorphous or crystalline materials. Amorphous substance involves random arrangement of the atoms whereas atoms are arranged in a regular pattern for the crystalline material.

The analyzing procedure is based on the diffraction of X-ray beam by the substance [77]. X-rays are electromagnetic radiation similar to light but with a much shorter wavelength of about 1\AA (10^{-10}m), which is about the same size as an atom. It is positioned between gamma-rays and ultraviolet region of electromagnetic spectrum. XRD involves a source of the monochromatic radiation and an X-ray detector as shown in Figure 2-12. The X-ray detector is situated on the circumference of a graduated circle centered on the powder specimen. Encounters between the X-ray

beam and a crystal lattice, result in scattering. The relation by which diffraction occurs is known as the Bragg law or equation. Because each crystalline material has a characteristic atomic structure, it will diffract X-rays in a unique characteristic pattern [78]. Bragg law (equation 2.13) explains the cleavage faces on the crystal which cause the X-rays to diffract at certain angles and wavelength.

$$2d (\sin \theta) = \lambda \quad (2-13)$$

Where

d = the lattice inter-planar spacing of the crystal

θ = the X-ray incidence angle (Bragg angle)

λ = the wavelength of the characteristic X-rays.

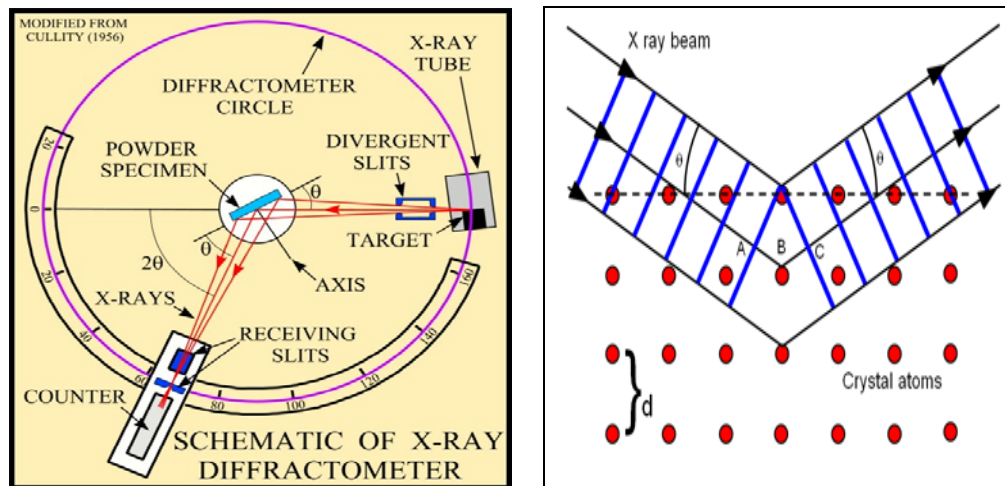


Figure 2-12: Flow diagram of the X-ray diffractometer and reflection of the X-ray [78] and [79]

2.3.4 Temperature-programmed reduction (TPR)

TPR is a technique to characterize the solid material and finding the most efficient reduction condition and studying the metal-support interaction. This technique consists of heating the catalyst at a linear temperature ramp in a flow of hydrogen while monitoring the hydrogen consumption. A quartz U-tube is used as a sample container and it is filled by known amount of the catalyst. The sample vessel is placed in a furnace. The sample has been pretreated to remove the moisture and impurities via heating in inert gas (nitrogen, argon or helium) at certain temperature and flow rate. Then flow is switched to 5%hydrogen in nitrogen and the temperature is

increased. The temperature is gradually increased, reaction rate increase depending on the activity and the actual degree of reduction of the solid material, until the material is completely reduced [80].

Jozwiak *et al.* [81] investigated the H₂ and CO reduction of various iron oxides by using TPR. They concluded that the change of the TPR profile shape was strongly influenced by the heating rate. They also found that when fast heating rate was used, the complete reduction moved to the higher temperatures of up to 800°C. They reported that reduction of Fe₂O₃ took place in two or three reduction stages. Two reduction stages represent transforming Fe₂O₃→Fe₃O₄→Fe which occurred at lower reduction temperature <500°C, while for the high reduction temperature 700-800°C, appearance of wüstite (FeO) phase proved the involvement of the third step in the reduction of Fe₂O₃.

2.4 Summary

Referring to the previous reports presented by many researchers confirmed that Fe-based catalysts was selected to catalyze the FT reaction at low H₂/CO ratio where it has higher WGS activity, higher flexibility at different reaction condition, higher selectivity to the heavy hydrocarbons and olefins compared with the Co-based catalyst. Furthermore, most of the prior studies showed that physical, chemical, and mechanical characteristics of Fe-based FTS catalysts was found to be significantly affected by applying different preparation techniques as well as supports, and promoters. Impregnation and precipitation methods were commonly used to synthesize the Fe-based catalysts. Al₂O₃ and SiO₂ supports are commonly used supports. Generally supported Fe-based catalyst was found to have lower catalytic activity compared to the unsupported one due to the strong interaction between the active metal and the support. Several alkali promoters were used to enhance the catalytic reducibility as well as the selectivity for hydrocarbons. Reaction condition such as temperature, pressure, space velocity, and reactant ratio strongly influenced the FTS catalytic performance.

CHAPTER 3

Research Methodology

3.1 Introduction

Although numerous studies have been conducted on the FTS over Fe-based catalyst, further investigations are required to determine the influence of different synthesis parameters on the performance of supported Fe catalyst in FTS process. Therefore, this study was aimed to apply various parameters on the catalyst synthesis steps and the reaction conditions to extract the effects of these parameters on the performance of the supported Fe-based catalyst in FTS. Accordingly, this chapter described the experimental work conducted in this study which is divided into three parts: preparation of the catalysts, characterization methods, and FT reaction studies.

The first part deals with the synthesis of the Fe-based catalysts for FT reaction. Fe-based catalysts with different Fe loading (3, 6, 10, and 15 wt %) supported on SiO₂ or Al₂O₃-SiO₂ supports were synthesized through two synthesis techniques, namely impregnation and precipitation methods. Moreover, supported Fe nanocatalysts were modified by adding promoters such as K or Cu.

The second part illustrated the influence of the synthesis techniques, Fe loading, supports, and promoters on the physical and chemical properties of the catalyst. Several analysis techniques such as N₂ physical adsorption, FESEM, TEM, XRD, and TPR methods were used to characterize the catalysts.

Finally, the influence of the synthesis parameters for the supported Fe catalysts and the operation conditions, such as flow rate, H₂:CO ratio and reaction temperature on the catalytic performance for FTS were tested in a microreactor system. A comparison was made between properties and performance of catalysts prepared using different synthesis techniques which have been subjected to the same

pretreatment and the reaction condition. The research methodology is summarized in the flow chart shown in Figure 3-1.

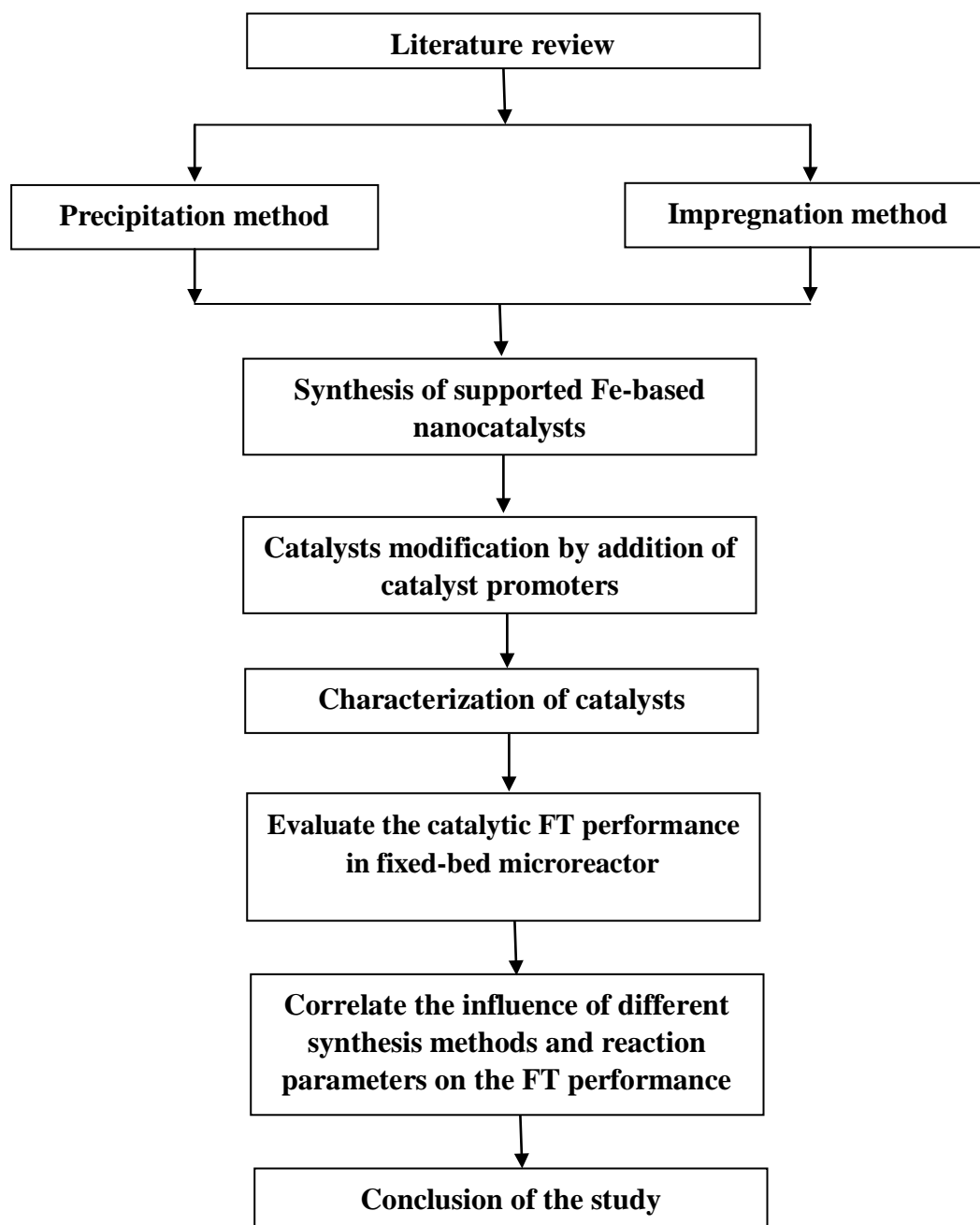


Figure 3-1: Methodology layout

3.2 Materials

Table 3-1: List of chemicals and gases used in this study

| Materials | Molecular weight (amu) | Supplier | Purity | purpose |
|-------------------------------|-------------------------------|---|---------------|-------------------------|
| Silica (aerosol OX50) | 60.1 | Evonik | 99.8% | Catalyst support |
| Aluminum nitrate nanohydrate | 375.1 | Fluka | 98.0% | Support precursor |
| Iron nitrate nanohydrate | 403.9 | Merck | 99.0% | Catalysts precursor |
| Copper nitrate nanohydrate | 241.8 | Merck | 99.0% | Promoter precursor |
| Potassium nitrate nanohydrate | 101.1 | Merck | 99.0% | Promoter precursor |
| Ammonia | 17.0 | Merck | 25.0% | Precipitating agent |
| 5%hydrogen/nitrogen | - | Malaysian oxygen (MOX) | 99.9% | Reduction |
| Nitrogen | 14.0 | MOX | 99.9% | Pretreatment |
| Hydrogen | 2.0 | MOX | 99.9% | Reactant gas |
| Carbon monoxide | 28.0 | MOX | 99.9% | Reactant gas |
| Helium | 2.0 | MOX | 99.9% | Purging gas and carrier |
| RGA standard gas | - | Praxair, Inc for Agilent technologies | - | Calibration standard |
| Scott specialty gas | - | Solution engineering SDN.BHD, (Agilent) | - | Calibration standard |

3.3 Synthesis technique of the FT catalysts

Generally the catalytic properties of the heterogeneous catalysts are strongly affected by every step of the preparation and the composition of the raw material. Although, numerous synthesis techniques were applied to synthesize Fe-based FT catalysts, such as impregnation, precipitation, sol-gel, colloidal, and micro-emulsion methods, impregnation and precipitation methods are commonly used. Therefore, in this study impregnation and precipitation methods were used to synthesize supported Fe nanocatalyst. Comparison was made between the properties of catalysts prepared by both synthesis techniques. The influence of the synthesis technique on the FT performance was investigated. The impregnation method was used to synthesize Fe nanoparticles on SiO₂ and Al₂O₃-SiO₂ supports. Fe-based catalysts supported by SiO₂ support were promoted by K and Cu promoters and the effect of the alkali promoter on the catalytic performance was investigated.

The preparation step consists of two parts. The first parts deal with synthesis of the oxide support using impregnation method, while the second part involved synthesis of supported Fe-based catalysts via impregnation and precipitation methods.

3.3.1 Preparation of the catalyst support

Two types of the catalyst supports used in this study were silica and alumina-silica. Commercial non-porous SiO₂, supplied by (aerosol OX50, Evonik Industries) with small surface area (40.9m²/g) was used as one of the support materials. The Al₂O₃-SiO₂ support with small surface area was synthesized via impregnation method to make the comparison between the two supports possible.

The Al₂O₃-SiO₂ support was prepared by impregnation method with weight ratios of Al₂O₃:SiO₂ set at (5:95, 15:85 and 25:75 w/w). The procedure followed was similar to that described by Zhang *et al.* [82]. Al₂O₃-SiO₂ support was synthesized by dissolving a desired amount of alumina precursor Al₂O₃ (NO₃)₃.9H₂O in glycol at 353K and stirred for 1h to form a homogenous solution (0.5M) of Al₂O₃ (NO₃)₃.9H₂O (amount of the precursor is shown in Appendix A). Then the solution was added dropwise on to the commercial SiO₂ at constant stirring for 12h. After impregnation,

the support was dried in air at 393K for 12h and calcined at 873K for 4h in following of air.

3.3.2 Preparation of the FT catalysts

3.3.2.1 Impregnation method

I. Supported Fe-based catalysts

Impregnation method is a simple technique that was used to synthesize the FT catalysts. Generally, impregnation method was a preferred method to synthesize the Fe-based catalysts having Fe loading (less than 10%). Catalysts with Fe loadings of 3, 6, 10, and 15 wt% were synthesized using the impregnation method. Iron nitrate nonahydrate ($\text{Fe}(\text{NO}_3)_3 \cdot 9\text{H}_2\text{O}$) was used as a metal precursor. Iron nitrate was chosen due to the availability of the precursor, high solubility in water, faster decomposition to oxide form compared to the other precursors and other safety and environment effects. The amount of each precursor was calculated to produce 5g of the total catalyst at different Fe loadings on SiO_2 and $\text{Al}_2\text{O}_3\text{-SiO}_2$ supports.

The procedure for synthesizing supported Fe-based FT catalysts are as follows. Desired amount of $\text{Fe}(\text{NO}_3)_3 \cdot 9\text{H}_2\text{O}$ was dissolved in deionized water to produce an aqueous solution (0.5M) of iron nitrate and then the solution was stirred for 1h to form a homogenous mixture (calculations are shown in detail in Appendix A). This precursor solution was dropped slowly onto the support under constant stirring. The impregnated sample was stirred for 24h. Equations 3.1 and 3.2 show the reaction which occur due to addition of precursor solution to the support [29].



Where,

aq = aqueous solution

p = powder

s = suspension

After the stirring period was completed, the sample was dried at 120°C for 12hr to remove the moisture and the impurities then calcined under the flow of air at 600°C for 4h [29].



Where, I.C is impregnated catalyst

II. Supported Fe-based catalysts incorporated with a promoter

Copper nitrate nonahydrate ($\text{Cu}(\text{NO}_3)_{2.3}\text{H}_2\text{O}$) and potassium nitrate (KNO_3) used as the metal precursors were supplied by Merck. Supported Fe-based catalysts were incorporated with alkali promoters (Cu, K, and double promotion of Cu/K) by impregnation method. In the case of catalysts promoted with individual promoter copper or potassium ($\text{Fe}/\text{Cu}/\text{SiO}_2$ or $\text{Fe}/\text{K}/\text{SiO}_2$), silica support was impregnated with an aqueous solution (0.5M) of iron nitrate and copper nitrate or iron nitrate and potassium nitrate. The amounts of the materials used are shown in Appendix A. Then each of those impregnated mixtures was stirred for 24hr, drying at 120°C for 12h and finally calcined for 4h under air flow at 600°C. for synthesis of the double promotion, supported Fe-based catalysts ($\text{Fe}/\text{Cu}/\text{K}/\text{SiO}_2$), an aqueous solution of iron nitrate and copper nitrate (0.5M) were added slowly to the desired amount of silica under a constant stirring for 4h. Then an aqueous solution (0.5M) of potassium nitrate was added dropwise to the iron-copper mixture, and the final mixture was stirred for 24h. The remaining steps were similar to the steps that were applied in the case for the Cu and K promotion.

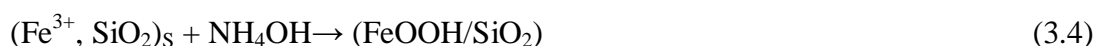
3.3.2.2 *Precipitation method*

Precipitation method involves the formation of a solid from a solution or inside another solid during a chemical reaction or by diffusion in a solid. The steps for the precipitation procedure are shown as follows: firstly, the Fe precursor, iron nitrate nonahydrate, was dissolved in deionized water and stirred for 1h to form a homogenous solution. This solution was slowly added to the silica support and the

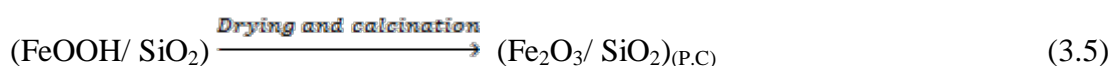
mixture was stirred for 4hr. Equation (3.3) explained the reaction that occurs due to the addition of metal solution to the support.



Ammonia hydroxide was chosen as the precipitation agent based on the study that was conducted by Diffenbach *et al.* [62]. NH_4OH was used to control the formation of the desired precipitate. The solution was heated up to 80°C and treated by adjusting the pH between 9 to 11 using 1- 2ml of NH_4OH (equation 3.4). This pH value was chosen referring to the studies that was published by Motjope and co-workers [63] on the influence of the pH where the pH of the solution was controlled by adding the precipitating agent dropwise under a constant stirring.



Then the solution was stirred for 24hr and after the precipitate was formed, the sample was washed several times by deionized water and carefully filtered. After filtration, the precipitate was dried at 120°C for 12h and calcined at 600°C for 4h under the air flow. The precipitate was dried and calcined in order to remove the moisture, and calcination step converting the precipitate to the more chemical stable form (oxide form) as shown in the following equation (3.5) [10].



Where, P.C is precipitated catalyst

3.4 Characterization techniques

3.4.1 N_2 -physical adsorption

BET theory provides a relationship between the pressure of a gas and the volume of the adsorbed monolayer across the surface of the material. The total surface area, pore volume and average pore size for all the synthesized Fe-based FT catalysts were

determined using micromeritics (ASAP 2000) adsorption equipment shown in Figure 3-2. This method is based on multipoint nitrogen adsorption-desorption principle. Nitrogen (99.9% purity) gas was used as an adsorbate. A sample was degassed by heating at 195⁰C over night under vacuum conditions to remove moisture or any adsorbed species or impurities.

BET equipment consisted of two parts as shown at Figure 3-2: the first part is the pretreatment where the sample is thermally pretreated under the flow of N₂ to remove the moisture or any other impurities. The second part is for sample analysis.



Figure 3-2: Micromeritics (ASAP 2000) equipment used to measure the surface area

Typically, 0.3 g of the catalysts was loaded in the pre-weighed quartz sample tube. The sample tube was placed at the degasser where it was degassed overnight under the flow of nitrogen at 195⁰C to remove the moisture and impurities. After finishing the degassing period, the sample was cooled to the ambient temperature. The sample tube was refilled with nitrogen and then the sample was removed from the degassing port and reweighed, to determine the actual sample mass before switching it to the analysis port. Subsequently, the sample tube was immersed inside a dewar

flask on an elevator filled by liquid nitrogen. Then all the information about the sample was keyed into the software to setup the system and to start the analysis. Finally, the value for the catalyst surface area was calculated according to the BET equation while the value for the pore size distribution was determined from the desorption branch of the adsorption isotherm by the Barrett-Joyner-Halenda (BJH) method.

3.4.2 Field-emission scanning electron microscopy (FESEM)

FESEM permits the surface morphology characterization of heterogeneous organic and inorganic material in nanometer (nm) to micrometer (μm) scale. The major reason for using the FESEM is to obtain high resolution in the nanometer range [72]. In addition, this technique is also known to be one of the most common techniques of imaging the surface area of the sample. This system also includes the energy dispersive X-ray analysis (EDX), which provides quantitative elemental analysis and element localization on samples being analyzed.

The FESEM analysis for the supported Fe-based catalysts was performed on Zeiss Supra 55 VP equipment. Samples of the catalysts powder were prepared by spreading powder on the carbon tape and the excess powder was simply shaken off. The FESEM was conducted under the following conditions:

Accelerating voltage = 5KV

Magnification = 100.00 KX

Working distance = 4 mm

3.4.3 Transmission electron microscopy (TEM)

TEM analysis was conducted to observe information about the catalysts particle size and the dispersion of these particles over the support. The powdered sample was suspended in heptane then it was sonicated for 30min. A portion of the sample was then deposited on a carbon-coated copper grid. Then the grid was placed in the TEM machine to analyze the shape of the nanoparticle, the metal particle size, and to

observe the metal coverage on the support. The TEM analysis for the supported Fe-based catalysts was performed on Zeiss LIBRA 200 FE equipment under the following conditions:

Voltage= 200KV

Magnifications= 1000KV

3.4.4 X-ray diffraction (XRD)

XRD is the most common technique used to investigate the characteristics of crystalline materials. This technique is attractive because it requires only small amount of material, easy of performance, and is non-destructive technique.

The composition of the synthesized catalysts was determined using the XRD. XRD analyses were performed using a Bruker A&S D8 Advanced Diffractometer instrument equipped with a $\text{CuK}\alpha$ radiation source, at 40 kV and 30 mA, in the scanning angle (2θ) range of $2\text{--}60^\circ$ at scanning speed of $1.2^\circ/\text{min}$. The respective XRD peak of the catalyst was compared with the literature to identify the phase composition of the catalyst.

3.4.5 Temperature-programmed reduction (TPR)

The TPR experiment was performed using a TPD/R/O 1100 CE Instrument equipped with a thermal conductivity detector (TCD) in two-stage procedure, namely pretreatment and analysis. The prepared catalyst (20mg) was placed between two layers of quartz wool inside a conventional atmospheric quartz flow reactor then the quartz cell was placed inside the electrical furnace, which is equipped with a programmable temperature controller. The sample was pretreated under flowing of pure N_2 and temperature was programmed to increase from the room temperature to 250°C at $10^\circ\text{C}/\text{min}$ then the sample was hold at 250°C for one hour in order to remove the impurities and the moisture. After completing the pretreatment step, the flow was switched to $5\% \text{H}_2/\text{N}_2$ (20ml/min) which was used as the reducing gas and temperature was ramped to 900°C at $10^\circ\text{C}/\text{min}$ and then the sample was hold at 900°C for 4 hours. The tail gas was directly passed to the thermal conductivity

detector (TCD) to determine the hydrogen consumption in the gas stream. Distinct reducible species in the catalyst were shown as peaks in the TPR profile.

3.5 General description of reactor rig

The fixed-bed microreactor was supplied by Aseptec Sdn Bhd. Figure 3-3 shows the assembly of the microreactor system. The reaction system consisted of three parts namely the gas supply, fixed-bed microreactor, and online gas analysis system. Figure 3-4 shows the schematic diagram of the microreactor system.

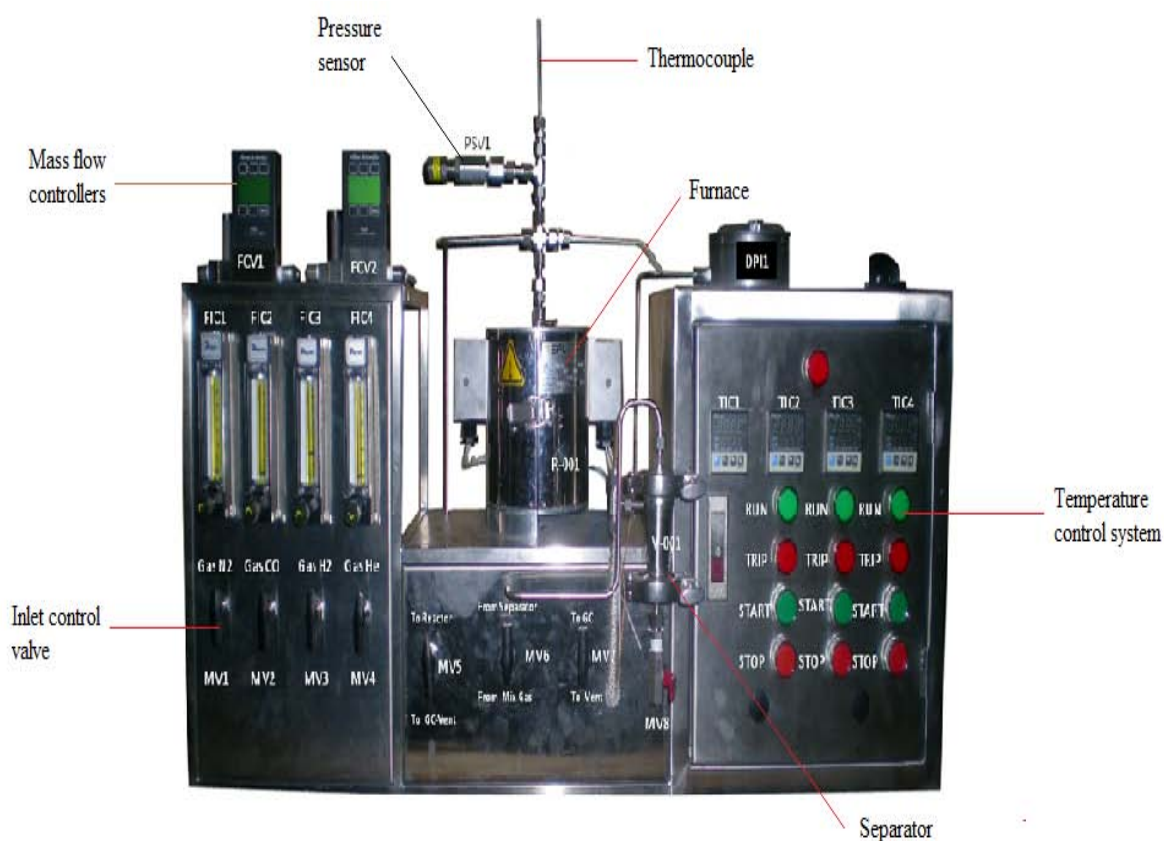


Figure 3-3: Overall reactor diagram

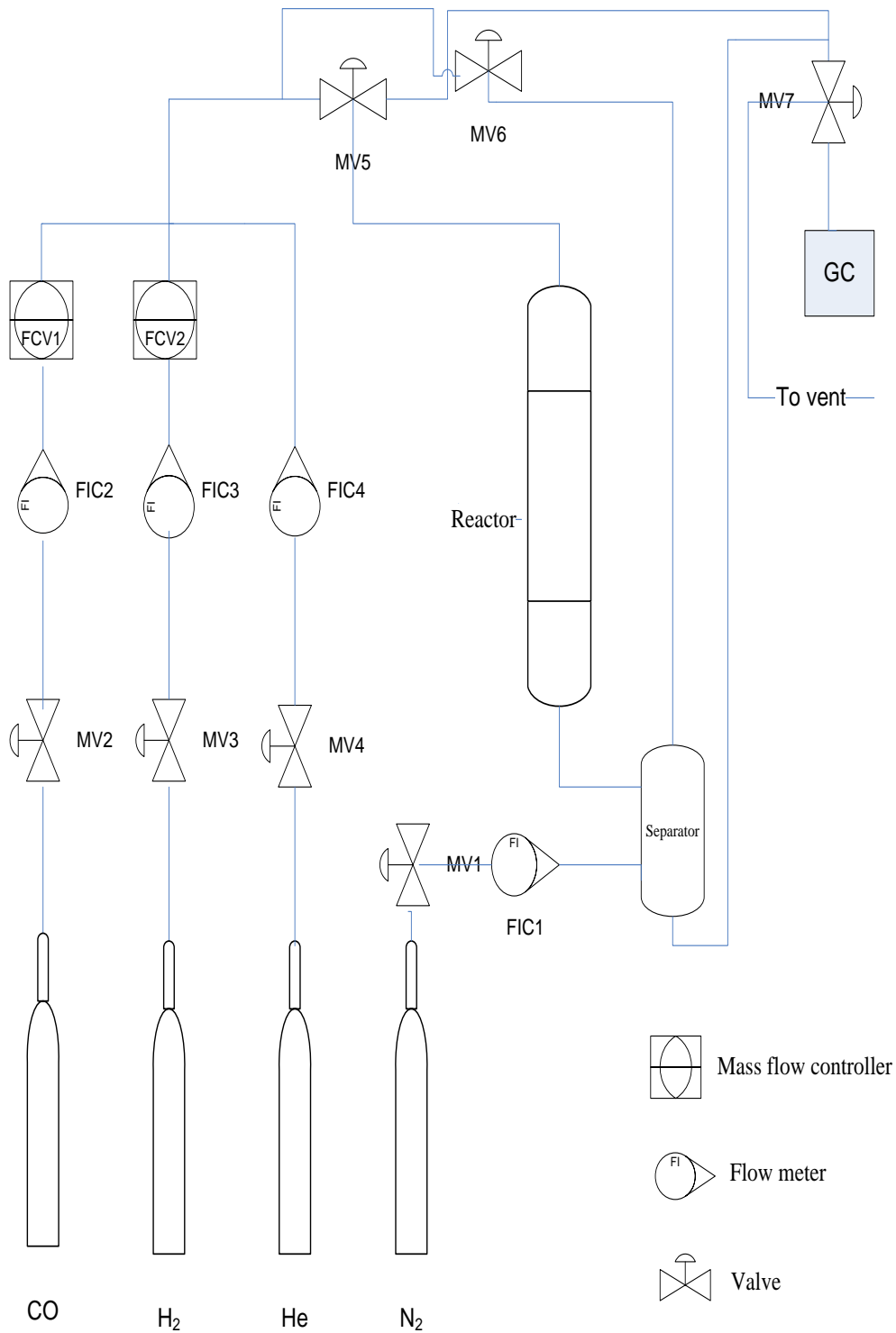


Figure 3-4: Schematic diagram of a microreactor system

3.5.1 Gas supplying system

Three gases used in the microreactor system were He, H₂, and CO (Figure 3-4). The inert gas helium was used as a purging gas to purge the overall system whereas; hydrogen and carbon monoxide were used as reactant gases. In addition, CO gas was also used as a reducing agent to activate the catalysts. Two-stage pressure gas regulators were used to control the gas outlet pressure to 2 bars for all the reactant gases. The reactant gases were transferred to the reactor through ¼ inch stainless steel tubings. Flow rate of the inlet gases CO and H₂ were controlled by mass flow controllers supplied by Alicat scientific (MC-100SCCM-D with flow rate range of 0-100ml/min and maximum pressure of 160psi). The flow rate of He and nitrogen were controlled using flow meters supplied by Dwyer (flow rate range between 0-60ml/min, 250^oF and 200psi).

3.5.2 Fixed-bed microreactor

The fixed-bed microreactor consisted of a vertical micro-tubular fixed-bed reactor fabricated from stainless steel (SS316). As shown in Figure 3-5 the fixed-bed microreactor has the following dimensions: outer diameter (OD) =5.97mm, inner diameter (ID) =5mm, length =100mm, and volume =1962.5mm³. Tubular reactor was placed in a vertical electrical furnace (SE799A) capable of producing a temperature up to 900^oC. The temperature inside the reactor was measured using thermo-couple equipped with a PID (proportional integral derivative) controller. This reactor system is equipped with separator (25ml) for separating the gas and liquid products. The separator has a tap to allow collecting liquid product for offline analysis. The gaseous products were analyzed online using a gas chromatography.

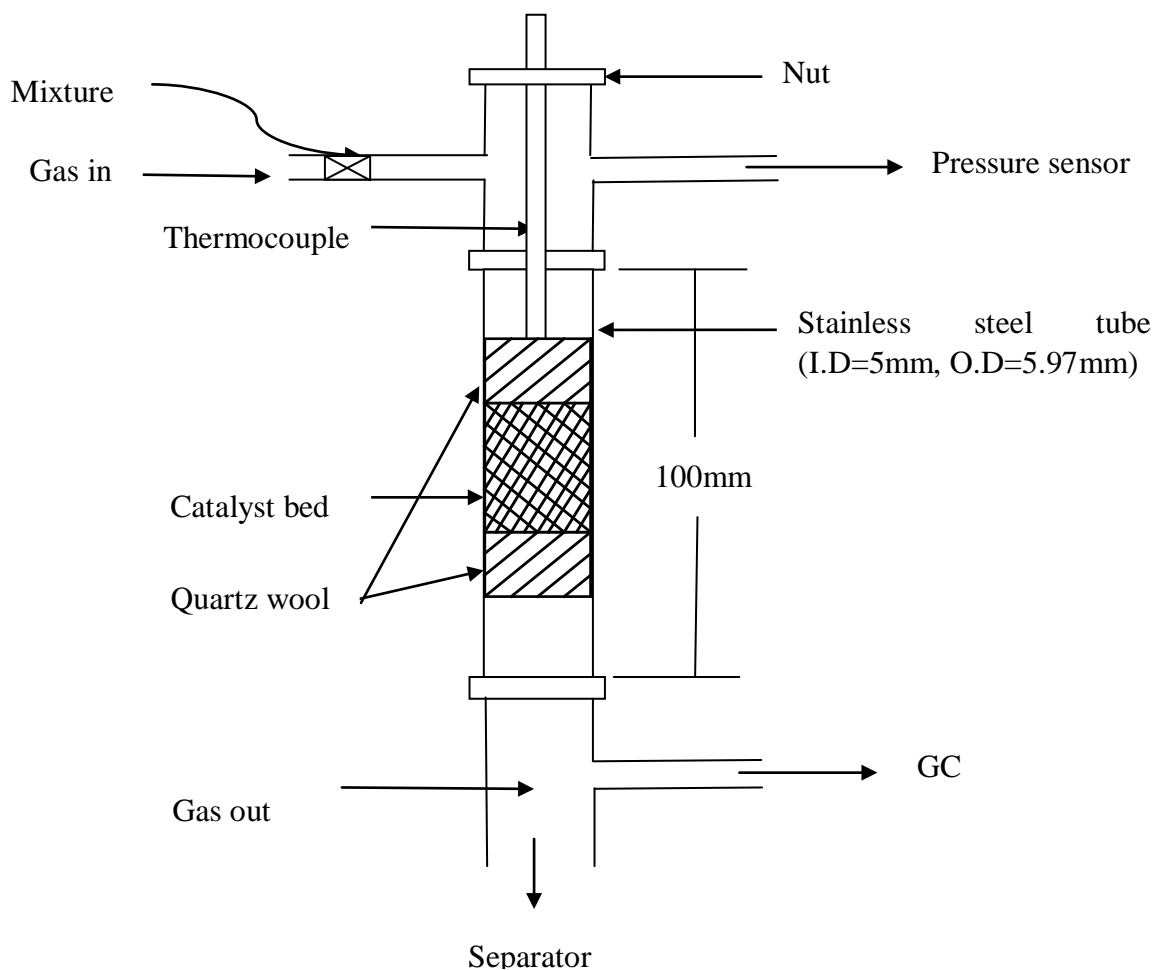


Figure 3-5: Schematic diagram of a fixed bed micro tubular reactor

3.5.3 On-line gas chromatograph (GC) system

The gaseous products were analyzed via on-line Agilent Hewlett Packard (HP) GC equipped with TCD and flame ionization detector (FID). The Gas chromatograph system consists of three columns designated as GC-AL/KCL, HP-Plot U, HP-Molesieve columns. The GC-AL/KCL column is ideal for separating hydrocarbon components that are gases at room temperature, while the other two columns are serially connected to separate light and gases hydrocarbons such as CH₄, CO₂, H₂O, CO, and H₂. Table 3-2 shows the specification of the GC columns. TCD and FID detectors were used to determine the specific components that were separated by those three columns. TCD (front detector) was used to identify components such as methane, CO, CO₂, and H₂. The FID (back detector) was applied to identify the

hydrocarbons. The GC-AL/KCL column was connected to the FID detector whereas the other two columns were connected serially to the TCD detector. He was used as a carrier gas where hydrogen was used for the FID detector.

Table 3-2: Specification of GC columns

| Column | Model | Dimension | | | Max Temp. (°C) | Flow rate (ml/min) |
|-----------|------------|------------|-----------|-----------|----------------|--------------------|
| | | Length (m) | I.D. (µm) | Film (µm) | | |
| GC-AL/KCL | 115-3332 | 29 | 530 | 3.0 | 200 | 8.0 |
| HP-Plot U | 19095P-U04 | 30 | 530 | 20 | 190 | 5.0 |
| HP-MolSiv | 19095P-MS9 | 15 | 530 | 50 | 300 | 5.0 |

3.5.3.1 Gas sampling system

The gas sampling system consisted of three pneumatic valves which are valve 1, valve 2, and valve 3. Figure 3-6 shows the flow diagram for the sequence of valves system. Gas analysis was started when these valves were opened at 0.00 min run time to allow the gas sample to be injected into the respective columns.

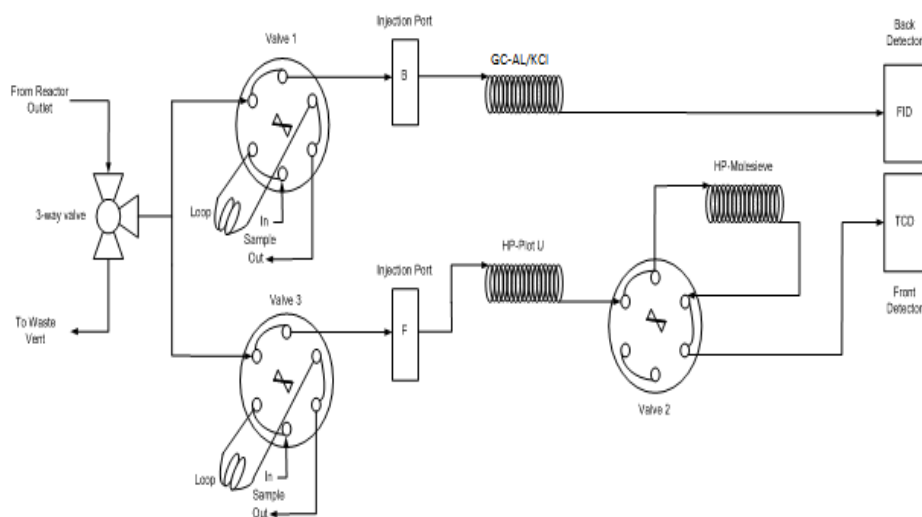


Figure 3-6: Gas sampling valve diagram in the GC

The procedures for analyzing the gaseous product from the microreactor are shown as follows:

- Analyze the gas via the front detector (TCD) (Table 3-3)
 - The gas sample entered the line where the valve 3 was turned on and the gas was flowed through the HP-Plot U and HP-Molesieve columns.
 - Valve 3 was closed at 0.5 min run time
 - Valve 2 was turned on at 2.6 min run time to prevent H₂O and CO₂ from entering the HP-Molesieve column which can damage the column.
 - Valve 2 was turned off at 3.3 min to let the gas sample to pass through the HP-Molesieve.
 - These gas sample was detected by TCD detector

Table 3-3: valve setting of the front detector

| Time (min) | Specifies | Parameter | Set-point |
|-------------------|------------------|------------------|------------------|
| 0.01 | Valve | 3 | On |
| 0.50 | Valve | 3 | Off |
| 2.60 | Valve | 2 | On |
| 3.30 | Valve | 2 | off |

- Analyze the gas through the back detector (FID) (Table 3-4)
 - Valve 1 was turned on at 0.01 min to allow the gas sample to enter the line
 - The sample was passed directly to the back line towards GC-AL/KCL
 - The separated gas was detected by FID detector

Table 3-4: valve setting of the back detector

| Time (min) | Specifies | Parameter | Set-point |
|-------------------|------------------|------------------|------------------|
| 0.01 | Valve | 1 | On |
| 0.50 | Valve | 1 | Off |

The GC calibration was carried out using Refinery Gas Analysis (RGA) standard, standard gas mixture containing (Scott specialty gas) CO, CO₂, H₂, and CH₄. The standard gases were injected into the GC to determine the retention time and peak

area corresponding to its amount. GC Calibration of standards are shown in Appendix B.

3.6 Catalyst pretreatment

All of the catalysts were reduced under the flow of the CO, 0.6L/h at 253K for 4h. This condition was selected based on prior studies in several laboratories [31] and [33]. Most of the researchers proposed CO to be the most preferable reducing gas especially for Fe-based catalyst, due to formation of Fe_2C_5 , which is considered as the primary active species during the FTS.

3.7 Catalysts testing

The performance of supported Fe-based catalysts in the FT reaction was examined in a fixed-bed microreactor (Figure 3-5) at atmospheric pressure. A detailed description of reactor and the product analysis system used in this study was illustrated in section 3.5.2 and 3.5.3. Briefly, 0.2g of the catalyst was held in the middle of the reactor tube between two layers of quartz wool. Then the reactor tube was placed in the electrical furnace. The reactor was purged with helium at flow rate of 1.2L/h for 15mins to purge the air out of the reactor tube and the line that was connected to the GC. The catalyst was firstly reduced in situ at atmospheric pressure in flowing carbon monoxide 3L/g-cat.h (0.6L/h) at the temperature of 553K for 4h.

After completion of the reduction step, the reactor was purged again with helium at 1.2L/h for 30mins until the temperature decreased from 553K to reaction temperature. The inert gas flow was then switched to a mixture of H_2 and CO at a desired feed ratio. Typically the FT reactions were conducted for 4h. Effluent gases from the reactor were analyzed by an on-line GC. Sampling was conducted at every 30mins and the evaluation of the CO conversion and product selectivity were made based on the average of the 4 reaction hours.

3.8 Reaction condition

FTS reaction was conducted at 1.5H₂/CO ratio, 3L/g-cat.h, 523K, and atmospheric pressure. Turn on procedure is shown in Appendix B. Additional study was conducted to investigate the effect of the reaction temperature (523, 543, and 563K), gas flow rate (0.6, 2.4, and 4.8L/h), and H₂/CO ratio (0.5, 1, 1.5, and 2) on the performance of impregnated and precipitated 6%Fe/SiO₂ catalyst.

CHAPTER 4

Results and Discussions

4.1 Introduction

One of the key elements to improve FT technology is to modify and develop the active catalyst with high FTS performance [66]. This chapter presents the results of catalysts characterization and reaction studies. The results are interpreted in terms of the catalytic structural properties and the catalytic performance. The catalytic properties such as textural properties, morphology, particles distribution, and catalyst reducibility were determined by N₂ physical adsorption, FESEM, TEM, XRD, and TPR. The effects of different synthesis techniques, supports, promoters, and Fe loading on the properties of the catalyst as well as the performance of Fe-based catalyst in the FTS under various reaction conditions are discussed in this section. The correlation between size of Fe nanoparticles and the performance in the FTS is also presented in this chapter.

4.2 Characterization of catalysts

4.2.1 Physical properties

The physical properties of the catalysts include the structural properties which had been determined through the N₂ physical adsorption measurement. The surface morphology and the size of the metal nanoparticles were measured using the FESEM and the TEM, respectively. XRD was used to determine the composition of the catalysts.

4.2.1.1 Textural properties

The surface area, pore volume, and average pore size of the catalysts were measured using N₂ physical adsorption. Measuring the surface area and pore volume is important since any changes on these properties are indicative of pore plugging and material sintering.

The textural properties of the SiO₂ and Al₂O₃-SiO₂ supports are shown in Table 4-1. The pore volume and the average pore size was determined using BJH method, as depicted in Figures 4-1 and 4-2 and their isotherms are shown in Figures 4-3 and 4-4. The raw data for N₂ adsorption studies are shown in Appendix C.

Addition of Al₂O₃ to the SiO₂ support increased the surface area and pore volume of the Al₂O₃-SiO₂ support. The BET surface area was strongly dependent on the ratio between Al₂O₃ and SiO₂. At Al₂O₃/SiO₂ ratio of (25:75) the largest surface area of 211.4m²/g was obtained compared to 54.9m²/g from that of the lower Al₂O₃/SiO₂ (5:95) ratio. The difference in the support's surface area could be due to the presence of the mesopores at higher ratio of Al₂O₃/SiO₂ support. Figure 4-2 shows two kinds of pores existed in support with higher Al₂O₃/SiO₂ ratio of (25:75) whereas only one kind of pore was obtained in the SiO₂ support (Figure 4-1). These indicate that textural properties of SiO₂ were changed from nonporous material (Figure 4-3) to porous support upon addition of Al₂O₃ (Figure 4-4). Similar trend was also obtained by Zhang and co-workers [82], who reported that increasing the surface area was due to impregnation of Al₂O₃ on silica gel to form Al₂O₃-SiO₂ bimodal, where Al₂O₃-SiO₂ bimodal had a surface area of 101 m²/g compared to silica-gel at 70m²/g.

Table 4-1: Textural properties of the supports

| Sample | Ratio (wt %) | BET surface area (m ² /g) | Pore volume (cc/g) | Average pore size (Å) |
|--|--------------|--------------------------------------|--------------------|-----------------------|
| SiO ₂ | - | 40.9 | 0.094 | 91.79 |
| Al ₂ O ₃ -SiO ₂ | 5:95 | 54.9 | 0.173 | 125.96 |
| Al ₂ O ₃ -SiO ₂ | 15:85 | 106.2 | 0.282 | 106.28 |
| Al ₂ O ₃ -SiO ₂ | 25:75 | 211.4 | 0.561 | 106.20 |

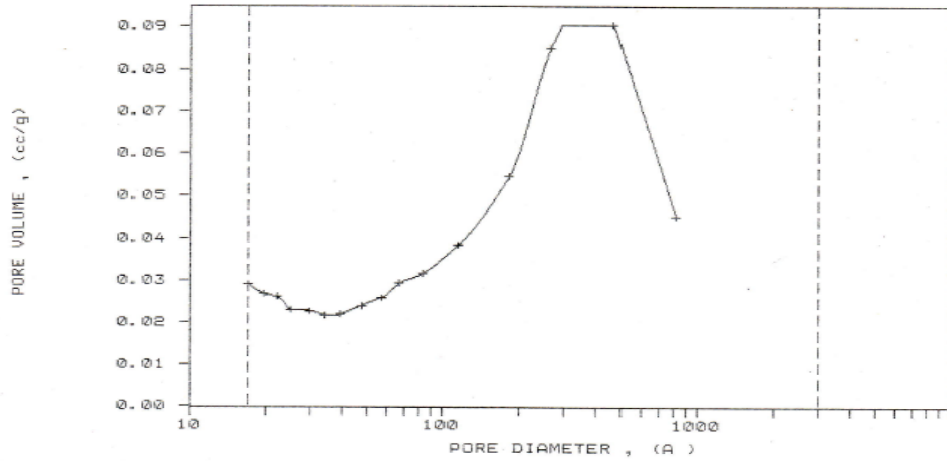


Figure 4-1: Desorption pore volume plot by BJH method of SiO₂ support

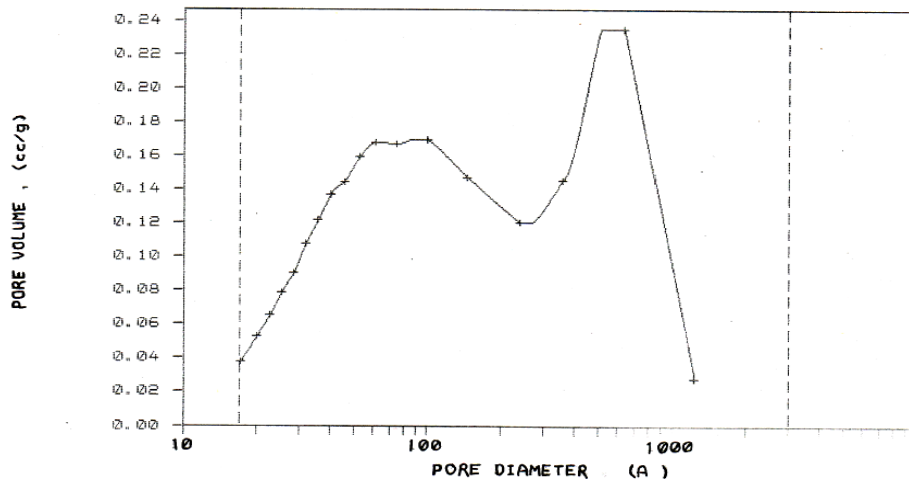


Figure 4-2: Desorption pore volume plot by BJH method of Al₂O₃-SiO₂ (25:50) support

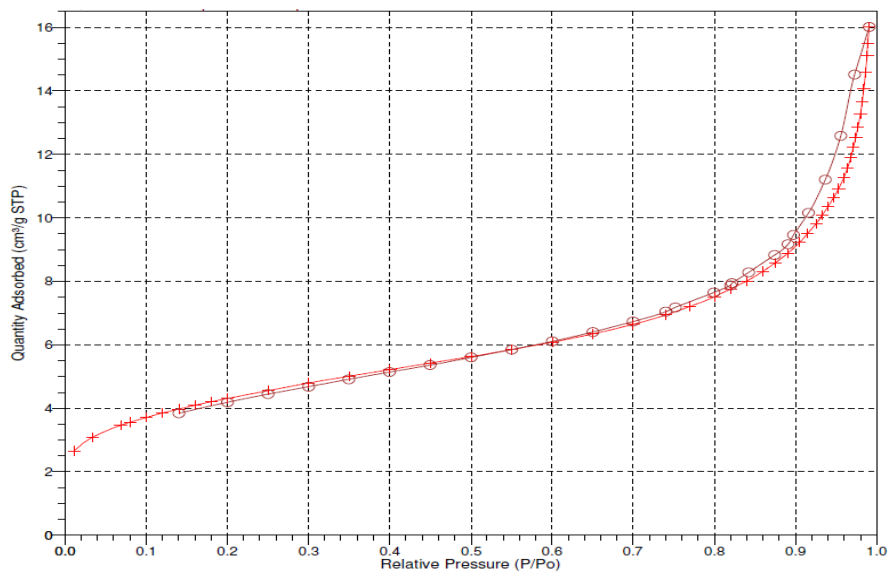


Figure 4-3: Isotherm linear plot of SiO₂ support

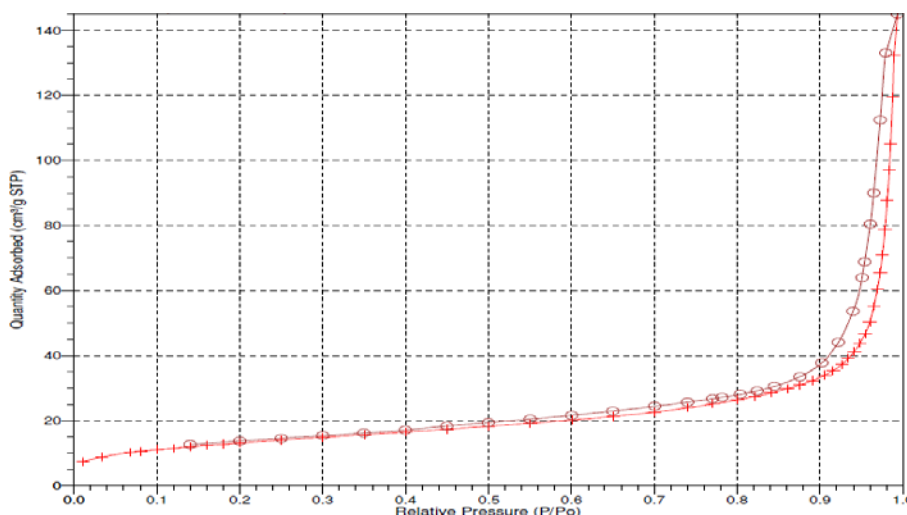


Figure 4-4: Isotherm linear plot of $\text{Al}_2\text{O}_3\text{-SiO}_2$ support

The BET surface area for SiO_2 -supported Fe-based catalyst prepared by impregnation and precipitation methods at different Fe loadings (3, 6, 10, 15 wt %) are shown in Table 4-2 and the data of BET calculation appear in Appendix C. An opposite trend was observed between the Fe loading and the BET surface area of the catalysts. The BET surface area decreased from $57.8\text{m}^2/\text{g}$ to $23.9\text{m}^2/\text{g}$ when Fe loading increased from 3% to 15%. This trend agreed with that reported by Pirola *et al.* [29] where they found that the catalyst surface area was strongly affected by the Fe loading. They also discovered that increasing Fe loading from 10 to 50 wt% resulted in a decrease in the BET surface area from 262 to $143\text{m}^2/\text{g}$, respectively.

The Fe/ SiO_2 catalyst synthesized via precipitation method displayed larger surface area and pore volume compared to samples that were prepared by impregnation method. For the same Fe loading e.g. 6wt% Fe/ SiO_2 catalysts prepared by impregnation method had surface area of $39.5\text{m}^2/\text{g}$ while the one prepared by precipitation method had surface area of $45.1\text{m}^2/\text{g}$. This difference can be explained in terms of the appearance of the small pores in the precipitated catalysts. The lower pore diameter permits greater number of pores to be existed in the catalyst structure and make it more porous and increased the catalyst surface area. Similar trend for the surface area of impregnated catalysts was also obtained due to the influence of the Fe loading on the surface area for the precipitated catalysts. BET surface area decreased from 45.1 to $40.6\text{m}^2/\text{g}$ when Fe loading increased from 6 to 15wt%.

Table 4-2: Textural properties of Fe/SiO₂ catalysts synthesized via impregnation and precipitation methods

| sample | Fe Loading (wt %) | BET surface area (m ² /g) | Pore volume (cc/g) | Average pore size (Å) | Preparation technique |
|---------------------|-------------------|--------------------------------------|--------------------|-----------------------|-----------------------|
| SiO ₂ | - | 40.9 | 0.094 | 91.79 | Commercial |
| Fe/SiO ₂ | 3 | 57.8 | 0.258 | 164.86 | Impregnation |
| Fe/SiO ₂ | 6 | 39.5 | 0.155 | 156.76 | Impregnation |
| Fe/SiO ₂ | 10 | 23.8 | 0.088 | 147.85 | Impregnation |
| Fe/SiO ₂ | 15 | 23.9 | 0.071 | 144.12 | Impregnation |
| Fe/SiO ₂ | 3 | 47.2 | 0.151 | 128.51 | Precipitation |
| Fe/SiO ₂ | 6 | 45.1 | 0.124 | 110.14 | Precipitation |
| Fe/SiO ₂ | 10 | 43.1 | 0.140 | 130.18 | Precipitation |
| Fe/SiO ₂ | 15 | 40.6 | 0.118 | 116.31 | Precipitation |

The textural properties of supported Fe-based catalysts having different Fe loadings on SiO₂ and Al₂O₃-SiO₂ supports, prepared by impregnation method are shown in Table 4-3. The BET surface area of the supported Fe nanoparticle catalysts was strongly dependent on the loading of the active site (Fe) and the type of the support. Increasing the Fe loading resulted in a decrease in the BET surface area of the catalysts. Surface areas of the catalysts were also affected by the type of the support. Fe-based catalysts supported on Al₂O₃-SiO₂ had bigger surface area and pore volume compared to those of SiO₂ support. This difference could be due to the bigger surface area of the Al₂O₃-SiO₂ compared to the SiO₂ support. An opposite trend was reported by Wan *et al.* [17] where larger surface areas were obtained for catalysts that were supported on SiO₂ and the surface area decreased by increasing of Al₂O₃/SiO₂ ratio, and reaches the minimum on the catalyst that was only supported on Al₂O₃ support. The difference in trend may be due to the fact that Al₂O₃ is more effective than SiO₂ in dispersing Fe particles. This discrepancy may be caused by the different catalyst preparation procedures, where they used a combination of co-precipitation and spray dried method for synthesis of the catalysts and also their catalyst was promoted by K and Cu which also influenced the change in surface area.

Table 4-3: Textural properties of Fe-based catalyst on SiO₂ and Al₂O₃-SiO₂ supported synthesized via impregnation method

| sample | Fe Loading (wt %) | BET surface area (m ² /g) | Pore volume (cc/g) | Average pore size (Å) | Preparation technique |
|---|-------------------|--------------------------------------|--------------------|-----------------------|-----------------------|
| SiO ₂ | - | 40.9 | 0.094 | 91.79 | Commercial |
| Fe/SiO ₂ | 3 | 57.8 | 0.258 | 164.86 | Impregnation |
| Fe/SiO ₂ | 6 | 39.5 | 0.155 | 156.76 | Impregnation |
| Fe/SiO ₂ | 10 | 23.8 | 0.088 | 147.85 | Impregnation |
| Fe/SiO ₂ | 15 | 23.9 | 0.071 | 144.12 | Impregnation |
| Al ₂ O ₃ -SiO ₂ (5:95) | - | 54.9 | 0.173 | 125.96 | Impregnation |
| Fe/Al ₂ O ₃ -SiO ₂ | 3 | 59.2 | 0.295 | 212.46 | Impregnation |
| Fe/Al ₂ O ₃ -SiO ₂ | 6 | 57 | 0.288 | 202.73 | Impregnation |
| Fe/Al ₂ O ₃ -SiO ₂ | 10 | 53 | 0.214 | 184.28 | Impregnation |
| Fe/Al ₂ O ₃ -SiO ₂ | 15 | 43 | 0.179 | 167.03 | Impregnation |

The effect of the promoters, such as K and Cu on the catalysts textural properties are illustrated in Table 4-4. The promoters influenced the values of surface area, pore volume, and average pore size. Fe/SiO₂ catalyst was chosen to study the effect of promoter because SiO₂ which had lower surface area and better morphology compared to Al₂O₃-SiO₂ support. Lower surface area at range of 20-60 m²/g is required because it showed nonporous material which it can be easily used to study the influence and distribution of the Fe particles over the support and the catalytic morphology. Addition of Cu to Fe/SiO₂ resulted in increase the surface area compared to un-promoted (Fe/SiO₂). The addition of Cu promoter may have facilitated the dispersion of the Fe crystallites which resulted in increase in the surface area of the catalyst. K promoter has an opposite trend compared to Cu. Surface area was reduced by introducing K as a promoter. This result could be due to the fact that K enhanced the agglomeration, enlarged the crystallite size of Fe₂O₃ after calcination, and blocked

the pores of the catalyst, which would result in the decrease in the surface area. Work of Yang *et al.* [83] over precipitated Fe/Mn/K catalyst have also led to a similar conclusion: increasing the K loading resulted in smaller pore diameters and lower specific surface area.

The effect of a double promotion on the surface area, pore volume and average pore size was also investigated using N₂ physical adsorption. Compared to Fe/SiO₂ catalyst, a greater loss on the catalyst surface area and pore volume were obtained for Fe/Cu/K/SiO₂ catalysts. This result showed that the addition of K promoter severely decreased the surface area and pore volume of Fe/K/SiO₂ and Fe/Cu/K/SiO₂ catalysts as compared to that of Fe/SiO₂ catalyst. Wan *et al.* [57] observed a similar trend over precipitated Fe-based catalysts promoted by K and Cu where they found that addition of Cu promoter resulted in a larger surface area compared to Fe, Fe/K, Fe/Cu/K catalysts while addition of K promoter resulted in a smaller surface area and pore volume.

Table 4-4: BET surface area, pore volume and average pore size of the promoted catalysts prepared via impregnation method

| Sample | Loading (wt %) | BET surface area (m²/g) | Pore volume (cc/g) | Average pore size (Å) |
|--------------------------|-----------------------|---|---------------------------|------------------------------|
| Fe/SiO ₂ | 6%Fe | 39.5 | 0.155 | 156.76 |
| Fe/SiO ₂ | 10%Fe | 23.8 | 0.088 | 147.85 |
| Fe/SiO ₂ | 15%Fe | 23.9 | 0.071 | 144.12 |
| Fe/Cu/SiO ₂ | 6%Fe/2%Cu | 39.7 | 0.109 | 109.90 |
| Fe/Cu/SiO ₂ | 10%Fe/2%Cu | 41.7 | 0.160 | 153.65 |
| Fe/Cu/SiO ₂ | 15%Fe/2%Cu | 65.4 | 0.196 | 120.10 |
| Fe/K/SiO ₂ | 6%Fe/4%K | 33.2 | 0.115 | 138.89 |
| Fe/K/SiO ₂ | 10%Fe/4%K | 34.3 | 0.108 | 125.51 |
| Fe/K/SiO ₂ | 15%Fe/4%K | 38.7 | 0.095 | 98.49 |
| Fe/Cu/K/SiO ₂ | 6%Fe/2%Cu/4%K | 15.5 | 0.022 | 52.91 |
| Fe/Cu/K/SiO ₂ | 10%Fe/2%Cu/4%K | 14.0 | 0.019 | 56.08 |
| Fe/Cu/K/SiO ₂ | 15%Fe/2%Cu/4%K | 6.3 | 0.032 | 204.83 |

The findings can be summarized as follows:

- The surface area of the catalyst was strongly influenced by the preparation technique. Precipitation method resulted in larger surface area, pore volume, and smaller average pore size compared to those of impregnation method.
- Both synthesis techniques show similar trend for the influence of the Fe loading. Increasing Fe loading from 6 to 15 wt% resulted in significant decrease of the surface area from 39.5 to 23.9m²/g, for the catalysts prepared by impregnation method and from 45.1 to 40.6m²/g for the catalysts synthesized via the precipitation technique.
- The catalytic textural properties were also affected by the type of the support. Fe-based catalyst supported by Al₂O₃-SiO₂ had a bigger surface area compared to that of SiO₂ support.
- Addition of Cu promoter resulted in a larger surface area and pore volume while the opposite trend was observed by the addition of K promoter.

4.2.1.2 Catalyst morphology

Field emission scanning electron microscopy and transmission electron microscopy were used to obtain information on the morphology of the catalyst.

I. Morphology and elemental analysis

FESEM-EDX analysis were carried out to study the surface properties of SiO₂ and Al₂O₃-SiO₂ supported Fe-based containing different Fe loading prepared by the impregnation and precipitation methods, and the promoted catalysts: Fe/Cu/SiO₂, Fe/K/SiO₂, and Fe/Cu/K/SiO₂.

The morphologies for the SiO₂-supported Fe-based catalyst at different Fe loadings synthesized via impregnation technique are shown in Figure 4-5. The SiO₂ particles were roughly spherical with diameter of 100-200nm. Some of the Fe particles were attached directly onto the surface of the SiO₂ support whereas some of them were positioned in between the SiO₂ spheres. Although, there was no great differences in morphologies among the catalysts with different metal loadings (Figure

4-5) higher amount of the Fe nanoparticles were deposited in between the support particles. FESEM reveals that the Fe/SiO₂ catalysts have diameters ranging from 90-170nm.

Compared to the catalysts prepared by impregnation method, precipitated catalysts (prepared by precipitation method) showed more agglomeration (Figure 4-6) which was due to difference in preparation procedure. As discussed in section 2.4.2 precipitation method occurred in three steps: super-saturation, nucleation, and growth and those steps, specially nucleation and growth of the particles affect the dispersion of those particles. This display the presence of agglomeration in the case of precipitated catalyst compare to those of impregnated catalyst.

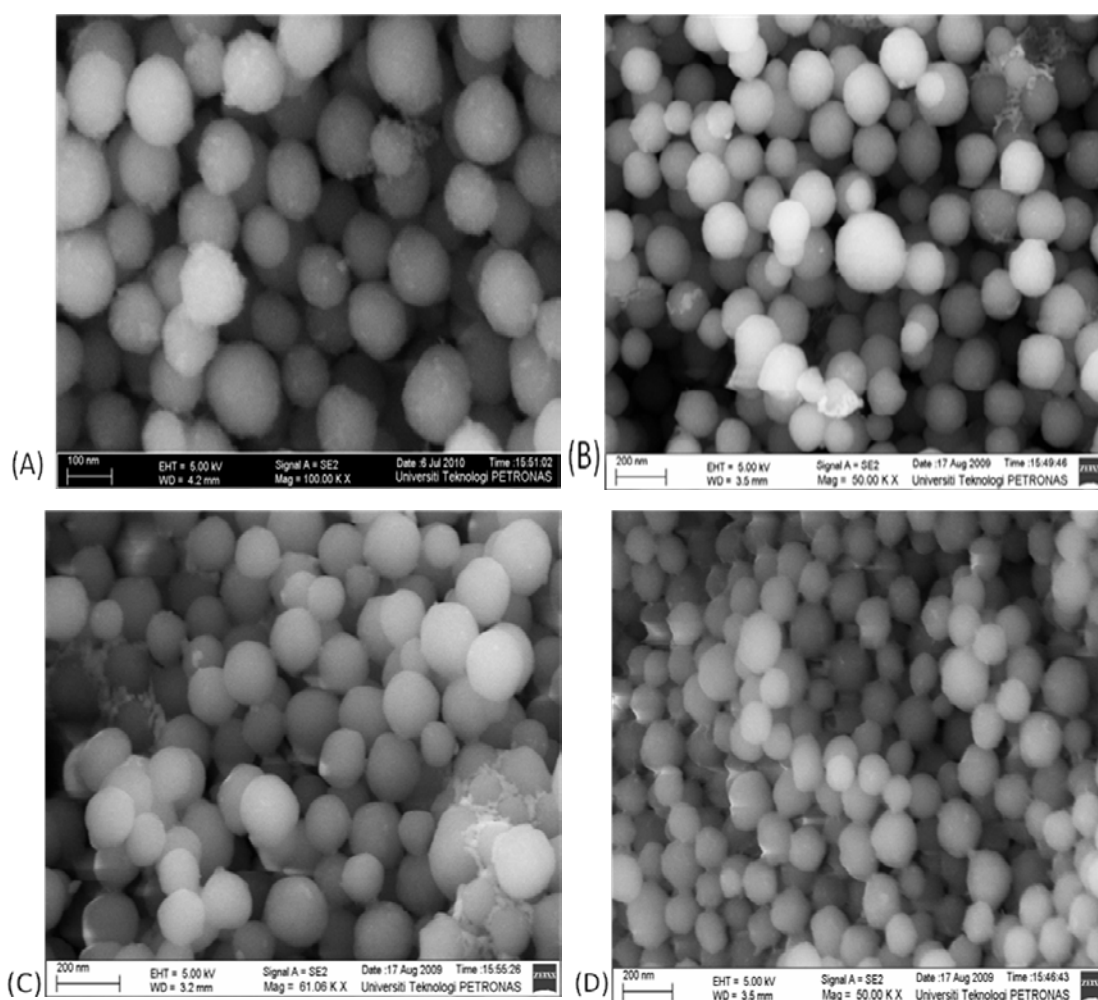


Figure 4-5: FESEM micrographs of Fe/SiO₂ catalysts prepared via impregnation method at Fe loading (A) 3, (B) 6, (C) 10, and (D) 15 wt %

The introduction of Al_2O_3 in SiO_2 support changed the textural properties of the support and led to more agglomeration (Figure 4-7). Better dispersion of the Fe nanoparticles was observed on the SiO_2 -supported catalyst prepared by impregnation method compared to those supported on Al_2O_3 - SiO_2 or synthesized via precipitation method.

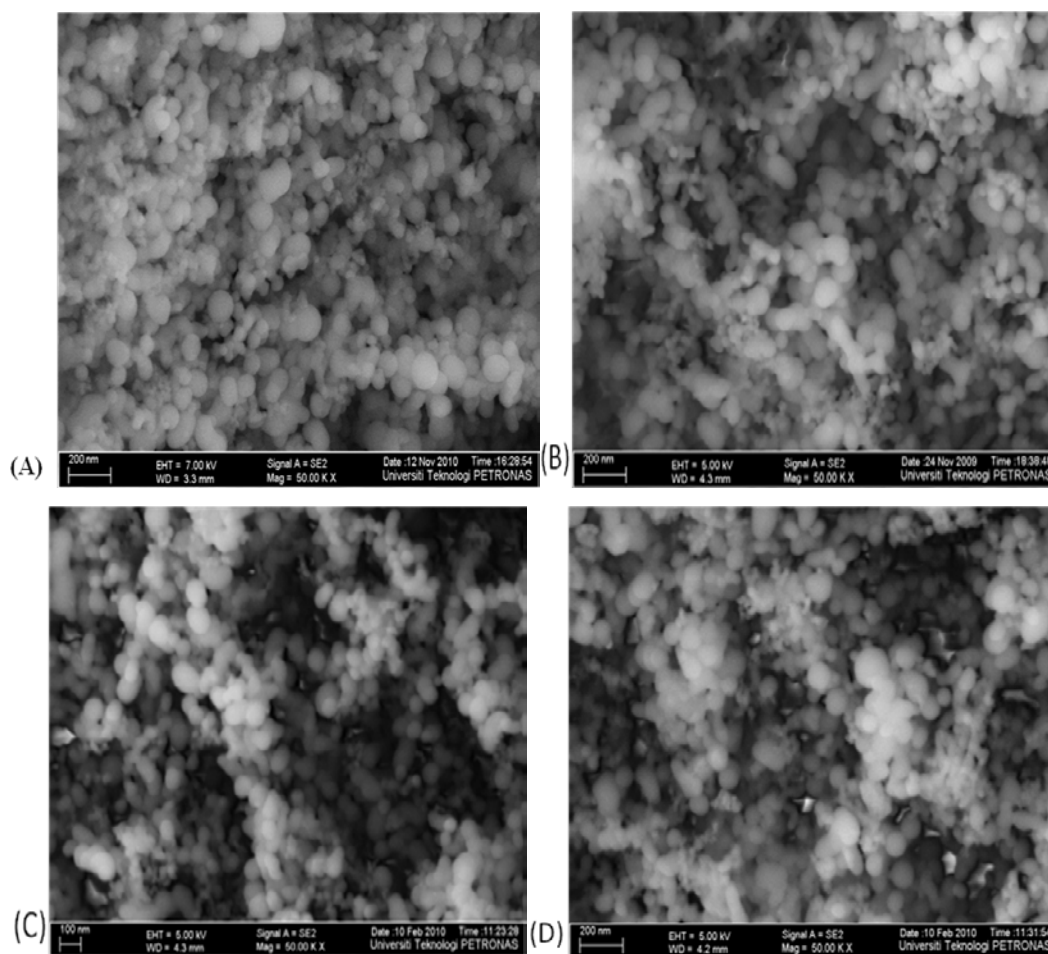


Figure 4-6: FESEM images of Fe/SiO_2 catalysts prepared by precipitation method at Fe loading (A) 3, (B) 6, (C) 10, and (D) 15wt%

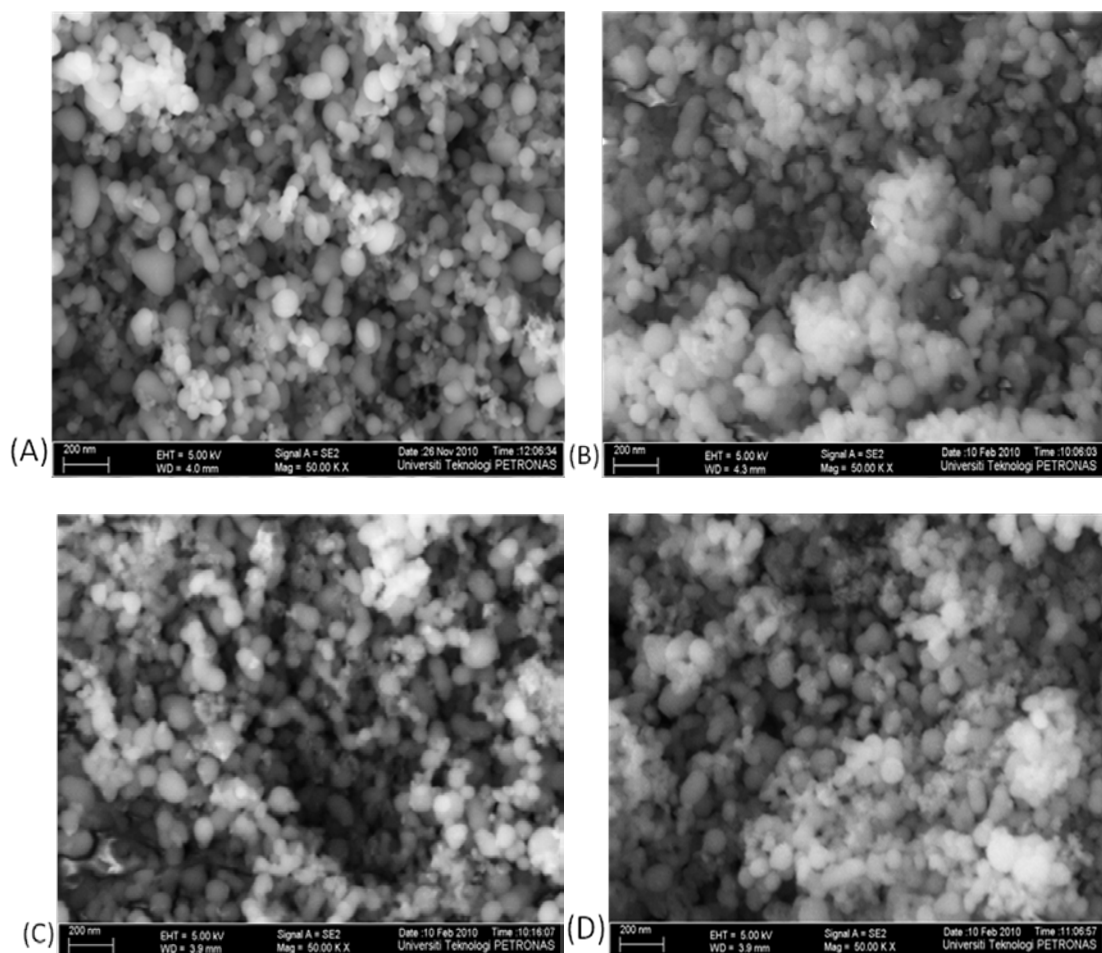


Figure 4-7: FESEM images Fe nanoparticles on Al₂O₃-SiO₂ prepared by impregnation method at Fe loading (A) 3, (B) 6, (C) 10, and (D) 15wt%

The morphological changes which occurred due to addition of promoters are shown in Figure 4-8. Compared to the unpromoted catalyst, catalysts promoted with Cu, K, and mixed promotion of Cu and K showed highly agglomerated particles with irregular shapes. These FESEM images confirmed the results obtained by the N₂ adsorption method where smaller surface areas were obtained for K-promoted Fe/SiO₂. The catalyst surface area was strongly dependent on the distribution or aggregation of the metal particles over the support.

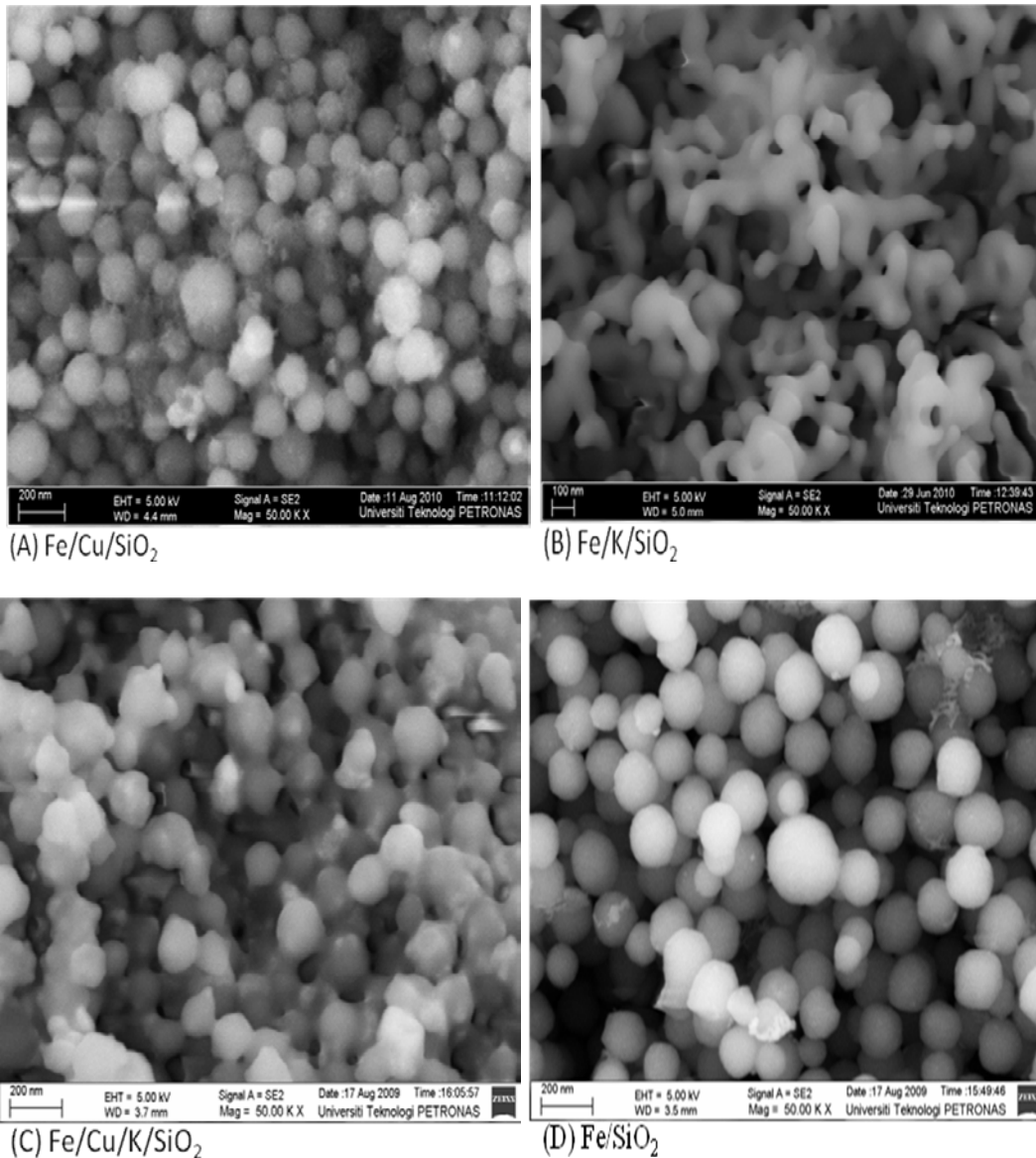


Figure 4-8: FESEM images of promoted and unpromoted Fe nanoparticles catalyst prepared by impregnation method

Elemental mapping from EDX was used to determine the distribution of the elements and the amount of the elements present over the support. The elemental mapping of Fe/SiO_2 catalysts prepared by impregnation method is shown in Appendix D. A uniform dispersion of the active sites (Fe) was observed on the Fe/SiO_2 catalyst prepared by impregnation method. This result is in good agreement with the FESEM image where it showed that better distribution of the Fe nanoparticles was observed for the impregnated catalysts. In addition, the elemental mapping showed that distribution of the active metal (Fe) over the support was not affected by the Fe loading and this was also confirmed by the FESEM images where no big change was

obtained by using different Fe loading. A similar trend was obtained for the Fe/Al₂O₃-SiO₂ catalysts (shown in Appendix D). While a slight change on the Fe distributions was observed by increasing the Fe loading from 6 to 15 wt% of Fe/SiO₂ prepared by precipitation method and led to more agglomeration of the Fe nanoparticles (Appendix D).

The elemental composition of the synthesized catalysts was determined using EDX and the results are shown in Tables 4-5, 4-6, and 4-7, as well as Figure 4-9. The values for the elements obtained by experiments were in good agreement with the estimated values, which were calculated based on the amount of each element compared to the total catalyst amount. A small deviation was observed between the calculated value and the measured value of the Fe. This deviation can be attributed to the loss of the elements during the preparation step or drying and calcination steps. The oxygen composition increased with increasing the metal loading as Fe existed in the oxide form.

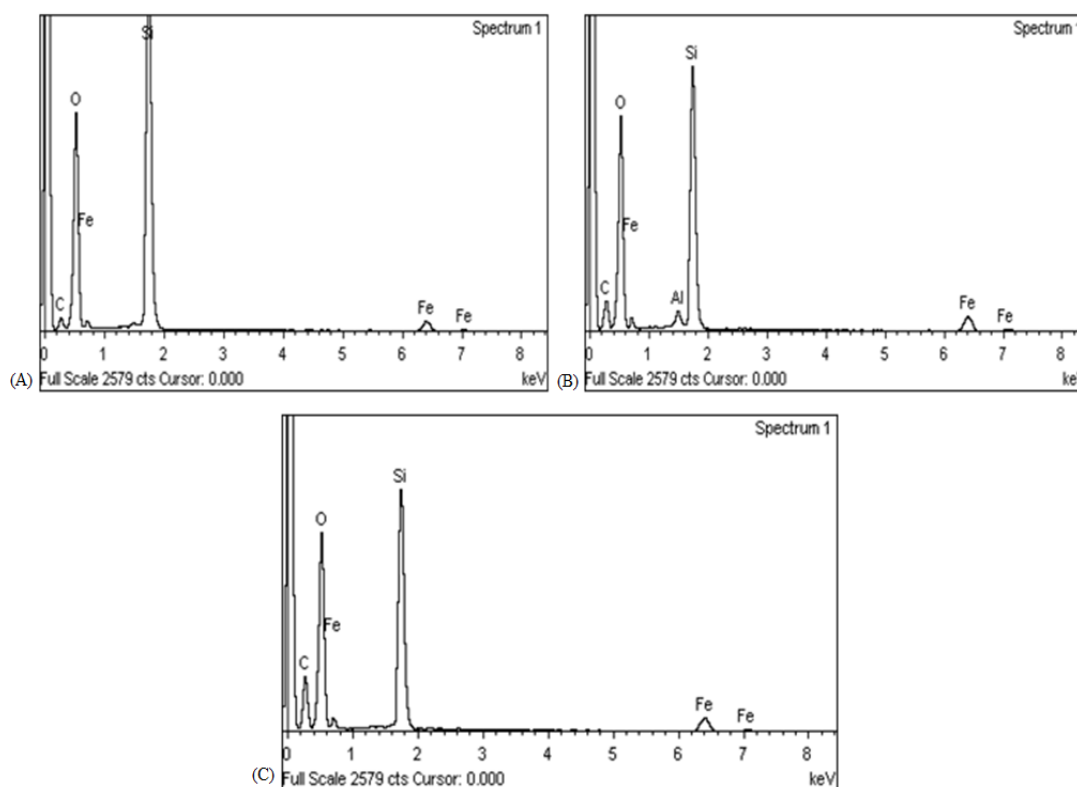


Figure 4-9: EDX spectrum of (a) Fe/SiO₂ catalyst prepared by impregnation method, (b) Fe/Al₂O₃-SiO₂ catalyst prepared by impregnation method, and (c) Fe/SiO₂ catalyst prepared by precipitation method

Table 4-5: EDX elemental analyses over Fe-based catalysts supported by SiO₂ and Al₂O₃

| Element | Element composition (wt %) | | | | | |
|-------------------|-------------------------------|-------|-------|---|-------|-------|
| | Fe/SiO ₂ catalysts | | | Fe/Al ₂ O ₃ -SiO ₂ catalysts | | |
| Theoretical value | 6%Fe | 10%Fe | 15%Fe | 6%Fe | 10%Fe | 15%Fe |
| Fe | 5.50 | 9.12 | 14.35 | 6.33 | 8.74 | 13.47 |
| Si | 26.94 | 26.57 | 26.01 | 24.83 | 20.61 | 20.23 |
| Al | - | - | - | 1.96 | 1.05 | 1.62 |
| O | 48.96 | 46.02 | 50.22 | 45.06 | 47.96 | 49.25 |
| C | 18.60 | 18.37 | 9.42 | 21.82 | 21.64 | 15.43 |

Table 4-6: EDX elemental analyses over SiO₂ supported Fe-based catalysts prepared by impregnation and precipitation

| Element | Element composition (wt %) | | | | | |
|-------------------|----------------------------|-------|-------|-----------------------|-------|-------|
| | Impregnated catalyst | | | Precipitated catalyst | | |
| Theoretical value | 6%Fe | 10%Fe | 15%Fe | 6%Fe | 10%Fe | 15%Fe |
| Fe | 5.50 | 9.12 | 14.35 | 4.27 | 7.77 | 12.68 |
| Si | 26.94 | 26.57 | 26.01 | 23.60 | 17.36 | 22.81 |
| O | 48.96 | 46.02 | 50.22 | 49.91 | 45.82 | 47.93 |
| C | 18.60 | 18.37 | 9.42 | 22.22 | 29.05 | 16.58 |

Table 4-7: EDX elemental analyses over SiO₂ supported Fe-based catalysts and promoted catalyst with Cu, K, and Cu/K

| Element | Element composition (wt %) | | | |
|-------------------|----------------------------|--------------------------|-------------------------|----------------------------|
| | 6%Fe/SiO ₂ | 6%Fe/Cu/SiO ₂ | 6%Fe/K/SiO ₂ | 6%Fe/Cu/K/SiO ₂ |
| Theoretical value | 6% Fe | 6% Fe, 2% Cu | 6% Fe, 4% K | 6% Fe, 2% Cu, 4% K |
| Fe | 5.50 | 4.00 | 4.92 | 6.07 |
| Si | 26.94 | 21.62 | 28.71 | 35.22 |
| O | 48.96 | 49.28 | 47.55 | 48.54 |
| C | 18.60 | 21.90 | 16.00 | 5.00 |
| Cu or K | - | 2.66 | 3.16 | 5.18 |

II. Particle size and distribution

TEM is a useful tool to determine size of crystallites and its distribution over the surface of the support. TEM technique was used in this study to measure the particle size of Fe crystallites and the dispersion of Fe particles over SiO₂ and Al₂O₃-SiO₂ supports. The effect of the synthesis technique, Fe loading, and type of the support on the particle size of Fe crystallites and distribution were also investigated using TEM technique. The average particles size of Fe was calculated using 15-20 Fe particles over the support.

Smaller particles and more uniform distribution of the Fe nanoparticles were observed on the Fe/SiO₂ catalyst prepared by impregnation method compared to those synthesized via the precipitation technique as shown in Figures 4-10 and 4-12. The catalyst particle has a strong potential to undergo either fragmentation or growth in size depending on the process conditions [84]. The difference in the size of Fe nanoparticles and distribution between impregnated and precipitated catalyst was due to difference in preparation condition where addition of the precipitating agent in the precipitation method accelerated the nucleation and growth of the Fe particles due to formation of the precipitate. This resulted in formation of less dispersed and bigger Fe nanoparticles over the support for the precipitated catalyst. TEM results show that Fe loading affected the distribution and the size of the Fe particles over the support. As can be seen from Figure 4-11, catalysts with low Fe loading have smaller particle size compared to those at higher loading for Fe/SiO₂ prepared by impregnation method. The 3%Fe/SiO₂ catalysts prepared via impregnation method had average particle size of 5.8 ± 1.3 nm whereas at Fe loadings of 6, 10, and 15wt%, average particle size increased to 8.6 ± 1.1 , 12.6 ± 1.3 and 13 ± 1.2 nm, respectively. Similar trend was observed on the Fe/SiO₂ catalysts prepared by precipitation where the average particle size increased by increasing the Fe loading (Figure 4-13). The precipitation method produced Fe nanoparticles with broader size distribution compared to that of impregnation method (Figures 4-11 and 4-13).

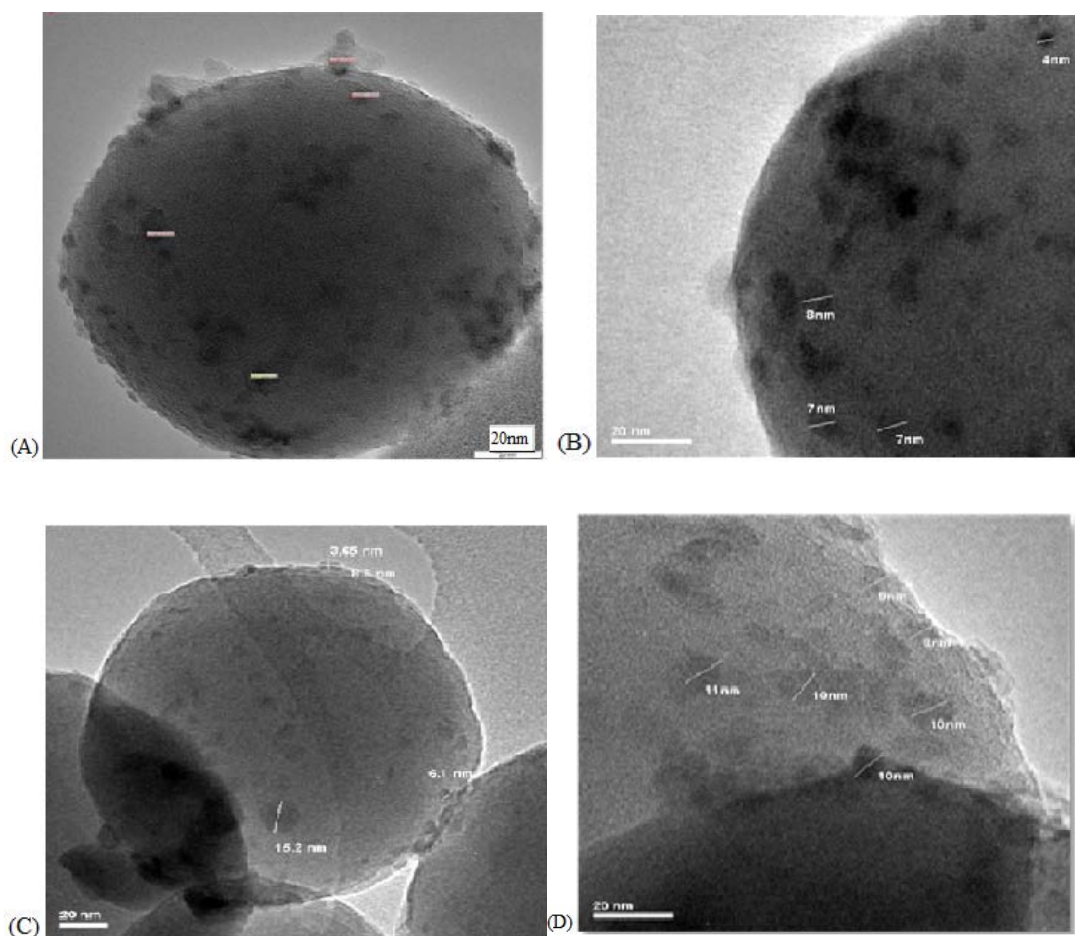


Figure 4-10: TEM image for silica supported Fe catalyst prepared by impregnation method at Fe loading (A) 3, (B) 6, (C) 10, and (D) 15wt%

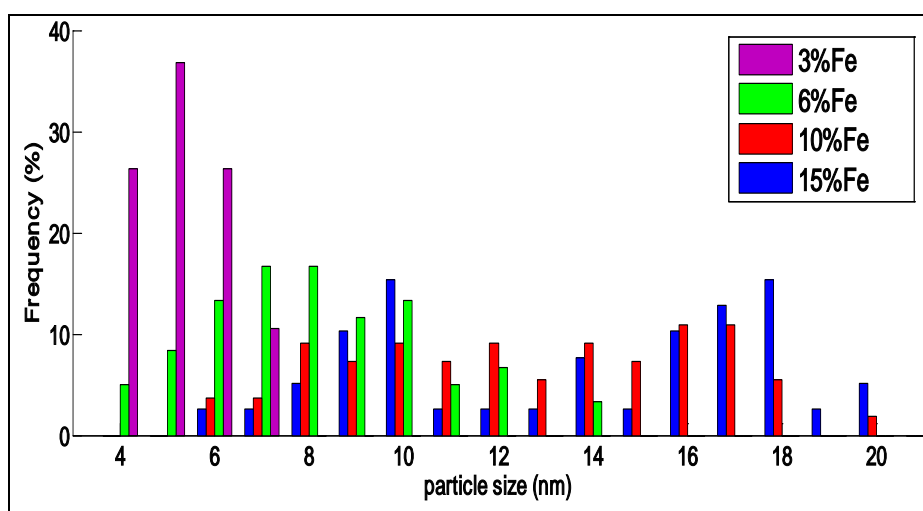


Figure 4-11: Particle size distribution for 3, 6, 10, and 15 wt % Fe/ SiO₂ catalysts prepared by impregnation method

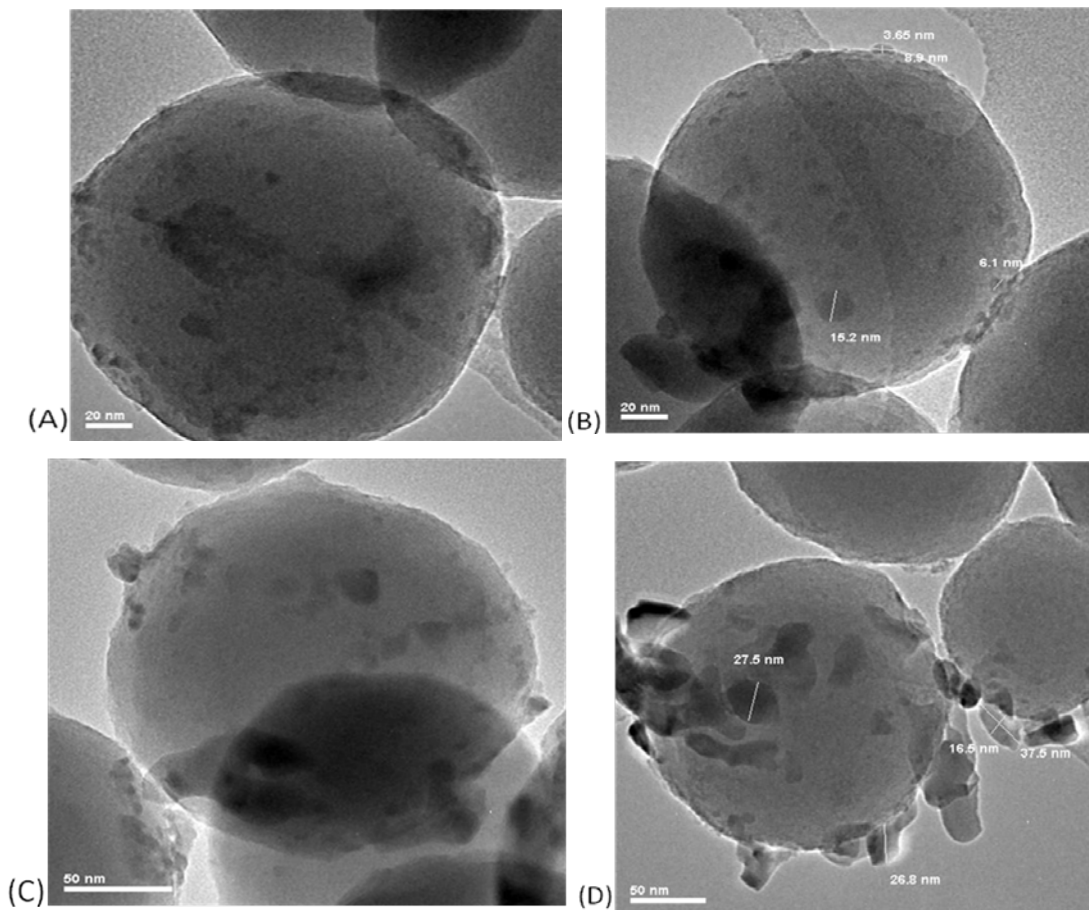


Figure 4-12: TEM image of silica supported Fe-based catalysts prepared by precipitation method at Fe loading (A)3, (B)6, (C) 10 and (D) 15wt%

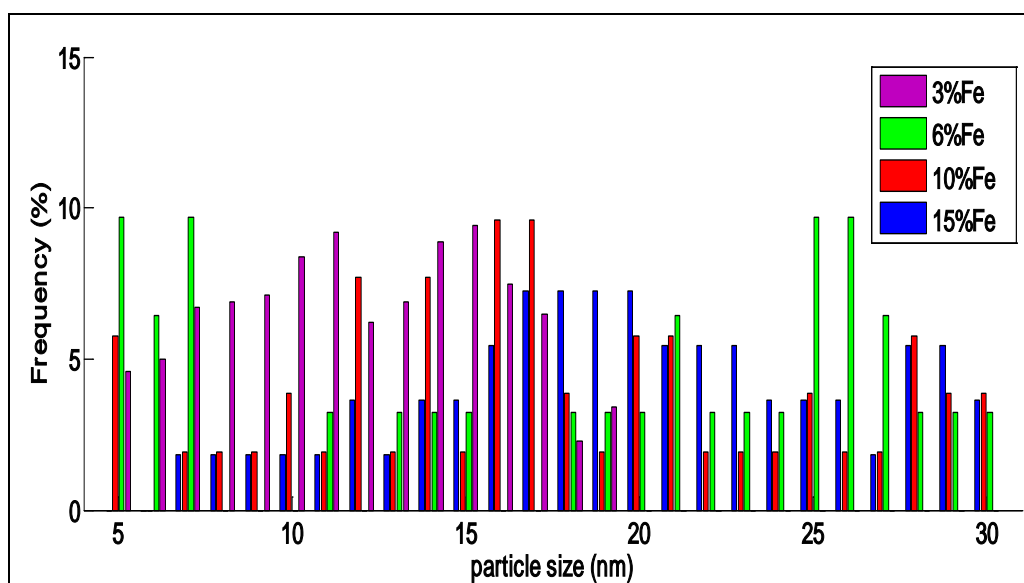


Figure 4-13: Particle size distribution for 3, 6, 10, and 15 wt %Fe on SiO₂ support prepared by precipitation method

Figure 4-14 shows the TEM image of Fe on $\text{Al}_2\text{O}_3\text{-SiO}_2$ support. The morphology of Fe nanoparticles was altered when the support was changed from SiO_2 to $\text{Al}_2\text{O}_3\text{-SiO}_2$ support. The particle size distribution for Fe on $\text{Al}_2\text{O}_3\text{-SiO}_2$ support is shown in Figure 4-15. Bigger particles with a broader range of distribution were observed on the $\text{Al}_2\text{O}_3\text{-SiO}_2$ support compared to those obtained on the SiO_2 support (Figure 4-11). The textural properties of the support play an important role in controlling the dispersion of the metal on the support. The support with a narrow pore range led to production of small metal particles compare to those of larger pore. SiO_2 has smaller average pore size of 91.79 nm compared to those of $\text{Al}_2\text{O}_3\text{-SiO}_2$ (125.95 nm). The effect of SiO_2 on the dispersion of catalyst crystallites compared to Al_2O_3 was reported by Hai-jun et al. [13] and they indicated that SiO_2 facilitated the dispersion of catalyst crystallites.

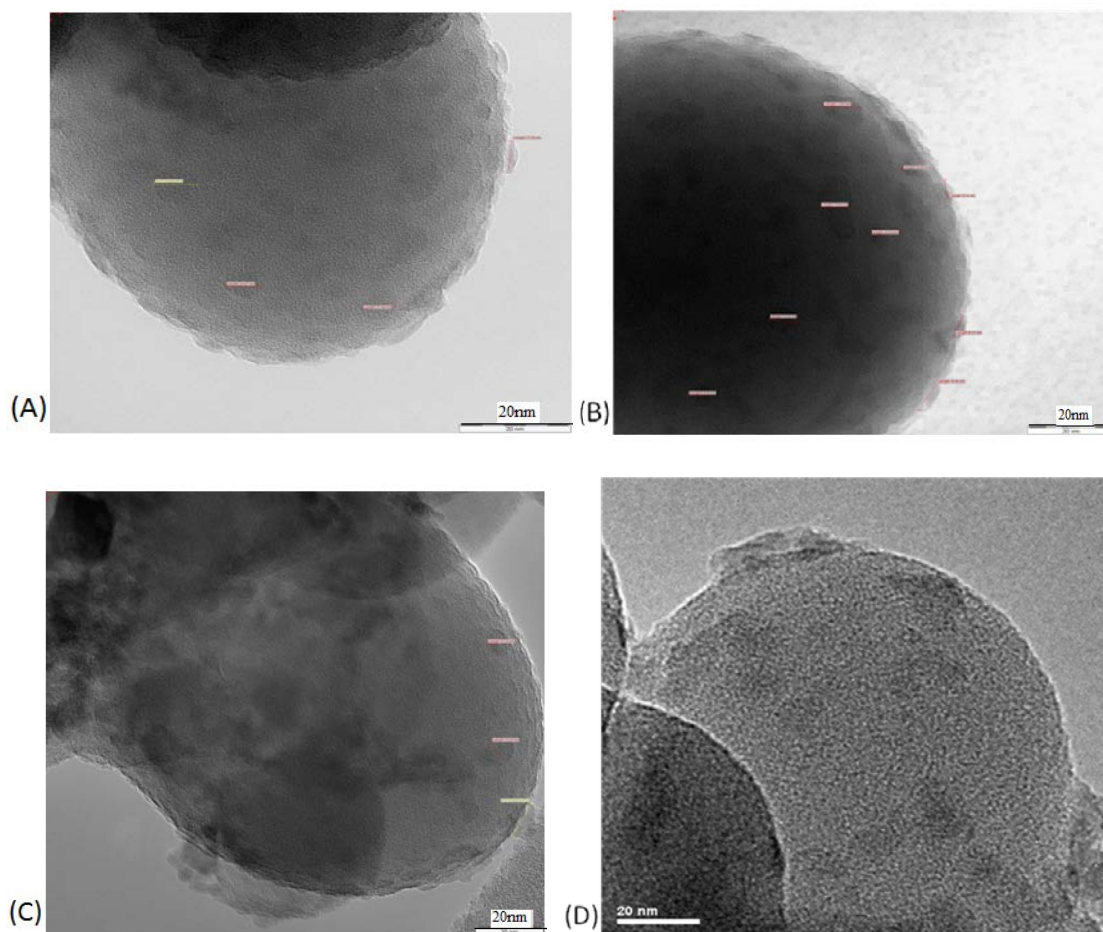


Figure 4-14: TEM image of $\text{Al}_2\text{O}_3\text{-SiO}_2$ supported Fe-based catalyst at different Fe content (A) 3, (B) 6, (C) 10, and (D) 15 wt%

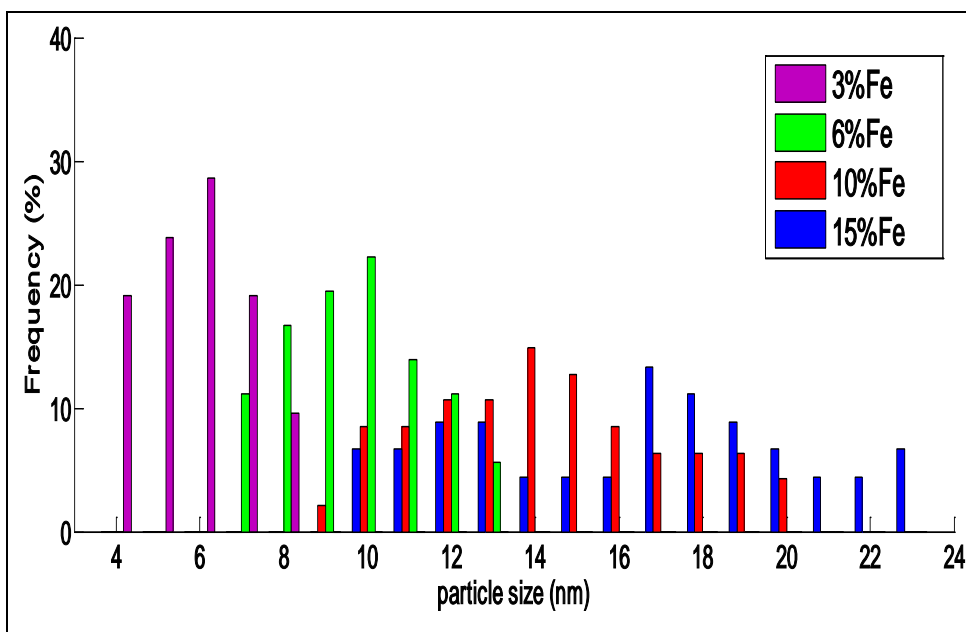


Figure 4-15: Particle size distribution for 3, 6, 10, and 15 wt %Fe on Al₂O₃-SiO₂ support

The effect of promoters on the Fe particle size and dispersion were investigated via TEM technique and the result is shown in Figure 4-16. Addition of Cu resulted in highly agglomerated Fe nanoparticles as shown Figure 4-16A, whereas more dispersed Fe particles was observed by the addition of K promoter. Compared to Cu and K-promoted catalyst, double promotion of Cu/K catalyst resulted in better Fe dispersion and smaller particle size (Figure 4-16C). Cu promoter resulted in highly agglomerated and bigger Fe particles. The synergistic effect of the Cu and K promoter on the catalyst produced well dispersed Fe particles.

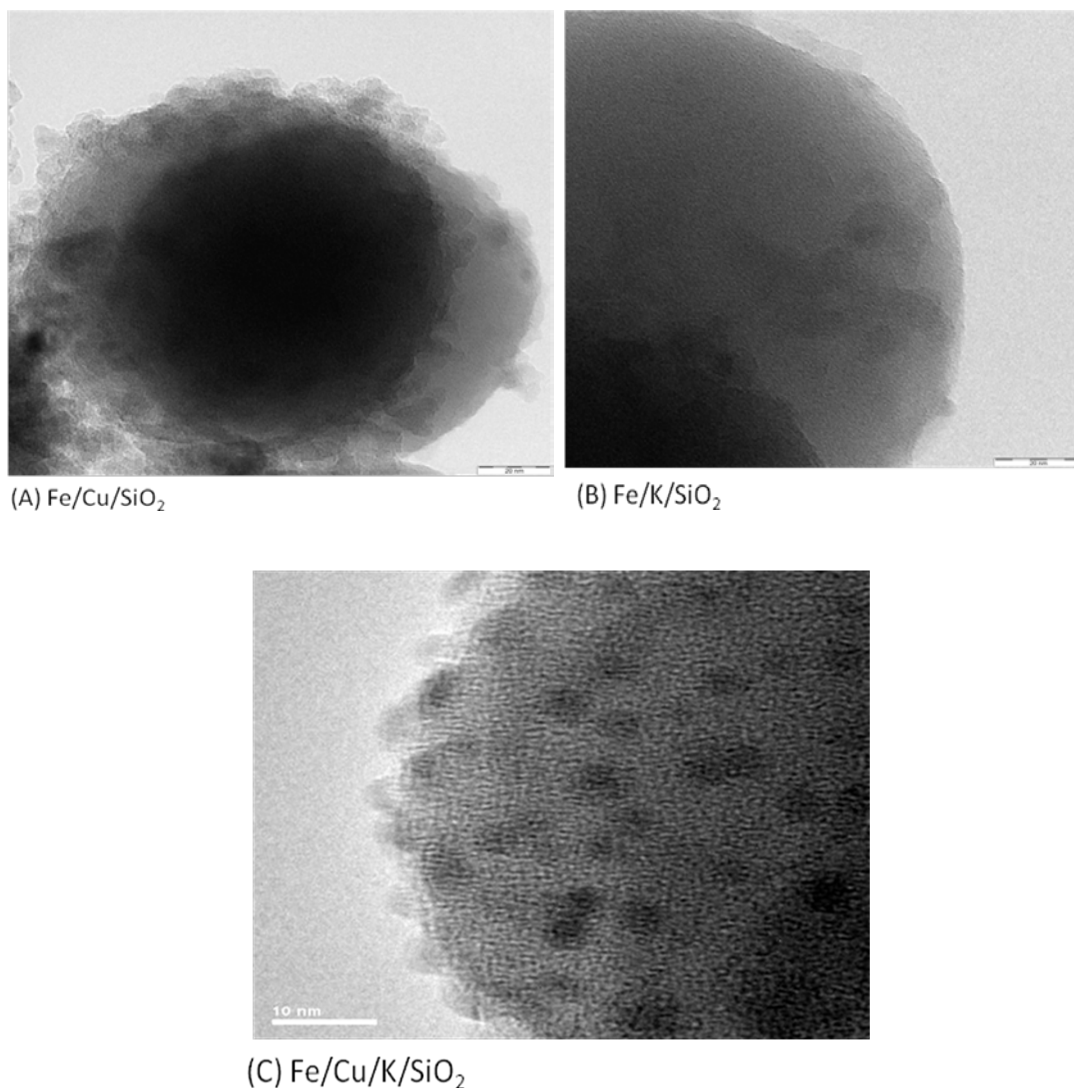


Figure 4-16: TEM image of promoted catalyst (A) 6%Fe/Cu/SiO₂, (B) 6%Fe/K/SiO₂ and (C) 6%Fe/Cu/K/SiO₂

Table 4-8 shows the average particle size Fe/SiO₂ catalysts prepared by impregnation and precipitation method and also the Fe/Al₂O₃-SiO₂ catalyst. The trend of increasing crystallite size with the Fe loading was reported previously by Hayashi *et al.* [85] where they concluded that for impregnated Fe/SiO₂, increasing the Fe content from 2 to 10 wt% resulted in an increase in Fe particles size from 5.6 to 14.2nm.

Fe loading had a significant effect on the average Fe particle size and catalyst surface area. Catalyst with low Fe loading has smaller average particle size and larger surface area compared to those at higher Fe loading.

Table 4-8: Average particle size of the synthesis supported Fe-based catalysts

| Sample | Fe loading (wt %) | Average particle size (nm) | Synthesis technique |
|---|-------------------|----------------------------|---------------------|
| Fe/SiO ₂ | 3 | 5.8±1.3 | Impregnation |
| Fe/SiO ₂ | 6 | 8.6 ± 1.1 | Impregnation |
| Fe/SiO ₂ | 10 | 12.6 ± 1.3 | Impregnation |
| Fe/SiO ₂ | 15 | 13.0 ± 1.2 | Impregnation |
| Fe/SiO ₂ | 3 | 12.8±4.2 | Precipitation |
| Fe/SiO ₂ | 6 | 17.3±7.3 | Precipitation |
| Fe/SiO ₂ | 10 | 19.3±6.6 | Precipitation |
| Fe/SiO ₂ | 15 | 19.3±6.6 | Precipitation |
| Fe/Al ₂ O ₃ -SiO ₂ | 3 | 6.2±1.6 | Impregnation |
| Fe/Al ₂ O ₃ -SiO ₂ | 6 | 10.0±2.0 | Impregnation |
| Fe/Al ₂ O ₃ -SiO ₂ | 10 | 14.0±3.3 | Impregnation |
| Fe/Al ₂ O ₃ -SiO ₂ | 15 | 17.8±5.3 | Impregnation |

As conclusion, the size of Fe nanoparticles and distribution were strongly affected by the synthesis technique, nature of support and Fe loading. The 3% Fe/SiO₂ catalyst prepared by impregnation method showed uniform dispersion of the Fe particles and had the smallest average particle size of 5.8±1.3nm.

4.2.1.3 Phase and crystallinity

Determining the phase composition is an important step in the characterization of the Fe-FT catalyst because Fe could exist in different forms such as oxides or carbides. XRD was used to investigate the type of phase present in the calcined catalysts. XRD patterns of the supported Fe -based catalysts are presented in Figure 4-17. Catalyst with low Fe loading of 6 wt% show amorphous phase compared to that of higher Fe loading of 15 wt%. The XRD peak of the 15% Fe/SiO₂ catalyst showed hematite phase Fe₂O₃ based on peaks detected between 2θ of 35° and 40°. The peaks at 2θ between 15° to 25° represent silica. The XRD results confirmed the presence of the crystalline phase in the catalyst with high Fe loading. XRD peaks were not detected for the catalyst with low Fe loadings and this could be due to the XRD detection limitation.

Lohitharn *et al.* [51] found that catalyst with small average crystallite sizes <4-5nm showed amorphous phase. Similar trend was obtained for the catalysts prepared by precipitation method and supported by Al₂O₃-SiO₂. This result is in good agreement with the result reported by Mansker *et al.* [86] where they found that catalyst incorporated with SiO₂ showed amorphous phase whereas Fe₂O₃ phase was present for SiO₂-free catalyst.

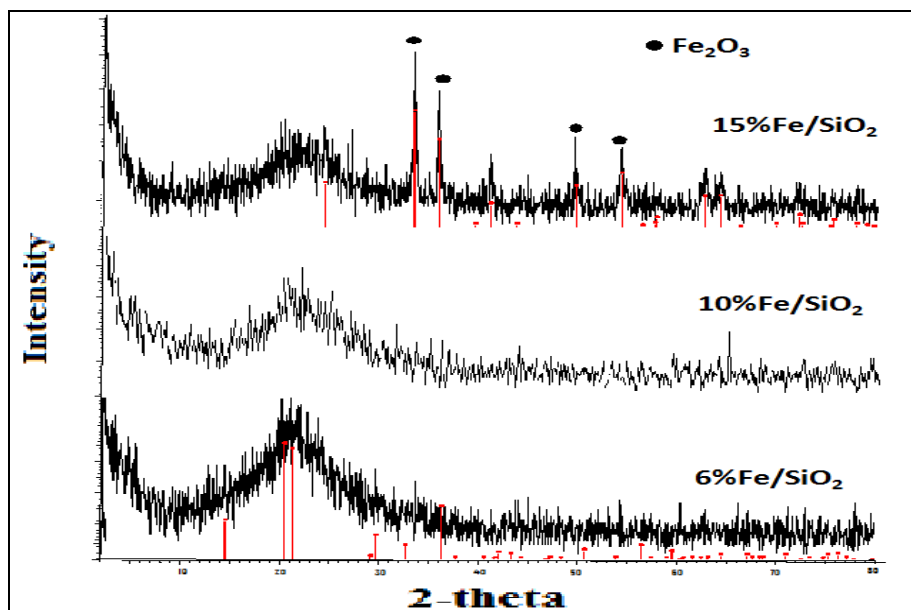


Figure 4-17: X-ray diffraction patterns of the Fe/SiO₂ catalyst prepared by impregnation method at Fe loading of 6, 10 and 15 wt%

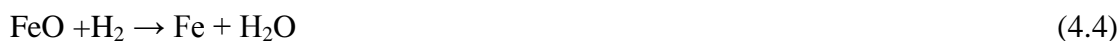
4.2.2 Catalyst reducibility

The phase transformation during the reaction plays a major role in influencing the overall FT performance (activity and selectivity). The Fe-based catalyst was found to be initially in the hematite phase (Fe₂O₃). Although, Fe₂O₃ is a more stable oxide phase of Fe, Fe₃O₄ and iron-carbide phases were described as the most active site for FTS [9] and [38]. Therefore, converting Fe₂O₃ phase to Fe₃O₄ or Fe phase was desirable. This transformation was proposed to occur in two or three stages depending on the composition of the catalyst. The two-step of the H₂-TPR profile can be represented by the equations (4.1 and 4.2) [81].





The step for transforming the magnetite to metallic Fe can be described by the sum of two subsequent steps (equation 4.3 and 4.4)



During H_2 -TPR reduction, chemical reaction was monitored when a reducing gas passed over an oxidized catalyst. Each hydrogen molecule reacted with interface oxygen atom giving water molecule and anionic vacancy. The initial stage of reducing the FeO involved chemisorptive dissociation of hydrogen molecule due to formation of intermediate hydroxyl (OH^-) group as shown in equation (4.5) [81].



Thus, the removal of individual water molecule represented by equation (4.5) could serve as the measurement reduction degree of the FeO.

The bulk phase reduction behavior of the catalysts was studied by H_2 -TPR. Table 4-9 shows summary of the TPR results for all the synthesized catalysts. The TPR profiles of the impregnated catalysts are shown in Figure 4-18.

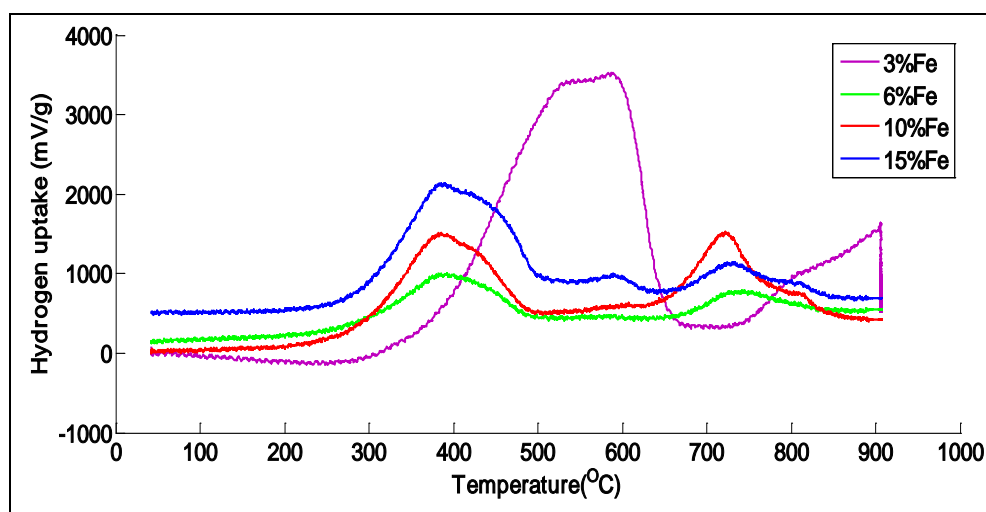


Figure 4-18: TPR profiles of impregnated Fe/SiO₂ catalysts with different Fe loading after calcination at 873K for 4h

The results from Figure 4-18 reveals that impregnated catalyst with Fe loading of 6, 10, and 15 wt% showed two distinct peaks at temperature of 380°C and 720°C. A big shift in the reduction peak position was observed for 3%Fe/SiO₂ catalyst. The

increase in the reduction temperature for the 3%Fe/SiO₂ catalyst was mainly due to the small size of Fe particles, which was more difficult to reduce at the lower temperature. As observed from TEM analysis, the smallest size of Fe particles was obtained from the catalyst with lowest Fe loading.

The results show that all synthesized catalysts were reduced at temperature higher than 450°C, except for the promoted catalysts. It is noted in some publications that supported catalysts suppressed the catalyst's reducibility due to the interaction between the active metal and the support [44] and [87]. The TPR results for Fe catalyst supported on SiO₂ suggested that the presence of SiO₂ on the catalyst increased the reduction temperatures of the Fe for both transformation steps, as discussed previously by Wan *et al.* [45] who reported that increasing of the SiO₂ content suppressed the reduction due to stabilization of the Fe₃O₄ phase.

The reduction profiles of the catalysts prepared by precipitation method are shown in Figure 4-19. The reduction peaks of the precipitated catalysts existed at higher temperature than those of the impregnated catalyst. Although, impregnated catalyst has smaller Fe particle size compared to precipitated catalysts, precipitated catalysts inhibit the catalyst's reducibility. The difference in the reducibility of the Fe₂O₃ particles between the impregnated and precipitated catalysts may be attributed to the difference in the interaction between Fe metals and SiO₂ support caused by the immobilization processes of the impregnation and precipitation methods.

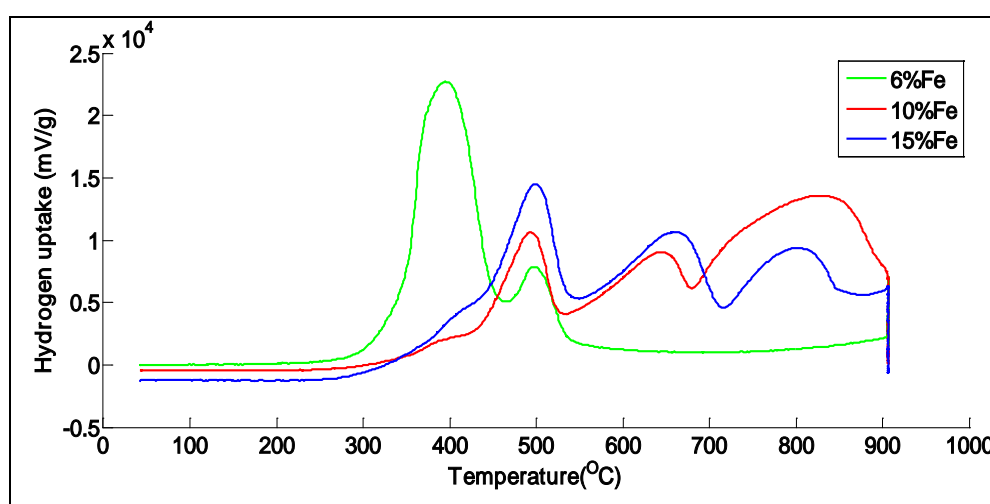


Figure 4-19: TPR profile of Fe/SiO₂ catalysts with different Fe loading prepared by precipitation method after calcination at 873K for 4h

Figure 4-20 shows the reduction peaks obtained from the catalysts supported on $\text{Al}_2\text{O}_3\text{-SiO}_2$. The reduction peak shifted to the higher temperature compared to those shown in Figure 4-18, for the catalysts supported on SiO_2 . As the electrons of the Fe atoms are attracted to O atoms of $\text{Al}_2\text{O}_3\text{-SiO}_2$ support, the fraction of Fe atoms interacted with O atoms of $\text{Al}_2\text{O}_3\text{-SiO}_2$ became larger and this resulted in stronger interaction between the metal (Fe) and the support [17]. The acidity of the Al_2O_3 also enhanced the interaction between Fe and the $\text{Al}_2\text{O}_3\text{-SiO}_2$ and resulted in stronger metal-support interaction than the catalysts on SiO_2 support [13].

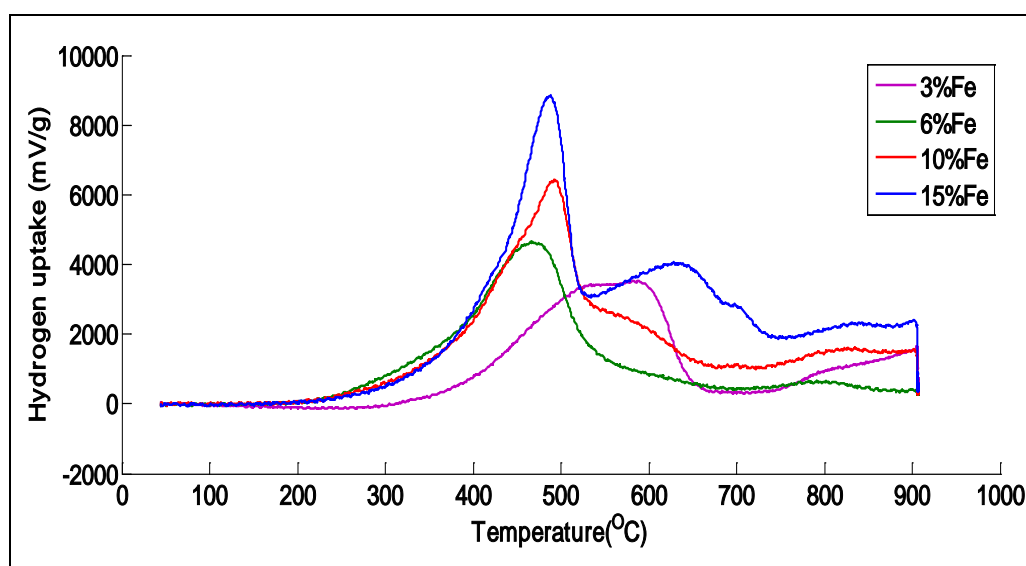


Figure 4-20: TPR profiles of $\text{Fe}/\text{Al}_2\text{O}_3\text{-SiO}_2$ catalysts with different Fe loading after calcination at 873K for 4h

The effects of Cu, K, and Cu/K promoters on the catalysts reducibility were also investigated via the TPR experiment. Figure 4-21 shows the TPR profile of the Fe/SiO_2 catalysts promoted by Cu. A big shift on the position of the reduction peaks was illustrated by adding Cu to the catalyst compared to those unpromoted catalysts (Figure 4-18). These results display that the presence of Cu promoter enhanced the reducibility as detected by the decrease in the reduction temperature. This result is in good agreement with the literature where most of the studies published confirmed that adding Cu facilitated the reducibility of the catalyst [51], [52], and [40]. The reduction of $\text{Fe}/\text{Cu}/\text{SiO}_2$ occurs in three steps: the first step which was presented at 220°C reflects the transformation of $\text{CuO} \rightarrow \text{Cu}$, the second step, illustrated at 300°C was related to the transformation of $\text{Fe}_2\text{O}_3 \rightarrow \text{Fe}_3\text{O}_4$, and the broad peak obtained at the temperature ranged between $450\text{-}800^\circ\text{C}$ was related to transformation of Fe_3O_4 to Fe.

The TPR profile of Fe/Cu/SiO₂ displayed the effect of Fe loading on the catalysts reducibility, where for 15%Fe/SiO₂ catalyst, the position of the first peak was shifted to higher temperature compared to those at other loadings, while the second peak was observed at the same temperature as those at other loadings (3, 6, and 10 wt%). This result could be due to the effect of the Fe particles where it inhibits the influence of the Cu because the percentage of the Cu (2%) was lower compared with the percentage of the Fe (15%).

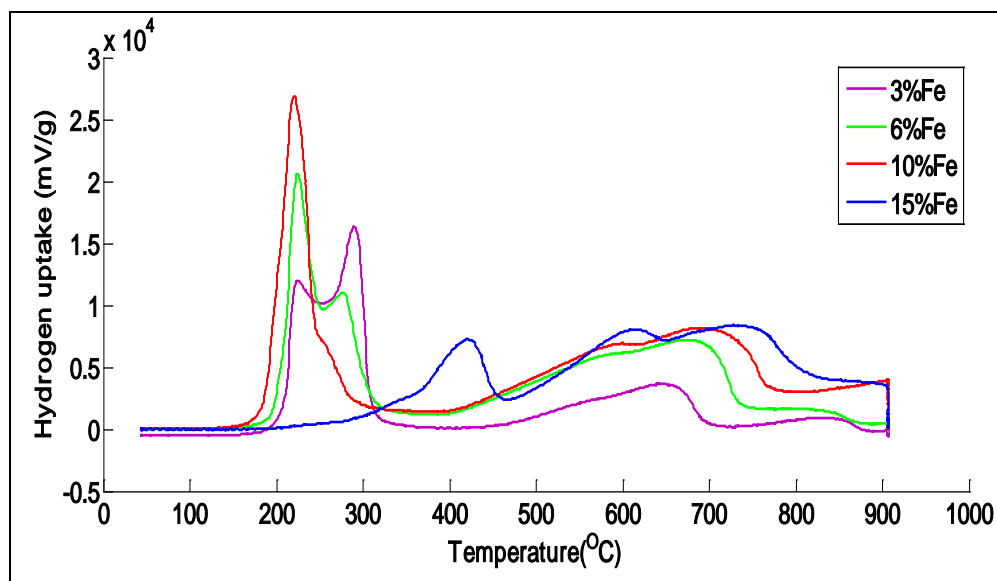


Figure 4-21: TPR profiles of Fe/Cu/SiO₂ catalysts with different Fe loading after calcination at 873K for 4h

However, K-promoter showed opposite trend compared to that of Cu-promoter as shown in Figure 4-22. TPR-profile for K-promoted catalyst showed only one reduction peak at temperature between 450-700°C, which indicated that K suppressed the catalyst reducibility. This effect might be due to small surface area obtained for the catalysts promoted with K promoters, which resulted in decreased contact area with H₂, thus suppressed the catalysts reducibility. A similar trend was also reported by other researchers [57].

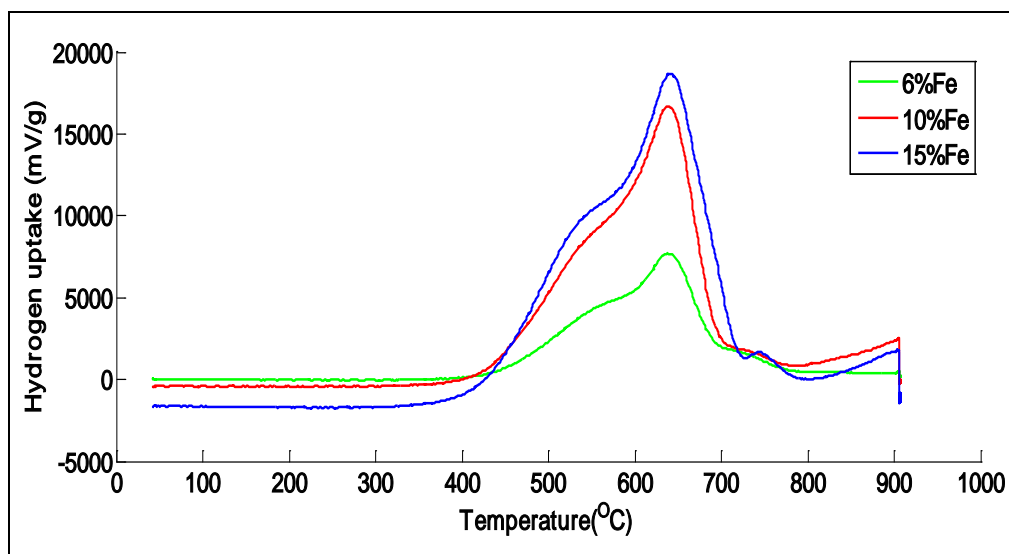


Figure 4-22 TPR profiles of Fe/K/SiO₂ catalysts with different Fe loading after calcination at 873K for 4h

The influence of the double promotion of Cu/K was also studied by the H₂-TPR analysis. Figure 4-23 shows the TPR profile of Fe/Cu/K/SiO₂ catalysts. Compared to Cu-promoted catalyst, the double promotion of Cu/K significantly suppressed the catalyst reducibility as both of the transformation stages were shifted to the higher temperature.

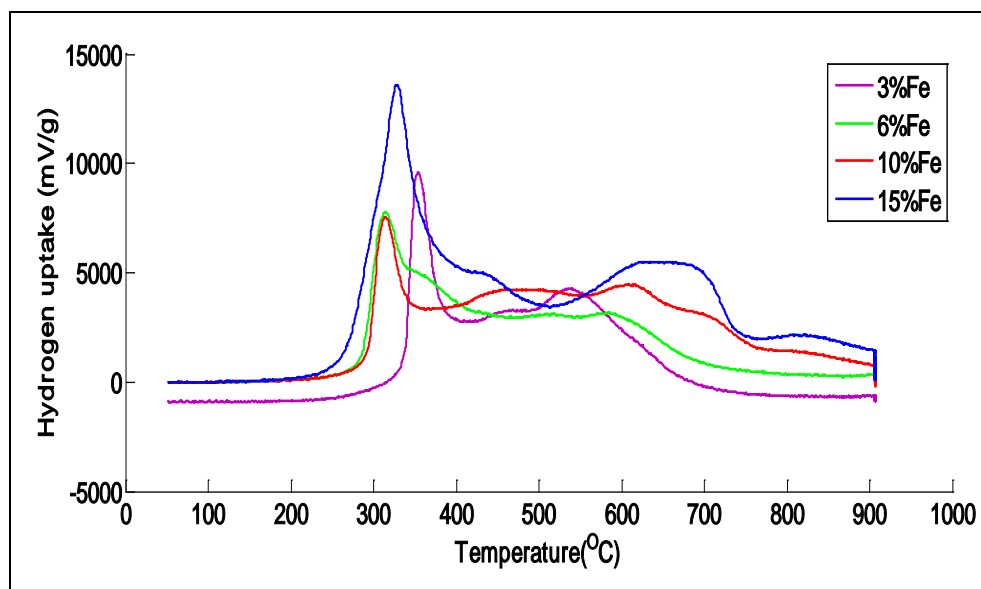


Figure 4-23: TPR profiles of Fe/Cu/K/SiO₂ catalysts with different Fe loading after calcination at 873K for 4h

The results of the catalyst reducibility using H₂-TPR are summarized in Table 4-9.

Table 4-9: Summary of the TPR results for all the synthesized catalysts

| Sample | T _{R1} (°C) | T _{R2} (°C) | T _{R3} (°C) |
|---|----------------------|----------------------|----------------------|
| 3% Fe/SiO ₂ | 400-680 | 780-900 | - |
| 6% Fe/SiO ₂ | 300-500 | 690-790 | - |
| 10% Fe/SiO ₂ | 300-500 | 690-790 | - |
| 15% Fe/SiO ₂ | 300-500 | 690-790 | - |
| 6% Fe/SiO ₂ | 340-490 | 500-550 | |
| 10% Fe/SiO ₂ | 450-550 | 600-700 | 700-850 |
| 15% Fe/SiO ₂ | 450-550 | 600-710 | 710-850 |
| 3% Fe/Al ₂ O ₃ -SiO ₂ | 410-670 | - | - |
| 6% Fe/Al ₂ O ₃ -SiO ₂ | 430-560 | 560-780 | - |
| 10% Fe/Al ₂ O ₃ -SiO ₂ | 430-560 | 560-780 | - |
| 15% Fe/Al ₂ O ₃ -SiO ₂ | 430-560 | 560-780 | - |
| 3% Fe/Cu/SiO ₂ | 190-240 | 260-310 | 540-710 |
| 6% Fe/Cu/SiO ₂ | 190-240 | 260-310 | 540-710 |
| 10% Fe/Cu/SiO ₂ | 190-240 | 260-310 | 540-710 |
| 15% Fe/Cu/SiO ₂ | 330-480 | 540-710 | - |
| 6% Fe/K/SiO ₂ | 430-730 | - | - |
| 10% Fe/K/SiO ₂ | 430-730 | - | - |
| 15% Fe/K/SiO ₂ | 430-730 | - | - |
| 3% Fe/Cu/K/SiO ₂ | 340-410 | 510-580 | - |
| 6% Fe/Cu/K/SiO ₂ | 290-390 | 580-750 | - |
| 10% Fe/Cu/K/SiO ₂ | 290-390 | 580-750 | - |
| 15% Fe/Cu/K/SiO ₂ | 290-390 | 580-750 | - |

4.3 Summary of the catalysts properties

The physicochemical properties of the catalysts were strongly affected by the preparation parameters such as synthesis technique, support, Fe loading, and

promoters. Impregnation method resulted in better properties compared to those of precipitation method in terms of particle size, distribution and reducibility. Physicochemical properties were strongly influenced by the Fe loading, where lower Fe loading resulted in larger surface area, smaller particle size, and better uniformity compared to those of higher Fe loading. However, lower Fe loading suppressed the reducibility of the catalysts possibly due to the decrease in Fe particle size. The physicochemical properties of the catalyst were also affected by the type of the support. The reduction of the catalyst and the dispersion of the Fe particles were better on SiO₂ compared to the Al₂O₃-SiO₂ support. Addition of Cu and K promoters also affected the catalyst properties. Cu promoter facilitated the reduction while K promoter enhanced the dispersion of Fe particles. The 3%Fe/SiO₂ and 6%Fe/SiO₂ catalysts prepared by impregnation method exhibited better properties in terms of all the physicochemical properties and particularly on dispersion and size distribution of Fe nanoparticles.

4.4 Fischer-Tropsch performance

The FTS performance of the supported Fe nanoparticles catalysts were evaluated in a fixed-bed microreactor at atmospheric pressure. The performances of the catalysts were evaluated in terms of the CO conversion and the product selectivity.

The CO conversion was calculated using the average CO content (mol %) in the feed stream, and in the reactor outlet's stream, at the respective reaction time (min) (equation 4.6) :

$$CO\ conversion = \left(\frac{\text{mole of } CO_{in} - \text{mole of } CO_{out}}{\text{mole of } CO_{in}} \right) \times 100 \quad (4.6)$$

The selectivity of the hydrocarbons (HC) produced in the FT reaction was determined as the ratio between respective product and the sum of products detected in the outlet stream using equation 4.7.

$$HC\ selectivity\ (\%) = \left(\frac{\text{mole of HC produced}}{\text{total mole of HC}} \right) \times 100 \quad (4.7)$$

The influence of the reaction conditions such as the ratio of reactant gases (H_2/CO ratio), reaction temperature, and the space velocity were investigated. Calculation and data for the CO conversion and product selectivity are shown in Appendix E. Products were analyzed using online GC and typical gas chromatograms are shown in Appendix E.

4.4.1 Pretreatment

The synthesized supported Fe-based catalyst was firstly reduced in the flow of carbon monoxide at 553K and 3L/g-cat.h for 4h. The reduction of Fe-based catalyst with CO occurred in two steps (equation 4.8 and 4.9) [88]:



The importance of the reduction step on the FT activity investigated by many researchers where they reported that reduced catalysts are more efficient in dissociating CO, where the disadvantage of the reduction step with CO was it favored the transformation of active carbon to an inactive carbon (graphite) [16]. The reduction condition that was used in this study was selected based on findings by previous studies. Davis [19] had pointed out that activation in CO at 280°C for 24h resulted in maximum conversion compared to those obtained by the other activation procedures. Compared to activation with H_2 and syngas, CO activation was found to provide higher fraction of iron carbide, which plays an important role in the catalytic activity [50]. Therefore, activation of Fe-based catalysts is generally practiced with CO or syngas [89].

4.4.2 Stability

The activity of the catalyst was represented by the conversion of the CO. The variation of the CO conversion with the time on stream (TOS) represents the stability of the catalyst. The stability of the impregnated and precipitated Fe/SiO₂ catalysts as

well as Fe/Al₂O₃-SiO₂ catalyst with different Fe loadings are demonstrated in Figures 4-24, 4-25, and 4-26, respectively. The CO conversion was found to be time-dependent. The activity of catalysts with different Fe loadings gradually increased with the time on stream and it reached the maximum at 30min (Figure 4-24). Compared with the catalysts at higher Fe loadings, the 6%Fe/SiO₂ catalyst exhibited higher stability where the catalytic activity slightly increased with the TOS. The activity of 3%Fe/SiO₂ catalyst decreased from 89% to 52% as the TOS increased from 30 min to 270 min. The rapid loss in the activity with the time on stream could be due to the accumulation of the inactive carbon on the surface of the catalyst, which was more pronounced on the 3%Fe which has the smallest Fe particle size.

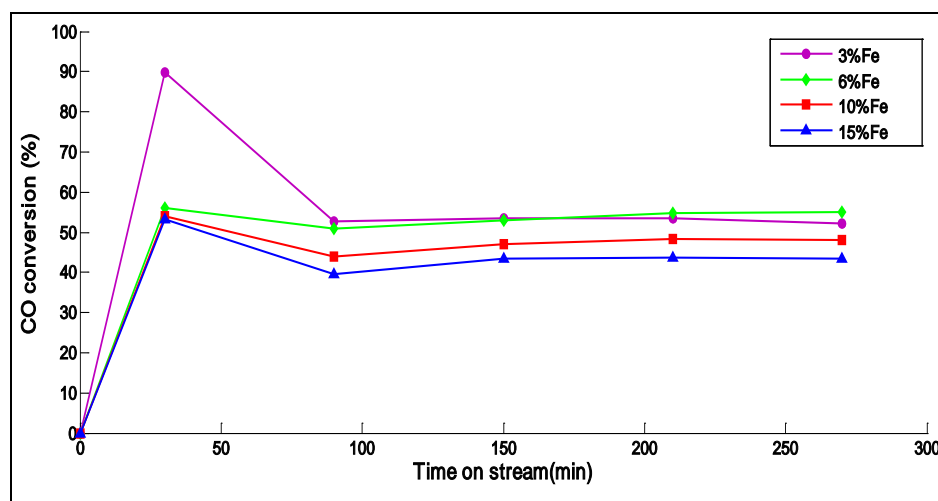


Figure 4-24: Stability of impregnated SiO₂ supported Fe-based catalyst at different Fe loadings 3, 6, 10, and 15 wt %Fe under reaction conditions of 523K, 1.5H₂/CO, and 3L/g-cat.h

Figure 4-25 shows the relation between the CO conversion and the TOS for the precipitated Fe/SiO₂. The CO conversion over the catalysts with high Fe loadings of (10% and 15%) rapidly increased at the beginning of reaction and reach the maximum at 30 min then remarkable decline was obtained where the CO conversion over 10%Fe/SiO₂ and 15%Fe/SiO₂ decreased from 65 to 21% and from 40 to 22%, respectively. The CO conversion over catalysts with low Fe loading (3 and 6 wt %) increased at the beginning of the reaction and keep increasing with the TOS and reached the maximum conversion at 150min. Although the initial CO conversions over the 3% and 6% of Fe/SiO₂ were lower than those at higher Fe loadings; however this trend changed after 90mins. The Fe loading influenced the catalyst stability where

low loading (3 and 6%) of Fe exhibited better catalytic stability than those of higher loading. At the same Fe loading (Figure 4-25), precipitation method resulted in catalysts with lower CO conversion compared to those synthesized via impregnation method (Figure 4-24).

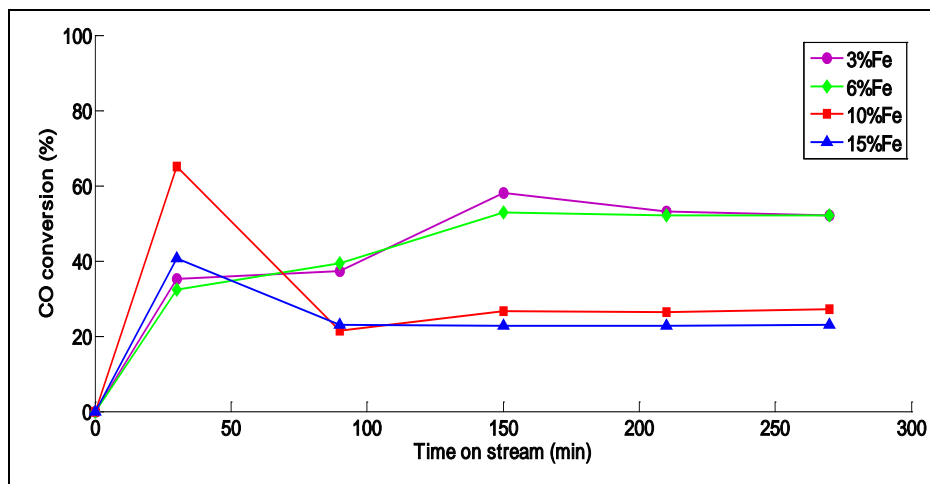


Figure 4-25: Stability of precipitated SiO₂ supported Fe-based catalyst at different Fe loadings of 3, 6, 10, and 15%Fe under reaction conditions of 523K, 1.5H₂/CO, and 3L/g-cat.h

The influence of the Al₂O₃-SiO₂ support and the Fe loading on the catalytic stability was also investigated during the FT reaction. The CO conversion over the Fe/Al₂O₃-SiO₂ catalysts at the different Fe loadings was found to be slightly increased with the TOS and reached the maximum at 30 min (Figure 4-26).

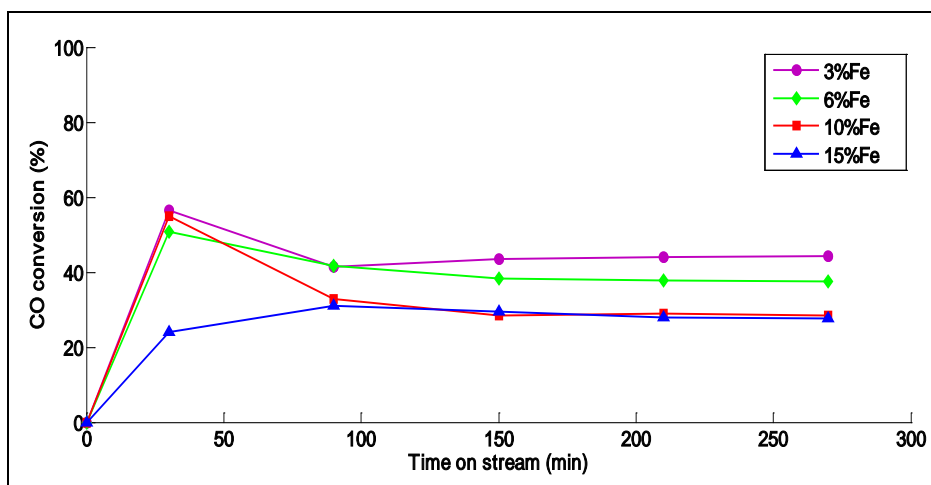


Figure 4-26: Stability of Al₂O₃-SiO₂ supported Fe-based catalyst at different Fe loadings of 3, 6, 10, and 15% Fe prepared by impregnation method under reaction conditions of 523K, 1.5H₂/CO, and 3L/g-cat.h

The effect of the promoter Cu, K, and Cu/K on the stability of the catalyst is shown in Figure 4-27. The CO conversion over the Fe/Cu/SiO₂ and Fe/Cu/K/SiO₂ catalysts increased with the time on stream and achieved the steady state after 90min. The CO conversion of silica-supported Fe/Cu catalyst dependent on TOS, where the maximum CO conversion was obtained at 30 min and then level off to a constant range. Addition of Cu facilitates the catalyst reduction (Figure 4-21) and according to the literature Cu also extends the catalyst carburization which enhanced the stability of FT catalyst [90].

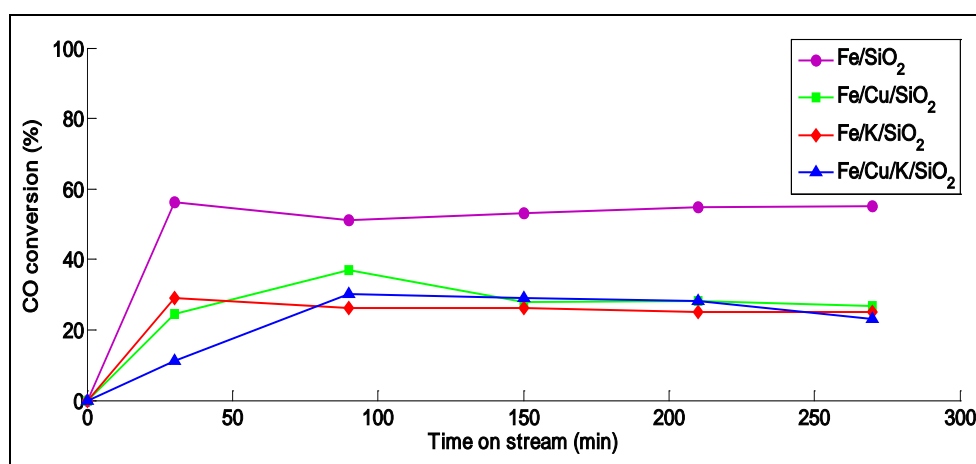


Figure 4-27: Stability of SiO₂ supported Fe-based catalyst incorporated with the promoter under reaction conditions of 523K, 1.5H₂/CO, and 3L/g-cat.h

The catalytic stability was found to be affected by the synthesis technique, support, Fe loading, and type of promoter. SiO₂-supported catalysts prepared by impregnation method exhibited higher stability than those of precipitation method in terms of increase in the CO conversion with the TOS.

4.4.3 Activity and Selectivity

The most important key factors for the performance of FT catalyst are activity and the product selectivity. The CO conversion was used as indication of the FTS activity; i.e. higher CO conversion implies higher catalyst activity. The influence of synthesis technique, support, Fe loading, promoter, and reaction conditions such as reactant ratio, space velocity, and temperature on the FTS performance was investigated.

Due to limitations in GC detection, hydrocarbon product larger than C₆ and H₂O were not quantified. Therefore, the selectivity of products were grouped as follows:

- Light HC = C₁-C₄
- Olefin = C₂⁼-C₄⁼
- Heavy HC (C₅-C₆) = C₅+
- Other product: CO₂

4.4.3.1 Effect of synthesis technique

The influence of the catalysts synthesis techniques on their activity for the FTS is displayed in Figure 4-28. The catalyst prepared by impregnation method exhibited higher conversion of CO compared to the catalyst that prepared by precipitation method. The difference in activity of the catalysts prepared by these techniques could be due to difference in physicochemical properties. Compared to impregnated catalysts, precipitated catalysts had larger size of Fe nanoparticles, higher agglomeration and lower reducibility. These finding suggested decreasing the catalytic activity to be affected by the pervious factors.

The effect of catalysts preparation method on the product selectivity is shown in Figure 4-29. Catalysts synthesized via impregnation method showed lower selectivity of the light hydrocarbon (C₁-C₄) and higher selectivity to the higher hydrocarbon (C₅+) and olefins (C₂⁼-C₄⁼) compared to those of precipitation method. These results were in good agreement with the result for stability and activity of those catalysts, where impregnated catalysts showed higher catalytic stability and activity compared to the precipitated catalysts.

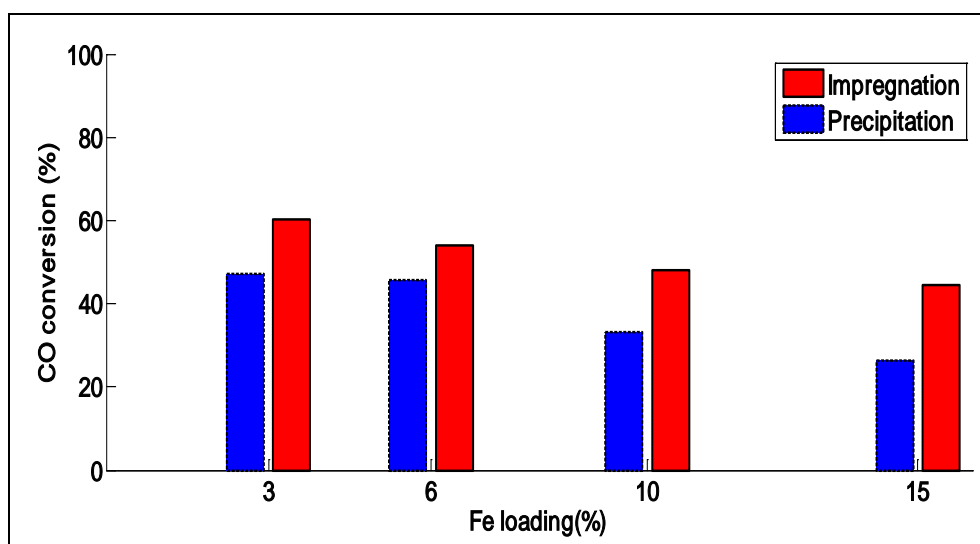


Figure 4-28: The activity of supported Fe-based catalysts prepared by impregnation and precipitation methods under reaction conditions 523K, $H_2/CO=1.5$, and $SV=3$ L/g-cat.h

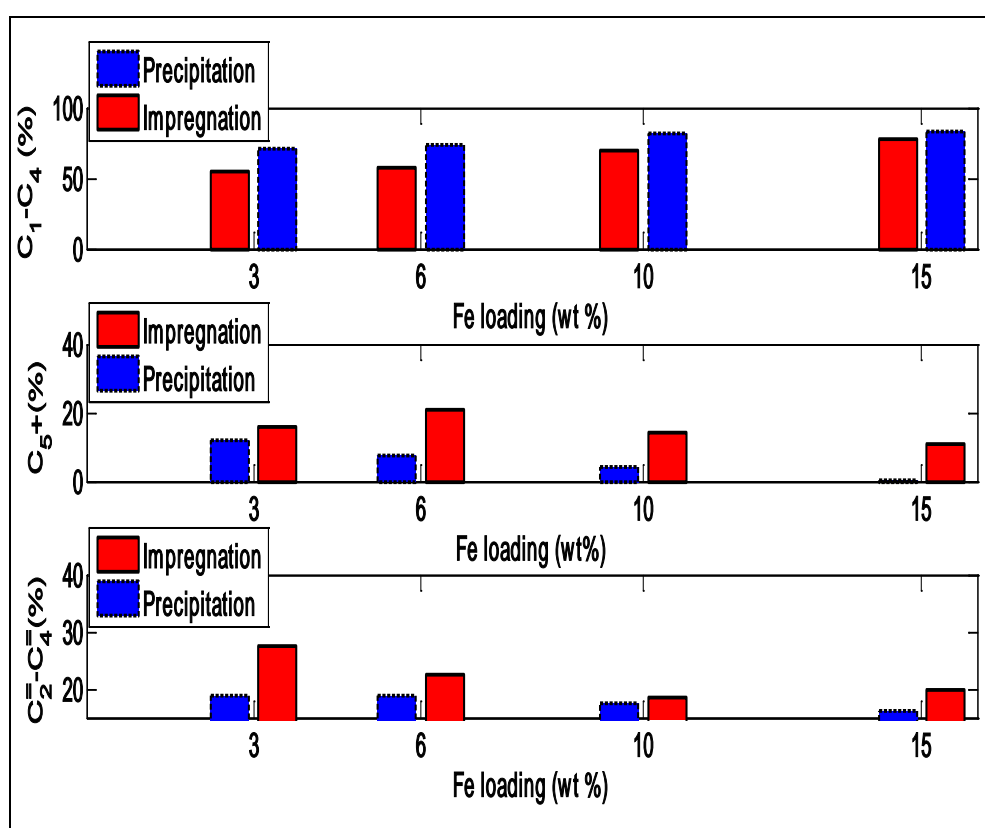


Figure 4-29: Comparison of the preparation methods on the selectivity of the hydrocarbons for SiO_2 supported Fe-based catalyst at different Fe loading at 523K, $1.5H_2/CO$ ratio, and $3L/g\text{-cat.h}$

4.4.3.2 Effect of the support

Hydrogenation of CO is susceptible to metal-support interaction effect. The catalytic activity and selectivity were influenced by the type of support that was used to synthesize the catalyst via impregnation method. In order to compare between the effect of SiO₂ and Al₂O₃-SiO₂ supports on FT performance, same synthesis techniques, Fe loading and reaction conditions have been used. The CO conversions over supported Fe nanoparticles synthesized via impregnation method, are shown in Figure 4-30. The catalyst supported on SiO₂ was more active than that which was supported on Al₂O₃-SiO₂. The differences in activity between Fe nanoparticles on Al₂O₃-SiO₂ and SiO₂ support may be partly attributed to difference in metal-support interaction. As shown by TPR analysis (Figure 4-18 and 4-20), Al₂O₃-SiO₂ support suppressed the catalytic reducibility which resulted in reduced catalyst activity. Similar trend have been pointed by Dlamini *et al.* [47] when they found that the catalyst with relatively strong interaction between the active metal and the support has lower catalyst activity. Addition of Al₂O₃ enhanced the catalytic acidity and decreased the catalytic carburization [17]. Carburization of Fe-based catalyst was represented by formation of the active site, FeC.

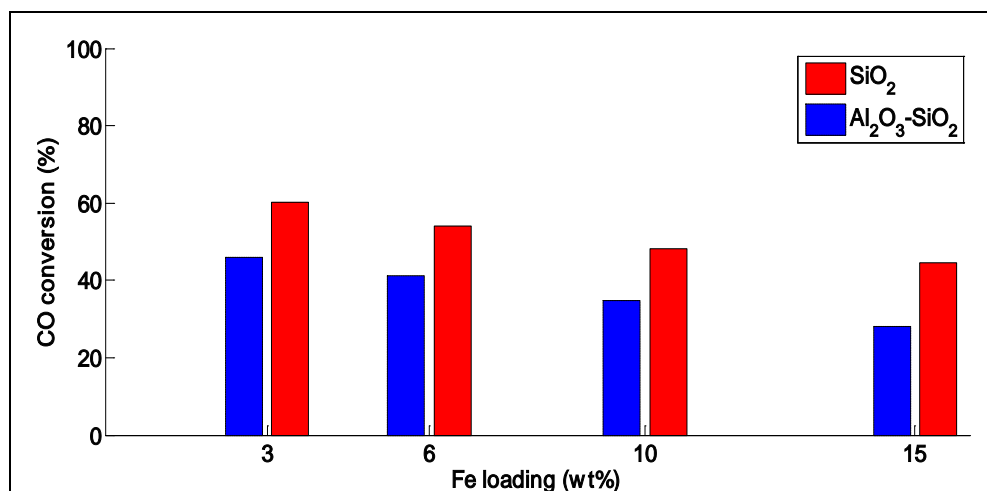


Figure 4-30: The activity of Fe-based catalysts supported on SiO₂ and Al₂O₃-SiO₂ under reaction conditions 523K, H₂/CO=1.5, and SV=3 L/g-cat.h

The influence of the support on the selectivity of hydrocarbons under the reaction condition of 523K, 1.5H₂/CO ratio and 3L/g-cat.h are observed in Figure 4-31. The Fe particles supported on SiO₂ showed higher selectivity toward heavy hydrocarbon

(C₅₊) and olefins and diminished the selectivity for the light hydrocarbon, compared to the catalyst that was supported on Al₂O₃-SiO₂. Al₂O₃ has higher acidity compared to SiO₂; therefore addition of Al₂O₃ to SiO₂ increased the acidity of the support which suppressed the catalyst carburization as well as the activity and selectivity to heavy hydrocarbons, while it enhanced the selectivity of light hydrocarbon. These results agree with the trend reported by Hai-jun *et al.*[13]. They reported that catalyst supported by Al₂O₃ has high selectivity to C₁-C₄, whereas lower selectivity of C₅₊ was obtained.

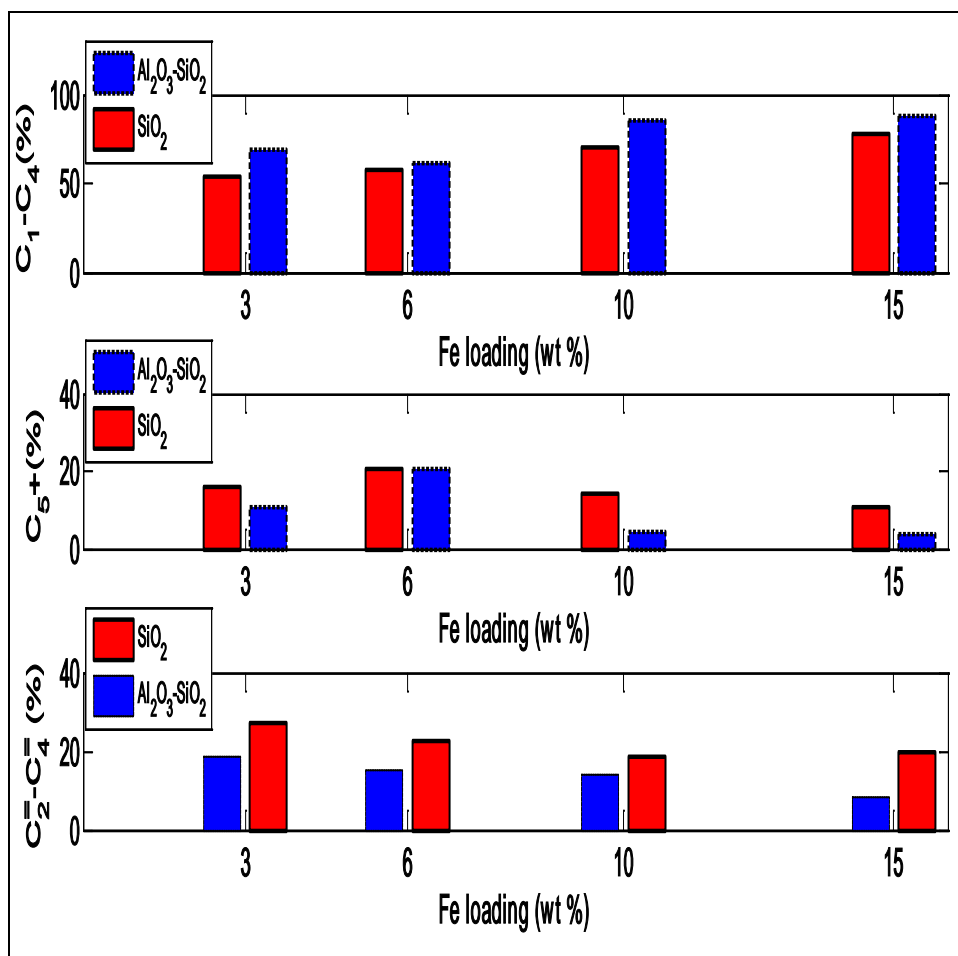


Figure 4-31: Selectivity of the hydrocarbons for Fe-based catalyst with different Fe loading prepared by impregnation method on SiO₂ and Al₂O₃-SiO₂ support under reaction conditions of 523K, H₂/CO=1.5, and SV=3 L/g-cat.h

4.4.3.3 Effect of the active metal (Fe) loading

The effect of the Fe loading on catalyst activity is demonstrated in Figure 4-32. The CO conversion was strongly influenced by the loading of the active metal, where the catalyst with the lower Fe loading resulted in the higher CO conversion. This trend could be due to difference in physicochemical properties, where catalyst with lower Fe loading has a higher surface area, dispersion of the active site over the support, and smaller particle size compared to those at higher Fe loading. Pirola *et al.* [29] indicated that the CO conversion is related to the number of Fe active site where it increased with increase the amount of Fe. And they also conclude that catalyst with Fe charge of 50% resulted in higher activity than the catalyst with lower Fe loading of 10% and 30%. It was expected that increasing Fe loading would increase the number of active sites, and enhanced the catalytic activity. However, our results showed an opposite trend, where the dispersion of the active site and the surface area decreased with increasing Fe loading.

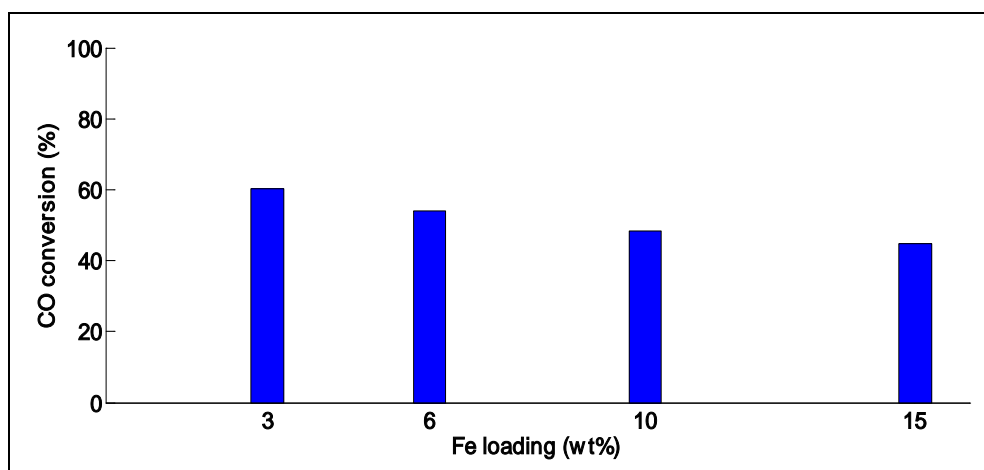


Figure 4-32: Effect of the Fe loading on the CO conversion for SiO₂ supported Fe-based catalyst at 523K, 1.5H₂/CO, and 3L/g-cat.h

The product selectivity was also examined using different Fe loading on SiO₂ at 523K, 1.5H₂/CO ratio, and 3L/g-Fe.h. The product selectivity was also found to be strongly affected by the loading of Fe. As can be seen from Figure 4-33, selectivity of the light hydrocarbon rapidly increased with increasing Fe loading from 3 to 15wt%, while the selectivity of C₅+ and olefins decreased. Although, the results showed decrease in the selectivity of C₅+ with increasing Fe loading, the catalyst with Fe

loading of 6 wt% displayed slightly higher selectivity of the C₅₊ at 20.85% compared to that of 3wt%, which was only at 10.8%.

The Fe/SiO₂ catalyst at 6%Fe loading resulted in a good balance between the CO conversion and the selectivity toward desired product (C₅₊) where, the catalytic activity and product selectivity rapidly declined with increasing the Fe loading (10% and 15%).

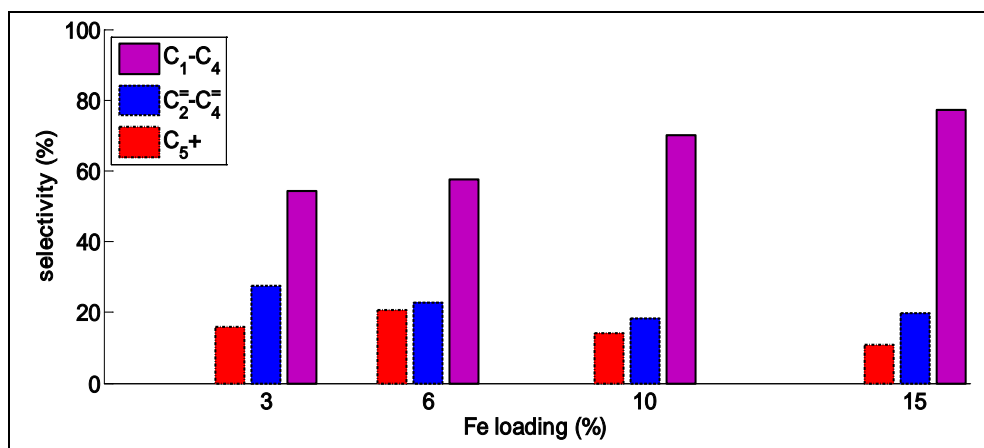


Figure 4-33: Effect of the Fe loading on the selectivity of hydrocarbons over SiO₂ supported Fe-based catalyst prepared by impregnation method at 523K, 1.5H₂/CO ratio, 3L/g-cat.h

4.4.3.4 Effect of Fe particle size

The size of Fe nanoparticle was found to be strongly dependent on the Fe loading. This finding has been illustrated by the TEM analysis. Increasing Fe loading resulted in bigger particles. Figure 4-34 shows the effect of Fe particle size on FT performance using the average Fe particle size obtained at each Fe loading on SiO₂ support prepared by impregnation method. For Fe/SiO₂ catalysts synthesized by impregnation method, Fe particle size ranged from 4-14 nm. The activity decreased from 54 to 30% by increasing the average Fe particles size from 8.6 to 13nm, respectively. Similar trend was obtained for the precipitated catalysts (Figure 4-35). Although, precipitated catalyst has bigger Fe average particle size (ranged between 17-19.5nm) compared to those of impregnated catalyst, similar trend was obtained in terms of the catalytic activity. The catalyst activity decreased from 45 to 26% by increasing the average Fe particles size from 17.3 to 19.3nm

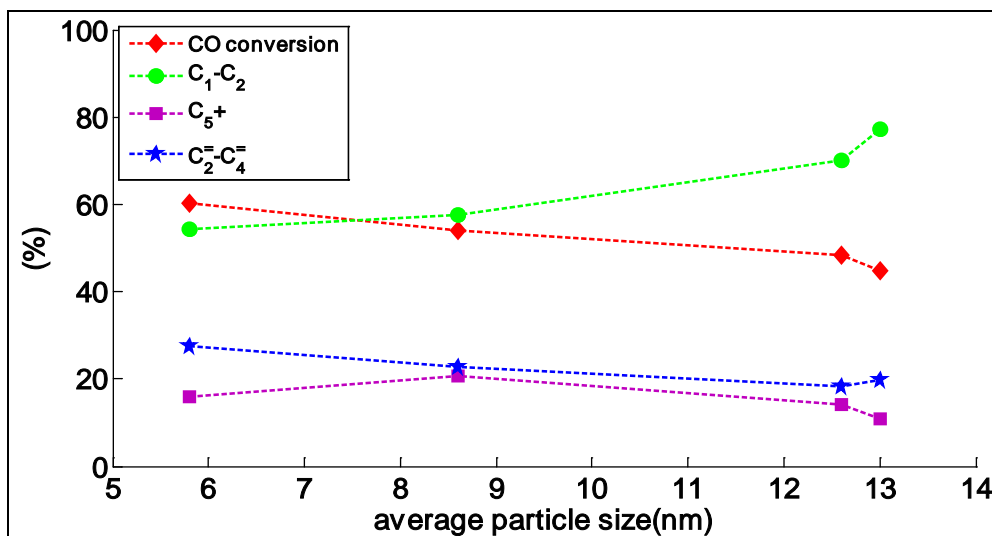


Figure 4-34: Variation of activity and hydrocarbon selectivity with Fe average particles size for the impregnated Fe-based catalysts supported by SiO₂

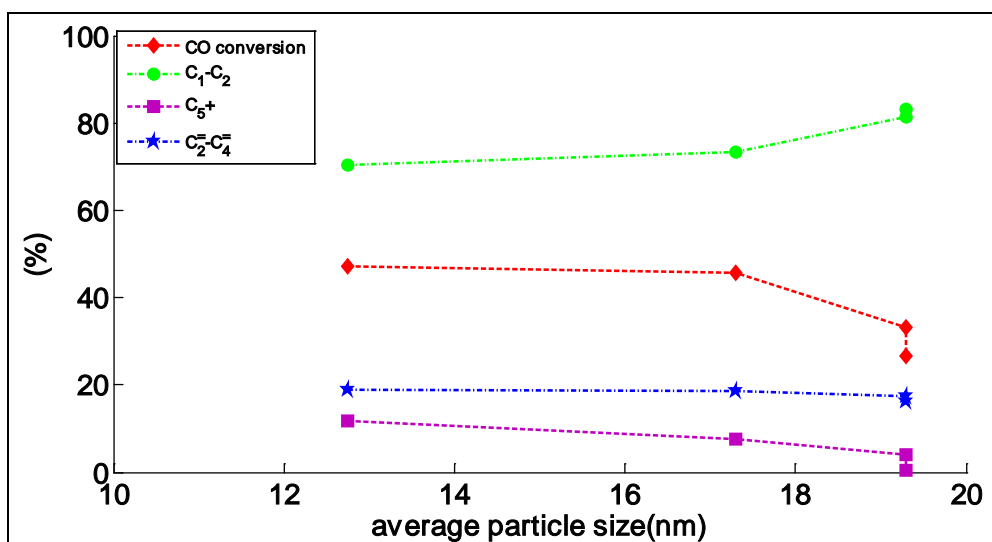


Figure 4-35: Variation of activity and hydrocarbon selectivity with Fe average particles size for the precipitated Fe-based catalysts supported by SiO₂

The Fe particle size was also affected by the type of support, where Al₂O₃-SiO₂ support resulted in bigger particles size (ranged between 4-23nm) (Figure 4-36) compared to those on SiO₂ support. Different particle size was obtained using different type of the support but similar trend of the catalytic activity was obtained.

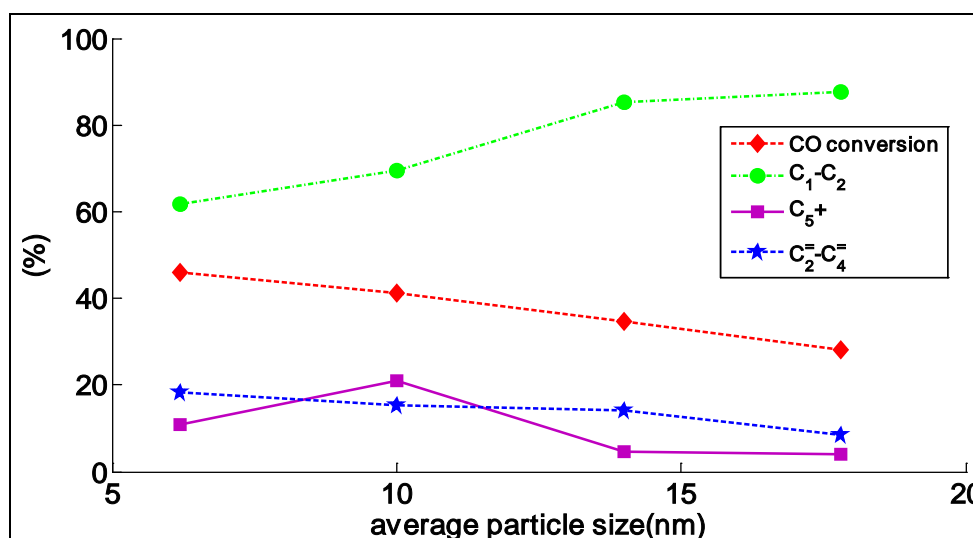


Figure 4-36: Variation of activity and hydrocarbon selectivity with Fe average particles size for the Fe-based catalysts supported by Al₂O₃-SiO₂

Increasing the Fe loading resulted in increasing Fe average particle size, which led to increase in the light hydrocarbon selectivity and decrease in both the CO conversion and selectivity of the heavy hydrocarbons (C₅⁺). The trend could be explained due to several factors such as lower dispersion of the Fe over the support which decreased the amount of the active site present over the support, agglomeration of the metal particles over the support which resulted in decrease of the contact area between the reactant and active site. All these factors result in decreasing CO conversion and selectivity of C₅⁺ while it increased the selectivity of the light hydrocarbon over larger Fe particles. Catalysts with average Fe particle size less than 9 nm exhibited higher activity and selectivity compared to the catalysts with bigger Fe particle size.

4.4.3.5 Effect of promoters

The effect of promoters on the performance of Fe-based catalyst in the FTS was investigated under reaction condition of 523K, 1.5H₂/CO ratio, and 3L/g-cat.h. Both K and Cu were found to be the most important alkali promoters which have been utilized in supported Fe-based FT catalyst. Table 4-10 shows the variation of the catalyst activity and product selectivity in the presence of promoters. Cu-promoted catalyst showed lower CO conversion compared to that of K and Cu/K promoted

catalyst. Higher activity (28.9%) and selectivity of heavy hydrocarbon (54.4%) was obtained by using Fe/K/SiO₂ catalyst. These results display that adding K-promoter enhanced the selectivity of heavy hydrocarbon and suppressed the light hydrocarbon (C₁-C₄) selectivity. Compared with unpromoted catalyst, catalyst promoted with K promoter shows lower CO conversion but higher selectivity of the heavy hydrocarbon. Addition of K promoter resulted in smaller surface area which led to small contact area between the reactant and active site. It also showed lower catalyst reducibility which resulted in small amount of the active sites but at the same time K-promoter enhanced the basicity of the catalyst and the carburization which resulted in enhancing the selectivity to the higher hydrocarbon. All these factors play important role in catalytic activity and selectivity. Several studies were carried out to determine the effect of both of Cu and K promoters on the performance of the Fe-based FTS. All of those studies confirmed that K promoters enhanced the catalytic activity and the selectivity of heavy hydrocarbons while an opposite trend was observed on the Cu promoters. Wan *et al.* [57] reported that incorporating of Cu and K promoters influenced the catalytic properties as well as FT performance. They concluded that the addition of Cu promoter decreased the activity and enhanced the deactivation of the catalyst because Cu facilitated conversion of iron carbide to magnetite. The addition of K enhanced the catalytic activity and the selectivity of heavy hydrocarbon.

Table 4-10: Effect of promoter on catalytic performance in fixed-bed microreactor (523K, 1.5H₂/CO, 3L/g-cat.h)

| Sample | Surface area (m ² /g) | CO conversion | selectivity | | |
|----------------------------|----------------------------------|---------------|--------------------------------|------------------|--|
| | | | C ₁ -C ₄ | C ₅ + | C ₂ ⁼ -C ₄ ⁼ |
| 6% Fe/SiO ₂ | 39.5 | 54.02 | 57.48 | 20.73 | 22.65 |
| 6% Fe/Cu/SiO ₂ | 39.7 | 24.37 | 72.04 | 8.16 | 20.66 |
| 6% Fe/K/SiO ₂ | 33.2 | 28.92 | 31.48 | 54.42 | 11.03 |
| 6% Fe/Cu/KSiO ₂ | 15.5 | 26.26 | 29.36 | 53.58 | 17.04 |

4.4.3.6 Effect of the reaction condition

Catalyst with the low Fe loading (6%) supported on SiO₂ prepared by impregnation method showed better performance towards FT activity compared to other catalysts. Due to the higher FT activity and stability exhibited by 6%Fe/SiO₂ catalyst prepared by impregnation method; this catalyst was selected to investigate the influence of the reaction conditions on the FT performance.

I. Reactant ratio (H₂/CO)

The effect of the reactant ratio (H₂/CO v/v ratio) on the FT catalytic performance of the silicSiO₂-supported Fe nanoparticles prepared by impregnation method at 523K, atmospheric pressure, and 3L/g-cat.h space velocity was investigated. The effect of the reactant ratio on the CO conversion is presented in Figure 4-37. The results show variation of the CO conversion with H₂/CO ratio. At the same Fe loading, the CO conversion increased significantly with increasing H₂/CO ratio and exhibited a maximum at H₂/CO ratio of 1.5 then declined with further increase of H₂/CO ratio. Davis [19] showed that the CO conversion was not strongly affected by the H₂/CO ratio over the range of 0.7-1.7, where it changed from 79 to 81% by increasing the H₂/CO ratio from 0.7 to 1.7. Similar conclusion was also published by Mirzaei *et al.* [66] on Fe/Mn/Al₂O₃ catalyst under atmospheric pressure. They reported that increasing the H₂/CO ratio from 1/1 to 3/1 resulted in increased the CO conversion from 84.4 to 97.2%, respectively.

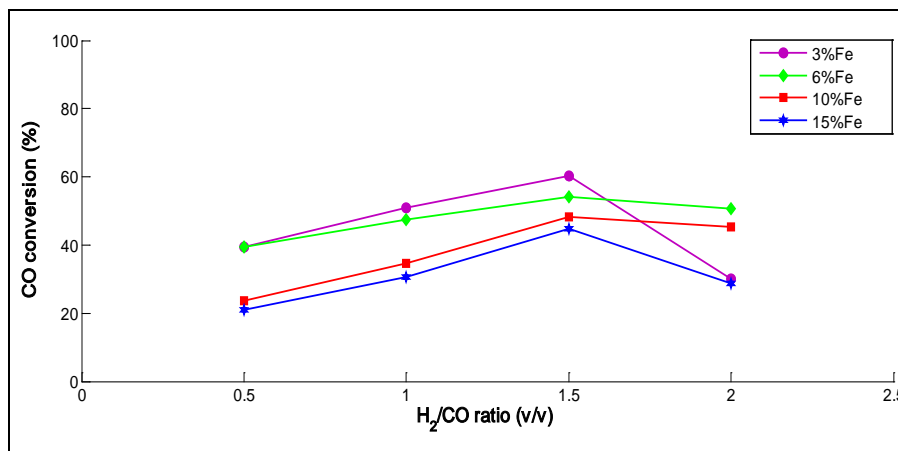


Figure 4-37: Effect of H₂/CO ratio on the CO conversion over Fe/SiO₂ catalysts prepared by impregnation method at 3, 6, 10, and 15% Fe loading

The product selectivity showed strong dependency on the H₂/CO ratio. As can be observed from Figures 4-38, 4-39, and 4-40, selectivity to C₅+ and C₂⁻-C₄⁻ respectively, were lower at the high ratio of the reactant, meanwhile selectivity of the light hydrocarbon showed opposite trend. Since Fe-based catalyst is also a water-gas-shift (WGS) catalyst, H₂ that was produced from this reaction (WGS) increased the H₂ content and facilitated the termination step and resulted in higher selectivity of saturated chain, especially methane.

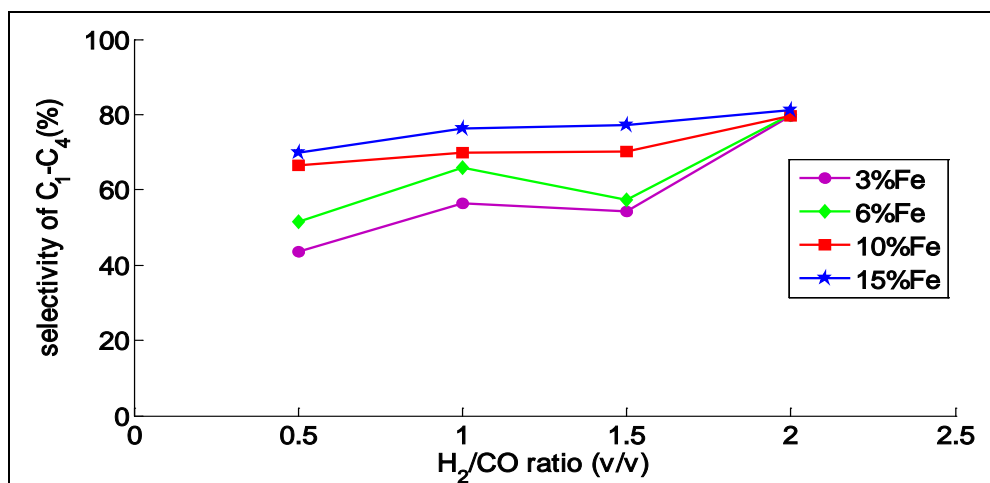


Figure 4-38: Effect of H₂/CO ratio at variety of the Fe loading on the selectivity of the light hydrocarbon (C₁-C₄) for SiO₂ supported Fe-based catalyst.

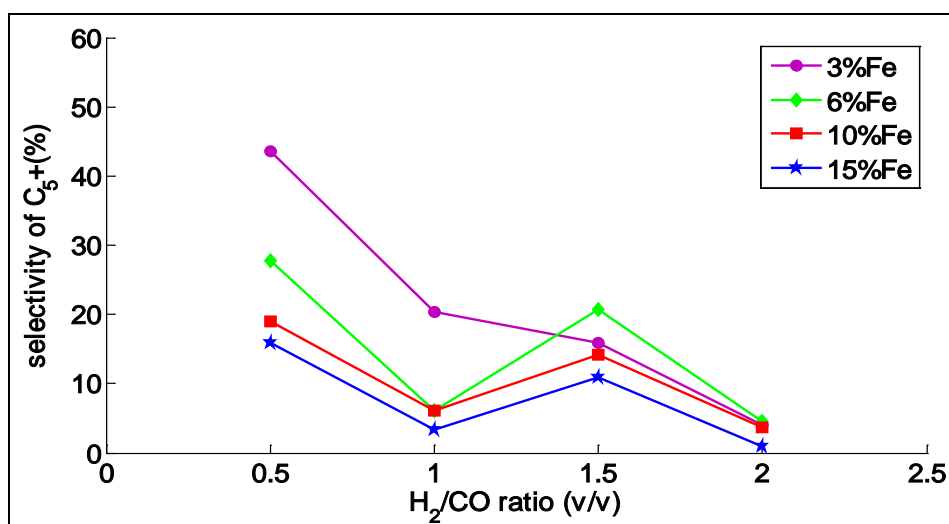


Figure 4-39: Effect of H₂/CO ratio at variety of the Fe loading on the selectivity of the heavy hydrocarbon for SiO₂ supported Fe-based catalyst.

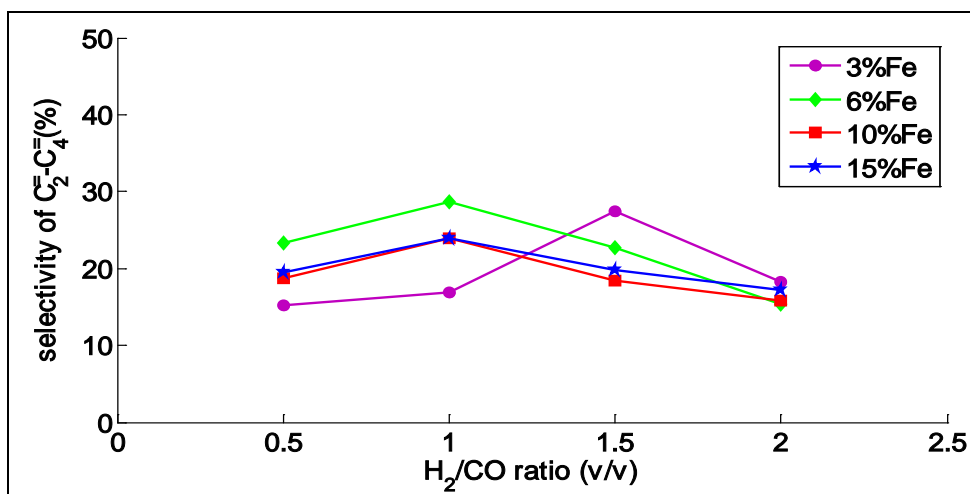


Figure 4-40: Effect of H₂/CO ratio at variety of the Fe loading on the selectivity of the olefins (C₂⁻-C₄⁻) for SiO₂ supported Fe-based catalyst.

II. Space velocity

The space velocity in the catalyst can be defined as mass space velocity (V_m), volumetric space velocity (V_v), and surface space velocity (V_s) where V represents the rate of the given reactant per unit mass or volume or surface area of the catalyst, respectively. The effect of the V_m on the catalytic performance of silica-supported Fe nanoparticles prepared by impregnation method at 523K and 1.5H₂/CO ratio was monitored as the total flow rate of reactant varied between 0.6, 2.4 and 4.8L/h. As seen in Figure 4-41, an opposite trend was obtained between the CO conversion and the V_m . The CO conversion decreased with increasing space velocity. The CO conversion decreased from 54 to 26% when the V_m increased from 3 to 24L/g-cat.h. The same trend was also observed by Liu *et al.* [15] over commercial Fe/Mn catalyst and they found that the CO conversion sharply decreased from 82 to 30% with increasing space velocity from 0.46×10^{-3} to 1.85×10^{-3} Nm³/Kg-cat.s. Davis [19] showed the dependency of the CO conversion on the V_m and he also found that increasing the space velocity from 5 to 50 NL/g-Fe.h resulted in decreasing CO conversion from 82 to 10%. Hayakawa *et al.* [21] reported that the CO conversion and the selectivity of the heavy hydrocarbons increased with increasing residence time (τ) or in other word by decreasing the V_m (F/W where W is the weight of the catalyst and F is the total flow rate). Results shown in Figure 4-41 show similar trend of the CO

conversion with space velocity obtained for different H₂/CO ratio of 0.5 and 1.5H₂/CO ratio.

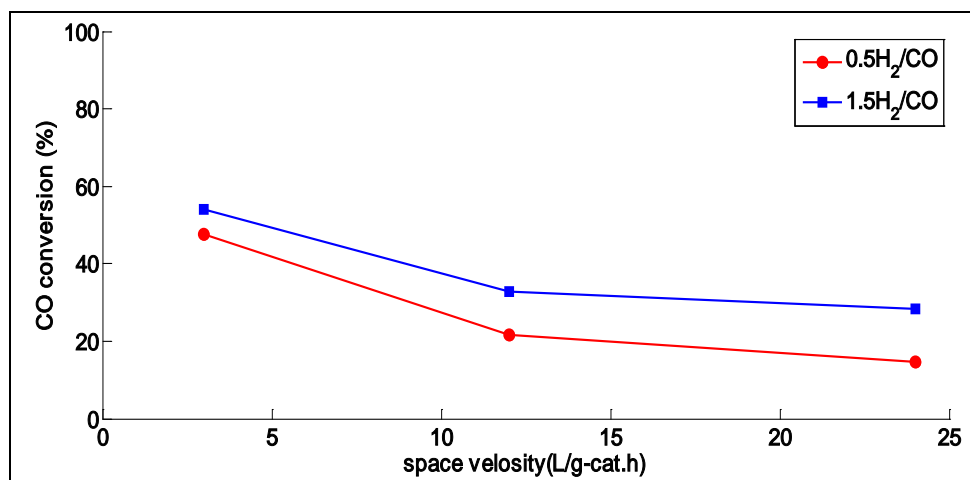


Figure 4-41: Effect of space velocity on CO conversion over 6% Fe/SiO₂ catalysts at 0.5 and 1.5 H₂/CO ratio

An increase in the V_m generally results in high selectivity of light hydrocarbon and lower selectivity of the C₅+ (Figure 4-42). The catalyst weight was constant at the different V_m which indicated that the V_m was only affected by the total feed flow rate. Accordingly, the difference in the product selectivity could be due to difference in flow rate. Increasing the feed flow rate resulted in shorter contact time between the reactant and catalyst thus reduced the probability of chain growth.

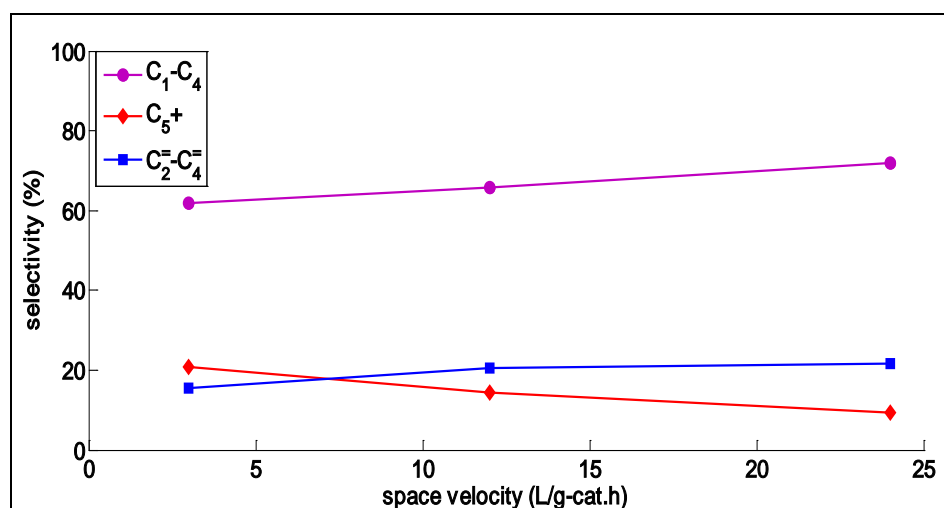


Figure 4-42: Effect of the space velocity on the selectivity of hydrocarbons for SiO₂-supported 6%Fe-based catalyst

III. Reaction temperature

Generally, Fe-based FT catalyst has higher flexibility to the reaction conditions compared to Co-based catalyst. Fe-based catalysts can be operated at a wide range of temperature; either at low (473-523K) or high (573-623K) temperature. Accordingly, Fe catalysts were used for the LTFT and HTFT. The effect of the reaction temperature at the range of temperature between 523 and 563K on the catalytic performance of impregnated 6%Fe/SiO₂ was studied under the reaction condition of 1.5H₂/CO ratio and 3L/g-cat.h. Figure 4-43 shows decreasing in CO conversion with increasing the reaction temperature where, the CO conversion decreased by 28% when the temperature was increased from 523 to 563K. Similar trend on the influence of reaction temperature on CO conversion was obtained for different H₂/CO ratio. For each temperature, higher H₂/CO ratio (1.5) resulted in higher activity compared to that at low H₂/CO ratio (0.5). The product selectivity was also affected by the reaction temperature, as can be observed from Figure 4-44. C₁-C₄ selectivity increased by 20% and C₅+ decreased by 15% as temperature was increased from 523 to 563K. The increase in C₁-C₄ selectivity could be due to higher reaction temperature which facilitated the chain termination step and resulted in production of light hydrocarbons. Liu *et al.* [15] reported that an exponential relation has been obtained between the temperature and the CO conversion where increasing the temperature from 533 to 563K caused the CO conversion to increase from 44.8% to 59.45%. The methane selectivity increased and the selectivity of heavy hydrocarbon decreased with increasing reaction temperature.

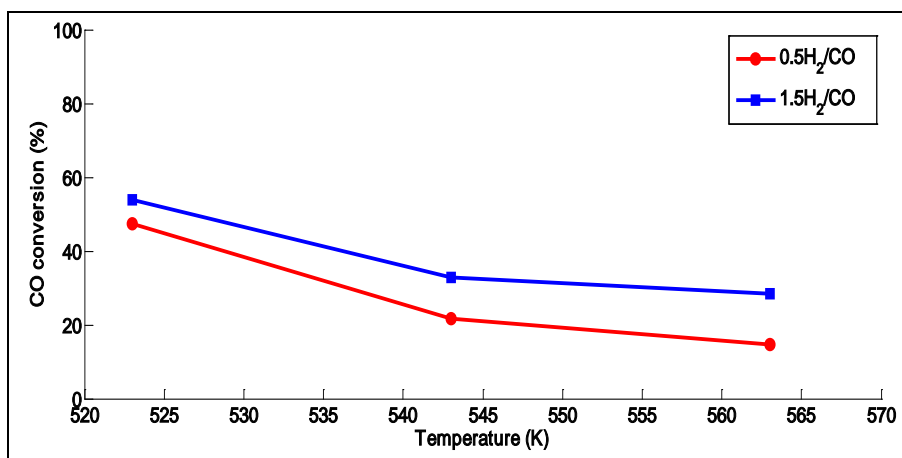


Figure 4-43: Effect of reaction temperature on the CO conversion for 6% Fe/ SiO₂ catalysts prepared by impregnation method at 0.5 and 1.5H₂/CO ratio

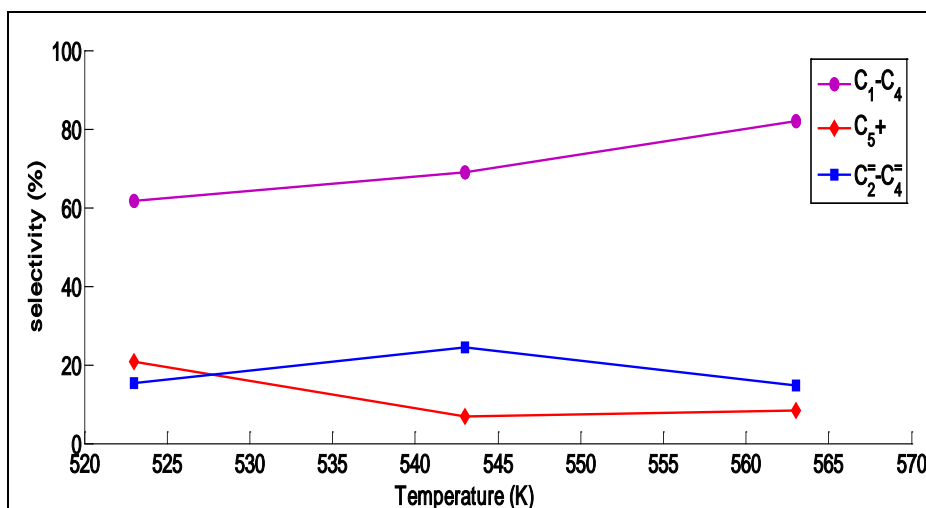


Figure 4-44: Effect of temperature on the selectivity of hydrocarbons for supported 6% Fe/ SiO₂ catalyst at 1.5H₂/CO ratio and 3L/g-cat.h

In summary, these studies were carried out to determine the effects of the reaction conditions such as reactant ratio, space velocity, and reaction temperature on the performance of the FTS over 6%Fe/SiO₂. The reaction conditions were found to be strongly influence the catalyst activity and the product selectivities. The FT performance changed with the variation of H₂/CO from 0.5 to 2, space velocity from 3 to 24L/g-cat.h, and the reaction temperature between 523 and 563K. The optimum reaction conditions were found to be at 1.5H₂/CO, 3L/g-cat.h, and 523K.

4.4.4 Kinetics of the FT reaction over Fe-based catalysts

The kinetics of the FT reaction over different types of catalysts has been studied. Generally many factors affect the reaction rate such as concentration of the reactants, temperature, and nature of the catalysts. The reaction rate is proportional to the temperature and concentration of the reactants raised to a simple power. The rate of reactions usually depends more strongly on temperature than concentration. The rate may double when the temperature is raised by only 10K. The influence of the temperature on rate of reaction was proposed by Arrhenius (1889) where he illustrated the dependence of rate constant (K_A) on temperature (T) according to equation (4.10).

$$\frac{\partial \ln K_A}{\partial T} = \frac{E_A}{RT} \quad (4.10)$$

Then

$$K_A = A \exp^{-E/RT} \quad (4-11)$$

Where,

K_A = specific rate constant, $L \text{ mol}^{-1} \text{ gcat}^{-1} \text{ h}^{-1}$

A = frequency factor for reaction, $L \text{ mol}^{-1} \text{ gcat}^{-1} \text{ h}^{-1}$

E_A = activation energy, KJ/mol

R = gas constant=8.314KJ/mol.K

T = temperature, K

The FT reaction kinetics was obtained under the reaction condition of 1.5 H_2/CO , residence time of 3139.9-392.5 second, reaction temperature between 523 and 563K, and total reactant flow rate of 0.6- 4.8L/h using constant weight of 0.2g of 6% Fe/SiO₂ catalyst prepared via impregnation and precipitation method. As can be seen from Figures 4-45 and 4-46 for the same reaction temperature, the CO conversion increased with increasing W/F (where W is the weight of the catalyst and F is the total flow rate) and seemed to reach equilibrium after 800 s, where selectivity of the light hydrocarbons and olefins decreased and selectivity to heavy hydrocarbon increased. Therefore, the mechanism of FT reactions appeared to be as followed (equation 4-12):



Where, LG is light hydrocarbon, Ol is olefins, and HC is heavy hydrocarbon

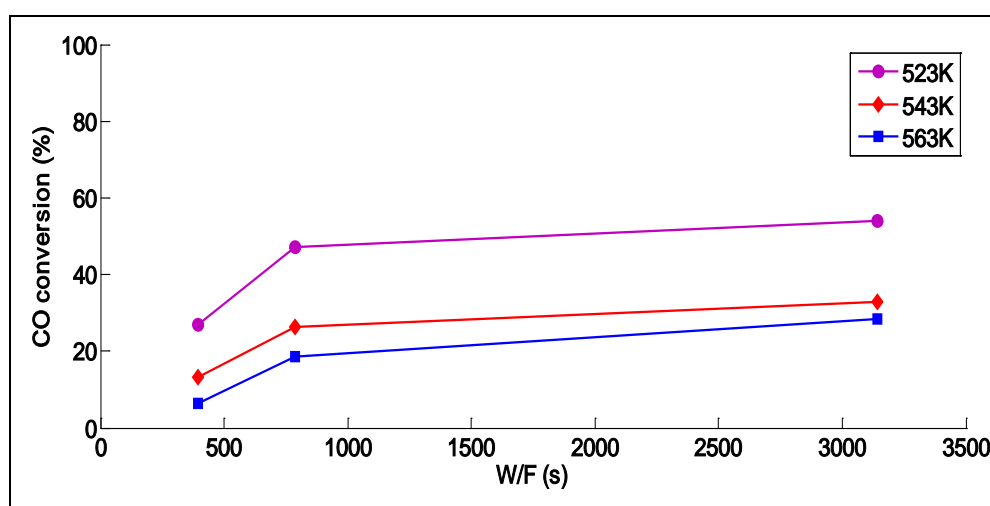


Figure 4-45: Variation of the CO conversion with residence time at different reaction temperature of impregnated 6% Fe/SiO₂ at 1.5 H_2/CO ratio

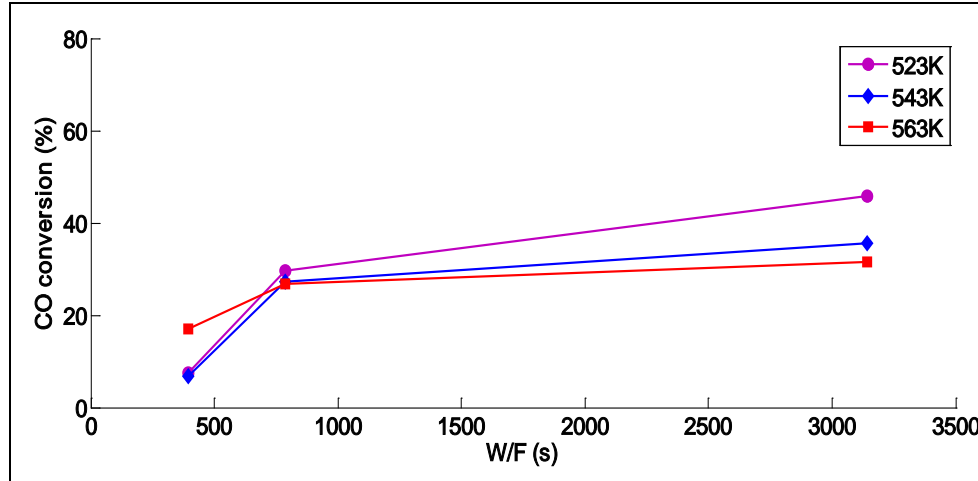


Figure 4-46: Variation of the CO conversion with residence time at different reaction temperatures over precipitated 6%Fe/SiO₂ at 1.5H₂/CO ratio

Reaction kinetics was determined using data presented in Figures 4-47, 4-48, and 4-49. In addition, for simplifying the kinetics of the CO conversion we assumed the reaction to be first order, reversible and at the steady-state. The rate constant was calculated by the formula shown in equation (4-13) [91]. Calculation data for k and E values is shown in Appendix E.

$$-\ln\left(1 - \frac{X_A}{X_{Ae}}\right) = X_{Ae} k \tau \quad (4-13)$$

Where

X_A = conversion of A

X_{Ae} = equilibrium conversion of A

k = constant rate

τ = residence time (W/F)

The values of rate constant (k) at different reaction temperature were determined from the slope of the plot of $(-\ln(1-XA/XAe))$ vs. τ , as shown in Figure 4-47, 4-48 and 4-49.

Figure 4-47, 4-48, and 4-49 show the comparison between the rate constant of impregnated and precipitated catalysts at different reaction temperatures. Precipitation method resulted in catalyst with higher value of k compared to that of impregnation method.

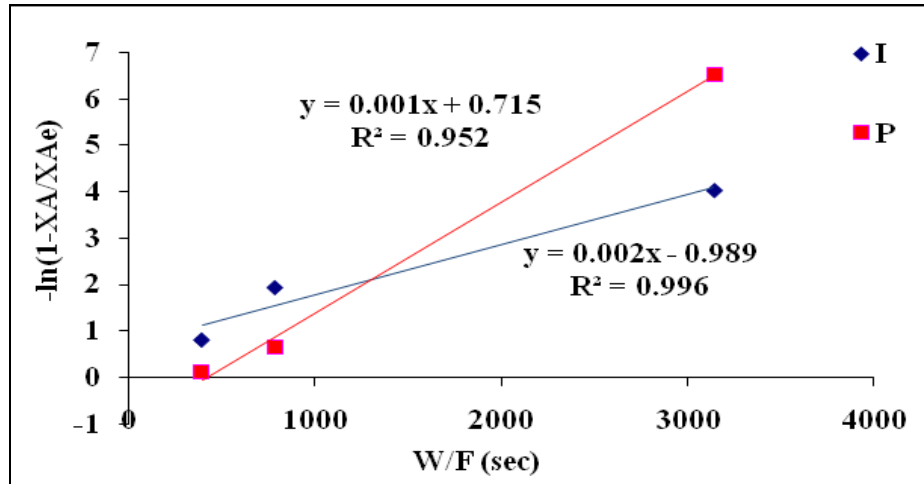


Figure 4-47: Comparison between rate constant of impregnated (I) and precipitated (P) Fe/SiO₂ at 523K and 1.5 H₂/CO ratio

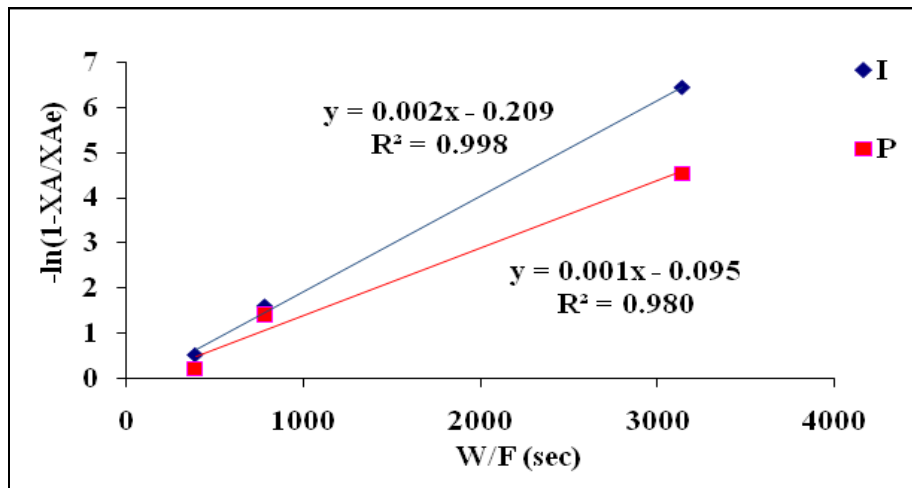


Figure 4-48: Comparison between rate constant of impregnated (I) and precipitated (P) Fe/SiO₂ at 543K and 1.5 H₂/CO ratio

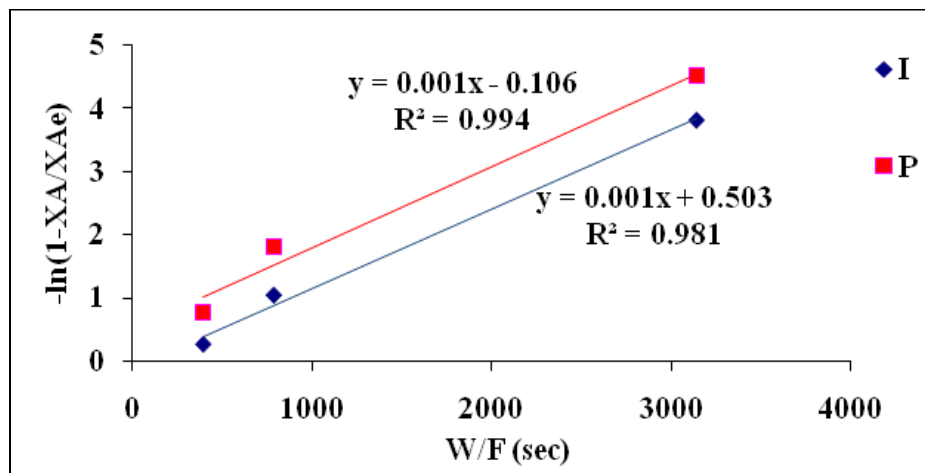


Figure 4-49: Comparison between rate constant of impregnated (I) and precipitated (P) Fe/SiO₂ at 563K and 1.5 H₂/CO ratio

Figure 4-50 shows the Arrhenius plot for the impregnated and precipitated catalyst. Precipitation method resulted in catalyst with higher activation energy compared to those synthesized via impregnation method. The activation energy increased from 9.3KJ/mol to 20.5KJ/mol for the precipitated catalyst compared to impregnated catalyst. higher values of activation energy have been published by Pirola *et al.* [29] where they found that depending on the reaction temperature, two different regimes can be observed and the activation energy for the FT regime on all the catalysts (Fe/SiO₂ with 10-50% Fe loading) range between 80-130KJ/mol and for the second regime (WGS) range between 10-40KJ/mol.

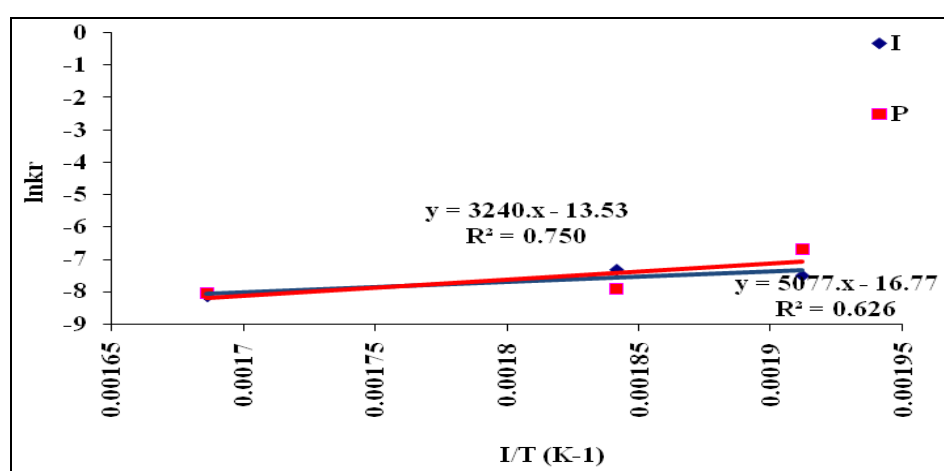


Figure 4-50: Arrhenius plot of 6% Fe/SiO₂ prepared by impregnation (I) and precipitation (P) methods at 1.5 H₂/CO

The results of kinetics studies are summarized in Table 4-11. The value of k decreased with increasing the reaction temperature.

Table 4-11: Activation energy

| Catalyst | Preparation method | Temperature (K) | H ₂ /CO ratio | Rate constant | Activation energy (KJ/mol) |
|------------------------|--------------------|-----------------|--------------------------|---------------|----------------------------|
| 6% Fe/SiO ₂ | impregnation | 523 | 1.5 | 0.00055 | 9.3 |
| 6% Fe/SiO ₂ | impregnation | 543 | 1.5 | 0.00033 | |
| 6% Fe/SiO ₂ | impregnation | 563 | 1.5 | 0.00029 | |
| 6% Fe/SiO ₂ | precipitation | 523 | 1.5 | 0.00122 | 20.5 |
| 6% Fe/SiO ₂ | precipitation | 543 | 1.5 | 0.00036 | |
| 6% Fe/SiO ₂ | precipitation | 563 | 1.5 | 0.00032 | |

4.5 Effect of the reaction conditions on the catalyst properties

The influence of the reaction conditions on the physical and chemical properties was investigated using N₂-physical adsorption, FESEM, and TEM. Comparison between the properties of the fresh and spent catalysts was carried out for the 6% Fe loading on SiO₂ prepared by impregnation and precipitation method, and 6% Fe on Al₂O₃-SiO₂ support after the catalysts were exposed to reaction condition of 523K, 5hr, 1.5H₂/CO and SV=3L/g-cat.h. Spent catalyst showed decrease in the surface area, pore volume and average particle size for catalyst. For the spent Fe/Al₂O₃-SiO₂ (Table 4-12) the surface area decreased by 20% compared to that of the fresh one. Fe/SiO₂ catalyst showed slight decrease in the surface area after exposure to the reaction atmosphere. The difference in the surface area and pore volume after exposure to reaction can be attributed to a partial collapse of the pore or formation of an inactive carbon.

Table 4-12: Textural properties of the supported Fe-based catalysts before and after the FT reaction

| Physical properties | Fresh catalyst | | | Spent catalyst | | |
|----------------------------------|---------------------------|---------------------------|---|---------------------------|---------------------------|---|
| | 6%Fe/SiO ₂ (I) | 6%Fe/SiO ₂ (P) | 6%Fe/Al ₂ O ₃ -SiO ₂ (I) | 6%Fe/SiO ₂ (I) | 6%Fe/SiO ₂ (P) | 6%Fe/Al ₂ O ₃ -SiO ₂ (I) |
| surface area (m ² /g) | 39.47 | 45.09 | 56.95 | 38.54 | 44.68 | 35.79 |
| Pore volume (cc/g) | 0.155 | 0.125 | 0.288 | 0.104 | 0.128 | 0.135 |
| Average pore size (Å) | 164.86 | 110.14 | 202.73 | 142.61 | 114.56 | 150.97 |

Spent catalysts were characterized by FESEM and TEM to determine the morphology of the catalyst after the FTS reaction. As shown in Figures 4-51, 4-52, and 4-53, significant change in the morphology of the catalyst was obtained after exposure to reaction. Small change was observed on the morphology of the Fe/SiO₂ after exposure to reaction (Figure 4-51) due to increasing the amount of the Fe particles between the SiO₂ spheres. Similar trend of the morphology change was

shown on the Fe/SiO₂ prepared by precipitation method (Figure 4-52). In addition, Figure 4-53 shows a drastic change on the morphology of Fe/Al₂O₃-SiO₂ catalyst after the reaction where the particles disintegrated into smaller particles and catalyst pores collapsed. This result is in a good agreement with the BET results where the surface area and the pore size decreased after the reaction.

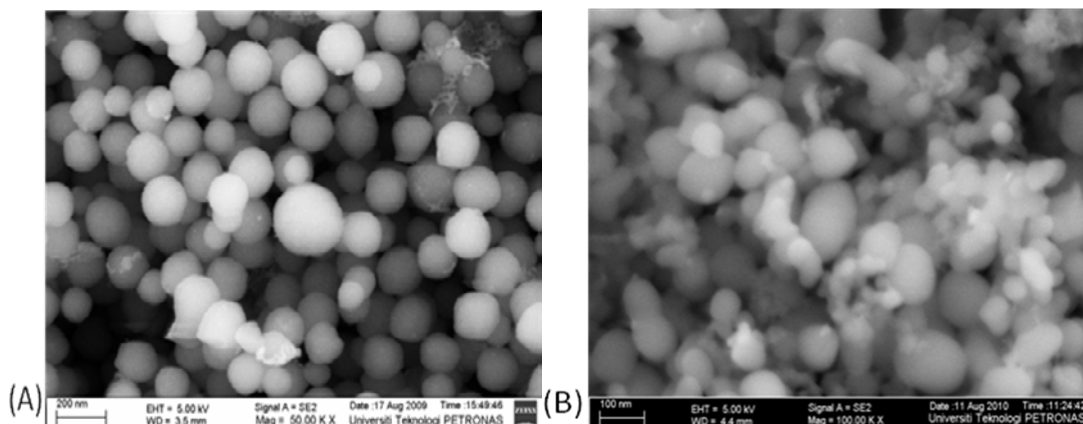


Figure 4-51: FESEM images of Fe/SiO₂ catalyst prepared by impregnation method before (A) and after (B) FTS reaction

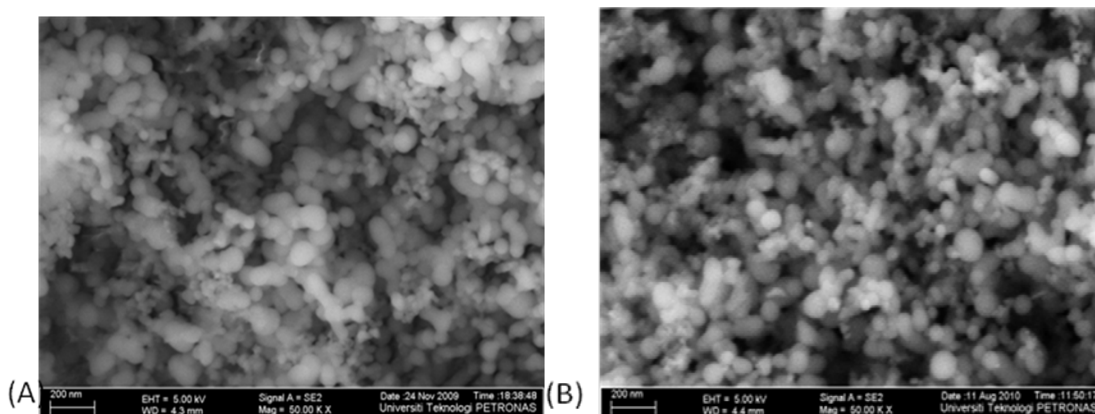


Figure 4-52: FESEM images of Fe/SiO₂ catalyst prepared by precipitation method before (A) and after (B) FTS reaction

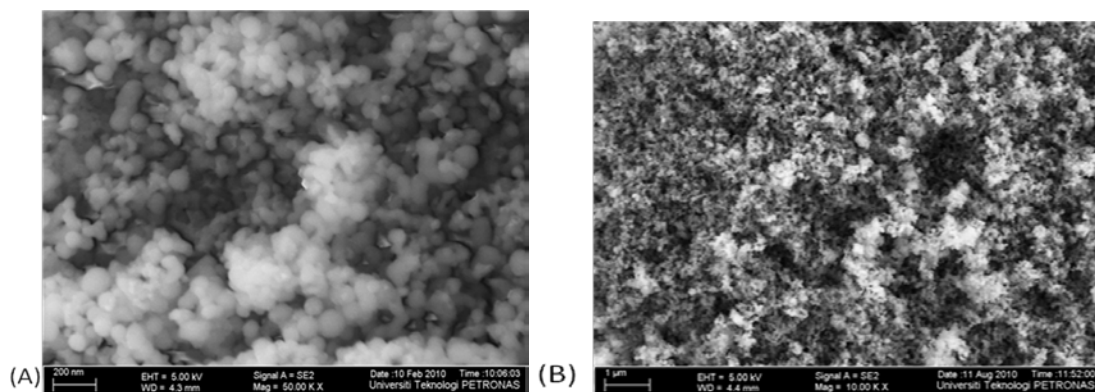


Figure 4-53: FESEM images of Fe/Al₂O₃-SiO₂ catalyst prepared by impregnation method before (A) and after (B) FTS reaction

Table 4-13 shows the changes in the elemental compositions after exposure to reaction atmosphere. The weight of carbon increased after the reaction while the weight of Fe component decreased. These results suggested that the decrease in the catalyst stability and activity with the TOS could be due to increase in of the carbon content and decrease in Fe content. The nature of the carbon plays an important role in the catalytic activity and stability, for example amorphous carbon influences the catalytic activity while graphitic carbon reinforced the catalyst deactivation [2].

Table 4-13: EDX elemental analyses of the fresh and spent catalysts

| Element | Element composition (wt %) | | | | | |
|---------|----------------------------|--------|----------------------------|--------|--|--------|
| | 6% Fe/SiO ₂ (I) | | 6% Fe/SiO ₂ (P) | | 6% Fe/Al ₂ O ₃ -SiO ₂ | |
| | Fresh | Spent | Fresh | Spent | Fresh | Spent |
| Fe | 5.50 | 4.62 | 4.27 | 3.99 | 6.33 | 4.98 |
| Si | 26.94 | 22.25 | 23.60 | 20.78 | 24.83 | 22.67 |
| Al | - | - | - | - | 1.96 | 1.19 |
| O | 48.96 | 41.01 | 49.91 | 46.47 | 45.06 | 46.11 |
| C | 18.60 | 32.12 | 22.22 | 28.76 | 21.64 | 24.33 |
| Total | 100.00 | 100.00 | 100.00 | 100.00 | 100.00 | 100.00 |

TEM images of the fresh and spent Fe/SiO₂ catalysts prepared by impregnation and precipitation methods as well as Fe/ Al₂O₃-SiO₂ catalyst are shown in Figure 4-54, 4-55 and 4-56, respectively. The morphology of the catalyst was changed after FT reaction. After exposure to FTS condition, the size of Fe particles increased, the shape became irregular, and SiO₂ surface coverage also decreased. An opposite trend was observed for Al₂O₃-SiO₂ supported catalyst which showed degradation of particles. SiO₂ support enhanced the sintering and resulted in bigger Fe particles for the spent catalyst compared to the fresh one.

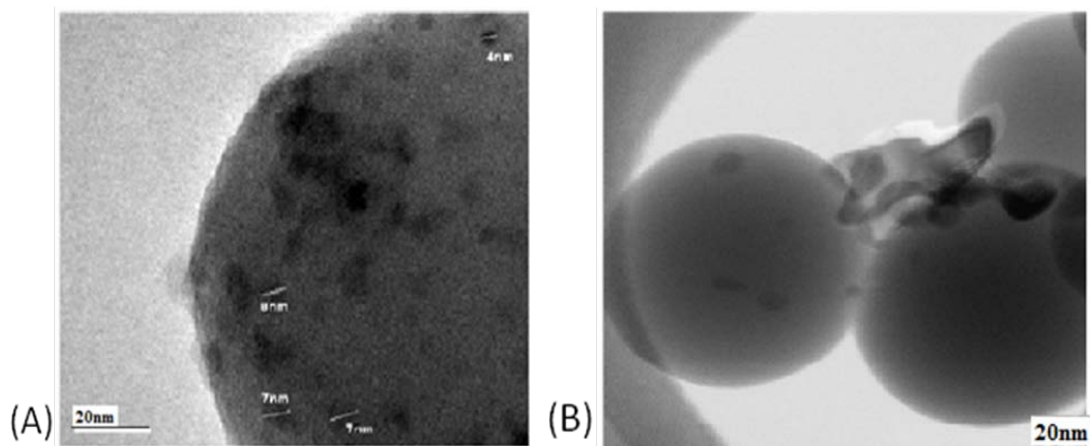


Figure 4-54: Comparison between the Fe particle distribution for impregnated 6% Fe/SiO₂ catalyst (a) before reaction and (b) after reaction

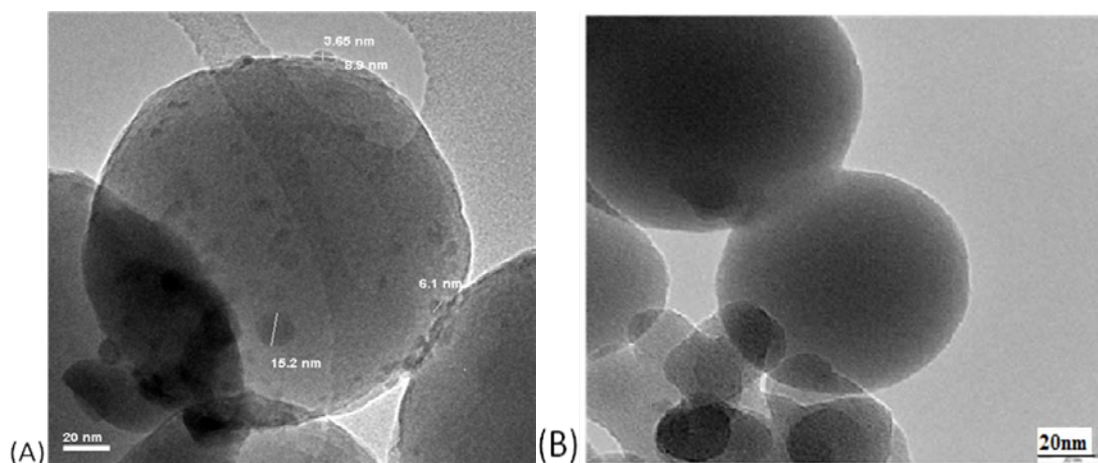


Figure 4-55: Comparison between the Fe particle distribution for precipitated 6% Fe/SiO₂ catalyst (a) before reaction and (b) after reaction

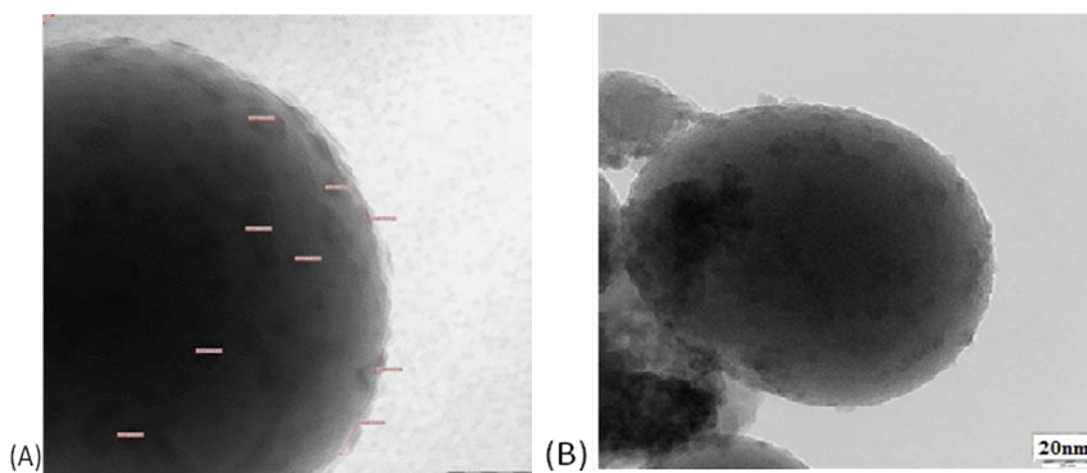


Figure 4-56: Comparison between the Fe particle distribution for impregnated 6% Fe/Al₂O₃-SiO₂ catalyst (a) before reaction and (b) after reaction

4.6 Summary of the reaction studies

The effects of synthesis technique, support, and Fe loading on the physicochemical properties of the catalysts were investigated. Good catalytic properties were exhibited by the catalyst with low Fe loading (≤ 6 wt %) on SiO₂ support, synthesized via impregnation method. The 6%Fe/SiO₂ catalyst resulted in relatively high CO conversion and production of desired hydrocarbon (C₅₊). Correlation between Fe particle size and the FT performance was performed. Small Fe particles resulted in higher catalytic activity and C₅₊-selectivity as well as lower selectivity to the light hydrocarbon. The effect of the promoter on the catalyst properties and the FT performance was also investigated. Addition of Cu promoter enhanced the reducibility of the catalysts whereas an opposite trend was obtained by the addition of the K promoter. Nevertheless, the addition of K promoter enhanced the selectivity of C₅₊ to a value of 54.42% compared to 20.73% for the unpromoted Fe/SiO₂ catalyst.

Comparisons between the results obtained in this study and those of previous studies are demonstrated in Table 4-14. Similar trend between the catalyst loading and surface area have been published by Pirola *et al.* [29] where they reported that the surface area of the catalyst decreased by increasing the loading of Fe. They also reported that the CO conversion increased with increasing the Fe loading but the opposite was observed for C₅₊ selectivity. The synthesized 10%Fe/SiO₂ catalyst in this study showed the CO conversion of 48.2% which was relatively higher than the CO conversion (6%) reported by Pirola *et al.* [29] at the same Fe loading 10wt%. Synthesized Cu promoted catalyst in this work showed higher activity and selectivity to C₅₊ and lower methane selectivity than that obtained by Lohitharn *et al.* [51]. The performance of the K promoter in this study was found to be lower than that prepared by Hayakawa *et al.* [21] in terms of the CO conversion and selectivity of C₅₊. This can be due to the difference in the reaction conditions as they used higher pressure and longer TOS and also due to the difference in the properties of the catalyst where they used catalyst with bigger surface area of 175m²/g and Fe loading compared to the catalyst that was synthesized in this study. As a comparison with different preparation method, 6%Fe/SiO₂ catalyst synthesized by impregnation method showed higher

activity and selectivity to heavy hydrocarbon than 5%Fe/SiO₂ catalyst synthesized by microemulsion method [10].

Table 4-14: Comparison of the Fe-based catalyst performance in FTS

| Catalyst | Fe loading (wt %) | Average particle size (nm) | BET surface area (m ² /g) | CO conversion (%) | Product Selectivity (%) | |
|---|-------------------|----------------------------|--------------------------------------|-------------------|--------------------------------|-----------------------|
| | | | | | C ₁ -C ₄ | C ₅ + |
| Fe/SiO ₂ ^A (I) | 6 | 8.6±1.1 | 39.47 | 54.02 | 57.48 | 20.73 |
| Fe/SiO ₂ ^A (I) | 10 | 12.6±1.3 | 23.82 | 48.24 | 70.07 | 14.13 |
| Fe/SiO ₂ ^A (I) | 15 | 13±1.2 | 23.98 | 44.68 | 77.37 | 11.00 |
| Fe/SiO ₂ ^A (P) | 6 | 17.3±7.3 | 54.1 | 45.7 | 63.43 | 9.68 |
| Fe/Cu/SiO ₂ ^A (I) | 6 | - | 39.73 | 24.37 | 72.04 | 8.16 |
| Fe/K/SiO ₂ ^A (I) | 6 | - | 33.20 | 28.92 | 31.48 | 54.42 |
| Fe/SiO ₂ ^B (I) | 10 | - | 362 | 6 | 19 (CH ₄) | 47 (<C ₇) |
| Fe/SiO ₂ ^B (I) | 50 | - | 143 | 74 | 9 (CH ₄) | 20 (<C ₇) |
| Fe/Cu/SiO ₂ ^C (P) | - | - | 329 | 10 | 95 | 5 |
| Fe/K/SiO ₂ ^D (P) | - | - | 175 | 66 | 26.6 | 73.4 |
| Fe/SiO ₂ ^E (ME) | 5 | - | 304 | 13.5 | 88.7 | 10.1 |

^A Reaction condition T=523K, P=1atm, W=0.2g, H₂/CO=1.5

^B Reaction condition T=523K, P=2MPa, W=1g, H₂/CO=2 [29]

^C Reaction condition T=553K, P=1.8atm, W=0.1g, H₂/CO=2, t=300min [51]

^D Reaction condition T=513-553K, P=1-2.85MPa, W=3g, H₂/CO=0.4-2, t=100hr [21]

^E Reaction condition T=573K, P=1.01MPa, W=4g, H₂/CO=2 [10]

I= catalyst prepared by impregnation method

P= catalyst prepared by precipitation method

ME= catalyst prepared by microemulsion method

CHAPTER 5

Conclusion and Recommendations

5.1 Conclusion

Fe nanoparticles on SiO₂ and Al₂O₃-SiO₂ supports were synthesized via impregnation and precipitation methods. The effects of different Fe loading (3, 6, 10, and 15 wt %), synthesis technique (impregnation and precipitation), type of support (SiO₂ and Al₂O₃-SiO₂), and promoter (Cu, K, and Cu/K) on the physicochemical properties of the catalysts and performance in the FTS were studied. The catalytic properties were evaluated by N₂ physical adsorption, FESEM, TEM, XRD, and H₂-TPR. Based on these characterization results the following conclusions can be drawn:

- Fe loading was found to have significant influence on the catalytic properties. The surface area decreased with increase in Fe loading. The results of FESEM and TEM investigations demonstrated that the dispersion of Fe particles over the support were uniform at Fe loading (≤ 6 wt %). Narrower particle size distribution and smaller size of Fe nanoparticles were obtained at lower Fe loading.
- Compared to the precipitation method, catalyst synthesized via impregnation method had smaller surface area, better distribution of Fe nanoparticles over the support, smaller particle size, and lower reduction temperature.
- SiO₂ served as a better support compared to Al₂O₃-SiO₂.
- Incorporation of Cu and K promoters to the Fe-based catalyst was found to have significant effects on the surface area, dispersion, and reducibility of the catalysts. Addition of Cu promoter was found to be more useful in term of enhancing the reducibility of the catalyst.

The supported Fe nanoparticles were evaluated for the FT reaction. The effects of different reaction conditions on the FT performance were also investigated. The following can be concluded from the catalytic studies:

- Catalyst with low Fe loading (≤ 6 wt%) resulted in higher catalytic stability and activity as well as higher selectivity to C_{5+} and olefins. Higher Fe loading suppressed the stability, decreased the CO conversion, and enhanced the C_1 - C_4 selectivity.
- Catalyst prepared by impregnation method exhibited better stability, activity, and selectivity to C_{5+} compared to the catalyst that was synthesized by precipitation method.
- Al_2O_3 - SiO_2 support decreased the catalytic stability and activity and increased the selectivity of C_1 - C_4 compared to that of SiO_2 support. This difference may be due to increase in metal-support interaction, resulted from increase in the catalyst acidity in the presence of Al_2O_3 .
- K promoter resulted in lower CO conversion and higher selectivity to heavy hydrocarbon (C_{5+}) compared to the unpromoted catalyst.
- Increasing the reactant ratio (H_2/CO), V_m , and reaction temperature resulted in lower CO conversion and higher C_1 - C_4 selectivity. The optimum reaction conditions for FT reaction were found to be at 523K, 1.5 H_2/CO ratio, and V_m of 3L/g-cat.h over the impregnated 6%Fe/ SiO_2 catalyst.

The comparison between properties and performance of Fe-based catalysts for the impregnation and precipitation methods and the effects of Fe particle size for supported Fe catalyst have not been reported in the literature. Correlation between Fe particle size and FT performance has been illustrated in this work. Particle size plays an important role in the catalytic activity and hydrocarbons selectivity. Conversion of CO and C_{5+} selectivity decreased with increase in Fe particle size.

Based on the results obtained in this study, catalysts with Fe particle size less than 9 nm exhibited good FT performance in terms of stability, CO conversion and product selectivity.

5.2 Recommendation

Based on the conclusion above, a few recommendations can be drawn for future work in this area:

- Due to the fact that physical and chemical properties of the catalyst affect the overall FT reaction performance therefore, improvement of the catalyst properties such as higher dispersion of Fe and lower reduction temperature can be made by varying the composition of the catalyst, loading of the active site, and synthesis technique.
- Supported Fe-based catalyst has different active sites and this mainly depends on the pretreatment step. Therefore, investigation on the effect of pretreatment conditions on the catalyst properties should be preformed.
- Due to the ability of using Fe-based catalyst in a wide range of the operation condition, varying the reaction pressure could help to understand the kinetic of the FT reaction and enhanced the selectivity of the higher hydrocarbons. Other parameters could also be varied such as type of the reactor and reaction time. The reaction time can be prolonged in order to study the reaction kinetic and dynamic and also the catalyst deactivation.
- This work presented the effect of the size of the Fe nanoparticles on the FT performance. In order to have better understanding of these phenomena, the catalyst should be synthesized at different particles size range, especially less than 5nm.

REFERENCES

- [1] C. Masters, "The Fischer-Tropsch Reaction," in *Advances in Organometallic Chemistry*, Vol. 17, Amsterdam, Netherland, 1979, pp. 61-100.
- [2] A. Steynberg, M. E. Dry, "Introduction to Fischer-Tropsch technology," in *Fischer-Tropsch Technology*, 1st edition, Amsterdam, Netherland, Elsevier, 2004, ch. 1, pp. 1-59.
- [3] A. P. Raje and B. H. Davis, "Fischer-Tropsch synthesis over iron-based catalysts in a slurry reactor: reaction rates, selectivities and implications for improving hydrocarbon productivity", *Catal. Today*, vol. 36, pp. 335-345, Jun. 1997.
- [4] C. H. Bartholomew and R. J. Farrauto, "Hydrogen production and synthesis gas reaction", in *Fundamentals of Industrial Catalytic Processes*, 2nd edition, New Jersey, John Wiley & Sons, Inc., Hoboken, 2006, ch. 6, sec. 6.5, pp. 398-457.
- [5] L. D. Mansker, "Characterization of working iron Fischer-Tropsch catalysts using quantitative diffraction methods", Ph.D. dissertation, Dept. Chem. Eng., UNM, New Mexico., USA, 1999.
- [6] M. E. Dry, "The Fischer-Tropsch process: 1950-2000", *Catal. Today*, vol. 71, pp. 227-241, Jan. 2002.
- [7] C. H. Bartholomew, "History of cobalt catalyst design for FTS", in *Proceedings of the National Spring Meeting of the American Institute of Chemical Engineers (AIChE'03)*, New Orleans, 2003.
- [8] H. N. Pham, "Agglomerate strength and attrition in slurry phase iron-based Fischer-Tropsch catalysts," Ph.D. dissertation, Dept. Chem. Eng., UNM., New Mexico, USA., 2001.
- [9] M. D. Shroff, D. S. Kalakkad, K. E. Coulter, S. D. Kohler, M. S. Harrington, N. B. Jackson, A. G. Sault and A. K. Datye, "Activation of Precipitated Iron Fischer-Tropsch Synthesis Catalysts", *Catal.*, vol. 156, pp. 185-207, Oct. 1995.

- [10] T. Herranz, S. Rojas, F. J. Pérez-Alonso, M. Ojeda, P. Terreros and J. L. G. Fierro, "Carbon oxide hydrogenation over silica-supported iron-based catalysts: Influence of the preparation route", *Appl. Catal. A: General*, vol. 308, pp. 19-30, Jul. 2006.
- [11] M. Bakhtiari, F. Khorasheh, A. Zamanian, A. Nakhaeipour and M. Irani, "Preparation, Evaluation and Characterization of Monolithic Catalysts for Fischer-Tropsch Synthesis", *Petroleum & Coal*, vol. 50, pp. 56–61, Sept. 2008.
- [12] J. Brown, J. McDonald and C. Wilson, "Microreactors for synthetic diesel production to optimize nanostructured cobalt catalyst", presented at the 15th IC on Solid-State Sensors, Actuators and Microsystems, Denver, Colorado, 2009, pp. 588-591.
- [13] W. Hai-jun, W. Bao-shan, L. Ting-zhen, T. Zhi-chao, A. Xia, X. Hong-wei and L. Yong-wang, "Effects of SiO₂ and Al₂O₃ on performances of iron-based catalysts for slurry Fischer–Tropsch synthesis", *Fuel Chem. and Tech.*, vol. 35, pp. 589-594, Oct. 2007.
- [14] B. Delmon, "Preparation of heterogeneous catalysts", *Thermal Anal. and Calorimetry*, vol. 90, pp. 49-65, Oct. 2007.
- [15] Y. Liu, B. Teng, X. Guo, Y. Li, J. Chang, L. Tian, X. Hao, Y. Wang, H. Xiang, Y. Xu and Y. Li, "Effect of reaction conditions on the catalytic performance of Fe-Mn catalyst for Fischer-Tropsch synthesis", *Mole. Catal. A: Chem.*, vol. 272, pp. 182-190, Jul. 2007.
- [16] W. J. Cannella, "Factors Influencing Kinetics and Product Distribution in Fischer-Tropsch Synthesis over Iron Catalysts", Ph.D. dissertation, Dept. chem. Eng., UC Berkeley, California, USA, 1984.
- [17] Y. Li, H. Wan, B. Wu, C. Zhang, B. Teng, Z. Tao, Y. Yang, Y. Zhu, and H. Xiang, "Effect of Al₂O₃/SiO₂ ratio on iron-based catalysts for Fischer–Tropsch synthesis", *Fuel*, vol. 85, pp. 1371-1377, Aug. 2006.
- [18] W. Ngantsoue-Hoc, Y. Zhang, R. J. O'Brien, M. Luo and B. H. Davis, "Fischer–Tropsch synthesis: activity and selectivity for Group I alkali promoted iron-based catalysts", *Appl. Catal. A: General*, vol. 236, pp. 77-89, Sept. 2002.

- [19] B. H. Davis, "Fischer-Tropsch synthesis: relationship between iron catalyst composition and process variables", *Catal. Today*, vol. 84, pp. 83-98, Aug. 2003.
- [20] J. Xu, "Rational design of silica-supported platinum-promoted iron Fischer-Tropsch synthesis catalysts based on activity-structure relationships", Ph.D. dissertation, chem. Eng. Chemistry, BYU, Provo, Utah, USA, 2003.
- [21] H. Hayakawa, H. Tanaka and K. Fujimoto, "Studies on catalytic performance of precipitated iron/silica catalysts for Fischer-Tropsch Synthesis", *Appl. Catal. A: General*, vol. 328, pp. 117-123, Sept. 2007.
- [22] Google Image, available: <http://www.zero.no/transport/biodrivstoff/hva-er-biodrivstoff/ft3.gif> , 2010.
- [23] Y. Wang, A. L. Tonkovich, T. Mazanec, F. P. Daly, D. Vander Wiel, J. Hu, C. Cao, C. Kibby, X. Li and M. D. Briscoe, "Fischer-Tropsch synthesis using microchannel technology and novel catalyst and microchannel reactor", U.S. Patent 7084180 Vol. Aug. 1, 2006.
- [24] C. Cao, D. R. Palo, A. L. Y. Tonkovich and Y. Wang, "Catalyst screening and kinetic studies using microchannel reactors", *Catal. Today*, vol. 125, pp. 29-33, 2007
- [25] A. Y. Khodakov, W. Chu and P. Fongarland, "Advances in the Development of Novel Cobalt Fischer-Tropsch Catalysts for Synthesis of Long-Chain Hydrocarbons and Clean Fuels", *Chem. Rev.*, vol. 107, pp. 1692-1744, 2007.
- [26] J. Gaube and H. Klein, "Studies on the reaction mechanism of the Fischer-Tropsch synthesis on iron and cobalt", *Molecular Catal. A: Chem.*, vol. 283, pp. 60-68, Mar. 2008.
- [27] J. Hagen, "The Phenomenon Catalysis", in *Industrial catalysis*, 2nd edition, Weinheim, Germany, WILEY-VCH, 2006, ch.1, sec. 1.1, pp. 1-11.
- [28] P. Biloen and W. Sachtler, "Mechanism of hydrocarbon synthesis over Fischer-Tropsch catalysts", *Adva. in Catal.*, vol. 30, pp. 165-216, 1981.
- [29] C. Pirola, C. L. Bianchi, A. Di Michele, S. Vitali and V. Ragaini, "Fischer Tropsch and Water Gas Shift chemical regimes on supported iron-based catalysts at high metal loading," *Catal. Comm.*, vol. 10, pp. 823-827, Feb. 2009.

- [30] M. A. Vannice, "The catalytic synthesis of hydrocarbons from H₂/CO mixtures over the group VIII metals: I. the specific activities and product distributions of supported metals", *Catal.*, vol. 37, pp. 449-461, Jun. 1975.
- [31] H. Wan, B. Wu, X. An, T. Li, Z. Tao, H. Xiang and Y. Li, "Effect of Al₂O₃ Binder on the Precipitated Iron-Based Catalysts for Fischer-Tropsch Synthesis", *Natural Gas Chem.*, vol. 16, pp. 130-138, Jun. 2007.
- [32] A. Khodakov, B. Peregryn, A. Lermontov, J. S. Girardon and S. Pietrzyk, "Transient studies of the elementary steps of Fischer-Tropsch synthesis", *Catal. Today*, vol. 106, pp. 132-136, 2005.
- [33] A. M. Saib, A. Borgna, J. van de Loosdrecht, P. J. van Berge, J. W. Geus and J. W. Niemantsverdriet, "Preparation and characterisation of spherical Co/SiO₂ model catalysts with well-defined nano-sized cobalt crystallites and a comparison of their stability against oxidation with water," *J. of Catal.*, vol. 239, pp. 326-339, Apr. 2006.
- [34] J. Niemantsverdriet, A. Van der Kraan, W. Van Dijk and H. Van der Baan, "Behavior of metallic iron catalysts during Fischer-Tropsch synthesis studied with Mössbauer spectroscopy, x-ray diffraction, carbon content determination, and reaction kinetic measurements", *J. Phys. Chem.*, vol. 84, pp. 3363-3370, 1980.
- [35] Y. Jin, "Phase transformation of iron-based catalysts for Fischer-Tropsch synthesis", Ph.D dissertation, Dept. Chem. Eng., UNM, New Mexico, USA, 1999.
- [36] D. B. Bukur, L. Nowicki, R. K. Manne and X. S. Lang, "Activation Studies with a Precipitated Iron Catalyst for Fischer-Tropsch Synthesis: II. Reaction Studies", *Catal.*, vol. 155, pp. 366-375, Sept. 1995.
- [37] M. Yamada, G. Bian, A. Oonuki, N. Koizumi, and H. Nomoto "Studies with a precipitated iron Fischer-Tropsch catalyst reduced by H₂ or CO", *Molecular Catal. A: Chem.*, vol. 186, pp. 203-213, Jul. 2002.
- [38] R. J. O'Brien, L. Xu, R. L. Spicer and B. H. Davis, "Activation Study of Precipitated Iron Fischer-Tropsch Catalysts", *Eng. Fuels*, vol. 10, pp. 921-926, 1996.
- [39] M. Ding, Y. Yang, B. Wu, J. Xu, C. Zhang, H. Xiang and Y. Li, "Study of phase transformation and catalytic performance on precipitated iron-based catalyst for

Fischer–Tropsch synthesis", *Molecular Catal. A: Chem.*, vol. 303, pp. 65-71, Apr. 2009.

[40] Y. Jin and A. K. Datye, "Phase transformations in iron Fischer-Tropsch catalysts during temperature-programmed reduction", *Catal.*, vol. 196, pp. 8-17, 2000.

[41] C. Ngamcharussrivichai, A. Imyim, X. Li and K. Fujimoto, "Active and Selective Bifunctional Catalyst for Gasoline Production through a Slurry-Phase Fischer Tropsch Synthesis", *Ind Eng Chem Res*, vol. 46, pp. 6883-6890, 2007.

[42] Y. Yang, H. W. Xiang, L. Tian, H. Wang, C. H. Zhang, Z. C. Tao, Y. Y. Xu, B. Zhong and Y. W. Li, "Structure and Fischer-Tropsch performance of iron-manganese catalyst incorporated with SiO₂", *Appl. Catal. A: General*, vol. 284, pp. 105-122, 2005.

[43] E. Iglesia, S. L. Soled and R. A. Fiato, "Fischer-Tropsch synthesis on cobalt and ruthenium. Metal dispersion and support effects on reaction rate and selectivity", *Catal.*, vol. 137, pp. 212-224, Sept. 1992.

[44] C. Zhang, H. Wan, Y. Yang, H. Xiang and Y. Li, "Study on the iron–silica interaction of a co-precipitated Fe/SiO₂ Fischer–Tropsch synthesis catalyst", *Catal. Comm.*, vol. 7, pp. 733-738, Sept. 2006.

[45] H. Wan, B. Wu, Z. Tao, T. Li, X. An, H. Xiang and Y. Li, "Study of an iron-based Fischer–Tropsch synthesis catalyst incorporated with SiO₂", *Molecular Catal. A: Chem.*, vol. 260, pp. 255-263, Dec. 2006.

[46] W. Hou, B. Wu, Y. Yang, Q. Hao, L. Tian, H. Xiang and Y. Li, "Effect of SiO₂ content on iron-based catalysts for slurry Fischer–Tropsch synthesis", *Fuel Process Tech.*, vol. 89, pp. 284-291, Mar. 2008.

[47] H. Dlamini, T. Motjope, G. Joorst, G. Ter Stege and M. Mdleleni, "Changes in Physicochemical Properties of Iron-Based Fischer–Tropsch Catalyst Induced by SiO₂ Addition", *Catal. Lett.*, vol. 78, pp. 201-207, 2002.

[48] D. B. Bukur, D. Mukesh and S. A. Patel, "Promoter effects on precipitated iron catalysts for Fischer-Tropsch synthesis", *Ind. Eng. Chem. Res.*, vol. 29, pp. 194-204, 1990.

- [49] J. Gaube and H. Klein, "The promoter effect of alkali in Fischer-Tropsch iron and cobalt catalysts", *Appl. Catal. A: General*, vol. 350, pp. 126-132, Nov. 2008.
- [50] M. Luo and B. H. Davis, "Fischer-Tropsch synthesis: activation of low-alpha potassium promoted iron catalysts", *Fuel Process Tech.*, vol. 83, pp. 49-65, Sept. 2003.
- [51] N. Lohitharn, J. G. Goodwin Jr and E. Lotero, "Fe-based Fischer-Tropsch synthesis catalysts containing carbide-forming transition metal promoters", *Catal.*, vol. 255, pp. 104-113, 2008.
- [52] H. Hayakawa, H. Tanaka and K. Fujimoto, "Studies on precipitated iron catalysts for Fischer-Tropsch synthesis", *Appl. Catal. A: General*, vol. 310, pp. 24-30, Aug. 2006.
- [53] S. Li, S. Krishnamoorthy, A. Li, G. D. Meitzner and E. Iglesia, "Promoted iron-based catalysts for the Fischer-Tropsch synthesis: Design, synthesis, site densities, and catalytic properties", *Catal.*, vol. 206, pp. 202-217, 2002.
- [54] A. N. Pour, S. M. K. Shahri, H. R. Bozorgzadeh, Y. Zamani, A. Tavasoli and M. A. Marvast, "Effect of Mg, La and Ca promoters on the structure and catalytic behavior of iron-based catalysts in Fischer-Tropsch synthesis", *Appl. Catal. A: General*, vol. 348, pp. 201-208, Oct. 2008.
- [55] A. P. Rajee, R. J. O'Brien and B. H. Davis, "Effect of potassium promotion on iron-based catalysts for Fischer-Tropsch synthesis", *Catal.*, vol. 180, pp. 36-43, 1998.
- [56] G. Zhao, C. Zhang, S. Qin, H. Xiang and Y. Li, "Effect of interaction between potassium and structural promoters on Fischer-Tropsch performance in iron-based catalysts", *Molecular Catal. A: Chem.*, vol. 286, pp. 137-142, May. 2008.
- [57] H. Wan, B. Wu, C. Zhang, H. Xiang and Y. Li, "Promotional effects of Cu and K on precipitated iron-based catalysts for Fischer-Tropsch synthesis," *Molecular Catal. A: Chem.*, vol. 283, pp. 33-42, Mar. 2008.
- [58] C. Perego and P. Villa, "Catalyst preparation methods", *Catal. Today*, vol. 34, pp. 281-305, Feb. 1997.
- [59] Andrew R. Barron, (2009, May), "Introduction to nanoparticle synthesis", [online], Available: <http://www.cnnexion.org>

- [60] Y. Bao, A. B. Pakhomov, and K. M. Krishnan", A general approach to synthesis of nanoparticles with controlled morphologies and magnetic properties", *Appl. Phys.*, vol. 97, pp. 10J317-1-10J317-3, May. 2005.
- [61] E. M. Assaf, L. C. Jesus and J. M. Assaf, "The active phase distribution in Ni/Al₂O₃ catalysts and mathematical modeling of the impregnation process", *Chem. Eng.*, vol. 94, pp. 93-98, Aug. 2003.
- [62] R. A. Diffenbach and D. J. Fauth, "The role of pH in the performance of precipitated iron Fischer-Tropsch catalysts", *Catalysis*. vol. 100, pp. 466-476, Aug. 1986.
- [63] T. R. Motjope, H. T. Dlamini, G. R. Hearne and N. J. Coville, "Application of in situ Mössbauer spectroscopy to investigate the effect of precipitating agents on precipitated iron Fischer-Tropsch catalysts", *Catal. Today*, vol. 71, pp. 335-341, Jan. 2002.
- [64] A. Pineau, N. Kanari and I. Gaballah, "Kinetics of reduction of iron oxides by H₂: Part I: Low temperature reduction of hematite", *Thermochimica Acta*, vol. 447, pp. 89-100, Aug. 2006.
- [65] M. E. Dry, "Advances in Fischer-Tropsch Chemistry", *Ind. Eng. Chem. Prod. Res. Dev.*, vol. 15, pp. 282-286, 1976.
- [66] A. Ali. Mirzaei, S. Vahid, and M. Feyzi, "Fischer-Tropsch Synthesis over Iron Manganese Catalysts: Effect of Preparation and Operating Conditions on Catalyst Performance", *Adv. In. phys. Chem.*, vol. 2009, pp. 1-12, Jun. 2008.
- [67] R. J. O'Brien, L. Xu, S. Bao, A. Raje and B. H. Davis, "Activity, selectivity and attrition characteristics of supported iron Fischer-Tropsch catalysts", *Appl. Catal. A: General*, vol. 196, pp. 173-178, Apr. 2000.
- [68] Google Image. *Basic Operating Principles of the SORPTOMATIC 1990*, Available: <http://saf.chem.ox.ac.uk/Instruments/BET/isotherms.jpg> , 2010.
- [69] A. Paul, Webb and Clyde Orr, "Surface area and pore structure by gas adsorption", in *Analytical Methods in Fine Particle Technology*, Norcross, GA USA, Micromeritics instrument Corp., 1997, ch. 3, sec. 3.3.2, pp. 60-63.

- [70] Ferret, *BET Surface Area Analysis by Tristar 3000*, Available: <http://www.ferret.com.au/odin/images/171429/BET-surface-area-analysis-by-Tristar-3000-171429.jpg> , 2010.
- [71] Google Image, *Electron Microscopy*, Available: <http://www.vcbio.science.ru.nl/images/TEM-SEM-electron-beam.jpg> , 2010.
- [72] Google image, *EDS SEM*, Available: <http://www.vcbio.science.ru.nl> , 2010.
- [73] J. Goldstein, D. Newbury, D. Joy, P. Echlin, C. Lyman, E. Lifshin, L. Sawyer, and J. Michael, "Introduction", in *Scanning Electron Microscopy and X-Ray Microanalysis*, 3rd edition, Springer USA, 2003, ch. 1, pp. 1-10.
- [74] H. Jasksch (1996 October), Filed Emission SEM for True Surface Imaging and Analysis, [online]. Available: <http://www.zeiss.de/C1256E4600307C70> , 2010.
- [75] Z. Wang, "Transmission electron microscopy of shape controlled nano-crystals and their assemblies," *Phys. Chem. B*, vol. 104, pp. 1153-1175, 2000.
- [76] BiovisioNZ, *Transmission Electron Microscopy*, Available: <http://www.mauricewilkinscentre.org/bioviz/forstudents/pharmacy/jpg> , 2010.
- [77] Scintag (1999), Inc, Basics of X-ray Diffraction. [online]. Available: www.scintag.com, 2010
- [78] L. J. Poppe, V. F. Paskevich, J. C. Hathwasy, and D. S. Blackwood (2001 October 10), A Laboratory Manual for X-Ray Powder Diffraction, [online]. Available: <http://pubs.usgs.gov/of/2001/of01-041/index.htm> , 2010.
- [79] Tutor Visto, Mechanism and laws involved in X-rays diffraction, [online]. Available: http://image.wistatutor.com/content/feed/u415/img_mid_5359.gif , 2010.
- [80] P. Heidebrecht, V. Galvita and K. Sundmacher, "An alternative method for parameter identification from temperature programmed reduction (TPR) data", *Chem. Eng. Sci.*, vol. 63, pp. 4776-4788, Oct. 2008.
- [81] W. Jozwiak, E. Kaczmarek, T. Maniecki, W. Ignaczak and W. Maniukiewicz, "Reduction behavior of iron oxides in hydrogen and carbon monoxide atmospheres", *Appl. Catal. A: General*, vol. 326, pp. 17-27, Mar. 2007.

- [82] Y. Zhang, M. Koike, R. Yang, S. Hinchiranan, T. Vitidsant and N. Tsubaki, "Multi-functional alumina-silica bimodal pore catalyst and its application for Fischer-Tropsch synthesis", *Appl. Catal. A: General*, vol. 292, pp. 252-258, Jul. 2005.
- [83] Y. Yang, H. W. Xiang, Y. Y. Xu, L. Bai and Y. W. Li, "Effect of potassium promoter on precipitated iron-manganese catalyst for Fischer-Tropsch synthesis", *Appl. Catal. A: General*, vol. 266, pp. 181-194, Apr. 2004.
- [84] A. Sarkar, D. Seth, A. K. Dozier, J. K. Neathery, H. H. Hamdeh and B. H. Davis, "Fischer-Tropsch Synthesis: Morphology, Phase Transformation and Particle Size Growth of Nano-scale Particles", *Catal. Lett.*, vol. 117, pp. 1-17, Jul. 2007.
- [85] H. Hayashi, M. Kishida and K. Wakabayashi, "Metal-support interaction and catalysis of the catalysts prepared using microemulsion", *Catal. Surveys*, vol. 6, pp. 9-17, Oct. 2002.
- [86] L. D. Mansker, Y. Jin and A. K. Datye, "Characterization of Iron Fischer-Tropsch Catalysts", *Appl. Catal. A: General*, vol. 186, pp. 277-296, 1999.
- [87] H. Wan, B. Wu, C. Zhang, H. Xiang, Y. Li, B. Xu and F. Yi, "Study on Fe-Al₂O₃ interaction over precipitated iron catalyst for Fischer-Tropsch synthesis", *Catal. Communications*, vol. 8, pp. 1538-1545, Oct. 2007.
- [88] M. Luo, H. Hamdeh and B. H. Davis, "Fischer-Tropsch Synthesis: Catalyst activation of low alpha iron catalyst", *Catal. Today*, vol. 140, pp. 127-134, Feb. 2009.
- [89] B. H. Davis, "Technology development for iron Fischer-Tropsch catalysis", Federal Eng. Tech. Cen., Morgantown, WV .USA, Tech. Rep. DE--AC22-94PC94055--13, Jul. 1998.
- [90] Y. Lu and P. Zhou, "Impact of promoters on the performance of the skeleton iron catalyst in the application to Fischer-Tropsch synthesis process", *Prepr. Pap.-Am. Chem. Soc., Div. Fuel. Chem.*, vol. 49, pp. 660-661, 2004.
- [91] Octave levenspiel, "Constant volume batch reactor," in *Chemical Reaction Engineering*, 3rd edition., Ken Santor, Ed. John Wiley & Sons, Inc, 1999, ch. 3, sec. 3.1, pp. 39-66.

Appendix A

- **Amount of chemical for the catalyst preparation**

1. Preparation of Al₂O₃-SiO₂ support

✓ For ratio of 5:95 Al₂O₃:SiO₂

A. Total weight is 20gm

weight of Al₂O₃ (g) = total weight of the support × percent of Al₂O₃

$$Al_2O_3 (g) = 20 \times \frac{5}{100}$$

$$= 1 \text{ g of } Al_2O_3$$

Then the weight of precursor (Al(NO₃)₃.9H₂O) is

weight of Al(NO₃)₃.9H₂O =

$$\frac{\text{molecular weight of } Al(NO_3)_3 \cdot 9H_2O \times \text{weight of } Al_2O_3}{\text{molecular weight of } Al_2O_3}$$

$$\text{weight of } Al(NO_3)_3 \cdot 9H_2O = \frac{375 \times 1 \times 2}{102}$$

$$= 7.35 \text{ g of } Al(NO_3)_3 \cdot 9H_2O$$

B. Weight of SiO₂

weight of SiO₂ (g) = total weight of the support – weight of Al₂O₃

$$= 20 \text{ g} - 1 = 19 \text{ g of } SiO_2$$

C. Volume of glycol (0.5M) solution

number of moles for Al(NO₃)₃.9H₂O = $\frac{\text{molarity} \times \text{volume}}{\text{liter of solution}}$

$$\text{Volume} = \frac{\text{number of moles} \times \text{liter of solution}}{\text{molarity}}$$

$$\text{Volume of glycol} = \frac{0.0196 \times 1000}{0.5}$$

$$= 39 \text{ ml of glycol}$$

5/95 wt% of Al₂O₃-SiO₂ support prepared by dissolving 7.35g of Al(NO₃)₃.9H₂O in 39ml of glycol and then impregnated the solution on 18g of SiO₂

2. Supported catalyst prepared by impregnation or precipitation

Since the total weight of the catalyst is 5gm, the amounts of the chemicals were based on the percentage of the metals.

✓ For 6% Fe/SiO₂ catalyst

A. The weight of Fe is calculated by the following equation:

$$\text{weight of Fe (g)} = \text{total weight of the catalyst} \times \text{percent of Fe}$$

$$\text{Fe (g)} = 5 \times \frac{6}{100}$$

$$= 0.3\text{g}$$

Then the weight of precursor (Fe(NO₃)₃.9H₂O) is

$$\text{weight of Fe(NO}_3)_3.9\text{H}_2\text{O} =$$

$$\frac{\text{molecular weight of Fe (NO}_3)_3.9\text{H}_2\text{O} \times \text{weight of Fe}}{\text{molecular weight of Fe}}$$

$$\text{weight of Fe(NO}_3)_3.9\text{H}_2\text{O} = \frac{403.86 \times 0.3}{56}$$

$$= 1.86\text{g of Fe(NO}_3)_3.9\text{H}_2\text{O}$$

B. weight of SiO₂

$$\text{weight of SiO}_2(\text{g}) = \text{total weight of the catalyst} - \text{weight of Fe}$$

$$= 5\text{g} - 0.3 = 4.7 \text{ g of SiO}_2$$

C. preparation of precursor solution 0.5M

$$\text{Number of moles of Fe(NO}_3)_3.9\text{H}_2\text{O} = \text{Molarity} \times \text{Volume}$$

$$\text{Volume} = \frac{\text{number of moles (mol)} \times \text{liter of solution (ml/L)}}{\text{molarity (mol / L)}}$$

$$\text{Volume of deionize water} = \frac{0.0046 \times 1000}{0.5}$$

$$= 9.2 \text{ ml of H}_2\text{O}$$

For preparing of 6% Fe/SiO₂ catalyst, 1.86g of Fe(NO₃)₃.9H₂O was dissolved in 9ml of deionized water and impregnated on 4.7gm of the SiO₂ support.

✓ For 10% Fe/SiO₂ catalyst

A. The weight of Fe is calculated by the following equation:

$$\text{weight of Fe (g)} = \text{total weight of the catalyst} \times \text{percent of Fe}$$

$$\text{Fe (g)} = 5 \times \frac{10}{100}$$

$$= 0.5 \text{g}$$

Then the weight of precursor (Fe(NO₃)₃.9H₂O) is

$$\text{weight of Fe(NO}_3)_3 \cdot 9\text{H}_2\text{O} =$$

$$\frac{\text{molecular weight of Fe(NO}_3)_3 \cdot 9\text{H}_2\text{O} \times \text{weight of Fe}}{\text{molecular weight of Fe}}$$

$$\text{weight of Fe(NO}_3)_3 \cdot 9\text{H}_2\text{O} = \frac{403.86 \times 0.5}{56}$$

$$= 3.61 \text{g of Fe(NO}_3)_3 \cdot 9\text{H}_2\text{O}$$

B. weight of SiO₂

$$\text{weight of SiO}_2 \text{ (g)} = \text{total weight of the catalyst} - \text{weight of Fe}$$

$$= 5 \text{g} - 0.5 = 4.5 \text{ g of SiO}_2$$

C. preparation of precursor solution 0.5M

$$\text{Number of moles of Fe(NO}_3)_3 \cdot 9\text{H}_2\text{O} = \text{Molarity} \times \text{Volume}$$

$$\text{Volume} = \frac{\text{number of moles (mol)} \times \text{liter of solution (ml/L)}}{\text{molarity (mol / L)}}$$

$$\text{Volume of deionize water} = \frac{0.0089 \times 1000}{0.5}$$

$$= 18 \text{ ml of H}_2\text{O}$$

For preparing of 10%Fe/SiO₂ catalyst, 3.61g of Fe(NO₃)₃.9H₂O was dissolved in 18ml of deionized water and impregnated on 4.5gm of the SiO₂ support.

✓ For 15% Fe/SiO₂ catalyst

A. The weight of Fe is calculated by the following equation:

$$\text{weight of Fe (g)} = \text{total weight of the catalyst} \times \text{percent of Fe}$$

$$\begin{aligned} \text{Fe (g)} &= 5 \times \frac{15}{100} \\ &= 0.75\text{g} \end{aligned}$$

Then the weight of precursor (Fe(NO₃)₃·9H₂O) is

$$\begin{aligned} \text{weight of Fe(NO}_3)_3 \cdot 9\text{H}_2\text{O} &= \\ &= \frac{\text{molecular weight of Fe(NO}_3)_3 \cdot 9\text{H}_2\text{O} \times \text{weight of Fe}}{\text{molecular weight of Fe}} \end{aligned}$$

$$\begin{aligned} \text{weight of Fe(NO}_3)_3 \cdot 9\text{H}_2\text{O} &= \frac{403.86 \times 0.75}{56} \\ &= 5.41\text{g of Fe(NO}_3)_3 \cdot 9\text{H}_2\text{O} \end{aligned}$$

B. weight of silica

$$\begin{aligned} \text{weight of SiO}_2 \text{ (g)} &= \text{total weight of the catalyst} - \text{weight of Fe} \\ &= 5\text{g} - 0.75 = 4.25\text{ g of SiO}_2 \end{aligned}$$

C. preparation of precursor solution 0.5M

$$\text{Number of moles of Fe(NO}_3)_3 \cdot 9\text{H}_2\text{O} = \text{Molarity} \times \text{Volume}$$

$$\text{Volume} = \frac{\text{number of moles (mol)} \times \text{liter of solution (ml/L)}}{\text{molarity (mol / L)}}$$

$$\begin{aligned} \text{Volume of deionize water} &= \frac{0.0134 \times 1000}{0.5} \\ &= 27\text{ ml of H}_2\text{O} \end{aligned}$$

For preparing of 15% Fe/SiO₂ catalyst, 5.41g of Fe(NO₃)₃·9H₂O was dissolved in 27ml of deionized water and impregnated on 4.25gm of the SiO₂ support.

3. Promoted catalyst

✓ For 6%Fe/SiO₂ catalyst promoted with copper (6%Fe/2%Cu/SiO₂)

A. The weight of Fe is

weight of Fe (g) = total weight of the catalyst × percent of Fe

$$\begin{aligned} Fe(g) &= 5 \times \frac{6}{100} \\ &= 0.3\text{g} \end{aligned}$$

Then the weight of precursor (Fe(NO₃)₃·9H₂O) is

weight of Fe(NO₃)₃·9H₂O =

$$\frac{\text{molecular weight of Fe (NO}_3)_3 \cdot 9\text{H}_2\text{O} \times \text{weight of Fe}}{\text{molecular weight of Fe}}$$

$$\begin{aligned} \text{weight of Fe(NO}_3)_3 \cdot 9\text{H}_2\text{O} &= \frac{403.86 \times 0.3}{56} \\ &= 1.86\text{g of Fe(NO}_3)_3 \cdot 9\text{H}_2\text{O} \end{aligned}$$

B. Weight of Cu promoter

weight of Cu (g) = total weight of the catalyst × percent of Cu

$$\begin{aligned} \text{Cu}(g) &= 5 \times \frac{2}{100} \\ &= 0.1\text{g} \end{aligned}$$

Then the weight of Cu(NO₃)₂·3H₂O

weight of Cu(NO₃)₂·3H₂O =

$$\frac{\text{molecular weight of Cu (NO}_3)_2 \cdot 3\text{H}_2\text{O} \times \text{weight of Cu}}{\text{molecular weight of Cu}}$$

$$\begin{aligned} \text{weight of Cu(NO}_3)_2 \cdot 3\text{H}_2\text{O} &= \frac{241.75 \times 0.1}{63.4} \\ &= 0.38\text{g of Cu(NO}_3)_2 \cdot 3\text{H}_2\text{O} \end{aligned}$$

C. weight of SiO₂

weight of SiO₂ (g) = total weight of the catalyst – weight of Fe

$$= 5\text{g} - 0.4 = 4.6\text{ g of SiO}_2$$

D. preparation of 0.5M precursor solution

Number of moles of $Cu(NO_3)_2 \cdot 3H_2O = Molarity \times Volume$

$$\begin{aligned} \text{Volume of deionize water} &= \frac{0.0016 \text{ mol} \times 1000 \text{ ml} / L}{0.5 \text{ mol} / L} \\ &= 3.14 \text{ ml of } H_2O \end{aligned}$$

6%Fe/2%Cu/SiO₂ was synthesized by dissolving 1.86g of Fe(NO₃)₃·9H₂O and 0.38g of Cu(NO₃)₂·3H₂O in 12.2ml of H₂O and impregnated the solution on 4.6g of SiO₂

✓ For 6%Fe/SiO₂ catalyst promoted with potassium (6%Fe/4%K/SiO₂)

A. The weight of Fe is

weight of Fe (g) = total weight of the catalyst × percent of Fe

$$\begin{aligned} Fe(g) &= 5 \times \frac{6}{100} \\ &= 0.3 \text{ g} \end{aligned}$$

Then the weight of precursor (Fe(NO₃)₃·9H₂O) is

$$\begin{aligned} \text{weight of } Fe(NO_3)_3 \cdot 9H_2O &= \\ &= \frac{\text{molecular weight of } Fe(NO_3)_3 \cdot 9H_2O \times \text{weight of Fe}}{\text{molecular weight of Fe}} \end{aligned}$$

$$\begin{aligned} \text{weight of } Fe(NO_3)_3 \cdot 9H_2O &= \frac{403.86 \times 0.3}{56} \\ &= 1.86 \text{ g of } Fe(NO_3)_3 \end{aligned}$$

B. Weight of K promoter

weight of K (g) = total weight of the catalyst × percent of K

$$\begin{aligned} K(g) &= 5 \times \frac{4}{100} \\ &= 0.2 \text{ g} \end{aligned}$$

Then the weight of KNO₃

$$\text{weight of } KNO_3 = \frac{\text{molecular weight of } KNO_3 \times \text{weight of K}}{\text{molecular weight of K}}$$

$$\begin{aligned} \text{weight of } KNO_3 &= \frac{101 \times 0.2}{39} \\ &= 0.52 \text{ g of } KNO_3 \end{aligned}$$

C. weight of SiO₂

$$\begin{aligned} \text{weight of SiO}_2(g) &= \text{total weight of the catalyst} - \text{weight of Fe} \\ &= 5\text{g} - 0.5 = 4.5 \text{ g of SiO}_2 \end{aligned}$$

D. preparation of 0.5M precursor solution

$$\text{Number of moles of KNO}_3 = \text{Molarity} \times \text{Volume}$$

$$\begin{aligned} \text{Volume of deionized water} &= \frac{0.0052 \text{ mol} \times 1000 \text{ ml} / \text{L}}{0.5 \text{ mol} / \text{L}} \\ &= 10.4 \text{ ml of H}_2\text{O} \end{aligned}$$

6%Fe/4%K/SiO₂ was synthesized by dissolving 1.86g of Fe(NO₃)₃.9H₂O and 0.52g of KNO₃ in 19.6ml of H₂O and impregnated the solution on 4.5g of SiO₂

Appendix B

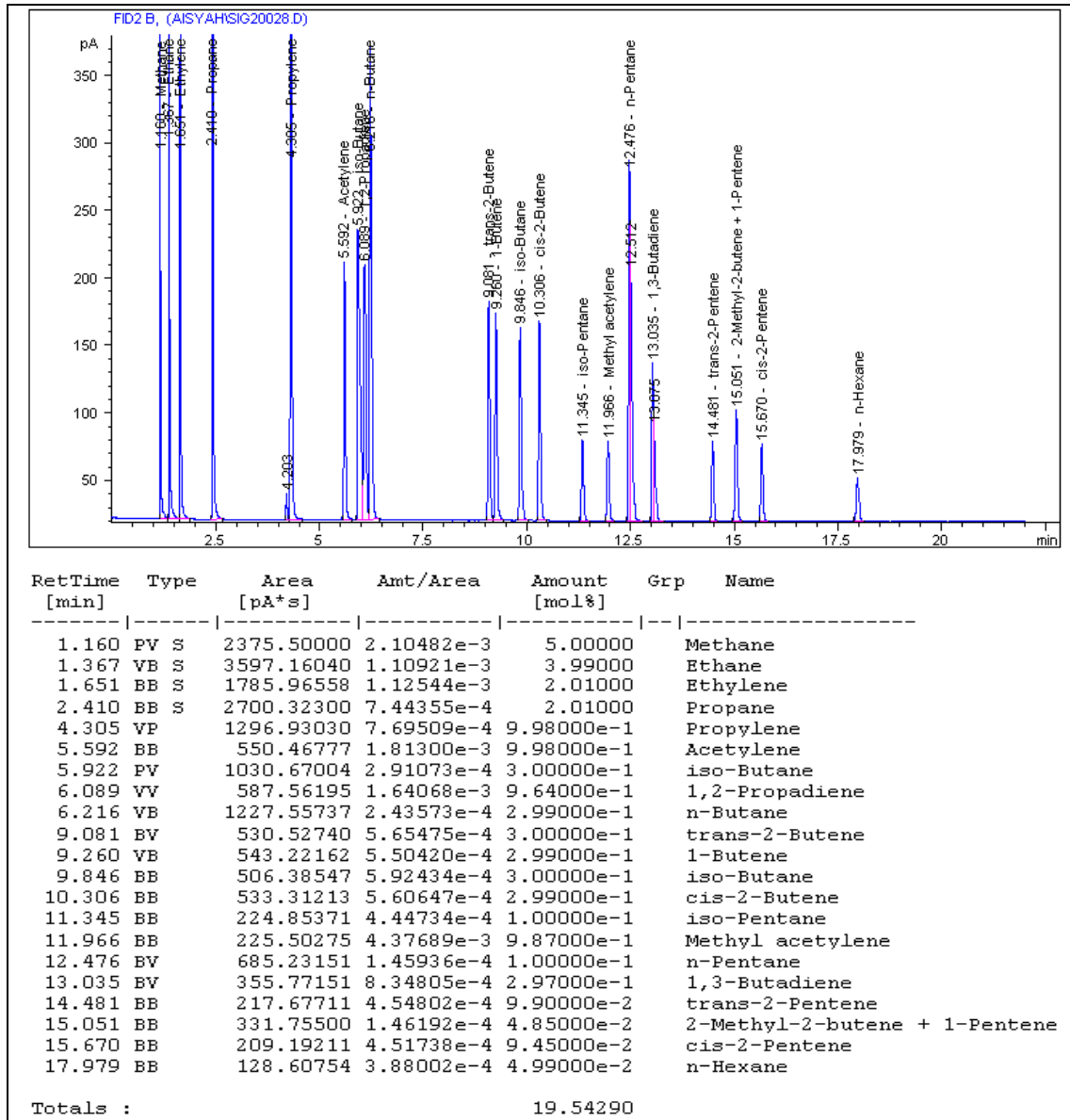


Figure B1: Chromatogram of GC calibration using RGA standard

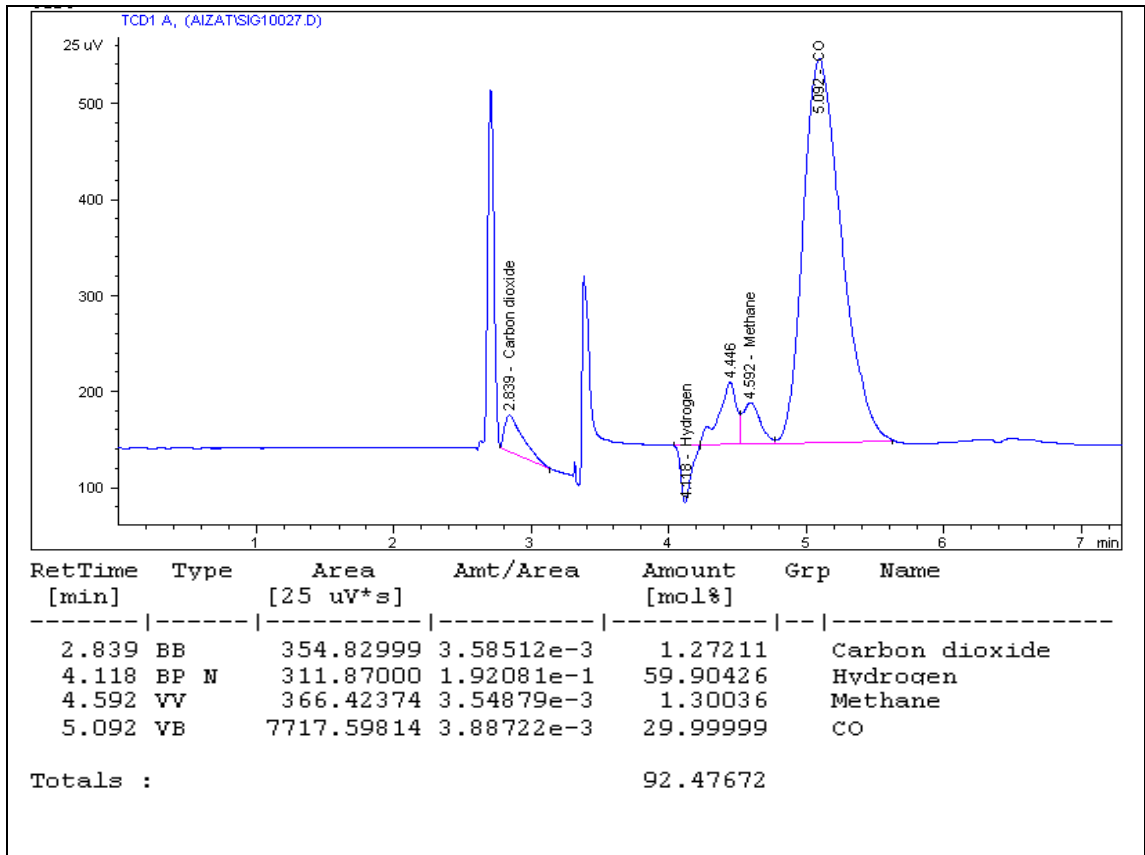


Figure B2: Chromatogram of GC calibration using CO, H₂, CO₂, and CH₄ gas mixture

Table B1: Gas Chromatograph calibration of standard gases

| | Retention time (min) | Signal | Compound | Amount (mol %) | Peak Area | Amount/ Area |
|-----|-----------------------------|---------------|-------------------|-----------------------|------------------|---------------------|
| 1. | 2.839 | TCD | Carbon dioxide | 1.272 | 354.83 | 3.58512 e-3 |
| 2. | 4.118 | TCD | Hydrogen | 59.904 | 311.87 | 1.92081 e-1 |
| 3. | 5.092 | TCD | Carbon monoxide | 29.999 | 7712.59 | 3.88722 e-3 |
| 4. | 1.174 | FID | Methane | 5.000 | 4163.85 | 1.20081e-3 |
| 5. | 1.426 | FID | Ethane | 3.990 | 6347.03 | 6.28640e-4 |
| 6. | 1.804 | FID | Ethylene | 2.010 | 3138.87 | 6.40357e-4 |
| 7. | 2.732 | FID | Propane | 2.010 | 4792.41 | 4.19413e-4 |
| 8. | 4.579 | FID | Propylene | 0.998 | 2288.50 | 4.36092e-4 |
| 9. | 5.587 | FID | Acetylene | 0.998 | 981.06 | 1.01726e-3 |
| 10. | 5.768 | FID | iso-Butane | 0.300 | 1865.35 | 1.60827e-4 |
| 11. | 5.937 | FID | 1,2-Propadiene | 0.964 | 922.21 | 1.04531e-3 |
| 12. | 5.993 | FID | n-Butane | 0.299 | 2232.55 | 1.33927e-4 |
| 13. | 7.757 | FID | Trans-2-Butene | 0.300 | 939.91 | 3.19179e-4 |
| 14. | 7.865 | FID | 1-Butene | 0.299 | 967.55 | 3.09026e-4 |
| 15. | 8.440 | FID | cis-2-Butene | 0.299 | 947.14 | 3.15685e-4 |
| 16. | 9.122 | FID | iso-Pentane | 0.100 | 399.56 | 2.50274e-4 |
| 17. | 9.456 | FID | Methyl acetylene | 0.987 | 396.55 | 2.48891e-3 |
| 18. | 9.593 | FID | n-Pentane | 0.100 | 2263.49 | 4.41795e-5 |
| 19. | 9.869 | FID | 1,3-Butadiene | 0.297 | 932.921 | 3.18355e-4 |
| 20. | 10.736 | FID | trans-2-pentene | 0.099 | 380.27 | 2.60340e-4 |
| 21. | 11.015 | FID | 2-Methyl-2-butene | 0.0485 | 144.63 | 3.35326e-4 |
| 22. | 11.050 | FID | 1-Pentene | 0.0997 | 438.67 | 2.27276e-4 |
| 23. | 11.353 | FID | cis-2-Pentene | 0.0945 | 366.40 | 2.57909e-4 |
| 24. | 12.657 | FID | n-Hexane | 0.0499 | 215.28 | 2.31784e-4 |

Microreactor operating procedure

The microreactor system (Figure B3) consists of three parts and the following steps show the operating procedure of microreactor system:

1. Connect the reactant gases carbon monoxide and hydrogen and purging gas (helium) to each gas inlet port.
2. Open the regulator for the He cylinder at 2bar to purge the reactor
3. Purge the reactor with helium for 15min through the following steps (Figure B3)
 - ✓ Turning on valve MV5 to reactor
 - ✓ Turn on valve MV6 to separator
 - ✓ Turn on valve MV7 to vent
 - ✓ Turn on valve MV4 to let He flow to the reactor
4. After 15min close all the valves that were mentioned at the purging step
5. Set the CO mass flow controller (MFC) at 10ml/min
6. Open the regulator for the CO cylinder at 2bar for the reduction step
7. Adjust the temperature TIC1 to the reduction temperature (280^oC)
8. Turn on MV5 to reactor, MV6 to separator, MV7 to vent, and MV2 to let CO flow to reactor
9. Turn on the heaters TIC2 and TIC3 to increase the temperature of the reactor to the reduction temperature.
10. Keep the temperature at 280^oC for 4h.
11. Turn off the heaters TIC2 and TIC3.
12. Set TIC1 to reaction temperature (250^oC).
13. Turn off the flow of CO by turning off valve MV2 and turn on the valve MV4 to let the He flow to reactor while the temperature decrease to reaction temperature.
14. Adjust the flow of the CO by FCV1 (mass flow controller) and the flow of H₂ by FCV2 (mass flow controller) to the desired ratio of H₂/CO
15. Turn on MV5 to GC vent, MV6 to “from mixed gas”, MV2 to let CO flow, MV3 to H₂ flow, and MV7 to GC for analyzing the mole percent of the reactant (Mole_{in}) before starting the reaction.
16. Turn on the heaters TIC2 and TIC3
17. Turn on MV5 to reactor, MV6 to separator, MV7 to vent, and MV2 and MV3 to let the reactant (CO and H₂)flow to start the reaction
18. After 30min from starting the reaction, turn on valve MV7 to GC to analyze the product and repeat this step every 30min during the 5h reaction.
19. After finishing the reaction period, turn off the heaters and purge the reactor system with He gas.

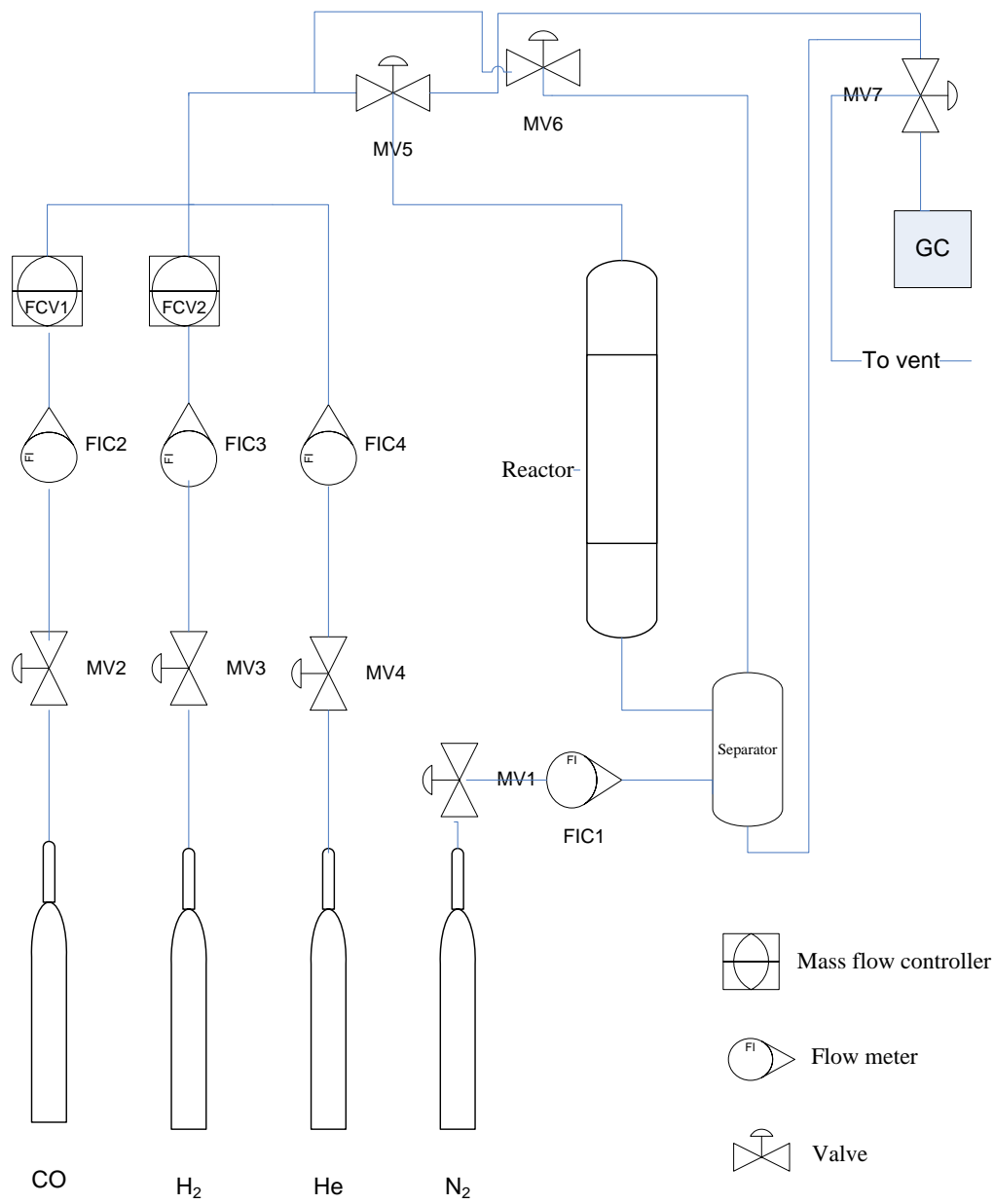


Figure B3: Schematic diagram of Reactor system

Appendix C

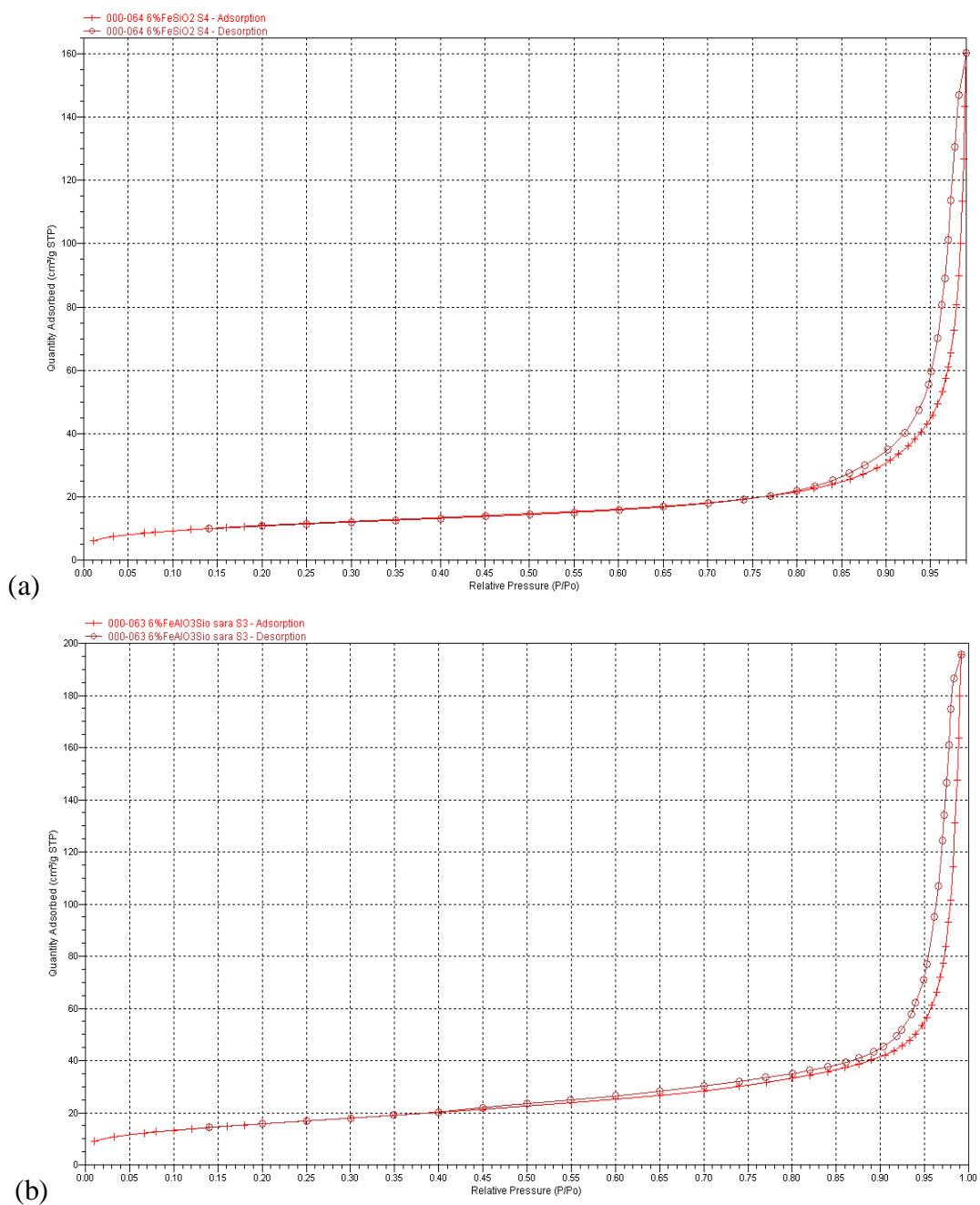


Figure C1 isothermal plot of (a) 6% Fe/SiO₂ and (b) 6% Fe/Al₂O₃-SiO₂ catalyst prepared by impregnation method

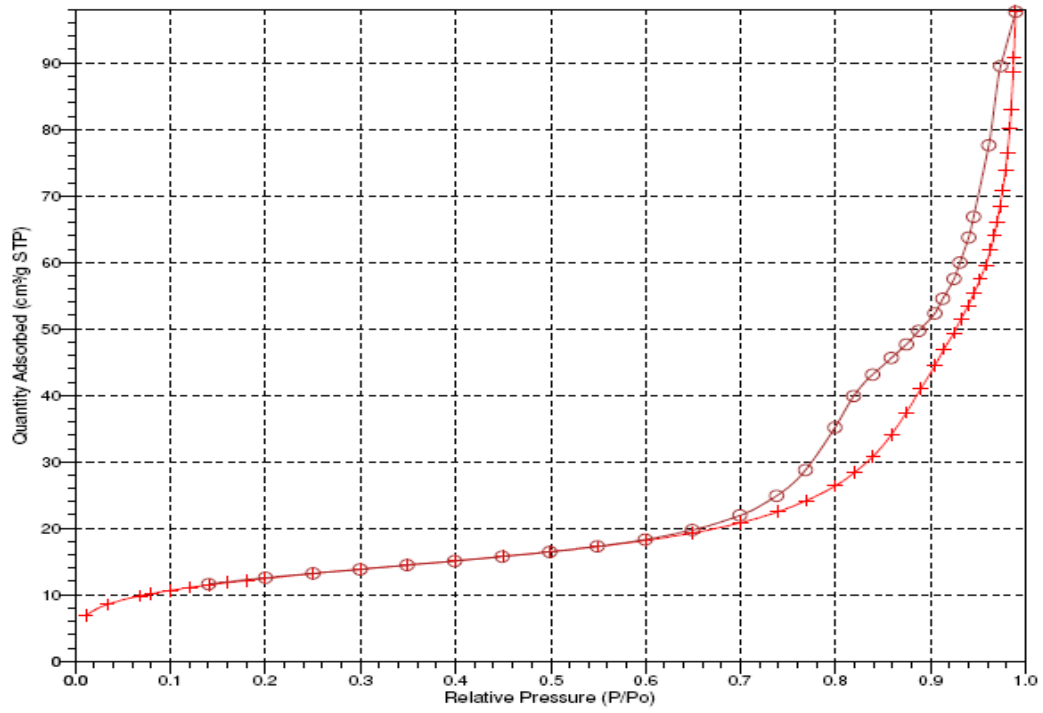


Figure C2 isothermal plot of 6% Fe/SiO₂ catalyst prepared by precipitation method

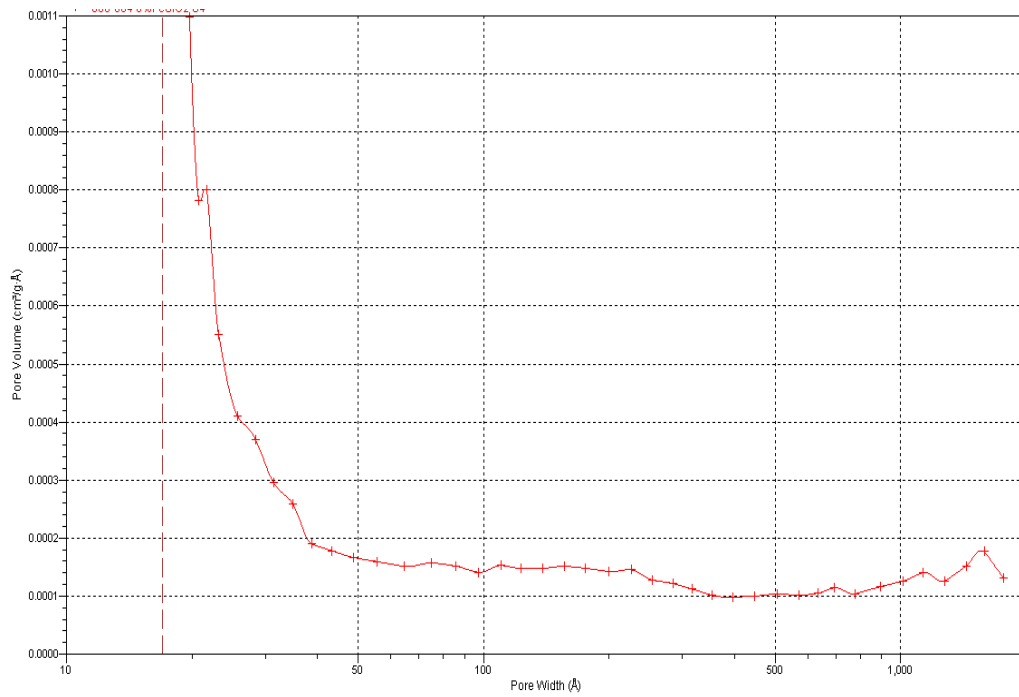


Figure C3 Pore size distribution of 6% Fe/SiO₂ catalyst prepared by impregnation method

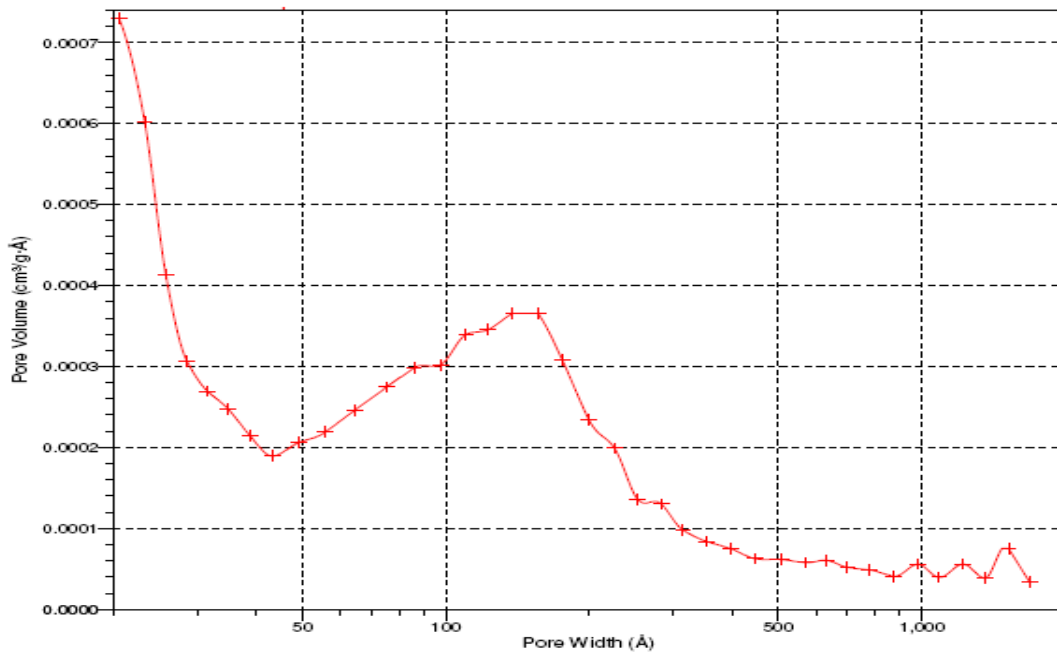


Figure C4 Pore size distribution of 6% Fe/SiO₂ catalyst prepared by precipitation method

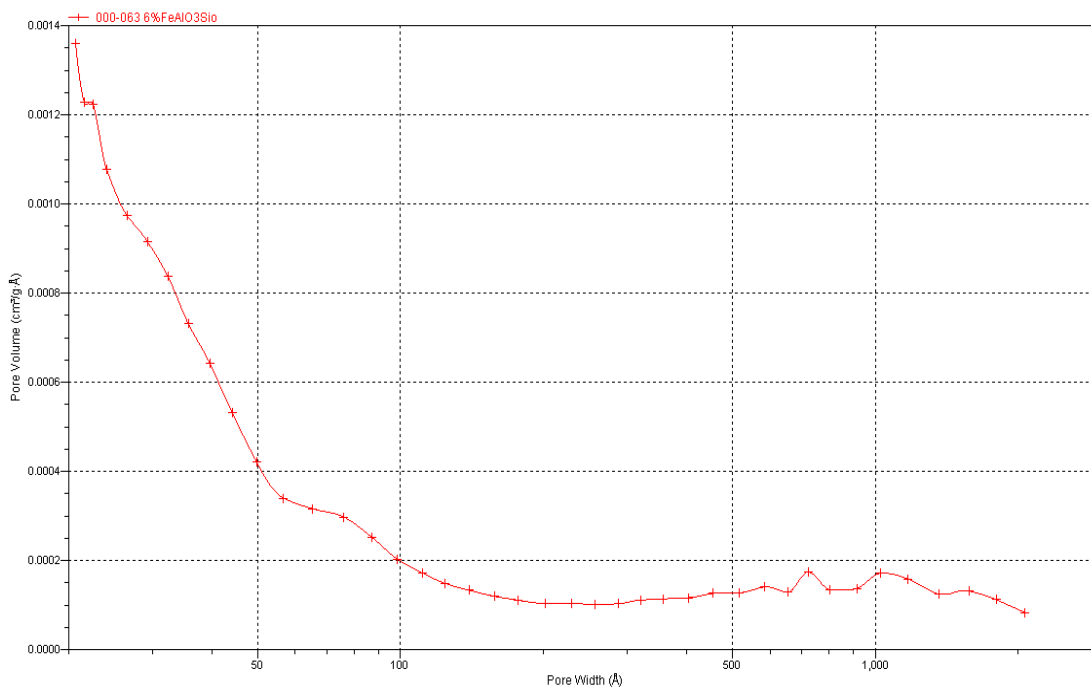


Figure C5 Pore size distribution of 6% Fe/Al₂O₃-SiO₂ catalyst prepared by impregnation method

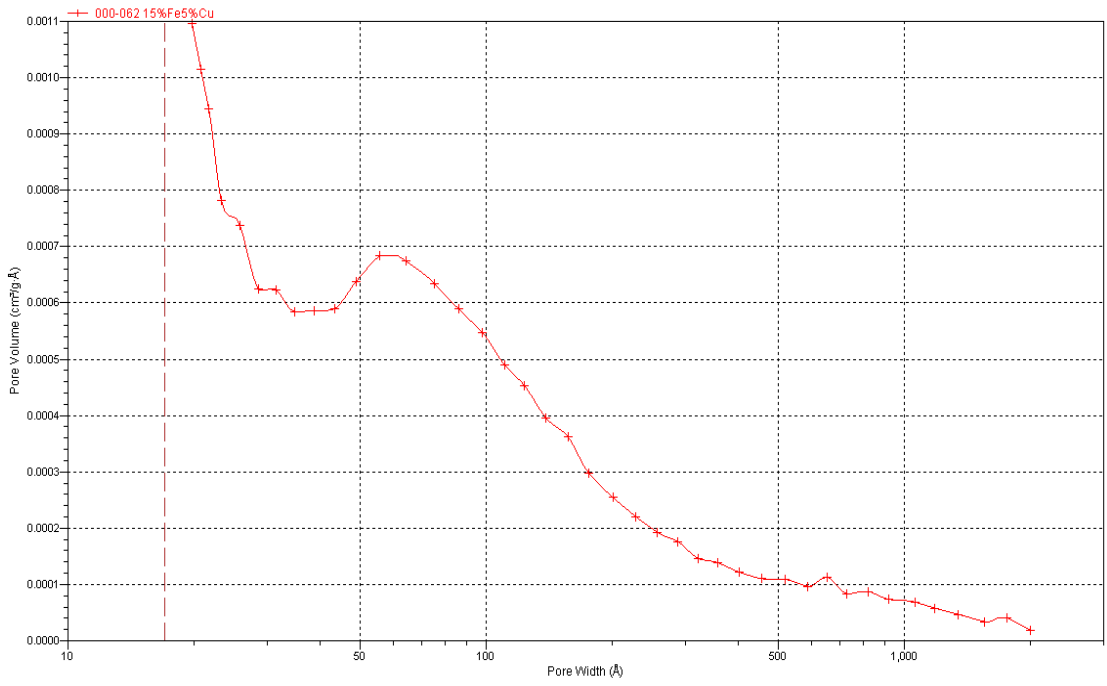


Figure C6 Pore size distribution of 15%Fe/Cu/SiO₂ catalyst prepared by impregnation method

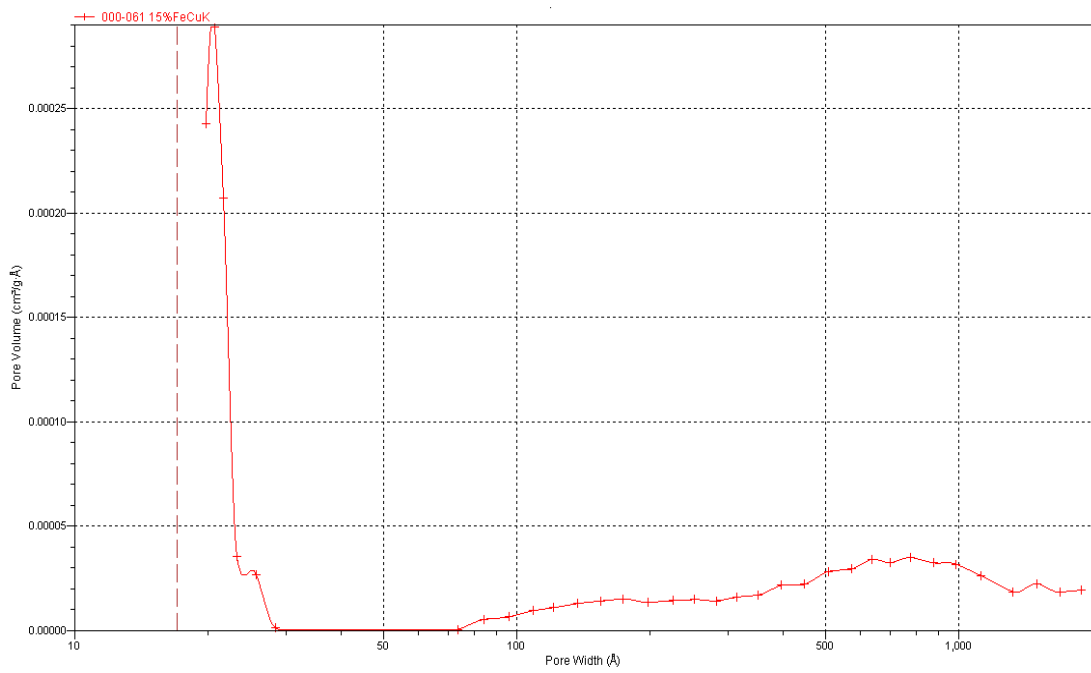
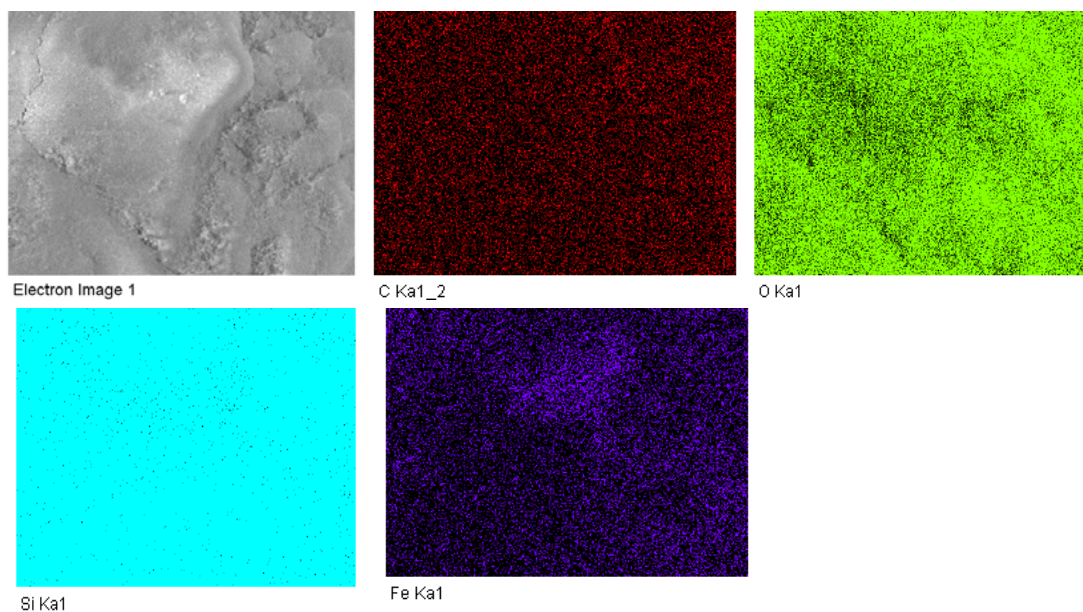


Figure C7 Pore size distribution of 15%Fe/Cu/K/SiO₂ catalyst prepared by impregnation method

Appendix D

(a)



(b)

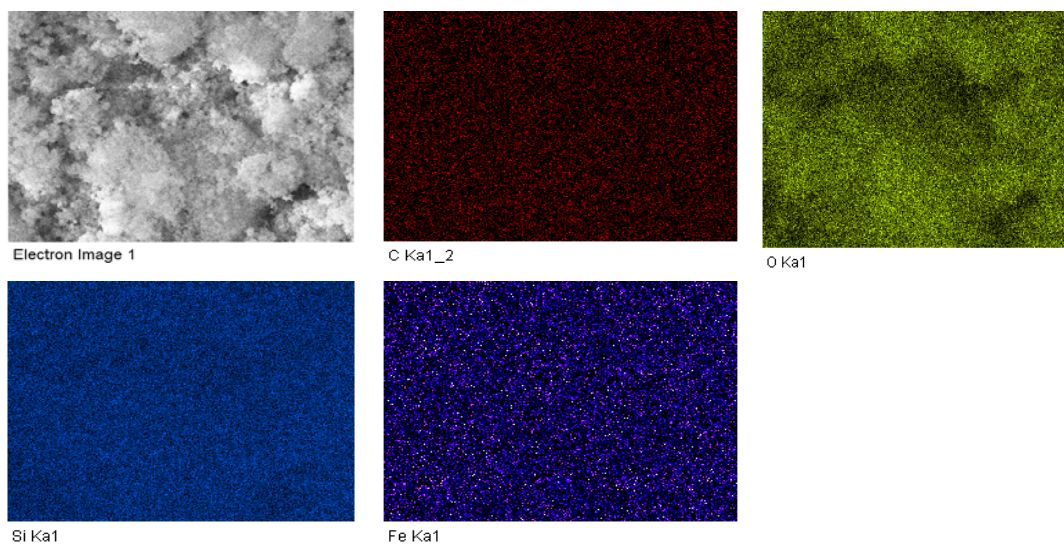


Figure D1 EDX mapping for SiO_2 supported Fe-based catalyst prepared via impregnation method at Fe loading of (a) 6 and (b) 15 wt%

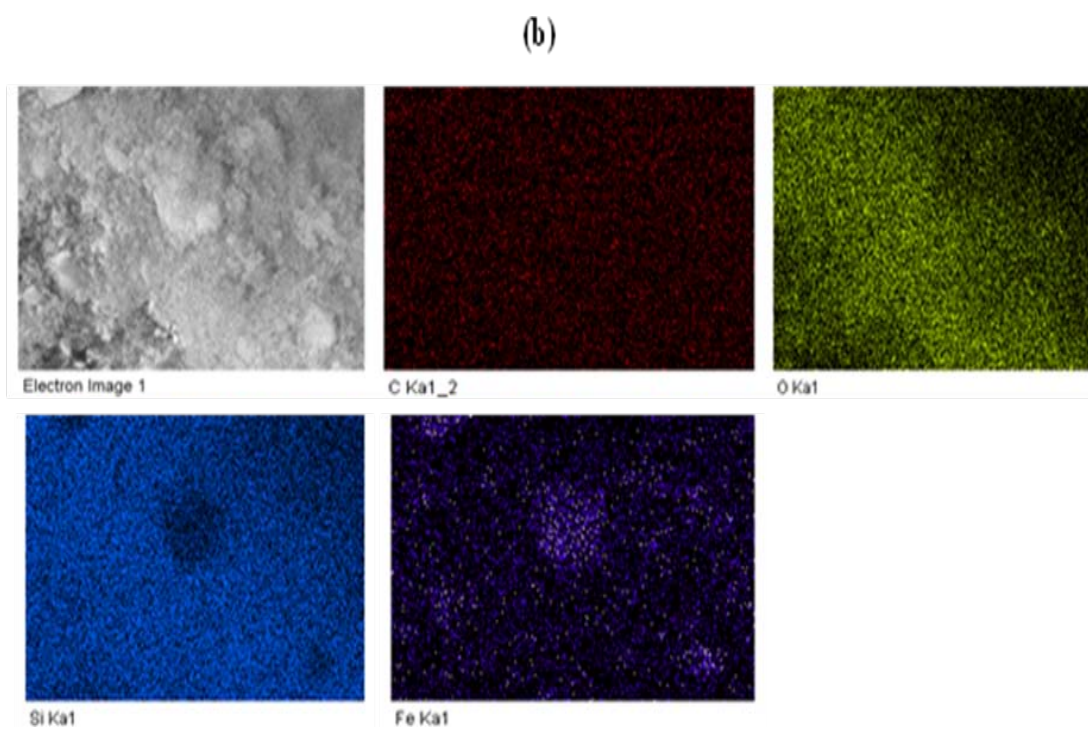
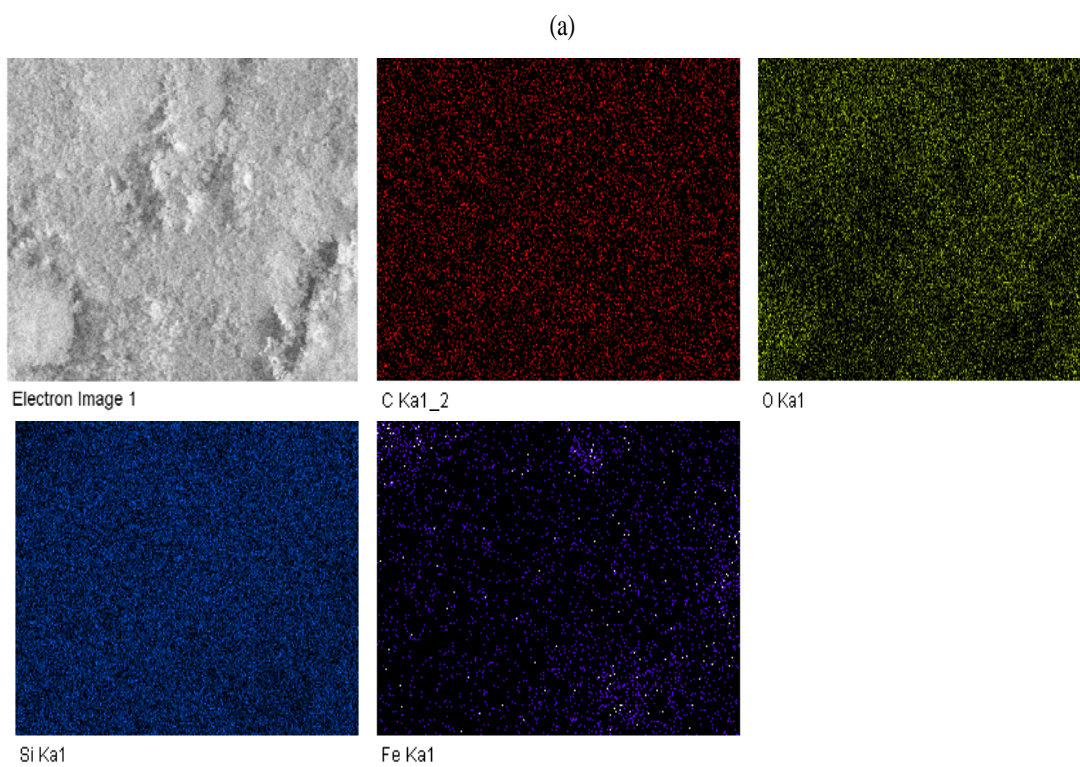
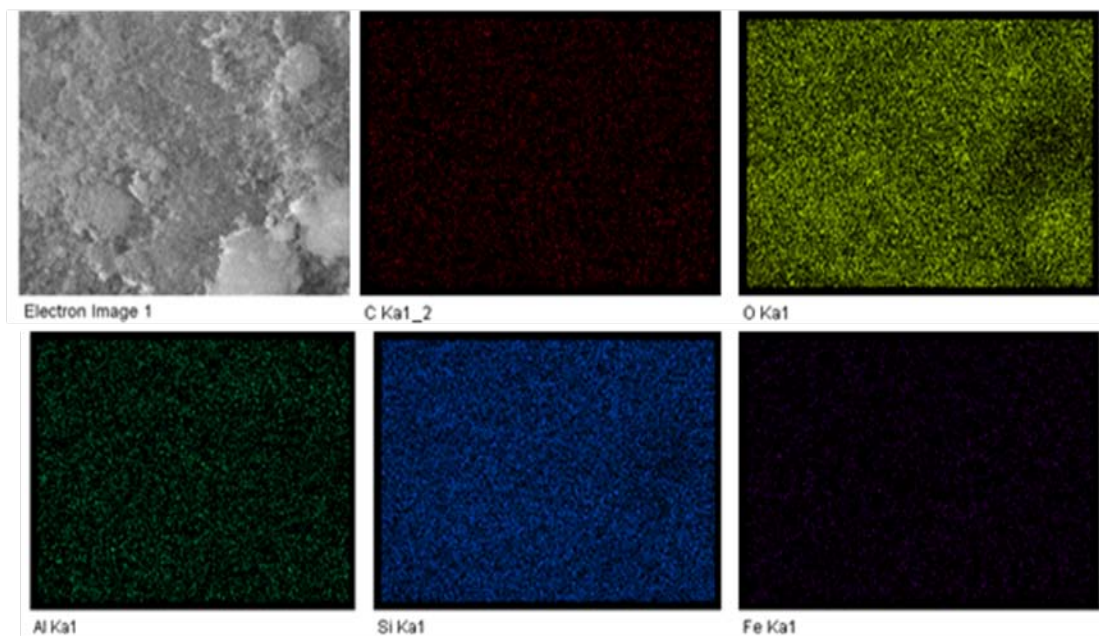


Figure D2 EDX mapping for SiO_2 supported Fe-based catalyst prepared via precipitation method at Fe loading of (a) 6, and (b) 15 wt%

(a)



(b)

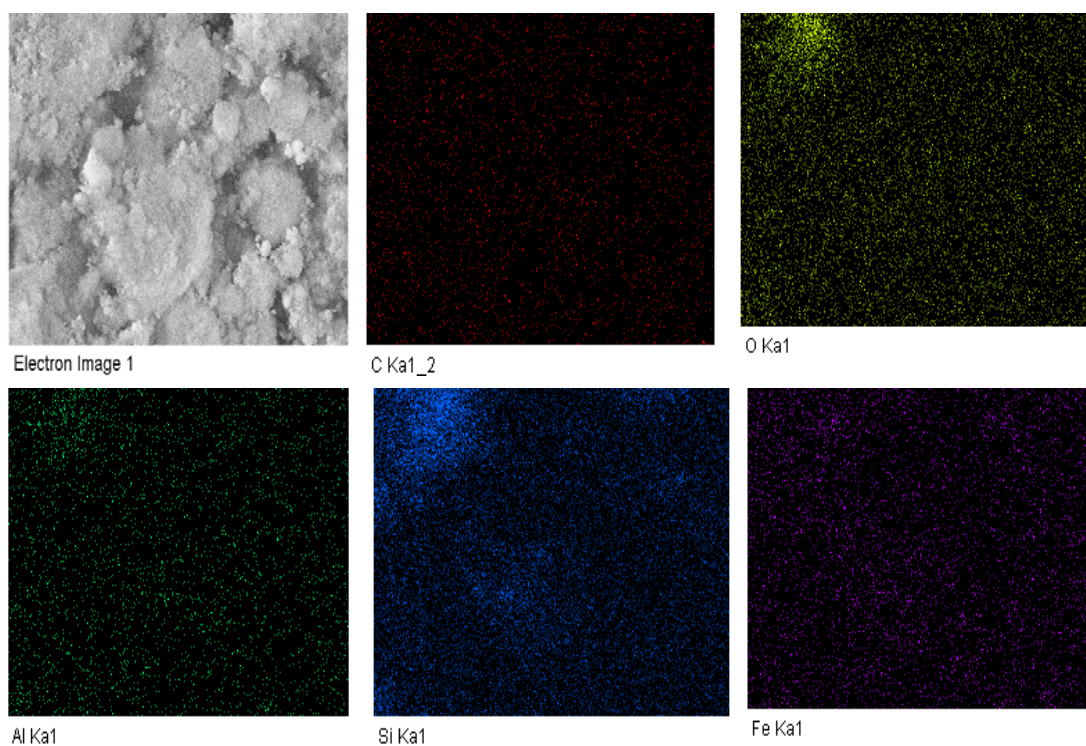


Figure D3 EDX mapping for Al_2O_3 - SiO_2 supported Fe-based catalysts at Fe loading of (a) 6, and (b) 15 wt%

Appendix E

- Chromatography of the FT reaction

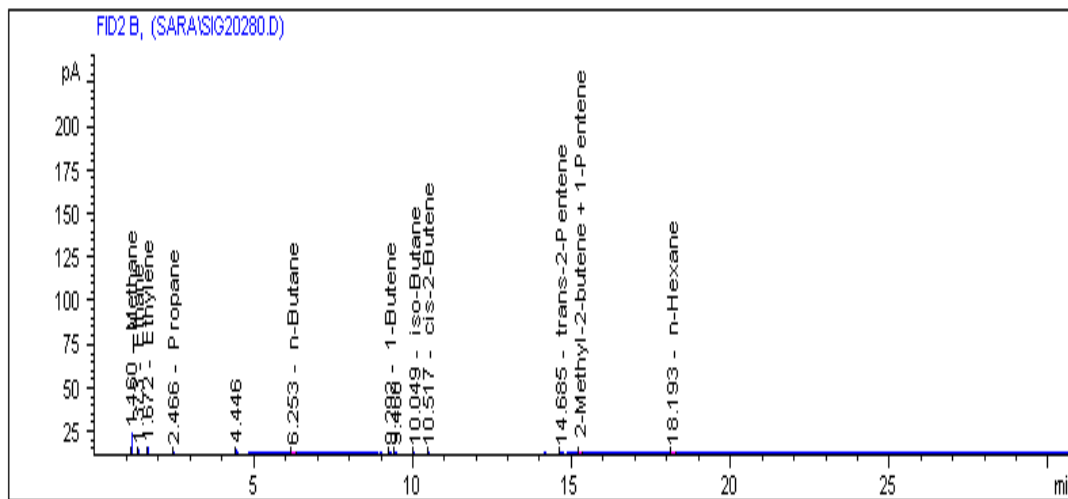


Figure E1: Example of reaction products FID chromatogram of impregnated Fe/SiO₂ at reaction condition of 523K, 1.5H₂/CO, 3L/g-Fe.h

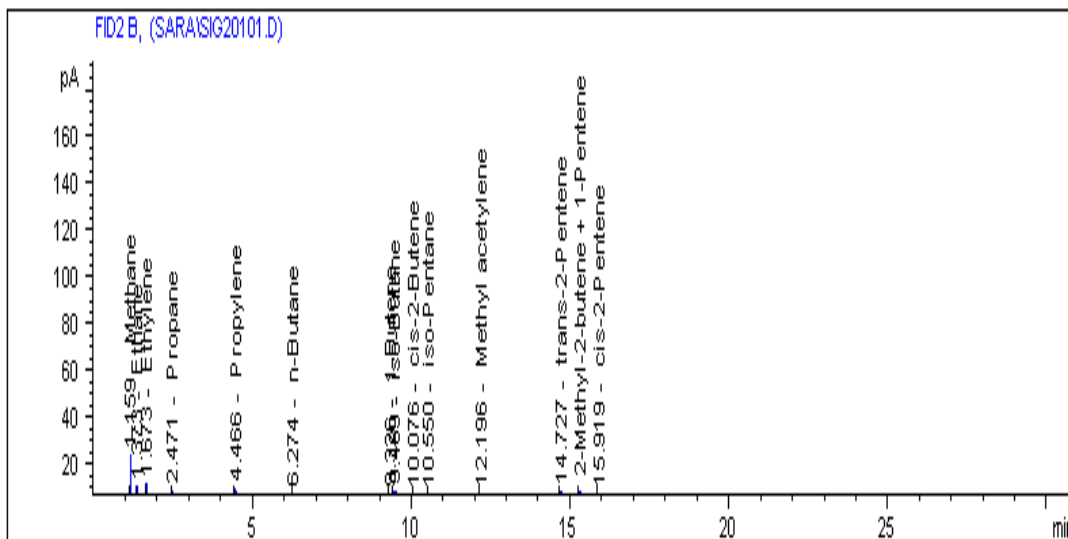


Figure E2: Example of reaction products FID chromatogram of Fe/Cu/SiO₂ at reaction condition of 523K, 1.5H₂/CO, 3L/g-Fe.

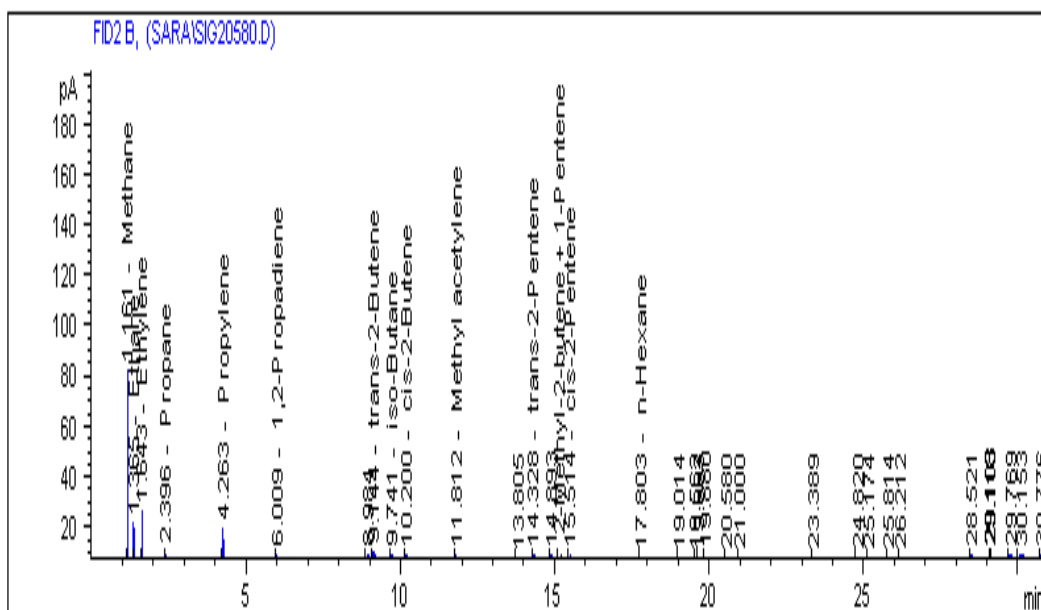


Figure E3: Example of reaction products FID chromatogram of Fe/K/SiO₂ at reaction condition of 523K, 1.5H₂/CO, 3L/g-Fe.h

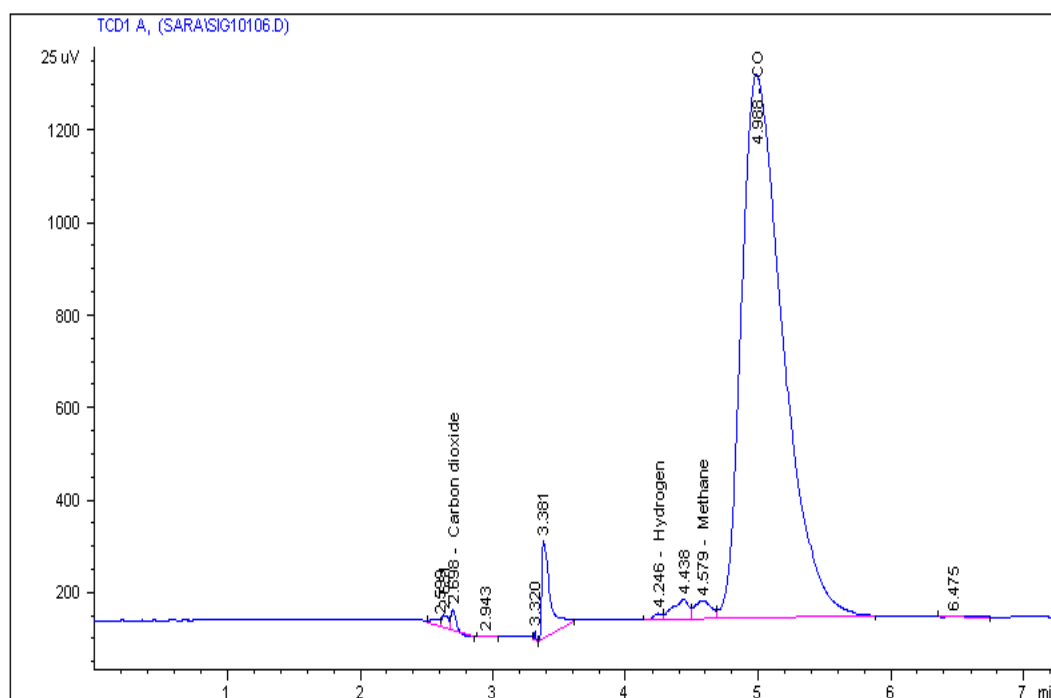


Figure E4: Example of reaction products TCD chromatogram of 6% Fe/SiO₂ at reaction condition of 523K, 1.5H₂/CO, 3L/g-Fe.h

- CO conversion and product selectivity calculations

1. CO conversion

$$X_{CO} = \left(\frac{CO_{in} - CO_{out}}{CO_{in}} \right) \times 100$$

Example for CO conversion calculation for 6%Fe/SiO₂ catalyst at reaction condition of 1.5H₂/CO, 523K and 5h

$$\begin{aligned} X_{CO} &= \left(\frac{98 - 44}{98} \right) \times 100 \\ &= 55\% \end{aligned}$$

2. Product selectivity

$$S_p = \frac{P}{\sum P_T} \times 100$$

Example for product selectivity calculation for 6%Fe/SiO₂ catalyst at reaction condition of 1.5H₂/CO, 523K and 90min

$$\begin{aligned} S_{CH_4} &= \frac{0.0140206}{0.0236106} \times 100 \\ &= 59.4 \end{aligned}$$

$$\begin{aligned} S_{C_5^+} &= \frac{0.004097}{0.0236106} \times 100 \\ &= 17.4 \end{aligned}$$

3. CO₂ selectivity

$$S_{CO_2} = \frac{\text{mole CO}_2 \text{ produced}}{\text{mole CO converted}} \times 100$$

Example for the calculation of CO₂ selectivity for 6%Fe/SiO₂ catalyst at reaction condition of 1.5H₂/CO and 523K

$$\begin{aligned} S_{CO_2} &= \frac{3.65}{52.94} \times 100 \\ &= 6.8 \end{aligned}$$

✓ Kinetics of FT reaction:

- Calculation of the rate constant

k value was calculated from equation 4-13 (section 4.4.4) and X_{Ae} was taken from figure 4-45 4-46 and 4-47 for the impregnated and precipitated catalyst.

$$k = -\frac{\tau}{X_{Ae}} \ln\left(1 - \frac{X_A}{X_{Ae}}\right)$$

$$k = X_{Ae} \times slope$$

Table E1 Calculation of the rate constant

| Sample | Temperature (K) | X_{Ae} (%) | k |
|----------------------------|-----------------|--------------|---------|
| 6% Fe/SiO ₂ (I) | 523 | 55 | 0.00055 |
| | 543 | 33 | 0.00033 |
| | 563 | 29 | 0.00029 |
| 6% Fe/SiO ₂ (P) | 523 | 46 | 0.00122 |
| | 543 | 36 | 0.00036 |
| | 563 | 32 | 0.00032 |

Then E value was calculated by drawing ln k versus 1/T (Figure 4-50)

$$E = R \times slope$$

- Data of CO conversion and product selectivity for all the synthesis catalyst at different reaction conditions

Table E2 Activity and selectivity of Fe/SiO₂ catalysts with different Fe loading prepared by impregnation at different H₂/CO ratio, 523K, 0.6L/h, and 5h

| H ₂ /CO ratio | Fe loading (wt %) | CO conversion (mol %) | CO ₂ selectivity (mol %) | Selectivity (%) | | |
|--------------------------|-------------------|-----------------------|-------------------------------------|--------------------------------|------------------|-----------------------------------|
| | | | | C ₁ -C ₄ | C ₅ + | C ₂ =-C ₄ = |
| 0.5 | 3 | 39.47 | 12.06 | 43.66 | 43.54 | 15.19 |
| | 6 | 39.42 | 16.41 | 51.38 | 27.70 | 23.27 |
| | 10 | 23.69 | 15.09 | 66.45 | 19.00 | 18.73 |
| | 15 | 20.96 | 26.22 | 69.77 | 15.94 | 19.53 |
| 1 | 3 | 50.87 | 7.36 | 66.29 | 20.32 | 16.87 |
| | 6 | 47.52 | 9.83 | 65.91 | 6.11 | 28.64 |
| | 10 | 34.67 | 14.10 | 69.83 | 6.18 | 23.99 |
| | 15 | 30.53 | 7.97 | 76.15 | 3.29 | 23.86 |
| 1.5 | 3 | 60.29 | 5.97 | 54.38 | 15.84 | 27.40 |
| | 6 | 54.02 | 6.89 | 57.48 | 20.73 | 22.65 |
| | 10 | 48.24 | 3.42 | 70.07 | 14.13 | 18.36 |
| | 15 | 44.68 | 20.88 | 77.37 | 11.00 | 19.87 |
| 2 | 3 | 29.96 | 24.79 | 79.59 | 3.98 | 18.26 |
| | 6 | 50.71 | 5.91 | 80.11 | 4.48 | 15.40 |
| | 10 | 45.22 | 4.81 | 79.58 | 3.62 | 15.88 |
| | 15 | 28.85 | 23.67 | 81.31 | 0.92 | 17.21 |

Table E3 Activity and selectivity of Fe/SiO₂ catalysts with different Fe loading prepared by precipitation method at 523K, 1.5H₂/CO ratio, 3L/g-cat.h

| Fe loading (wt %) | CO conversion (mol %) | CO ₂ selectivity (mol %) | Selectivity (%) | | |
|-------------------|-----------------------|-------------------------------------|--------------------------------|------------------|-----------------------------------|
| | | | C ₁ -C ₄ | C ₅ + | C ₂ =-C ₄ = |
| 3 | 47.16 | 6.89 | 70.31 | 11.70 | 18.98 |
| 6 | 45.76 | 8.54 | 73.31 | 7.70 | 18.72 |
| 10 | 33.31 | 17.12 | 81.51 | 3.91 | 17.36 |
| 15 | 26.49 | 22.21 | 83.24 | 0.44 | 16.32 |

Table E4 Activity and selectivity of Fe/Al₂O₃-SiO₂ catalysts with different Fe loading prepared by precipitation method at 523K, 1.5H₂/CO ratio, 3L/g-cat.h

| Fe loading (wt %) | CO conversion (mol %) | CO ₂ selectivity (mol %) | Selectivity (%) | | |
|-------------------|-----------------------|-------------------------------------|--------------------------------|------------------|-----------------------------------|
| | | | C ₁ -C ₄ | C ₅ + | C ₂ =-C ₄ = |
| 3 | 45.96 | 9.45 | 69.40 | 10.80 | 18.40 |
| 6 | 41.24 | 11.93 | 61.78 | 20.84 | 15.41 |
| 10 | 34.76 | 13.69 | 85.17 | 4.61 | 14.21 |
| 15 | 27.98 | 23.25 | 87.61 | 3.87 | 8.52 |

Table E5 Activity and selectivity of Fe/SiO₂ catalysts by impregnation method at 1.5H₂/CO ratio and different reaction temperature and flow rate

| Temperature (K) | Flow rate (L/h) | Fe loading (wt %) | CO conversion (mol %) | CO ₂ selectivity (mol %) | Selectivity (%) | | |
|-----------------|-----------------|-------------------|-----------------------|-------------------------------------|--------------------------------|------------------|-----------------------------------|
| | | | | | C ₁ -C ₄ | C ₅ + | C ₂ =-C ₄ = |
| 523 | 0.6 | 6 | 54.02 | 6.89 | 57.48 | 20.73 | 22.65 |
| 543 | | | 32.95 | 20.52 | 68.82 | 8.54 | 24.31 |
| 563 | | | 28.36 | 21.04 | 81.29 | 8.29 | 14.75 |
| 523 | 2.4 | 6 | 47.61 | 9.77 | 65.64 | 14.32 | 20.40 |
| 543 | | | 26.27 | 24.52 | 70.73 | 2.89 | 28.95 |
| 563 | | | 18.71 | 35.70 | 64.44 | 0.56 | 35.56 |
| 523 | 4.8 | 6 | 26.35 | 24.62 | 71.87 | 9.31 | 21.75 |
| 543 | | | 13.20 | 26.45 | 72.43 | 0.59 | 26.98 |
| 563 | | | 6.50 | 37.56 | 79.51 | 0.34 | 20.38 |

Table E6 Activity and selectivity of Fe/SiO₂ catalysts by precipitation method at 1.5H₂/CO ratio and different reaction temperature and flow rate

| Temperature (K) | Flow rate (L/h) | Fe loading (wt %) | CO conversion (mol %) | CO ₂ selectivity (mol %) | Selectivity (%) | | |
|-----------------|-----------------|-------------------|-----------------------|-------------------------------------|--------------------------------|------------------|-----------------------------------|
| | | | | | C ₁ -C ₄ | C ₅ + | C ₂ =-C ₄ = |
| 523 | 0.6 | 6 | 45.76 | 8.54 | 73.31 | 7.70 | 18.98 |
| 543 | | | 35.61 | 11.89 | 75.68 | 5.85 | 20.41 |
| 563 | | | 31.65 | 15.60 | 83.89 | 0.67 | 16.11 |
| 523 | 2.4 | 6 | 29.54 | 13.92 | 77.03 | 3.67 | 20.40 |
| 543 | | | 27.15 | 19.93 | 79.54 | 1.04 | 19.40 |
| 563 | | | 26.69 | 23.86 | 85.83 | 0.31 | 16.92 |
| 523 | 4.8 | 6 | 7.52 | 17.88 | 79.07 | 0.12 | 20.81 |
| 543 | | | 6.72 | 22.80 | 82.23 | 0.45 | 17.75 |
| 563 | | | 17.14 | 26.77 | 87.10 | 0.73 | 12.09 |

Appendix F

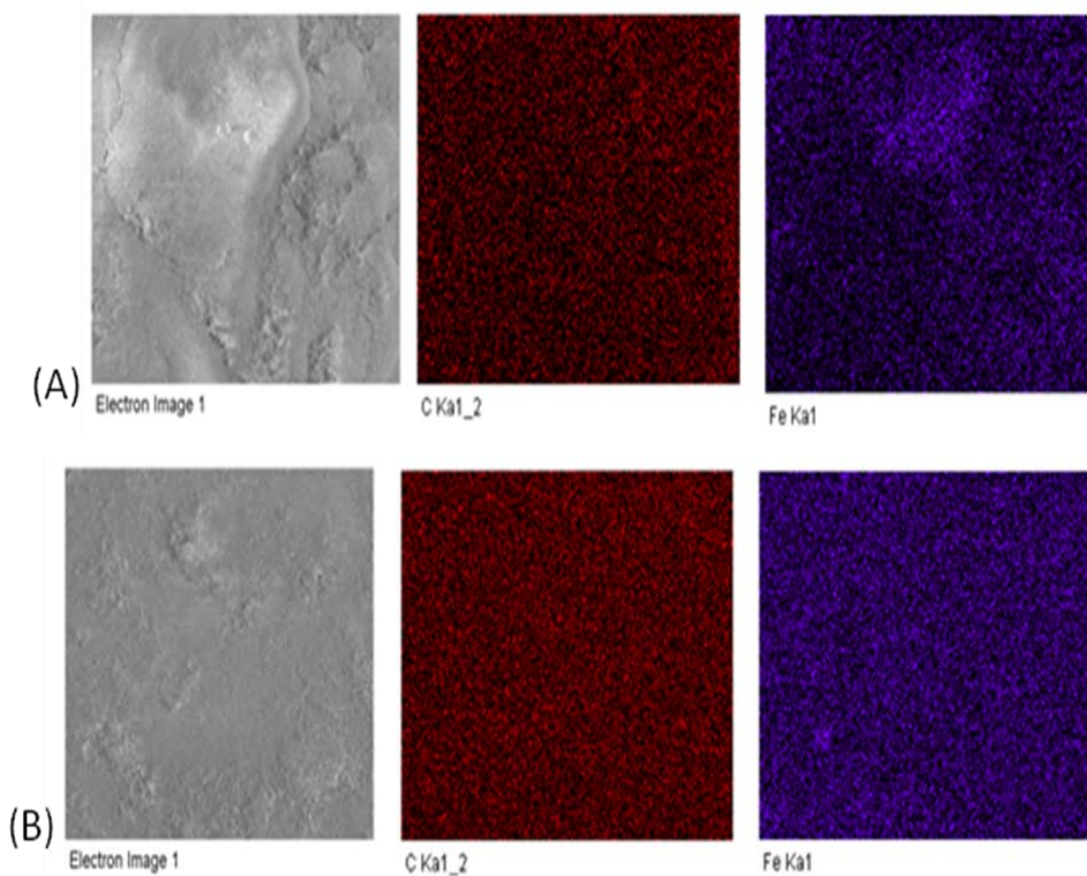


Figure F1: EDX mapping of 6%Fe on SiO₂ catalyst prepared by impregnation method (A) fresh catalyst before reaction and (B) spent catalyst after reaction

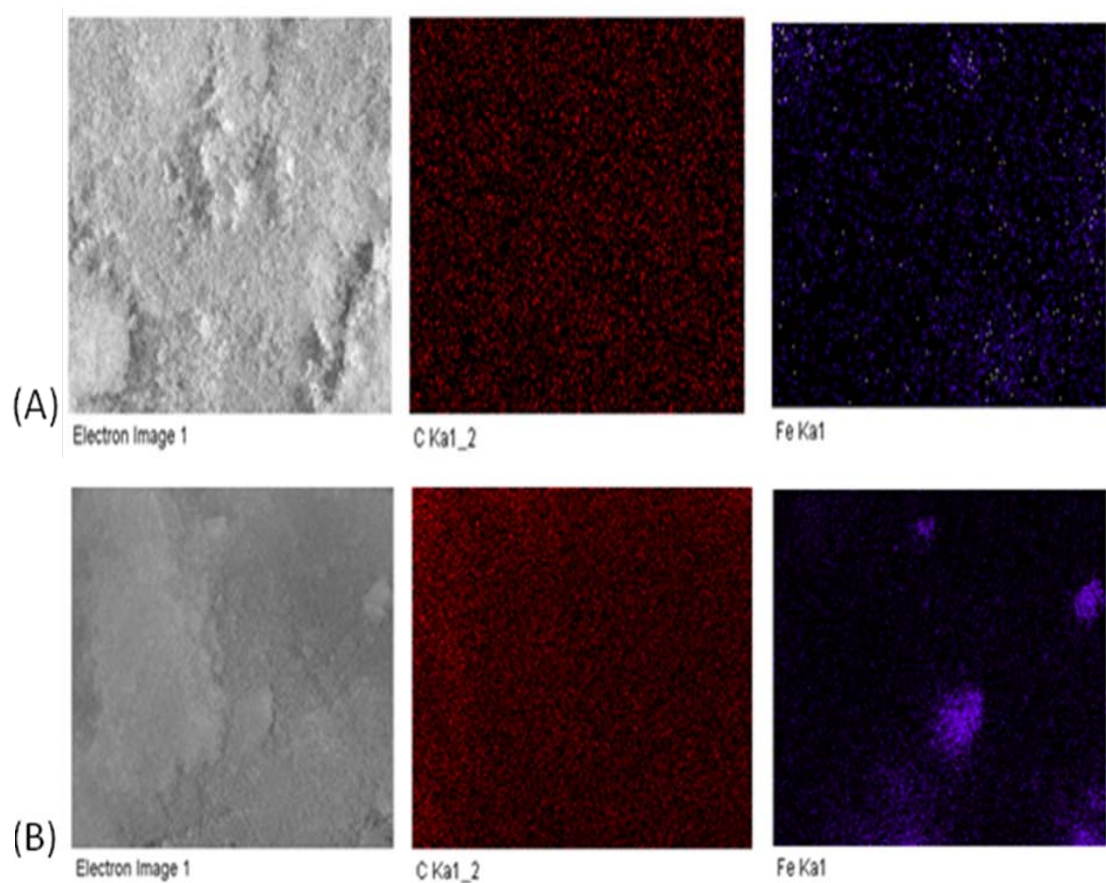


Figure F2: EDX mapping of 6%Fe on SiO₂ catalyst prepared by precipitation method (A) fresh catalyst before reaction and (B) spent catalyst after reaction

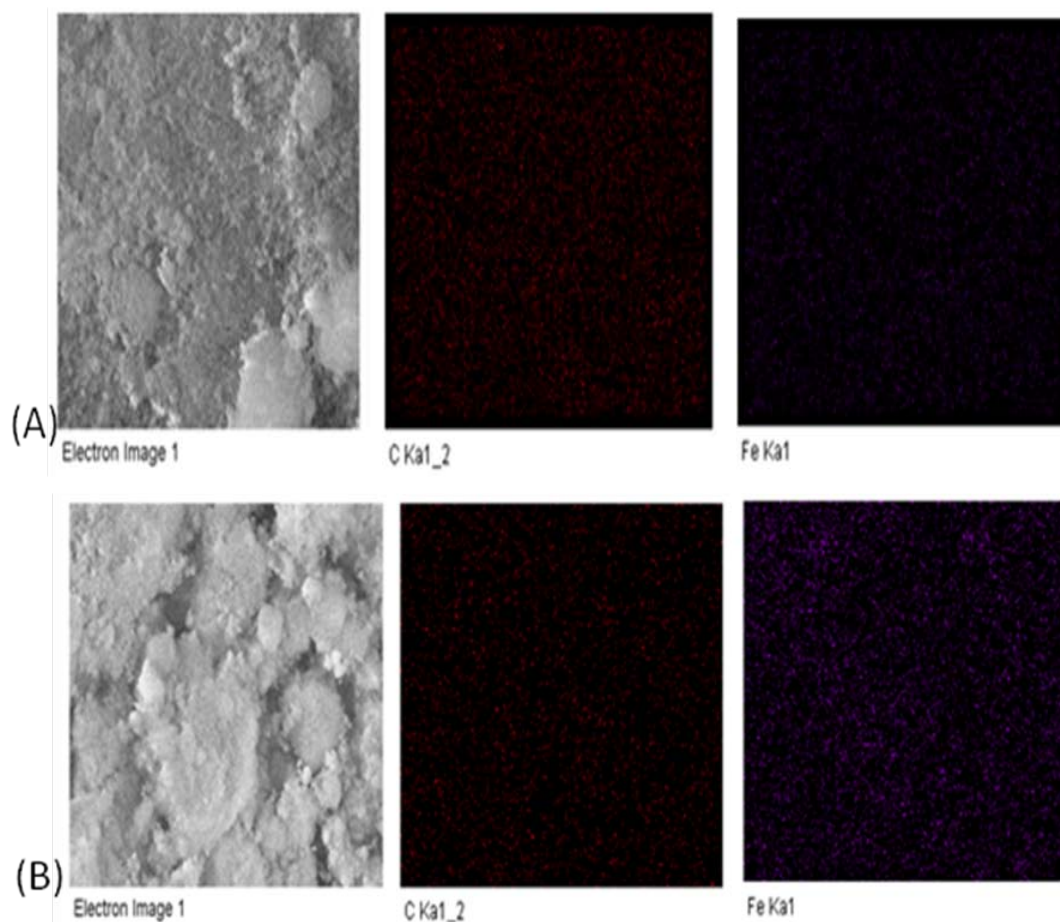


Figure F3: EDX mapping of 6%Fe on Al₂O₃-SiO₂ catalyst (A) fresh catalyst before reaction and (B) spent catalyst after reaction